Regulation of Synapse Development by Activity Dependent Transcription in Inhibitory Neurons

Dissertation Advisor: Professor Michael E. Greenberg Alan Robert Mardinly

Regulation of Synapse Development by Activity Dependent Transcription in Inhibitory Neurons

Abstract

Neuronal activity and subsequent calcium influx activates a signaling cascade that causes transcription factors in the nucleus to rapidly induce an early-response program of gene expression. This early-response program is composed of transcriptional regulators that in turn induce transcription of late-response genes, which are enriched for regulators of synaptic development and plasticity that act locally at the synapse.

The main focus of this thesis is to describe the activity-induced transcriptional program in inhibitory neurons and identify its functional roles. We find strong similarity of the early-induced transcription factors induced by activity in excitatory and inhibitory neurons, but significant differences in the late-response genes. This finding suggests that commonly induced transcription factors may regulate distinct sets of target genes to perform cell-type specific functional roles. To test this hypothesis we focused on the immediate early transcription factor Npas4, which in excitatory neurons transcribes Bdnf to promote increased inhibition. While Npas4 is highly induced in response to activity in inhibitory neurons, Bdnf is not expressed, suggesting that Npas4 may perform a unique function in inhibitory neurons.

Conditional deletion of Npas4 in somatostatin (SST) expressing inhibitory neurons causes a decrease in excitatory – but not inhibitory – synapses both *in vitro* and *in vivo,* showing that Npas4 functions to promote development of excitation onto SST neurons. This function is the reciprocal if its function in promoting inhibition to excitatory neurons, demonstrating that the functional role of activity-

dependent transcriptional programs is uniquely adapted to the requirements of a specific cell-type within a circuit.

To investigate the mechanisms by which Npas4 controls development of excitatory input to SST neurons, we identified Npas4 target genes in inhibitory neurons and found that Npas4 regulates a unique transcriptional program of activity-induced late-response genes distinct from the program that it regulates in excitatory neurons. Finally, we demonstrate that SST neurons *in vivo* induce expression of a subset of Npas4 target genes. These genes include Nptx2, which has a well-characterized role in clustering AMPA receptors specifically to non-spiny excitatory synapses, suggesting a possible mechanism by which activity-dependent transcription in inhibitory neurons mediated by Npas4 controls the development of excitation.

TABLE OF CONTENTS

List of Figures

ACKNOWLEDGEMENTS

"*We have to watch ourselves most carefully. The real preparation for education is a study of one's self. The training of the teacher who is to help* ***life*** *is something far more than a learning of ideas. It includes the training of character; it is a preparation of the spirit."*

Montessori, *The Absorbent Mind*

This PhD is in a narrow sense a record, or catalogue, of the work that I have performed over the last six years, but the contents of no thesis are ever truly reflective of the nature of the labor that went into producing it. It is perhaps the curse of modern biology that the conceptual ideas are relatively simple compared to the long, laborious, and technically demanding experiments demanded to test them. Therefore doctoral training is only partially a purely intellectual challenge; the demands placed upon the trainee and the advisor are extended, to quote Montessori, to "the training of character...the preparation of the spirit." It has been my good fortune to train with Dr. Michael Greenberg, who understands this aspect of mentorship more than anybody I have ever encountered. I stand in awe of Mike's capacity for clarity and incisiveness in the face of complexity, and I would consider my training a success if I have made even a small fraction of this capacity my own. Equally as important is his capacity for patience, understanding, and to allow people to come to their own conclusions. Even more than his great capacity for teaching how to think, Mike has a gift for teaching how to live life within science, how to behave, to persevere, be generous, and learn the appropriate lessons from adversity. I owe any success in my future scientific pursuits to his mentorship.

I have been very fortunate to be guided throughout my graduate school career by a supportive and generous group of faculty advisors. Chinfei Chen has been a great mentor, confidant, and friend. She generously took me into her lab at the start of graduate school, and provided advice, support, and a sympathetic ear throughout the entire process. Beth Stevens has also been a great mentor, collaborator, and friend. Her enthusiasm, energy, and passion for science are

infectious. I have been equally lucky to be guided by Chuck Weitz, Jeff Lichtman, and Clay Reid on my dissertation advisory committee. They offered constant support, good and frank advice, and patience during my inevitable missteps. I left every single meeting feeling that I had learned a lot, and that I had a lot to learn. I would also like to thank my examination committee, Chinfei Chen, Takao Hensch, and Gordon Fishell for their time, guidance, support, and – hopefully – for passing me.

Science is not performed in a vacuum, and the development of any scientist is profoundly related to the environment where they work. The Greenberg lab has been an incredible place to learn how to be a scientist and to grow and mature. I have been very fortunate to work closely with Ivo Spiegel during the second half of my graduate training. Ivo is incredibly smart, but he is successful because he is thorough, organized, prepared, plans far into the future, is rigorous, thinks broadly and conceptually, and is strong willed. These things make him an excellent collaborator, will make him an excellent primary investigator, and are all things that I hope I have learned from him. I've also been very fortunate to work with Jeremy Bazinet and Cameron Couch, who have worked very hard on experiments relating to my thesis work. I've been very fortunate to work with and learn from a large group of talented and supportive post-doctoral fellows in the Greenberg lab and the Harvard neuroscience community, including Sarah Ross, Zak Wills, Seth Margolis, Harrison Gabel, Bulent Ataman, Tim Cherry, Dan Ebert, Mac Hooks, and Dori Shaffer.

The graduate students in the Greenberg lab have provided camaraderie, intellectual stimulation, moral support, and friendship. I could not have done this without them. In particular, I cannot imagine graduate school without my baymate, Caleigh Mandel-Brehm, who is one of the most imaginative, fun, and enthusiastic people I have met. She is also technically brilliant and extremely generous with her time, and I have learned an incredible amount of science through conversations with her. I entered the Greenberg lab at the same time as Mike Soskis, John Salogiannis, and Athar Malik, and we helped each other survive, grow, and succeed. I also had to great fortunate to work with, learn from, and befriend a number of other extraordinary members of the Greenberg lab including Sonia Cohen, Milena Andzelm, and Paul Greer.

In dealing with the inevitable trials and tribulations of graduate school, I have looked constantly to my loving and supportive family. My mother and father – Sue and Peter Mardinly – are the best any child could hope for. They provided me with infinite support and every opportunity in life. It has been a great pleasure to become close with my sister Shaina over the last several years. We have always loved each other, but now we are close friends. My grandparents have been inspirations throughout my life, like my parents I have no words to describe what they mean to me, for words will by definition limit, restrict. In particular I would like to acknowledge that my grandfather, a great psychoanalyst, first fired my interest in the inner workings of the brain. I would note with some disappointment that after several-hundred mouse brains dissected, I have as of yet found no evidence of the Id, Ego, or Superego.

Finally, I have been fortunate to enjoy the company of a wonderful group of friends during my time at Harvard; they have provided a never-ending fun and enrichment, kept me happy and sane. My greatest thanks to Jesse Raber, Clara Raubertas, Dan Pratt, Andrew Klock, Matty McFeely, Maia Raber, Hanna Buettner, Alex Amman, Tucker Bennett, Sarah Elgart, Erin Braswell, Tami Lieberman, Yitzhak Wasileski, Joan Wolkerstorfer, Jess Lent, John Payne, Dan Kimmel, and Maren Christensen for their friendship and support.

COLLABORATOR CONTRIBUTIONS

Chapter 2: Chapter 2 is based on a manuscript in preparation for submission that is the result of a close and equal collaboration between Alan Mardinly and Ivo Spiegel under the guidance and supervision of Michael Greenberg. Alan Mardinly was involved in either the planning, execution, or analysis of every experiment except the initial characterization of MGE and E14 Cortical cultures presented in figure 2.1, which were performed by Ivo Spiegel. Ivo Spiegel also performed microarray studies of MGE cultures that while not explicitly discussed in this chapter, provided the intellectual basis for this project. Ivo Spiegel purified all RNA and performed all quantitative RT-PCR for experiments in this chapter, including the Ribotag experiment. Jeremy Bazinet helped perform Sholl analysis experiments. Cameron Couch, a summer student working under Alan Mardinly, participated in immunohistochemistry experiments and Sholl analysis experiments.

Chapter 3: Alan Mardinly performed and analyzed all experiments for which data is shown as part of an ongoing collaboration with Ivo Spiegel. The discussion references unpublished or preliminary experiments performed by Ivo Spiegel and analyzed by Alan Mardinly, as well as unpublished or preliminary work performed independently by Ivo Spiegel and Harrison Gabel in the laboratory of Mike Greenberg.

Chapter 4: includes both unpublished work performed by Alan Mardinly and collaborators in Mike Greenberg's laboratory, as well as work drawn from publications from the laboratories of Michael E. Greenberg or Beth Stevens.

Developing the capacity to perform array tomography experiments at Harvard would not have been possible without an ongoing and generous collaboration with Beth Stevens and her laboratory, as well as the generosity of Stephen Smith, Christina Micheva, and Brad Busse.

Experiments performed on Ube3a mutant animals were performed by Alan Mardinly in collaboration with Paul Greer under the guidance of Michael Greenberg.

Experiments performed on Ephexin 5 mutant animals were performed by Alan Mardinly in collaboration with John Salogiannis and Seth Margolis, under the guidance of Michael Greenberg.

Experiments performed on CR3 and C3 mutant animals were performed by Dori Shaffer and Amanda Kautzman in the Beth Stevens' laboratory, in consultation with Alan Mardinly, and analysis was performed by Alan Mardinly

Chapter 1:

Activity-Dependent Transcription and GABAergic Neurons in the Nervous System

Forward

Mammalian nervous systems have evolved to gather information about the environment, form associations, and modify innate patterns of behavior to promote the animal's survival and reproduction. In order to perform the complex computations required for these tasks, the nervous system must form appropriate synaptic connections early in development and subsequently rewire itself in response to new experiences. The wiring of a complex nervous system is unlikely to be strictly deterministic: the mouse cortex consists of ~1.0×10^7 neurons that form 8.1×10^{10} synaptic connections (Schuz and Palm, 1989); with ~24,000 protein-coding genes in the mouse genome, the deterministic specification of every synaptic connection would require the utilization of most of the genome for that purpose. Instead, the nervous system relies on emergent properties of gene expression networks to guide synaptic development. The membrane dynamics necessary to fire action potentials can be established using relatively few genes products; subsequent patterns of activity driven by the dynamic interplay between excitation and inhibition provide a vast information space to guide activity-dependent processes.

The realization that the brain is modified by experience is as old as the rejection of mind-body dualism by the scientific community. To accept that the physical brain is the seat of cognition is to accept that the act of learning or memory formation is to physically modify the brain. The specific role of sensory experience in shaping the development of functional responses of the nervous system was demonstrated by the seminal work of Hubel and Wiesel in the 1960s (Wiesel and Hubel, 1963). Their discovery of nervous system plasticity was followed a decade later by the discovery of long term potentiation (LTP) by Bliss and Lomo (Bliss and Lomo, 1973). This realization that the strength of an individual synapse could be acutely modified by neuronal activity opened new doors for potential mechanistic understanding of nervous system plasticity. The appreciation that the late phase of LTP required new protein synthesis tied neuronal plasticity irrevocably to the cell biology of a neuron, and dovetailed with a new emerging understanding that

transcription itself can be regulated by extracellular signals (Frey et al., 1989), (Greenberg and Ziff, 1984), (Greenberg et al., 1986).

The discovery of operons in the early 1960s in prokaryotes demonstrated that extracellular signals could directly affect transcription. The subsequent discovery that addition of growth factors to quiescent fibroblasts induces transcription of c-Fos showed that transcriptional responses to extracellular stimuli could occur in eukaryotes (Greenberg and Ziff, 1984). This discovery was remarkable for two additional reasons: the rapid kinetics with which c-Fos is induced suggested that extracellular signaling to the nucleus could occur rapidly enough to read out specific, acute signals from the extracellular environment. Additionally, the massive magnitude of c-Fos induction showed that stimulus-induced transcription could occur over a large dynamic range necessary for reading out complex temporal patterns of signaling (Greenberg and Ziff, 1984). The extension of this finding to the nervous system opened a new era of molecular insight into activity-dependent changes in the nervous system (Montminy and Bilezikjian, 1987),(Greenberg et al., 1986; Sheng et al., 1990).

Since Hubel and Wiesel's groundbreaking studies, the study of activity in the nervous system has proliferated at an astonishing rate. The sheer volume of publications relating to neuronal activity (over 60,000 pubmed hits) speaks to the profound importance and far reach of activity dependent processes. Because of an ever-increasing realization that many, if not most, aspects of the nervous system are somehow dynamically regulated, the term "activity-dependent" can refer to things as varied as potassium chloride and real-time dynamic changes in sensory experience. In this introduction, I briefly review selected topics relating to activity dependent transcriptional control of synapse development. This review is followed by a short review of inhibitory neuron function in the nervous system, as well as a discussion of how activity impacts inhibitory neurons.

I. Activity-induced transcription in the nervous system

Activity in the developing nervous system

The developing nervous system faces a number of immense challenges as it assembles itself into an active network. Cells of the correct type must be born and migrate into appropriate positions, axons must navigate across vast domains to precisely defined target regions, and synaptic contacts must develop with exquisite selectivity (Hooks et al., 2011). Remarkably, the synaptic microarchitecture of the brain can be assembled without canonical synaptic vesicle release, suggesting that early nervous system development does not require synaptic neurotransmitter signaling (Verhage et al., 2000). However, synaptic connectivity is massively refined later in life, and synaptic activity elicited by both intrinsic and mechanisms and sensory experience is vital for this and other aspects of nervous system development.

The visual system has historically been an appealing model in which to study activity in the nervous system: visual input is very easy to manipulate by dark rearing, eyelid suturing, or pharmacologically through eye injections. In mammals, retinal ganglion cells (RGCs) send a major projection to the lateral geniculate nucleus (LGN). These axons are initially guided to appropriate locations by gradients of signaling molecules, and are subsequently refined by activity to define discreet zones of the LGN that receive input from either the ipsi- or contra-lateral eye (Feldheim and O'Leary, 2010). Intrinsic activity is required for this refinement: although the retina does not respond to light for several days after birth, retinal ganglion cells fire action potentials from the first day of life (Masland, 1977),(Galli and Maffei, 1988). Blocking these action potentials blocks eye-specific segregation of RGC axons into their proper target areas in the LGN, demonstrating that spontaneous activity contributes to the organization of the visual system (Shatz and Stryker, 1988). Spontaneous RGC firing is highly correlated amongst groups of neighboring cells; large cohorts of RGCs fire high frequency bursts in waves that are necessary for eye-specific segregation of RGC axons in the LGN (Meister et al., 1991),

(Torborg et al., 2005),(Wong et al., 1993),(Maffei and Galli-Resta, 1990). This synchronization ensures that groups of afferents from the ipsilateral eye fire in patterns distinct from contralateral afferents; the acorrelated nature of this bursting is required for map refinement (Zhang et al., 2012). In addition to map refinement, intrinsic activity is necessary for much of the strengthening and refinement of RGC input to thalamic relay neurons that occurs prior to eye opening, with visual input only necessary for later stages of refinement (Hooks and Chen, 2006). Finally, desynchronization of retinal waves around the time of eye opening disrupts refinement of RGC axons in the LGN, indicating that patterned intrinsic activity is also important for the maintenance of eye-specific segregation (Demas et al., 2006).

Intrinsic activity also occurs in developing cortex, which is partitioned into distinct domains of electrically coupled coactive neurons spanning cortical layers (Yuste et al., 1992). Coherent calcium waves , which require synaptic activity for propagation, travel across the visual cortex before eye opening. These waves dissipate around the time when GABA becomes hyperpolarizing, consistent with a role for GABAergic inhibition in stopping these oscillations (Garaschuk et al., 2000). In the visual cortex, large coherent oscillations take place layer II/III after the onset of inhibition, recruiting up to 75% of LII/III neurons per wave; these waves gradually become sparser after eye opening (Rochefort et al., 2009). The precise function of intrinsic activity in the cortex is not fully understood, but it is theorized to play key roles in the emergence of a number of cortical visual properties that emerge before the onset of visual experience, including direction selectivity, receptive field formation, and initial wiring of ocular dominance columns (Rochefort et al., 2011), (Espinosa and Stryker, 2012),(Horton and Hocking, 1996) (Feller and Scanziani, 2005),(Godecke and Bonhoeffer, 1996).

One of the most well characterized examples of experience-dependent plasticity is the critical period for ocular dominance plasticity, during which visual deprivation causes a permanent decrease in the acuity of the deprived eye. First described by Hubel and Wiesel in cats, monocular deprivation during the visual critical period results in a dramatic shift in the responsiveness of normally binocularly driven neurons away from the deprived eye and towards the spared eye

(Wiesel and Hubel, 1963). In addition to causing a shift in the functional responsiveness of the cortex, monocular deprivation during the critical period results in anatomical changes, with geniculate afferents from the deprived eye shrinking to innervate reduced territory in layer 4 (Shatz and Stryker, 1978),(Hubel et al., 1977). Indeed, the spacing of ocular dominance columns can be affected by decorrelation of visual input by experimentally induced strabismus, implying that pattern – not simply the presence - of binocular input is important for shaping the connectivity of the cortex (Lowel, 1994).

Visual critical periods also occur in mice; although the mouse visual cortex does not feature ocular dominance columns, nearly one third of murine V1 receives binocular input (Hubener, 2003). The mouse visual critical period begins at P19, several days after eye opening, and persists until P32; during this timeframe the visual acuity of the mouse increases to mature levels, and a process of binocular orientation matching occurs (Prusky and Douglas, 2003; Wang et al., 2010). Similarly to cats, monocular deprivation during this critical period in mice causes a shift in cortical responsiveness towards the spared eye that results in amblyopia (Gordon and Stryker, 1996). Blockade of vision in one eye during the critical period results in two distinct synaptic events in binocular V1; first, a rapid depression of responses from the deprived eye, followed by a delayed potentiation of responses to the spared eye through a process that requires homeostatic scaling (Frenkel and Bear, 2004),(Ranson et al., 2012). The expression of OD plasticity is also critically dependent on spine motility facilitated by activation of extracellular protease cascades by tissue plasminogen activator, a gene induced by synaptic activity (Mataga et al., 2004),(Oray et al., 2004),(Mataga et al., 2002),(Qian et al., 1993). Critically, the timing during which critical periods plasticity occurs is intimately dependent upon the maturation of cortical inhibition (Hensch, 2005). Thus, neuronal activity plays critical roles at every stage of neuronal development, from LGN map refinement to the emergence of mature functional response in the visual system and control of cortical plasticity.

Activity-Dependent Transcription

What are the mechanisms by which activity and experience shape the development of the nervous system? One of the many ways in which activity can influence the development of the nervous system is by regulating gene expression. Excitatory neurotransmission results in membrane depolarization and calcium influx that activates signaling cascades that culminate in the activation of transcriptional regulators. These regulators rapidly induce the transcription of a set of early-response genes, many of which are themselves transcriptional regulators that promote activation of other genes enriched for regulators of synaptic development. This activity-dependent transcriptional program regulates many aspects of nervous system development including, but not limited to, synaptic development and plasticity.

The first description of activity-dependent transcription in neuronal cells was the observation in PC12 cells that application of acetylcholine receptor agonists induces transcription of the immediate early gene c-Fos through a pathway that requires calcium influx through the L-type calcium channel (Greenberg et al., 1986a). Activity-dependent mRNA induction can be induced through other stimuli as well; application of forsklin, an adenylate cyclase activator, causes the upregulation of somatostatin (SST) mRNA in PC12 cells. This regulation was found to be critically dependent upon a region of DNA in the SST promoter region termed the CRE (cAMP Response Element). The cAMP dependent upregulation of SST mRNA levels was also critically dependent on the PKA mediated phosphorylation of a 43 kDa protein that binds to the CRE in the promoter region. This protein was termed CREB (CRE Binding protein) (Montminy and Bilezikjian, 1987), (Gonzalez and Montminy, 1989). In addition to cAMP signaling, a number of other stimuli can induce CREB phosphorylation at Serine 133, which results in activation of CREB and transcription of immediate early genes, including c-Fos (Sheng et al., 1990). One such stimulus is the influx of calcium ions into the cytoplasm. Calcium influx into the cell results in the binding of free calcium ions to calmodulin (CaM), a small effector protein that dramatically changes its conformation upon binding to calcium, whereupon it activates a number of signaling pathways, including the CaM kinase II

pathway. Activation of this pathway results in phosphorylation and activation of CREB (Dash et al., 1991), (Sheng et al., 1990). Additionally, neurotrophin signaling through receptor tyrosine kinases activates Ras, a small GTPase that activates the MAPK signaling cascade, to phosphorylate CREB (Bonni et al., 1995),(Ginty et al., 1994). In addition to S133, calcium signaling can selectively phosphorylate S142, conferring CREB with the ability discriminate between the various signaling pathways that converge upon it (Kornhauser et al., 2002).

CREB phosphorylation on both S133 and S142 occur in the suprachiasmatic nucleus (SCN) in response to light, and mutations that abolish S142 phosphorylation impair light entrainment of the SCN. This mutation also disrupt temporally regulated patterns of c-Fos expression in the SCN, demonstrating that CREB mediated transcription occurs *in vivo* and has biological significance (Ginty et al., 1993),(Kornhauser et al., 1996),(Gau et al., 2002). Furthermore, CREB mediated transcription, as reported by a CRE-LacZ reporter, is activated in the visual cortex in response to monocular deprivation during visual critical period, suggesting that CREB-activated transcription has a role in nervous system plasticity (Pham et al., 1999). The specific role of CREB in synaptic plasticity is the subject of some debate, but reports have indicated that CREB is required for expression of the late phase of LTP, and that ectopic expression of constitutively active CREB primes synapses for the late phase of LTP, abolishing the requirement of post-tetanic transcription for late phase LTP (Barco et al., 2002). Acute *in vivo* expression of CREB results in increased numbers of silent synapses, suggesting that CREB mediated transcription regulates multiple aspects of synaptic development and plasticity (Marie et al., 2005).

As discussed, CREB does not act directly at synapses, but binds widely across the genome at CRE sequences. CREB is constitutively bound to CRE elements on the DNA at thousands of discreet sites, 72% of which are within 1 KB of a CRE (Impey et al., 2004). Activation of CRE-bound CREB is necessary for the activation of a broad program of gene expression, but it is not sufficient: transcription of many activity-regulated genes requires the binding of additional factors. One of these factors is CBP (Creb Binding Protein), a transcriptional coactivator that is activated by

CaMKIV-mediated phosphorylation. CBP binds to phosphorylated CREB, and augments the CREB-mediated activation of cAMP-responsive genes by recruiting TFIIB and the basal transcriptional machinery through an interaction in its C-terminus (Kwok et al., 1994),(Impey et al., 2002). CBP is mutated in Rubinstein-Taybi syndrome, and deletion of CBP in excitatory neurons of the neocortex impairs memory formation, lending further evidence of the critical importance of activity-dependent transcription for proper neuronal function (Petrij et al., 1995),(Chen et al., 2010a). Phosphorylated CBP binds to activity-regulated enhancers, where its native histone acetyltransferase activity helps open chromatin to promote enhancer function (Bannister and Kouzarides, 1996),(Kim et al., 2010). These studies demonstrated the electrical activity of the neuronal membrane can lead directly to changes in the chromatin state of the nucleus, as well as alter gene transcription.

Routes of Calcium Influx

The nature of the activity-dependent signal depends upon the route of calcium entry into the cell. Calcium is kept at micromolar concentrations inside the cell through highly regulated active processes. This exclusion of calcium from the cytoplasm allows calcium sensors such as calmodulin to respond to exquisitely small, local, and transient changes in calcium concentration. Calcium can enter a neuron through calcium permeable AMPA receptors, NMDA receptors, and L-type calcium channels. AMPA receptor activation is a necessary precondition for calcium influx through NMDA receptor or voltage sensitive calcium channels, both of which only flux calcium at elevated membrane potentials.

AMPA receptors are tetramers composed of varying compositions of four subunits GluA1-4 (formerly termed GluR1-4 or GluRA-D). In excitatory neurons, most AMPA receptors are hetero-tetramers consisting of two GluA2 subunits and either two GluA1 or two GluA3 subunits, though GluA1 homo-tetrameric AMPA receptors are synthesized and preferentially inserted into synaptic sites in some forms of plasticity including LTP (Plant et al., 2006). GluA4 is enriched in inhibitory neurons, at the expense of GluA2, which is not widely expressed in those cells. Of

the AMPA receptor subunits, only GluA2 undergoes a post-transcriptional mRNA editing event that converts a glutamine to an arginine residue in the pore-forming region of the channel. The introduction of this bulky positively charged moiety in the channel pore affects two aspects of AMPA receptor function: edited GluA2-containing AMPA receptors do not conduct calcium ions and, unlike calcium permeable AMPA receptors, they are not blocked by intracellular polyamines at depolarized membrane potentials (Jonas et al., 1994),(Dingledine et al., 1999), (Isaac et al., 2007). Despite this intracellular polyamine block, calcium influx through CP-AMPA receptors can elicit activity-dependent gene expression directly, without the involvement of NMDA receptors or L-type channels (Perkinton et al., 1999).

Different types of AMPA receptors have distinct roles in synaptic plasticity. GluA2 AMPA receptors are required for homeostatic synaptic scaling of mEPSC amplitudes after activity blockade through a mechanism critically dependent on the C-terminal tail of GluA2 (Gainey et al., 2009). However, distinct sequences on the GluA1 subunit C-terminal tail mediate a PDZ domain interaction sufficient to recruit GluA1/2 heterotetramer receptors to synapses during LTP (Shi et al., 2001), (Hayashi et al., 2000). Strikingly, this GluA1 tail sequence, but not channel conductance, is required for stabilization of increased spine size after LTP (Kopec et al., 2007). Consistent with the requirement for GluA1-containing receptors in synaptic plasticity, local dendritic synthesis of GluA1 occurs in response to retinoic acid mediated synaptic plasticity; other, distinct forms of plasticity including stimulation with activity-induced TNFα, preferentially recruit GluA1 containing receptors to the cell surface (Maghsoodi et al., 2008), (Stellwagen et al., 2005). These studies suggest a general model in which calcium impermeable receptors are constitutively inserted into the membranes and induction of activity-dependent plasticity mechanisms increases the fraction of calcium permeable receptors sent to synaptic sites.

Seemingly every aspect of AMPA receptor function and trafficking, including surface expression, lateral mobility, endocytosis, post-translation modification, and

function are under some degree of regulation (Groc et al., 2004),(Dingledine et al., 1999). This tight control over AMPA receptor function is accomplished through direct interaction with a host of proteins including GRIP, TARPs, Cornichons, and other post-synaptic scaffolds (Ye et al., 2000),(Chen et al., 2000),(Schwenk et al., 2009),(Sheng and Pak, 1999). The full complexity of the dynamic interplay between the activities of these proteins remains under investigation, and is likely to be differentially regulated across development, and neuron-type (or even synapse type), and to be affected by the recent activity history of the cell.

Like AMPA receptors, NMDA receptors are gated by glutamate, but the two channels have a number of important differences. Unlike the majority of (GluA2-containing) AMPA receptors, NMDA receptors conduct calcium ions; furthermore, NMDA receptors are blocked by intracellular magnesium ions at resting membrane potentials. This blockade means that they serve as ideal 'coincidence detectors,' since NMDA receptors will conduct current only when they are both bound to glutamate and when the membrane is depolarized. NMDA receptors have a higher affinity for glutamate than AMPA receptors, but they open more slowly and have considerably longer inactivation kinetics.

Structurally, NMDA receptors are tetramers consisting of two constitutively expressed GluN1 (NR1) subunits, and two other subunits, most of which are GluN2 (NR2) subunits. GluN2 subunits come in four variants, GluN2A-D; expression of these variants is differentially regulated over development. They have distinct functional roles in part due to distinct C-terminal sequences, which contain phosphorylation sites important for regulation of channel kinetics as well as interaction domains important for tethering them to scaffolding proteins in the post synaptic density such as PSD-95 (Myers et al., 1999). Early in development, NMDA receptors are present at synaptic sites without complementary AMPA receptors, but addition of AMPA receptors over development 'unsilences' these immature synapses (Petralia et al., 1999). The developmental ratio of NMDA to AMPA receptors is dynamically regulated: early in development very few AMPA receptors are present, and this ratio increases steadily until adulthood, when it stabilizes (Watt et al., 2000). The function of the NMDA receptor is also developmentally

regulated; this is accomplished by experience-dependent modifications in the ratios of different GluN subunit variants that compose the complement of NMDARs. Early in development some NMDA receptors contain GluN3A subunits that have an antagonistic effect on receptor function. These GluN3A subunits serve as a developmental brake on synapse development, and their removal is required for synapse maturation, LTP, and development of mature NDMA current (Roberts et al., 2009). Later in postnatal development, NMDA receptors preferentially contain GluN2B subunits. These subunits have slow inactivation kinetics, allowing for increased calcium influx; the GluN2B subunits also actively suppress TARP expression, limiting AMPA receptor insertion into synaptic sites (Hall et al., 2007). In the visual cortex, onset of visual experience drives a decrease in the size of NMDA responses (Carmignoto and Vicini, 1992). This change is driven by an experience dependent increase in GluN2A containing NMDA receptors, which decrease the time constant of the receptors, attenuating NMDA mediated current (Flint et al., 1997),(Philpot et al., 2001),(Quinlan et al., 1999).

The NMDA receptor physically associates with a large cadre of signaling molecules that are enriched at the synapse including calmodulin, CaMKII, calcineurin, Tiam1, and a large number of MAPK pathway signaling components (Tolias et al., 2007) (Husi et al., 2000). Calcium influx through synaptic NMDA receptors can activate signaling cascades mediated by these interacting proteins that promote CREB phosphorylation and activation of transcription, providing a direct link between synaptic transmission and the nucleus (Bading et al., 1993). Calcium influx through the NMDA receptor does not require a generalized increase in calcium concentration throughout the cell; instead, local increases in calcium in a microdomain near the channel pore is sufficient to trigger recruitment of the MAPK pathway and transcriptional activation of immediate early genes (Hardingham et al., 2001),(Xia et al., 1996). The duration of CREB phosphorylation that results from stimulation of NMDA receptors decreases over development; this could be the result of decreased calcium influx resulting from expression of GluN2A subunits, or the physical association of protein phosphatase 1 (PP1) with the NMDA receptor, which may actively suppress kinase-based signaling cascades to the nucleus (Sala et al.,

2000). Strikingly, the subcellular localization of activate NMDA receptors has important consequences for the transcriptional response it initiates: calcium signaling through synaptic NMDA receptors mediates pro-survival transcriptional pathways, whereas activation through extrasynaptic NMDA receptors has the opposite effect, resulting CREB inactivation and promoting cell death (Wittmann et al., 2009),(Hardingham et al., 2002). The distinct signaling mediated by synaptic versus extrasynaptic NMDA receptors may reflect differential localization of NMDA receptors containing alternately spliced GluN1 subunits, which can differentially affect NMDA dependent gene expression without altering channel kinetics (Bradley et al., 2006).

Calcium influx through L-type voltage sensitive calcium channel (CaV 1.2) is responsible for robust activity-dependent gene expression. L-type calcium channels are localized in the soma and dendrites, open in a voltage dependent manner, and exhibit a large single channel calcium conductance and slow inactivation kinetics. Basal expression of IEGs such as c-Fos, Jun, Zif268, and FosB is suppressed by antagonizing the L-type channel, and rapidly induced by activating it (Murphy et al., 1991). Coupling of calmodulin to an interaction motif on the L-type channel C-terminus is necessary for calcium influx through the L-type channel to activate the Ras/MAPK signaling pathway and promote subsequent transcriptional activation; this configuration allows the activation of signaling pathways in response to local increase in calcium concentration in a sub-channel microdomain, and does not require global elevation of intracellular calcium levels (Dolmetsch et al., 2001),(Rosen et al., 1994). In addition to activating signaling pathways in the nucleus, activated calmodulin coupled to the L-type channel promotes channel inactivation, effectively attenuating calcium influx once the signal has been transduced. This dual action of calmodulin may imply an all-or-none signaling response from an individual L-type channel (Peterson et al., 1999). L-type calcium channels are also coupled to additional signaling cassettes by binding of AKAP70/150, a scaffolding molecule that can anchor both calcineurin and PKA. Calcium-dependent PKA activity increases L-type channel activity, but is dominantly suppressed by calcineurin activation, adding another layer of dynamic regulation of

L-type channel function. Additionally, AKAP binding to the L-type channel is required for the activation and nuclear transport of the transcription factor NFAT4c (Oliveria et al., 2007).

Consistent with the vital role of activity-dependent transcription for cognitive function, mice lacking CaV1.2 in the neocortex have impaired spatial memory and LTP, as well as the expected decrease in MAPK pathway activation (Moosmang et al., 2005). In humans, mutation of the L-type channel causes Timothy Syndrome, a multisystem disorder that includes learning disability and autism-like phenotypes (Splawski et al., 2004). CamKII mediated phosphorylation of a serine residue on the S6 loop of the L-type channel causes the L-type channel to enter mode 2 gaiting, which increases channel opening for long durations. Intriguingly, L-type channel mutations in Timothy syndrome may actually be gain of function mutations that cause calcium-dependent inactivation to become dysfunctional and potentiate mode 2 gating, resulting in calcium excitotoxicity (Erxleben et al., 2006), (Barrett and Tsien, 2008).

In summary, stimulus-dependent induction of mRNA levels of specific genes can occur in response to a variety of stimuli that induce distinct signal transduction cascades that signal to the nucleus. Neuronal activity can result in calcium influx at synaptic sites through CP-AMPA or NMDA receptors, and the dendritic compartment through L-type calcium channels. These calcium-induced signaling pathways converge on CREB, which acts to promote transcription of activity-induced genes. While CREB was the first nuclear transcription factor known to receive input from these activity-induce signaling cascades, it is only one of many factors that modulate transcription in response to activity-dependent signaling events.

MEF2 and Activity-Dependent Regulation of Excitation

Another important set of transcriptional activators that responds to activity-dependent signaling is the MEF2 (myocyte enhancer factor-2) family. The MEF2 family of transcriptional activators consists of four isoforms, MEF2A-D; which are

expressed in overlapping yet distinct sets of neurons (Lyons et al., 1995). Neuronal activity dynamically regulates the post-translational modification state of MEF2. The exact set of modifications that active MEF2 remains unknown, but both PKA mediated phosphorylation and calcineurin-mediated dephosphorylation contribute to a complex landscape of post-translational modification that includes both acetylated and sumoylated residues. The mechanisms by which individual modifications precisely affect MEF2 activity are still under investigation; however, it is known that calcineurin-mediated dephosphorylation is necessary to induce activation and subsequent transcriptional activity in membrane depolarized neurons (Mao and Wiedmann, 1999),(Wang et al., 2005),(Shalizi et al., 2006).

Like other activity-regulated factors, MEF2 has multiple ascribed functions across different stages in development. MEF2 family members are required for the survival of cerebellar granule neurons in the face of activity, and brain specific deletion of multiple MEF2 family members results in early postnatal lethality caused by massive increases in neuronal apoptosis (Akhtar et al., 2012),(Mao et al., 1999). Deletion of MEF2C is sufficient to impair neural precursor differentiation and integration into neural circuits, indicating that MEF2C plays an important role in neuronal maturation. Mice in which MEF2C has been deleted from then nervous system also present with behavioral abnormalities reminiscent of autism-related disorders (Li et al., 2008).

In addition to its function in promoting neural differentiation and survival, MEF2 activation suppresses the number of excitatory synapses formed on hippocampal pyramidal neurons. Deletion of MEF2 A and D results in an increase in the number of excitatory synapses formed onto excitatory neurons, suggesting that in response to activity, MEF2 mediated transcription either promotes synapse elimination or suppresses excitatory synapse formation. This regulation of synapse number may be related to MEF2's control of neuronal survival, as restricting excitation onto a neuron may be protective against excitotoxicity (Flavell et al., 2006). MEF2 restricts synapse number *in vivo* as well: suppression of MEF2 activity in the nucleus accumbens is required for cocaine mediated increases in spine density, and activation of MEF2 is necessary for activity-dependent spine loss in

striatal medium spiny neurons (Pulipparacharuvil et al., 2008), (Tian et al., 2010). Furthermore, acute over-activation of MEF2 negatively regulates learning-induced spine addition and memory formation in the hippocampus (Cole et al., 2012).

MEF2 family members modulate the transcription of hundreds of genes by directly binding to DNA in the nucleus. Activated MEF2 binds throughout the genome, including near transcriptional start sites, where it modulates transcription of immediate early genes including *Nr4a1-3*, *Egr1-4*, several kruppel-like factors, as well as multiple Fos family members. Additionally, MEF2 is a transcriptional activator for a host of genes intimately associated with synaptic functions including Ube3a, Homer1, Arc, synGAP, and Bdnf. MEF2 activation also promotes the use of alternate exons that preferentially contain internal poly-adenylation sites, resulting in preferential production of truncated mRNAs (Flavell et al., 2008).

This poly-A switching is particularly prominent in the case of Homer1, a scaffolding protein that selectively binds metabotropic glutamate receptors (Brakeman et al., 1997). MEF2 activation promotes an activity-dependent switch in the expression of two different isoforms of the Homer1 genes, from the long Homer1b to the shortened Homer1a. This switch changes the direction of mGluR1/5-mediated signaling from promoting stabilization of spine synapses to promoting their elimination. This change in directionality of mGluR plasticity mediated by MEF2 is consistent with MEF2's synapse-suppressing effect (Van Keuren-Jensen and Cline, 2006),(Sala et al., 2005).

MEF2-mediated synapse elimination is further tied to mGluR signaling by its relationship to Fragile-X Mental Retardation Syndrome. Fragile-X Syndrome is caused by mutation of FMRP, which suppresses local translation at sub-synaptic sites. When FMRP function is ablated, local translation is disinhibited, and mGluR-mediated LTD is hyperactive (Bear et al., 2004). Consistent with the hypothesis that runaway LTD may be a disease-causing insult in Fragile-X syndrome, multiple phenotypes of FMRP knockout mice can be rescued by either genetically or pharmacologically attenuating mGluR function (Dolen et al., 2007),(Dolen and Bear, 2008). FMRP normally inhibits the constitutive translation of a set of activity-induced MEF2 target genes; when FMRP is disrupted these genes are constitutively

expressed. Accordingly, in FMRP knockout mice, activation of MEF2 fails to suppress synapse number, and knockdown of MEF2 fails to result in increased synapse number (Pfeiffer et al., 2010). The MEF2-mediated transcriptional program is linked to mGluR plasticity through a target gene other than Homer1: expression of hyperactive mGluR-mediated LTD in FMRP knockout mice requires the MEF2 target gene Arc (Park et al., 2008).

Multiple components of the activity dependent signaling pathway converge on Arc: binding of activated MEF2, as well as activated CREB and SRF, to a 100 base pair region 5 kbs upstream of the Arc promoter is required for activity dependent transcription of Arc (Kawashima et al., 2009). Unlike many other immediate early genes, Arc mRNA localizes to the dendritic locations that received strong synaptic activation (Steward et al., 1998). Arc, or **A**ctivity-**R**egulated **C**ytoskeleton-associated protein, is so named because it interacts directly with F-actin (Lyford et al., 1995). Arc also interacts with elements of the endocytic machinery coupled to the cytoskeleton, including dynamin and endophilin, to mediate endocytosis of cell-surface localized AMPA receptors (Chowdhury et al., 2006). This biochemical activity is consistent with Arc's role in mediating mGluR dependent long-term depression. Intriguingly, Arc becomes enriched at inactive synapses by associating with inactive CaMKIIβ, where it then promotes internalization of AMPA receptors (Okuno et al., 2012). Since Arc mRNA is trafficked to active dendritic branches, Arc mediates the weakening or elimination of synapses that fail to become active during local depolarization events, in effect tuning neighboring synapses to be more coactive.

Arc-mediated AMPA receptor internalization is required for aspects of synaptic plasticity other than weakening of inactive synapses. Loss of Arc results in increased basal AMPA currents, and abolishes homeostatic decreases in AMPA current in response to elevated activity. Arc overexpression blocks increases in AMPA receptor current after activity blockade (Shepherd et al., 2006). This requirement for Arc in homeostatic plasticity is conserved *in vivo*; Arc knockout mice fail to induce normal homeostatic downregulation of AMPA current amplitude in layer 2/3 pyramidal neurons in visual cortex that normally occurs after onset of

visual experience (Gao et al., 2010). Finally, although Arc knockout mice have very few baseline abnormalities in synaptic transmission, they are unable to maintain the late phase of hippocampal LTP. This synaptic defect is associated with an apparent inability to form long lasting memories (Plath et al., 2006).

Together, these data suggest that Arc is vital for mediating experience dependent changes in synaptic transmission. The dynamic interplay between calcium-dependent transcription, trafficking, and translation of Arc mRNA, in addition to sub-synaptic sorting of Arc protein provides rich substrates for the expression of multiple forms of plasticity. In addition to these forms of regulation, Arc protein is also regulated by degradation through the ubiquitin/proteasome system mediated by an interaction with the E3 ubiquitin ligase Ube3a.

Ube3a, another activity regulated MEF2 target gene, is an E3 ubiquitin ligase whose mutation is sufficient to cause Angelman Syndrome, a developmental disorder characterized by learning disability, seizure, and ataxia. Mutation of Ube3a causes ~90% of Angelman syndrome cases; because the Ube3a gene is located in a chromosomal region subject to genomic imprinting, only the maternal Ube3a allele is expressed; thus a phenotypically normal mother can be a carrier for a silenced mutant Ube3a allele inherited from her father (Clayton-Smith and Laan, 2003). Mouse mutants with a disrupted maternal allele of the Ube3a gene recapitulate important aspects of Angelman Syndrome, including motor dysfunction, seizure presentation, and learning deficits (Jiang et al., 1998), (Miura et al., 2002).

As an E3 ubiquitin ligase, Ube3a covalently links target proteins to ubiquitin moieties, which promote subsequent trafficking of the ubiquitylated protein to the proteasome for degradation. Although Ube3a is known to ubiquitylate multiple targets in the nucleus, including p53 (Jiang et al., 1998), the identity of these targets do not readily explain the synaptic abnormalities associated with Angelman Syndrome. Neuronal activity broadly regulates the composition of the postsynaptic density through ubiquitylation, and one component of this general response is Ube3a mediated ubiquitylation of Arc (Ehlers, 2003; Greer et al., 2010). Consistent with this interaction, Arc levels are elevated in Ube3a maternal null mice; these mice have decreased surface AMPA receptor expression and resulting synaptic

dysfunction (Greer et al., 2010). Intriguingly, Ube3a mutant mice also have profound defects in inhibitory input to pyramidal cells arising from defective presynaptic vesicle cycling in inhibitory neuron nerve terminals, implying that other synaptic Ube3a targets may be relevant for the etiology of Angelman Syndrome (Wallace et al., 2012).

Together, these synaptic defects underlie altered cortical plasticity in Ube3a mutant animals: animals lacking the maternal copy of the Ube3a allele have impaired ability to shift the responsiveness of the visual cortex from the deprived to the spared eye in response to monocular deprivation during the visual critical period. This defect was associated with reduced spine density on pyramidal neurons in the binocular zone of the cortex, consistent with Arc over-activation (Sato and Stryker, 2010). Intriguingly, Ube3a mutant phenotypes can be rescued by crossing Ube3a null mice to mice harboring a mutation of an inhibitory phosphorylation residue on CaMKII. This genetic cross rescues a number of behavioral phenotypes of the Ube3a mutant, including audiogenic seizures and rotarod defects (van Woerden et al., 2007). The mechanism by which hyper-activation of CaMKII signaling rescues these behavioral changes is not known. Naively, increased activation of CaMKII signaling may be expected to upregulate the levels of activity-induced genes, including Arc. However, Arc levels are already abnormally elevated in Ube3a knockout mice, making it unclear how increasing activity-dependent transcription would rectify synaptic defects through an Arc-dependent mechanism. One possible explanation is that Ube3a ubiquitylates other targets whose misregulation may contribute to Angelman Syndrome etiology.

One such target may be the RhoA-GEF Ephexin 5, which is expressed early in postnatal development, and associates directly with EphB receptors at non-synaptic sites. Ephexin 5 serves as a brake on synaptogenesis: deletion of Ephexin 5 results in a dramatic increase in excitatory synapse number. EphBs phosphorylate Ephexin 5 progressively as development advances, and this phosphorylation event marks Ephexin 5 for ubiquitylation by Ube3a and subsequent degradation by the proteasome. Ube3a mediated degradation of Ephexin 5 thus relieves a developmental brake on synapse formation; in the absence of Ube3a, Ephexin 5

levels may persist, possibly causing either fewer synapses to form, or a developmental delay in their formation (Margolis et al., 2010).

Npas4 and regulation of inhibition by activity

In addition to restricting excitation, one of the primary functions of the activity-induced transcriptional response in excitatory neurons is to promote increased inhibition on excitatory neurons. One of the key mediators of activity-mediated development of inhibition is Npas4, which is an immediate early gene transcribed rapidly after initiation of calcium-dependent signaling. Unlike many other immediate early genes, robust Npas4 expression cannot be induced by neurotrophin stimulation; this unusual selectivity for calcium signaling suggests that Npas4 may be specially tuned to read out and respond to electrical signals resulting from increases in action potential frequency.

Deletion of Npas4 from cultured hippocampal excitatory neurons results in a large decrease in the number of inhibitory synapses formed onto the both soma and dendrites, but deletion of Npas4 does not alter the number of excitatory synapses on hippocampal excitatory neurons. Furthermore, activity-dependent overexpression of Npas4 increases the density of inhibitory, but not excitatory, synapses received by hippocampal excitatory neurons (Lin et al., 2008). Npas4's regulation of inhibitory synapse number is mediated cell-autonomously by the postsynaptic excitatory neuron. This function directly links the level of excitatory input to control of inhibition, placing Npas4 in an ideal place to mediate important aspects of neuronal homeostasis.

In vivo, Npas4 is expressed very sparsely in the neocortex of mice housed in a standard laboratory cage. Dark housing for one week during the visual critical period and subsequent exposure to light robustly and rapidly induces Npas4 expression throughout the visual cortex, but not the hippocampus (Lin et al., 2008). In contrast, exposure of mice to enriched environment induces Npas4 expression robustly in the CA3 region of the hippocampus, but not visual cortex (A Mardinly, personal observations). Npas4 is also upregulated in the nucleus accumbens in

response to amphetamine administration and in the lateral amygdala and CA3 after fear conditioning (Guo et al., 2012) (Ploski et al., 2011) (Ramamoorthi et al., 2011). Thus, Npas4 can be activated *in vivo* in relevant brain structures and neuron types in response to experience tuned to activate those structures.

Strikingly, *in vivo* removal of Npas4 from the hippocampus of a mouse in standard housing does not alter the number of inhibitory synapses on pyramidal neurons; however, exposure to an enriched environment or induction of a kainate seizure causes the expected phenotype to emerge. This observation reflects the activity-dependent nature of Npas4: a phenotype associated with Npas4 can only emerge in a context where Npas4 would normally be induced (Bloodgood et. al., 2013 in review). These observations may be generally true for all phenotypes related to activity-induced genes.

Consistent with its control of inhibitory connectivity, deletion of Npas4 has profound consequences for cognitive function. Npas4 knockout mice are hyperactive in new environments, are aggressive and socially dominant, have deficiency in pre-pulse inhibition, and impaired short- and long-term memory (Coutellier et al., 2012). Selective deletion of Npas4 in either CA3 or the lateral amygdala results in impaired contextual memory recall (Ramamoorthi et al., 2011),(Ploski et al., 2011). Taken together, these data suggest that Npas4 is vital for cellular function, including proper organization of inhibition, and that knockout of Npas4 from a given set of neurons is likely to impair their ability to mediate their normal function.

Npas4 is a bHLH-PAS domain family transcriptional regulator, and it controls inhibitory synapse number through transcriptional mechanisms. Upon induction, Npas4 is imported into the nucleus, where it binds to thousands of enhancer elements that are activated in response to activity, where it presumably serves to promote transcriptional activation (Kim et al., 2010). Npas4 forms heterodimers with Arnt1 or Arnt2 in the brain, but the specific functional significance these interactions, as well as the identity of other binding partners, remain unknown (Ooe et al., 2009). Deletion of Npas4 in excitatory neurons in neuronal cultures results in the misregulation of hundreds of transcripts. The genes that are misregulated in the

absence of Npas4 are involved in all aspects of cellular physiology, but strikingly, they include well known activity-induced genes such as c-Fos, Bdnf, Arc, and Nptx2 (Ramamoorthi et al., 2011),(Lin et al., 2008). Bdnf is a notable Npas4 target for several reasons: it is the most misregulated gene in the absence of Npas4, Npas4 uncharacteristically binds directly to its promoter region (in addition to nearby enhancers), and Bdnf has been extensively linked to the development of inhibition. Finally, knockdown of Bdnf attenuates the increase in inhibitory synapses that results from overexpression of Npas4, suggesting that Npas4's transcriptional activation of Bdnf is one of the mechanisms by which it promotes increased inhibitory synapse number (Lin et al., 2008).

Bdnf has a very complex genomic structure, featuring at least 8 alternate promoter exons and two 3' UTR variants, coding for at least 16 distinct mRNAs that all encode an identical protein (Timmusk et al., 1993). The utility of having eight independent promoters has yet to be fully appreciated, but it is clear that transcripts driven from promoters I and IV are most responsive to neuronal activity. Activity induced transcription of BDNF requires the recruitment of calcium signaling culminating in the phosphorylation and activation of CREB (Tao et al., 1998). However, there a number of other transcriptional regulators that contribute to normal activity-dependent transcription of BDNF, including MEF2, Npas4, CaRF, and USF (McDowell et al., 2010),(Tao et al., 2002),(Flavell et al., 2006),(Chen et al., 2003). Interestingly, Bdnf mRNA containing promoter IV is preferentially expressed in the cortex, while promoter I containing transcripts are preferentially induced in the hippocampus in response to neuronal activity; thus, distinct promoters mediated brain-region specific activity-induced transcription of Bdnf. The biological significance of this distinct regulation remains unknown (Metsis et al., 1993). Transcripts from all BNDF promoters have either a short or long form 3` UTR, and these different UTRs mediate distinct functions. Transcripts with the short 3' UTR are retained in the soma, while mRNAs containing the long 3` UTR are transported to the dendrites; specific mutation of the long UTR results in defects in dendritic spine morphology (An et al., 2008). In addition to regulating subcellular localization, the two 3' UTRs have different effects on translation. The short 3' UTR

variant mediates active translation, while the long form UTR is a cis-active translational repressor that is relieved by calcium signaling, lending an activity-dependent component to Bdnf translation (Lau et al., 2010),(Oe and Yoneda, 2010). Thus somatic transcripts are actively translated, whereas dendritcally localized transcripts are translated in response to activity, and have specific effects on plasticity.

This intense regulation of Bdnf transcription, trafficking, and translation reflects the many known functions of Bdnf. Bdnf, but not other neurotrophins, is critical for neuronal survival in the face of activity (Ghosh et al., 1994), as well as for the maintenance and stabilization of dendrites in cortical neurons (McAllister et al., 1995),(Gorski et al., 2003). Bdnf has also consistently been implicated in long-term potentiation of excitatory synapses in the hippocampus, though the mechanisms by which it acts is the subject of debate (Kang and Schuman, 1995),(Patterson et al., 1996),(Kovalchuk et al., 2002),(Pang et al., 2004),(Barco et al., 2005). Strikingly, Bdnf synthesis is also required for the activity-dependent formation of new synaptic connections underlying plasticity in the cortex in response to whisker stimulation (Genoud et al., 2004). In addition to its role in LTP, Bdnf greatly affects the development of inhibition. Bath application of BDNF to cortical cultures increases the amplitude of mEPSCs onto interneurons, whereas it decreases the quantal amplitude of mEPSCs onto excitatory neurons (Rutherford et al., 1998). In addition to increasing excitatory drive onto interneurons, bath application of BDNF increase the frequency of mIPSCs onto excitatory neurons, as well as leading to increased number and size of inhibitory presynaptic terminals that form on excitatory neurons (Bolton et al., 2000). Abolition of the activity-dependent component of Bdnf transcription in the cortex results in selective defects in inhibition, including reduced inhibitory synapse number, and reduced inhibitory neurotransmission onto cortical pyramidal neurons (Hong et al., 2008),(Sakata et al., 2009).

The potent and far reaching roles of Bdnf in synaptic development underlie an important role in the development of neuronal plasticity. Bdnf levels are developmentally upregulated; as activity increases, Bdnf transcription is induced, and Bdnf is secreted into the extracellular space where it is cleaved into its mature

form by tPA (Pang et al., 2004). This process is critical for functional development of the nervous system; dark rearing stops the developmental rise in Bdnf levels in the visual cortex, but exposure to light rescues Bdnf levels (Castren et al., 1992). Strikingly, overexpression of Bdnf is sufficient to rescue the visual system from many of the effects of dark rearing, including restoration of visual acuity, receptive field size, and maturation of intracortical inhibition (Gianfranceschi et al., 2003). Transgenic mice that precociously express Bdnf in the cortex have accelerated development of visual acuity, critical period onset and the maturation of inhibition (Huang et al., 1999),(Hanover et al., 1999). Taken together, this evidence suggests that the timing of Bdnf expression over postnatal development controls the maturation of cortical inhibition, which in turn sets the window for critical period plasticity (Hensch, 2005). Although the specific effects of Bdnf on subtypes of cortical inhibitory neurons has yet to be systematically investigated, it is extremely likely that BDNF is important for development of parvalbumin positive fast spiking inhibitory neurons whose maturation is critical for critical period plasticity (Fagiolini et al., 2004),(Fagiolini and Hensch, 2000),(Chattopadhyaya et al., 2004).

Finally, there is substantial evidence that the various functions described for Bdnf are meaningful for human cognition. In addition to being linked to obsessive-compulsive disorder by a genome wide association study (Hall et al., 2003), a specific amino acid substitution in Bdnf (Val66met) in humans has been associated with poor episodic memory and abnormal hippocampal activation during memory recall tasks (Egan et al., 2003). A mouse model of this polymorphism has normal Bdnf expression, but impaired secretion of Bdnf from dendritic granules and synaptic sites, as well as defective hippocampal LTP. These mice also display increased anxiety-related behaviors that are not corrected with fluoexetine (Bath and Lee, 2006),(Chen et al., 2006),(Ninan et al., 2010). Taken together, these data show that Bdnf is tightly regulated by activity both pre- and post-transcriptionally, and has important functions ranging from survival and dendritic growth to LTP and development of inhibition that controls the timing of the visual critical period.

Although Npas4's activity in promoting inhibition is known to act in part through Bdnf, many other genes are regulated by Npas4, and presumably act to

mediate its function. One such Npas4 target is Nptx2; although it is not understood how regulation of Nptx2 may mediate Npas4's function in excitatory neurons, Nptx2 is a well-known activity-regulated gene known to be involved in synapse development. Nptx2, or neural pentraxin 2, encodes a protein called Narp (**N**euronal **A**ctivity **R**egulated **P**entraxin), which is a secreted protein structurally related to the pentraxins that are prominent pattern recognition receptors in the immune system (Tsui et al., 1996). Extracellular narp is enriched at synaptic sites in cultured spinal excitatory neurons, and overexpression increases the number of excitatory, but not inhibitory synapses formed onto cultured spinal neurons. Overexpression of Narp in heterologous cell lines is sufficient to induce AMPA receptor clustering on co-cultured neurons (O'Brien et al., 1999). Expression of a dominant negative form of Narp (DN-Narp), which can bind endogenous Narp but prevents its synaptic accumulation, severely impairs the ability of a transfected neuron to cluster AMPA receptors on a non-transfected postsynaptic target, consistent with a role for narp originating in the presynaptic neuron in AMPAR clustering. Conversely, transfection of a single neuron with DN-Narp is sufficient to reduce AMPA receptor clustering and the number of excitatory synapse formed onto that neuron by wild-type presynaptic neurons. These results suggest complementary or redundant roles for pre- and post-synaptic sources of Narp in AMPA receptor clustering and synapse stabilization. However, it remains unclear whether there is a specific requirement for narp originating in both the pre- and post-synaptic neuron, or if the source of narp is irrelevant for its clustering activity. Strikingly, Narp does not localize to gephryin or GAD65 puncta, nor does it affect inhibitory synapse number or GABA-A receptor clustering, indicating that it is selectively involved in excitatory synapse formation (O'Brien et al., 2002).

Narp mediates its pro-synaptic activity by forming hetero-pentamers with its closely related family member, Nptx1 (NP1 or Neural Pentraxin 1). These pentamers are covalently linked by disulfide bonds in their N-terminal domains, and localized to the extracellular matrix. The clustering activity of these pentamers depends on the relative ratio of NP1/Narp: pentamers composed entirely of NP1 are not effective at clustering AMPA receptors, and pentamers composed entirely of

Narp have increased clustering activity. However, hetero-pentamers have a super-additive increase in clustering activity (Xu et al., 2003). Since Nptx1 is not regulated by neuronal activity and Nptx2 is, the history of activity levels experienced by the neuron determine the ratios of different types of pentamers, allowing a neuron to tune AMPA receptor clustering in response to activity (Xu et al., 2003). NP1 directly binds the N-terminal domain of the GluR4 subunit of the AMPA receptor, which may help mediate its recruitment to developing synapses; the mechanism by which Narp homo-pentamers recruit AMPA receptors is unknown (Sia et al., 2007).

Consistent with its activity-dependent role in synapse development, mice in which both Nptx1 and Nptx2 are knocked out have defects in eye-specific segregation in the LGN, despite having normal retinal waves (Bjartmar et al., 2006). Single fiber stimulation experiments on these mice indicate that loss of neural pentraxins causes a profound deficit in both AMPA receptor currents and number of fibers innervating thalamic relay neurons early in postnatal development. Strikingly (and confusingly), this phenotype reverses itself later in development: thalamic relay neurons that had fewer inputs with reduced AMPA current early in development end up with more inputs with greater AMPA current later in development. These results have been interpreted to be consistent with a role of neural pentraxins in recruiting AMPA receptors to nascent synapses, in effect 'unsilencing' them. A defect in this process is presumably over-compensated for by an independent mechanism for recruiting AMPA receptors that become dominant later in development (Koch and Ullian, 2010).

Interestingly, the body of experiments on neural pentraxins has been conducted in cell-types not commonly used for biochemical studies. Most of the biochemical work was conducted in neuronal cultures derived from spinal cord; these neurons, though excitatory, do not have dendritic spines. Excitatory thalamic relay neurons also do not receive the majority of their excitatory synapses on dendritic spines. In contrast to the large effects of narp deletion in these cells, synapse formation onto spiny hippocampal excitatory neurons is not perturbed by loss of narp. Accordingly, neural pentraxins have been proposed to specifically regulate non-spiny excitatory synapses. Consistent with this hypothesis, secreted

narp has been reported to regulate homeostatic scaling of excitatory inputs to parvalbumin positive interneurons, which are also lack dendritic spines. Curiously, PV neurons do not seem to express Nptx2, implying that extracellular narp secreted from surrounding excitatory neurons is sufficient to mediate this plasticity (Chang et al., 2010).

Conclusion

Neuronal activity has profound consequences for the transcriptional landscape of a neuron, including altering the geometry of the nucleus and inducing widespread modification of the chromatin landscape (Fischer et al., 2007; Levenson et al., 2004; Wittmann et al., 2009). This overview has highlighted several particularly well-studied molecules in the activity-dependent transcriptional pathway. However, there are over 50 acutely regulated genes; and up to 800 genes regulated by neuronal activity with delayed kinetics. This number vastly increases when we include genes that are down regulated by activity, or when we lower the threshold for calling a gene regulated.

Such a vast program of activity dependent gene expression is likely to affect a number of cellular functions besides synapse formation: for instance, NeuroD, CREB, and CREST all mediate aspects of dendritic morphogenesis (Gaudilliere et al., 2004),(Redmond et al., 2002),(Aizawa et al., 2004). In addition to MEF2 and BDNF, the activity dependent factor NFAT3 mediates neuronal survival (Benedito et al., 2005). In contrast, SRF regulates synaptic plasticity but not neuronal viability (Ramanan et al., 2005), while CaRF and Zif268 impact synaptic plasticity and memory formation, but not survival or dendrite morphogensis (Tao et al., 2002),(McDowell et al., 2010),(Jones et al., 2001), (Bozon et al., 2003). The specific biochemical activity or biological function of only a small fraction of activity-regulated genes has been determined, and understanding the temporal dynamics by which activity dependent gene products execute their functions to produce a coherent cell biological response remains a major challenge. Additionally, the importance of activity-dependent transcription in other cell-types in the brain,

including GABAergic neurons, which underlie vital aspects of neuronal circuit function, remains to be determined.

II. Neuronal Activity in Inhibitory Neurons

GABAergic inhibitory interneurons are integral components of all neural circuits. Inhibition is essential for shaping the temporal dynamics of excitatory neuron action potentials, thereby regulating how information is propagated through the nervous system (Shadlen and Newsome, 1998). Distinct types of inhibitory input delivered with precise temporal dynamics to specific subcellular compartments exert intimate control over excitatory neurons across behavioral (Lapray et al., 2012),(Somogyi and Klausberger, 2005). In keeping with these vital roles of inhibition, disruption of synaptic input to inhibitory neurons results in widespread neural circuit dysfunction, including defects in oscillatory behavior, and learning and memory deficits (Wulff et al., 2009), (Korotkova et al., 2010),(Fuchs et al., 2007). Additionally, inhibitory neuron dysfunction has been widely linked with psychiatric disorders such as schizophrenia and neurodevelopmental disorders including autism (Marin, 2012),(Chao et al., 2010),(Gogolla et al., 2009b). Accordingly, it is of great interest to classify interneurons, understand their function roles in the nervous system, and to identify the mechanisms by which they develop and exhibit plasticity.

Diversity of Inhibition

The many and varied functions of inhibition in the nervous system are performed by an astounding diversity of inhibitory cell types. This diversity exists from the birth of inhibitory neurons in the ganglionic eminences, where distinct subtypes of inhibitory neurons are specified on the basis of a combinatorial code of transcription factor expression. Transcription factor expression is correlated with responsiveness to morphogens, birth date, and the specific location of an interneuron within the eminence (Wonders and Anderson, 2006),(Flandin et al.,

2011),(Zhao et al., 2008). Interneurons born early in development migrate tangentially out of the eminence and into the developing neocortex where they extend processes and form synaptic connections. Many aspects of interneuron identity have already been specified during these early stages of development, , as gene expression profiles in young post-mitotic inhibitory neurons are highly related to their mature identity (Batista-Brito et al., 2008). However, not all aspects of interneuron identity is specified: neuronal activity acts on distinct classes of interneurons to influence their migration, mature identity, and the development of their neuronal processes (Denaxa et al., 2012),(De Marco Garcia et al., 2011),(Close et al., 2012).

The exact number of distinct subtypes of cortical interneurons is the subject of debate. Inhibitory interneurons all release GABA; besides having this in common, they seem to vary from one another on every possible axis of diversity. Inhibitory neurons can be defined based on the distinct sets of transcription factors that they express early in development, as well as on the basis of their mature gene expression profiles. Genetic classification is most commonly based on a combinatorial code of marker proteins, most of which are calcium binding proteins or neuropeptides. Different types of inhibitory neurons also exhibit distinct forms of both pre- and post-synaptic plasticity, and they form synapses on postsynaptic targets on distinct subcellular locations. Interneurons can be classified on the basis of their action potential characteristics, and the dynamics with which they are recruited upon activation of a circuit (Ascoli et al., 2008). Thankfully, not every variable is independent: some groups of interneurons characteristics tend to co-distribute, and these patterns provide a basis for classification of inhibitory neurons subtypes. For example, fast spiking neurons are either basket cells that form synapses on the soma and dendrites of post-synaptic targets, or chandelier cells that form axo-axonic synapses. Many – but not all - of both basket and chandelier cells express the calcium binding protein parvalbumin. These categories describe general trends, and they are not absolute: for instance, some fast spiking neurons are calbindin positive, and some basket cells stain positive for CCK and are not fast spiking (Kawaguchi and Kubota, 1997),(Cauli et al., 1997),(Kawaguchi and Kondo,

2002),(Kawaguchi and Kubota, 1998). Experimentally, classification on the basis of specific markers is often the most useful way to identify distinct populations of interneurons. To this end, interneurons can broadly be grouped into three non-overlapping classes on the basis of marker expression: parvalbumin (PV), somatostatin (SST), and 5HT3aR – the majority of which express vasointesinal peptide (VIP) (Rudy et al., 2011),(Xu et al., 2010). Although these groups are mutually exclusive, they are not homogeneous, as each major group is further subdivided into distinct sub-classes of interneurons (Markram et al., 2004).

Parvalbumin positive neurons are enriched for fast spiking basket cells that are densely and promiscuously connected to the soma and dendrites of pyramidal neurons and other fast spiking neurons throughout the cortex; these cells specifically form synapses that contain the α1 GABA-A receptor subunit (Packer and Yuste, 2011),(Nusser et al., 1996), (Klausberger et al., 2002). PV neurons are directly innervated by multiple release cites from thalamocortical afferents; these synapses rapidly and robustly activate PV neurons to mediate feedforward inhibition (Cruikshank et al., 2007),(Bagnall et al., 2011). Excitatory synapses formed onto PV neurons are rapidly depressing, meaning that in response to excitatory input they respond rapidly and reliably - but not in a sustained manner (Glickfeld and Scanziani, 2006),(Reyes et al., 1998).

Like PV neurons, somatostatin positive interneurons densely innervate pyramidal neurons in the cortex; however, they preferentially target distal dendrites of pyramidal neurons (Fino and Yuste, 2011). Somatostatin expressing neurons are never fast spiking; they may be either regular spiking or low threshold spiking. On the basis of action potential characteristics, marker expression, morphology and other features, SST neurons segregate into three distinct subtypes (Ma et al., 2006),(McGarry et al., 2010). In contrast to PV neurons, most SST neurons do not receive thalamocortical input; instead, their excitatory input tends to come from local cortical or horizontally connected afferents, enabling them to mediate disynaptic feedback inhibition between local cortical pyramidal neurons (Tan et al., 2008),(Silberberg and Markram, 2007),(Xu and Callaway,

2009),(Adesnik et al., 2012). Unlike PV neurons, excitatory synapses formed onto SST neurons are facilitating; thus, in response to excitatory input, SST neurons are recruited with delayed kinetics, but they can maintain consistent firing rates even in the face of persistent excitatory input (Reyes et al., 1998),(Hayut et al., 2011). The facilitating nature of excitatory input to SST neurons allows them to fire tonically during theta oscillations associated with quiet wakefulness (Fanselow et al., 2008; Gentet et al., 2012),(Goldin et al., 2007).

Parvalbumin and somatostatin expressing interneurons together make up the majority of inhibitory neurons in the cortex, and they have relatively stereotyped connectivity and function. While many other types of inhibitory neurons have been identified and studied, their specific functions and connectivity have not been extensively characterized, though they are the subjects of current active investigation. Because of the longstanding availability of reagents allowing genetic access, PV neurons have become the most well studied type of interneurons, followed by SST neurons. For this reason, the discussion that follows will be focused on these types of neurons.

Functions of Inhibition

Inhibition exerts its influence on all aspects of nervous system function. Beyond simple balancing of excitation, inhibition has a number of important roles in shaping neuronal activity, including controlling cortical oscillations, sharpening feature selectivity, and dynamically tuning the response of the cortex to excitation. A major feature of both PV and SST neurons is their dense, promiscuous connectivity to pyramidal neurons. This connectivity allows them to synchronize the activity of large groups of excitatory neurons, entraining them to fire in phase with each other. Synaptic transmission from a single inhibitory neuron can entrain the firing of over 1000 pyramidal neurons by providing a common temporal reference (Cobb et al., 1995). Distinct groups of interneurons are electrically coupled with one another, ensuring that inhibitory neurons fire in phase with one another. This synchronization amongst inhibitory neurons provides a mechanism

to bind the oscillatory behavior of cohorts of pyramidal neurons entrained by individual inhibitory neurons. Importantly, inhibitory neurons of similar types are coupled with each other, but not other interneuron types: fast-spiking neurons form an electrically coupled network that responds to thalamocortical input, while low threshold spiking neurons (probably SST expressing) are electrically coupled to each other, but not to fast-spiking cells (Gibson et al., 1999),(Galarreta and Hestrin, 1999). When activated, these two distinct networks of coupled inhibitory neuron networks can each induce synchronization of pyramidal neuron firing: the fast-spiking network promotes synchrony in response to ascending input, while the low threshold spiking network is activated by neuromodulators such as acetylcholine (Galarreta and Hestrin, 2001),(Beierlein et al., 2000). Interestingly, synchronization of inhibitory neuron firing is possible both within and across interneuron subtypes without electrical coupling or glutamatergic neurotransmission: activation of chemical inhibitory synapses between pairs of fast-spiking interneurons or between somatostatin and fast-spiking interneurons are sufficient to induce synchronous firing (Hu et al., 2011).

The ability of inhibitory neurons to promote synchrony in neuronal networks is intimately related to their ability to dynamically modulate oscillatory behavior in neural circuits. Two oscillatory regimes dominate the waking cortex: theta oscillations (3-8 Hz) associated with quiet wakefulness, and gamma oscillations (20-80 Hz), which are though to reflect active processing of the cortex, and are commonly disrupted in neuropsychiatric disorder (Bartos et al., 2007). Theoretical modeling studies suggested that networks of fast-spiking inhibitory neurons firing in synchrony with each other may be sufficient to induce both local gamma oscillations as well as gamma oscillation coupled across distal brain regions (Wang and Buzsaki, 1996), (Traub et al., 1996), (Bartos et al., 2007). Supporting these models, direct optogenetic activation of parvalbumin positive neurons – but not pyramidal neurons – is sufficient to induce gamma oscillations in the cortex (Cardin et al., 2009),(Sohal et al., 2009). Inhibition does more than simply increase the power of gamma oscillations: rapid balancing of inhibition with highly variable

excitation can modulate both the frequency and amplitude of gamma oscillations (Atallah and Scanziani, 2009).

The ability of feedforward inhibition to instantaneously balance excitation underlies signal normalization, another important function of inhibition. The cortex can maintain a set dynamic range of responsiveness in the face of large variations in the strength of excitatory input. To do so, the cortex requires some form of gain control over excitatory input in order to elicit adequate responses to weak input and to avoid saturation when it receives strong excitatory input. Gain normalization is mediated by feedforward inhibition, which is dynamically and rapidly recruited to linearly match the magnitude of excitatory input. This feature of inhibition ensures that the relative weight of an individual excitatory input is inversely proportional to the number of active afferents, in essence normalizing the excitatory input (Pouille et al., 2009),(Atallah et al., 2012),(Wilson et al., 2012).

Somatostatin positive and other non-fast spiking interneurons do not appear to participate in input normalization, and they do not seem to either influence the initiation of gamma oscillations or to respond to them. However, SST neurons do exhibit strong activation during theta oscillations (Fanselow et al., 2008),(Gentet et al., 2012). Inhibitory tone to dendrites mediated by SST neurons actively suppresses the response of pyramidal neurons to excitatory input; indeed, optogenetic silencing of SST neurons increases pyramidal cell burst firing (Royer et al., 2012),(Lovett-Barron et al., 2012). However, unlike PV neurons, dendritic inhibition mediated by SST neurons does not mediate gain control; instead, it linearly diminishes the responsiveness of a pyramidal neuron to a given stimuli (Wilson et al., 2012).

Dynamic control of excitation by inhibition causes the emergence of key features of pyramidal neuron responsiveness to stimuli. In particular, inhibition sharpens feature selectivity of excitatory neurons. Theoretically, broadly tuned inhibition could subtract from more narrowly tuned excitation, resulting in feature responsiveness substantially more selective than the net selectivity of excitatory input (Isaacson and Scanziani, 2011). Indeed, there is substantial experimental evidence indicating that inhibitory neurons are broadly tuned across feature space.

In the visual cortex, inhibitory neurons in layer 2/3 have receptive fields that are much larger than neighboring excitatory neurons, and they also display weaker orientation tuning to visual stimuli (Liu et al., 2009),(Sohya et al., 2007). This lack of orientation selectivity is not specific to any specific inhibitory neuron subtype: PV, SST, and VIP neurons in layer 2/3 of the visual cortex all exhibited significantly less selectivity for stimulus orientation or spatial frequency than pyramidal neurons. Moreover, any existing response bias in the inhibitory neurons reflected the net bias of neighboring pyramidal neurons, suggesting that feature selectivity of inhibitory neurons reflects averaging of excitatory inputs from surrounding cells (Kerlin et al., 2010),(Hofer et al., 2011). Independent studies suggest that the fast-spiking interneurons in layer 4 of the visual cortex also display broader feature selectivity than their pyramidal neighbors; however, the tuning of the excitatory inputs to neighboring pyramidal cells and FS cells is identical, suggesting that the broader selectivity of the fast-spiking neurons may arise solely from intrinsic membrane properties (Cardin et al., 2007).

These features of inhibition give rise to multiple functional properties of pyramidal neurons. In the barrel cortex, blockade of GABAergic transmission results in expansion of receptive field size and loss of angular tuning, consistent with the emergence of multi-whisker thalamocrotical input in the absence of GABAergic transmission (Kyriazi et al., 1996). In the visual system, broadly tuned inhibition underlies receptive field structure and sharpens pyramidal cell orientation selectivity by expanding the neurons dynamic range, allowing robust and selective output in response to strong but weakly tuned excitatory input (Liu et al., 2011),(Liu et al., 2010). These functions have direct functional consequences for visual feature dynamics: optogenetic activation of PV neurons in V1 sharpens feature selectivity and improves perceptual discrimination, while activation of SST neurons mediates surround suppression (Lee et al., 2012),(Adesnik et al., 2012).

Intriguingly, at least one key feature of inhibition, its nonselective orientation tuning, is not present in juvenile animals, and emerges over development (Kuhlman et al., 2011). This finding implies that activity-dependent developmental processes in inhibitory neurons may govern the emergence and maintenance of key features of

inhibitory neurons function in the mature nervous system. Given the importance of these roles, it is of great interest to understand how inhibitory neurons change over development and in response to activity, as well what molecular mechanisms underlie these changes.

Activity and Inhibitory Neurons

The visual critical period highlights how inhibition can affect activity-dependent cortical plasticity. As previously mentioned, the visual critical period for monocular deprivation plasticity is dynamically regulated by the maturation of PV-expressing inhibitory neurons. Genetic ablation of GAD65, which selectively impairs high frequency inhibitory neurotransmission, causes the cortex to remain in a permissive state for ocular dominance (OD) plasticity well past the normal developmental closure of the critical period. Enhancement of GABAergic transmission by administration of diazepam can rescue ocular dominance plasticity in GAD65 KO mice, as well as induce precocious critical periods in wild-type juvenile mice. These data show that this form of plasticity is bidirectionally regulated by the efficacy of cortical inhibition (Hensch et al., 1998),(Fagiolini and Hensch, 2000). The ability of diazepam to control critical period plasticity is ablated by a point mutation of the $\alpha 1$ subunit of the GABA-A receptor that removes its sensitivity to diazepam. The $\alpha 1$ subunit is strongly enriched at synapses formed by PV positive basket cells; moreover, similar mutations in other GABA-A receptor α subunits do not alter the effect of diazepam on critical period onset, indicating that the specific maturation of fast-spiking neurons controls the timing of the critical period (Fagiolini et al., 2004),(Klausberger et al., 2002). The finding that critical period plasticity is controlled by development of PV neurons is supported by the observation that over-expression of Bdnf – which promotes development of inhibition - early in development induces both precocious development of inhibitory neurons and early critical periods (Huang et al., 1999), (Hong et al., 2008). Given their obligate role in

controlling cortical plasticity, it is of great interest to understand how PV positive interneurons mature, and what molecular mechanisms control this maturation.

Parvalbumin interneurons undergo dramatic changes between the first postnatal week and the end of the visual critical period that include decreased input resistance, decreased spike width, and increased maximal firing rate. These changes in membrane properties are accompanied by increased excitatory and inhibitory synaptic input, as well as transcriptional changes in gene modules involved in synaptic development, the development of perineuronal nets, and membrane properties (Okaty et al., 2009). In particular, two potassium channels, Kv3.1 and Kv3.2, are developmentally upregulated in PV neurons with kinetics corresponding to the onset of fast-spiking activity. These channels have positively shifted voltage dependencies and extremely fast deactivation rates, which make them excellent mediators of rapid action potential repolarization, perhaps accounting for the developmental decrease in spike width in PV neurons. In addition, they allow action potential after-hyperpolarizations with more negative membrane potentials, helping sodium channels recover more rapidly from inactivation. Together, these properties make Kv3 channels excellent mediators of fast-spiking activity, and suggest that their upregulation over development may be a key event in PV neuron maturation (Rudy and McBain, 2001),(Erisir et al., 1999),(Lien and Jonas, 2003).

Another hallmark of PV neuron maturation is the emergence of complex perineuronal nets (PNNs) composed of chondroitin sulphate proteoglycans and extracellular matrix proteins. The functional roles attributed to PNNs are varied, but they include buffering the ionic composition of the extracellular space, possibly to support fast-spiking (Hartig et al., 1999). Perineuronal nets can influence synaptic transmission as well: loss of the ECM protein tenascin-R, which associates with PV neuron perineuronal nets through an interaction with a specific carbohydrate, results in decreased perisomatic inhibition delivered to pyramidal neurons and subsequent network hyperactivity (Saghatelyan et al., 2001). Strikingly, degradation of extracellular matrices in adult animals is sufficient to reactivate ocular dominance plasticity well after critical period closure, suggesting that PNNs are required to maintain a mature state of inhibitory neuron function

(Pizzorusso et al., 2002). A key molecular mechanism by which PNNs may mediate this function is by promoting the accumulation of the homeobox transcription factor Otx2 in PV neurons. Otx2 is a key molecular regulator of PV neuron development; infusion of Otx2 into the cortex of juvenile mice is sufficient to induce precocious PV neuron development and critical period plasticity, whereas its deletion abolishes critical period plasticity (Sugiyama et al., 2008). Otx2 is expressed postnatally in retinal ganglion cells, but in response to visual experience, it translocates to the cortex, where it accumulates on PV neurons through a specific interaction with chondroitin sulfates that compose the PNNs that decorate PV cells. Cortical infusion of a small peptide that competitively inhibits the specific interaction of Otx2 with the perineuronal net is sufficient to reopen critical period plasticity in the adult cortex. This finding suggests that persistent association of Otx2 with PV neurons is necessary to maintain mature PV neuron function, and suggests a potential mechanism by which degradation of PNNs reopens OD plasticity (Beurdeley et al., 2012),(Sugiyama et al., 2008).

Visual experience during the critical period is also important for development of appropriate synaptic connectivity of PV neurons. Dark rearing during the critical period occludes developmental increases in the number perisomatic axonal boutons formed by PV neuron axons, and it also prevents upregulation of GABAergic synaptic transmission onto excitatory cells (Morales et al., 2002),(Chattopadhyaya et al., 2004). Normal patterns of activity may be required for maintenance of inhibitory connectivity in the adult: loss of sensory input rapidly induces structural changes in inhibitory neuron axons, including axon branch retraction, and disappearance of inhibitory boutons (Keck et al., 2011),(Chen et al., 2011).

In addition to structural changes, long term changes in activity levels in a circuit can induce homeostatic plasticity in interneurons, although these changes are distinct from classical homeostatic synaptic scaling of synapse strength observed in pyramidal neurons (Turrigiano, 2011),(Turrigiano et al., 1998). In contrast to excitatory neurons, increased activity can promote increased strength of excitatory synapses onto PV positive inhibitory neurons. This homeostatic increase

in excitation onto PV neurons is thought to arise from molecules synthesized in excitatory neurons in an activity-dependent manner and subsequently secreted. Two of these molecules, Bdnf and Narp, are not synthesized in parvalbumin expressing interneurons, yet they both act to increase the amplitude of miniature EPSCs of excitatory synapses formed onto interneurons (Chang et al., 2010), (Rutherford et al., 1998). These data support a model in which increased levels of activity throughout a local circuit increases the extracellular concentration of factors that promote increased excitatory inputs to inhibitory neurons.

However, disruption of visual input by monocular deprivation during the critical period markedly increases the number of inhibitory connections to layer 4 pyramidal neurons, and also potentiates the strength of inhibitory synapses (Maffei et al., 2006). These data suggest that both increases and decreases in activity levels can, under specific conditions, potentiate inhibition. In striking contrast, bath application of TTX to cortical slices significantly decreases the size of unitary IPSCs from PV neurons to connected pyramidal cells; TTX application also reduced the number of inhibitory synapses formed by PV neurons (Bartley et al., 2008). Suppressing the activity of a single basket cell reduces the number of pyramidal neurons innervated by the PV neurons, without altering the pattern of perisomatic innervation to the remaining cells. Surprisingly, this effect is completely reversed later in development, suggesting that the directionality by which activity modifies inhibitory function can differ over development, brain region, or specific experimental preparation (Turrigiano, 2011),(Baho and Di Cristo, 2012).

Different types of inhibitory neurons display distinct homeostatic mechanisms. SST neurons become more excitable over postnatal development in response to sensory experience, but in response to activity blockade, they down regulate a potassium leak current and become even more excitable (Lazarus and Huang, 2011),(Gibson et al., 2006). In contrast to PV neurons, activity blockade does not diminish the size of unitary IPSCs delivered by SST neurons. However, the short-term plasticity of synapses both on and from SST neurons is altered by activity blockade: in response to TTX, EPSCs onto SST neurons become less facilitating, and IPSCs from SST neurons become more depressing (Bartley et al., 2008). Together,

these studies show that inhibitory neurons actively adapt to long-term changes in activity levels, but they do so through a surprising diversity of mechanisms that may vary between inhibitory subtypes, brain region, developmental stage, and experimental preparation.

In addition to exhibiting homeostatic synaptic changes in response to sustained changes activity levels, the properties of synaptic connectivity to and from inhibitory neurons are acutely regulated by short-term changes in local activity. As previously discussed, the short term plasticity dynamics of excitatory synaptic inputs to PV and SST neurons are respectively depressing and facilitating; these differences underlie important aspects of subtype specific function, including the temporal dynamics of their activation (Reyes et al., 1998). The mechanisms by which these synapses acquire these short-term plasticity properties have only recently begun to be uncovered. A recent study has identified a role for Elfn1 (extracellular leucine-rich repeat fibronectin containing 1) in trans-synaptically specifying the facilitating nature of excitatory input. Elfn1 is expressed in SST neurons, but not PV neurons in the hippocampus; ablation of Elfn1 in SST neurons destroys the facilitating nature of their excitatory inputs, while ectopic expression of Elfn1 in PV neurons causes their excitatory inputs to flip from depressing to facilitating (Sylwestrak and Ghosh, 2012). This finding is the first evidence that an interneuron can specify the presynaptic properties of its excitatory inputs, and suggests that programs of gene expression in specific interneuron subtypes may intimately regulate important aspects of their connectivity. It remains to be determined whether there are similar molecules expressed by PV neurons that can induce excitatory inputs to PV neurons to become depressing, or whether short-term depression is a default state for excitatory afferents to interneurons. Intriguingly, the short-term plasticity exhibited by inhibitory synapses to pyramidal cells is the reciprocal of the excitatory inputs to those interneurons: PV inhibitory input to excitatory neurons is facilitating, while SST inhibitory input to excitatory neurons is depressing (Ma et al., 2012). Discovering whether and how the short-term plasticity properties of these distinct types of inhibitory synapses are

regulated by the post-synaptic neuron remains a major goal of molecular neurobiology.

Excitatory inputs to inhibitory neurons undergo long term, as well as short term, plasticity. Excitatory synapses onto cortical SST neurons under long term potentiation in response to strong theta bursts through a presynaptic mechanism activated by forskolin but insensitive to calcium signaling (Chen et al., 2009). In non-fast spiking neurons in the hippocampus, an intriguing form of anti-Hebbian LTP occurs through a post-synaptic mechanism reliant on calcium permeable AMPA receptors. CP-AMPARs are blocked by polyamines during depolarization, so they cannot pass current when the cell is depolarized. This anti-Hebbian LTP is induced by presynaptic activity, but occluded by post-synaptic depolarization; in essence, this mechanism is induced when active presynaptic terminals fail to elicit depolarization. This plasticity has been hypothesized to occur in interneurons that are silent during periods of intense pyramid neuron firing (Lamsa et al., 2007).

Inhibitory neurons express less GluA2 and more GluA4 than excitatory neurons, so their AMPA receptors are mostly calcium permeable. Calcium permeable AMPA receptors are thought to be an important mediator of synaptic plasticity across multiple types of inhibitory neurons (Szabo et al., 2012). In contrast to the hundreds of proteins known to be active at the post-synaptic density of spiny excitatory synapses, very little is known about the molecules that specifically regulate CP-AMPA receptors. However, it is likely that the milieu of proteins that regulate calcium impermeable AMPA receptors in dendritic spines in excitatory neurons is significantly different form those that associate with CP-AMPA receptors on dendritic shafts in inhibitory neurons. As discussed, Nptx1 and Nptx2 cluster AMPA receptors specifically at shaft synapses through a direct interaction with GluA4, and it is likely that additional functions of proteins uniquely involved in regulating CP-AMPA receptors will be uncovered. Two such proteins may be the atypical TARPs, γ-5 and γ-7, which specifically interact with CP-AMPA receptors in Bergmann glia, and are enriched in inhibitory neurons relative to other TARP family members (Kato et al., 2008),(Soto et al., 2009).

Long and short-term plasticity of synapses onto and from inhibitory neurons occurs widely, and utilizes a startling diversity of molecular mechanisms (Kullmann et al., 2012). Although our mechanistic understanding of the plasticity of inhibition is incomplete, it is far more advanced than our understanding of the molecular mechanisms underlying the formation and development of synaptic input to inhibitory neurons. One of the only signaling pathways known to be involved in regulating formation of excitatory synaptic connections to inhibitory neurons is the ErbB4/neuregulin 1 pathway. ErbB4 expression in parvalbumin neurons regulates the formation of excitatory synapses onto those cells through an interaction with presynaptic neuregulin 1 (Fazzari et al., 2010). This trans-synaptic interaction is also important for subsequent long-term potentiation of existing synapses, and its disruption causes deficient pre-pulse inhibition and other schizophrenia-like phenotypes in mice (Wen et al., 2010), (Chen et al., 2010b). This work supports genetic evidence linking ErbB4 and NG1 to schizophrenia, as well as experimental evidence showing that ablation of NMDA receptors in 40-50% of corticolimbic interneurons causes schizophrenia-like phenotypes (Belforte et al., 2010).

The role of activity-regulated transcription in the development of synaptic connectivity onto inhibitory neurons remains a large gap in knowledge. Activity-induced molecules synthesized in excitatory neurons and subsequently secreted regulate synaptic plasticity of synapses to inhibitory neurons. For instance, though Bdnf potentiates excitatory input to inhibitory neurons, inhibitory neurons have never been observed to express Bdnf (Gorba and Wahle, 1999; Rutherford et al., 1998). Furthermore, although Narp regulates activity-dependent homeostatic scaling of excitatory input to PV neurons, PV neurons themselves apparently do not express Nptx2 (Chang et al., 2010). However, inhibitory neurons do express mediators of activity-depending signaling including CREB, MEF2, and SRF, and these factors undergo activity-dependent post-translation modifications in inhibitory neurons (A. Mardinly, Personal Observations). Moreover, these factors are probably capable of inducing gene transcription in interneurons, as c-Fos induction has been widely used to label populations of activated inhibitory neurons. Intriguingly, a recent study found that deletion of CREB in inhibitory neurons in the hippocampus

results in abnormal plasticity of excitatory synapses onto these neurons, suggesting that activity-dependent transcription in interneurons may have a role in synaptic development (Ran et al., 2012). The identity of the genes induced by activity in inhibitory neurons, as well a their specific function in synaptic development were not previously characterized, and this gap in knowledge is a major topic of this thesis.

Chapter 2:

Npas4 regulates excitatory input onto somatostatin positive inhibitory neurons through a unique activity-dependent transcriptional program

Introduction

Cortical inhibition is mediated by a subset of neurons that release the neurotransmitter GABA (γ-aminobutyric acid) at synapses and function to sharpen sensory inputs (Kyriazi et al., 1996),(Liu et al., 2011), entrain synchronous oscillations on cohorts of pyramidal neurons (Somogyi and Klausberger, 2005), (Cobb et al., 1995), (Cardin et al., 2009) and specify the onset and closure of critical periods (Hensch, 2005), (Fagiolini and Hensch, 2000). GABAergic inhibitory neurons are highly diverse with respect to their developmental lineage, morphology, gene expression program, electrophysiological properties, and post-synaptic targets (Cauli et al., 1997; Kawaguchi and Kubota, 1997), (Ascoli et al., 2008), (Sugino et al., 2006) (Batista-Brito et al., 2008). Historically, this diversity has made it difficult to define the function of distinct classes of inhibitory neurons within neural circuits. However, recent technical advances have provided genetic access to specific subtypes of inhibitory interneurons and has revealed that different classes of inhibitory neurons have distinct functions in the nervous system (Lapray et al., 2012), (Lovett-Barron et al., 2012), (Wilson et al., 2012).

Many distinct types of inhibitory neurons have been characterized to date, and these neurons can be grouped into three non-overlapping subtypes based on whether they neurons express somatostatin, parvalbumin or the 5HT3a receptor. Somatostatin (SST) expressing neurons, which are the focus of the current study, constitute about a third of all cortical GABAergic neurons (Rudy et al., 2011). Unlike the soma-targeting fast-spiking PV-positive basket cells, SST neurons are non fast-spiking and preferentially form synapses on the distal dendrites of pyramidal neurons (Fino and Yuste, 2011), (Kawaguchi and Kondo, 2002). Recent reports suggest that, in the mouse cortex, SST neurons are predominately activated by local excitatory afferents and horizontal connections in layer 2/3 and 4, and mediate feedback inhibition through release of GABA onto distal dendrites of pyramidal neurons (Xu and Callaway, 2009),(Adesnik et al., 2012),(Silberberg and Markram, 2007).

SST neurons receive weak but facilitating excitatory synaptic input that allows them to maintain tonic firing during quiet wakefulness and during regimes of elevated activity (Hayut et al., 2011),(Gentet et al., 2012),(Fanselow et al., 2008),(Reyes et al., 1998). During brain development, sensory experience promotes the maturation of SST neurons by increasing their excitability (Lazarus and Huang, 2011). In response to acute activity, excitatory inputs to SST neurons can undergo long-term potentiation through a presynaptic mechanism, while chronic activity blockade recruits homeostatic mechanisms that modulate both membrane excitability and short-term plasticity of synapses both on and from SST neurons (Chen et al., 2009),(Bartley et al., 2008),(Gibson et al., 2006). The specific molecular mechanisms by which neuronal activity affects the development, maturation, and plasticity of excitatory synapses on SST neurons are not yet known.

Studies of excitatory neurons have revealed that neuronal activity regulates synapse development and function by inducing post-translational modifications of synaptic proteins as well as the transcription and/or translation of key regulators of synaptic function (Jackson and Nicoll, 2011),(Anggono and Huganir, 2012). For example, our laboratory has shown that synaptic activity activates a transcriptional network that functions to restrict the number of excitatory synapses while increasing the number of inhibitory synapses that form on pyramidal neurons (Lin et al., 2008), (Flavell et al., 2006). In particular, neuronal activity and the subsequent influx of calcium stimulate expression of Npas4, a transcription factor that induces expression of brain derived neurotrophic factor (Bdnf) that then functions locally to increase the number of inhibitory synapses on excitatory neurons (Lin et al., 2008),(Hong et al., 2008),(Sakata et al., 2009). Whether similar mechanisms operate in SST neurons and other inhibitory neurons to control excitatory and inhibitory inputs to these neurons remained to be determined.

Using cultured GABAergic neurons derived from the medial ganglionic eminence and *ex vivo* acute cortical slice recording, we show here that neuronal activity induces a transcriptional program that is unique to inhibitory neurons and functions to promote the development of excitatory synapses on SST neurons. While early-response transcription factors such as Npas4 are induced in both

excitatory and inhibitory neurons, the targets of these transcription factors are different in these two types of neurons. This allows the synapses that form on inhibitory and excitatory neurons to be uniquely modified by neuronal activity in a manner that is tailored to the function of the specific neuron within a neuronal circuit. In excitatory neurons, Npas4 activates transcription of Bdnf, thereby promoting an increased number of inhibitory synapses on excitatory neurons; however, the activation of Npas4 in SST neurons has an entirely different outcome. In SST neurons, activity-dependent induction of Npas4 triggers activation of a unique set of target genes that serve to increase excitatory input onto SST neurons, likely resulting in enhanced inhibition within cortical circuits.

Results

Activity-dependent gene expression regulates the development of synaptic connectivity throughout the nervous system. While this transcriptional program has been extensively studied in excitatory neurons, it is poorly described in inhibitory neurons in part because of the technical difficulty of isolating RNA selectively from inhibitory neurons. To overcome this obstacle, we prepared neuronal cultures that are highly enriched for inhibitory neurons. This was accomplished by taking advantage of the fact that early in their development, inhibitory neurons are localized to specialized regions of the embryonic brain, the ganglionic eminences, that are devoid of excitatory neurons (Flandin et al., 2011),(Wonders and Anderson, 2006). We dissected the medial ganglionic eminence (MGE) at embryonic day 14, dissociated the tissue, and cultured the resulting cells. We found by immunostaining, western blot, and quantitative RT-PCR analysis that MGE-derived cultures are highly enriched for the inhibitory markers GAD65/67; furthermore, MGE cultures are almost completely devoid of proteins such as Vglut1 and Tbr1 that are selectively expressed in excitatory neurons (Figure 2.1A-B, 2.2A). These results indicate that MGE-derived cultures are highly enriched for inhibitory neurons. Using antibodies directed against several markers of inhibitory neuron subtypes (Parvalbumin, Somatostatin, VIP, NPY, Calbindin,

Figure 2.1: Neuronal cultures enriched for inhibitory and excitatory neurons

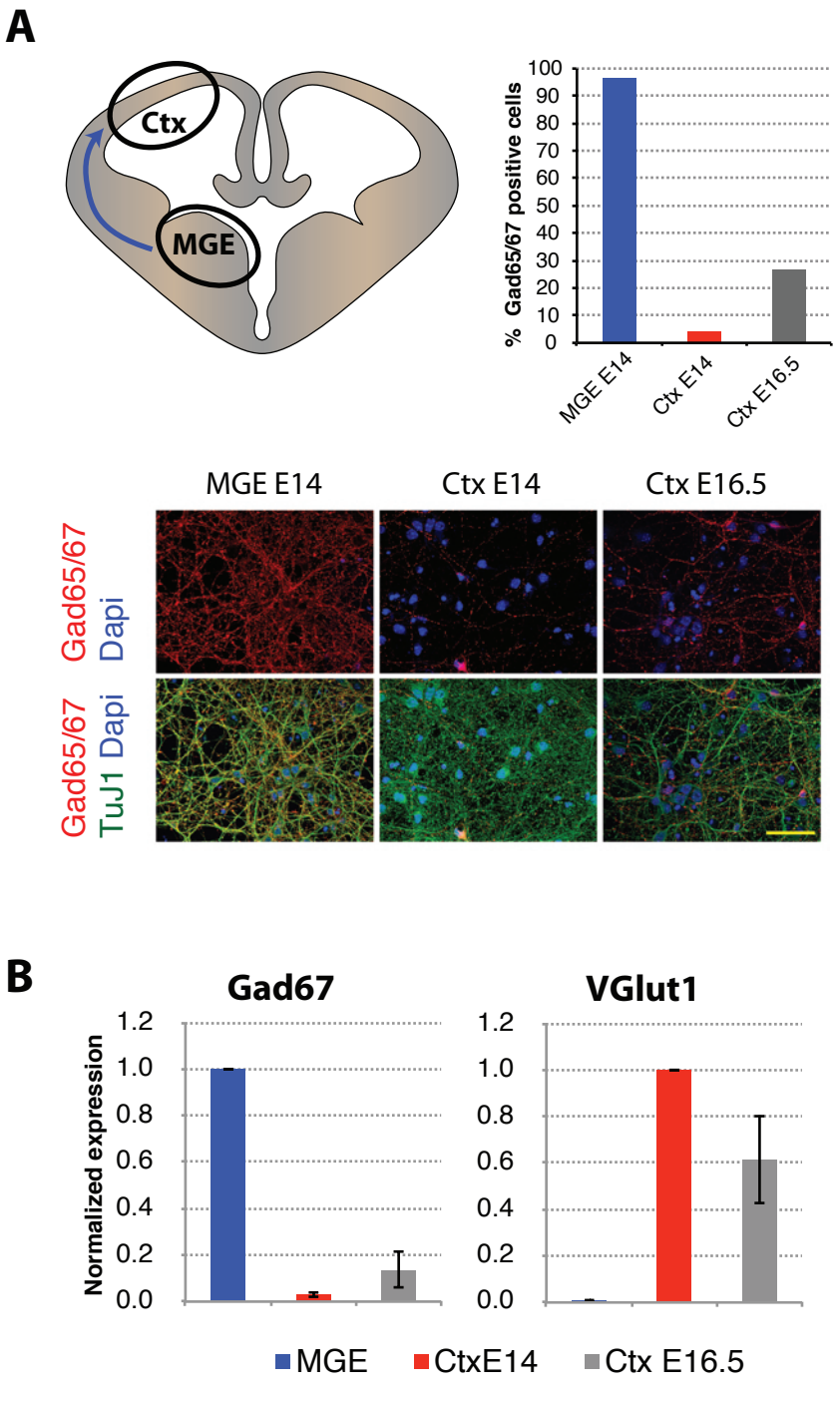

Figure 2.1 (Continued): Neuronal cultures enriched for inhibitory and excitatory neurons

A) Left, schematic showing the embryonic brain regions dissected to prepare MGE-derived cultures and E14 cortical cultures. At embryonic day 14, most of the inhibitory neurons born in the MGE have not yet migrated to the cortex. Physical isolation of the cortex and the MGE yield separate cultures highly enriched for excitatory and inhibitory neurons, respectively. Standard cortical cultures are prepared from E16.5 embryos, after many inhibitory neurons have migrated to the cortex. Right, quantification of the percentage of neurons in each type of culture that are positive for GAD65/67 immunostaining. Bottom, example images of GAD65/67 staining (red) with Tuj-1 (green) and DAPI (blue) to label neuronal processes and nuclei, respectively, in each culture type. Scale bar is 50 μm.
B) Quantitative RT-PCR analysis of GAD67 and Vglut1 mRNA from DIV9 MGE and E14 cortical cultures and DIV7 E16.5 cortical cultures. Signal was normalized to the most highly expressed condition in the experiment. Error bars represent the SEM of three biological replicates.

Calretinin), we found by immunostaining that a wide variety of inhibitory neuron subtypes are present in the MGE-derived cultures (data not shown) (Markram et al., 2004). Finally, using double immunolabeling for pre- and post-synaptic marker proteins and electrophysiological recordings of miniature synaptic currents, we detected a large number of inhibitory synapses, but very few excitatory synapses in MGE-derived cultures (data not shown). These data confirm that MGE-derived cultures contain a low percentage of excitatory neurons and indicate that inhibitory neurons in MGE-derived cultures form functional synapses. For the purpose of comparison, we prepared cultures that are devoid of inhibitory neurons by dissecting and dissociating the mouse cortex at embryonic day 14, a time during brain development before inhibitory neurons have migrated to the cortex (E14 cortical cultures). We found by immunostaining that E14 cortical cultures are almost completely devoid of GAD65/67 positive neurons and by qPCR analysis that these cultures express substantially more Vglut1 mRNA than MGE cultures (Figure 2.1A-B). These findings indicate that MGE derived cultures and E14 cortical cultures should be useful for examining how neuronal activity affects gene expression in inhibitory and excitatory neurons respectively.

Activity induced transcription in inhibitory neurons

To begin to identify mechanisms by which neuronal activity controls the development of synaptic input onto inhibitory neurons, we asked if membrane depolarization induces gene expression in inhibitory neurons and if so, whether the gene expression program is similar to or different from the program induced by activity in excitatory neurons. Previous studies have shown that activity-regulated genes can be divided into two classes, early and late response genes, that are induced maximally at one and six hours after stimulation, respectively. The early induced genes in excitatory neurons primarily encode transcription factors (e.g. Npas4, Zif268, Fos) that regulate the expression of late response genes, many of which encode proteins that function directly at synapses (e.g Bdnf, Homer1, Narp) (Flavell et al., 2008), (Cohen and Greenberg, 2008). We hypothesized that neuronal

activity induces a program of early and late gene transcription in inhibitory neurons that is distinct from the program activated in excitatory neurons, and is tailored to the specific functions of inhibitory neurons within a neural circuit.

To identify the gene program that is activated in inhibitory neurons in response to membrane depolarization, MGE-derived cultures were incubated overnight with TTX and AP-5 to block sodium channels and NMDA receptors, and then exposed to elevated levels of potassium chloride (KCl) to induce membrane depolarization and calcium influx. MGE-derived cultures were incubated with elevated levels of KCl (55mM) for 0, 1 or 6 hours; we then purified RNA and performed genome-wide microarray analysis. To compare this program with the program that is induced in excitatory neurons, we performed a similar membrane depolarization experiment using E14 cortical cultures and carried out microarray analysis to identify activity-regulated genes in excitatory neurons.

To determine the purity of the MGE and E14 cortical cultures used in these experiments, we assessed the microarray signal from probesets directed against known cell-type specific mRNAs. We found that the signal from probesets directed against Vgat, Gad1 and Gad2 was more than ten times higher in MGE cultures than in E14 cortical cultures across all experimental conditions. Similarly, microarray signal from probesets directed against Vglut1 and Tbr1 was more than ten times higher in E14 cortical cultures across all conditions, indicating that the MGE and E14 cortical cultures used in this analysis were highly enriched for inhibitory and excitatory neurons, respectively (Figure 2.2C).

Analysis of these microarray experiments revealed that membrane depolarization of inhibitory neurons induces a gene program that consists of both early and late responses genes. We find that in inhibitory neurons the early transcriptional response to neuronal activity is very similar to the early response that occurs in excitatory neurons, while the sets of late-response genes induced upon membrane depolarization of inhibitory and excitatory neurons are clearly distinct (Figure 2.3A,C). In MGE-derived cultures, the majority of probesets that were maximally induced after one hour of KCl depolarization (35 out of 39) was also maximally induced after one hour in E14 cortical cultures, indicating that the early

Figure 2.2: Neuronal culture systems to assay cell-type specific inducible transcriptional programs

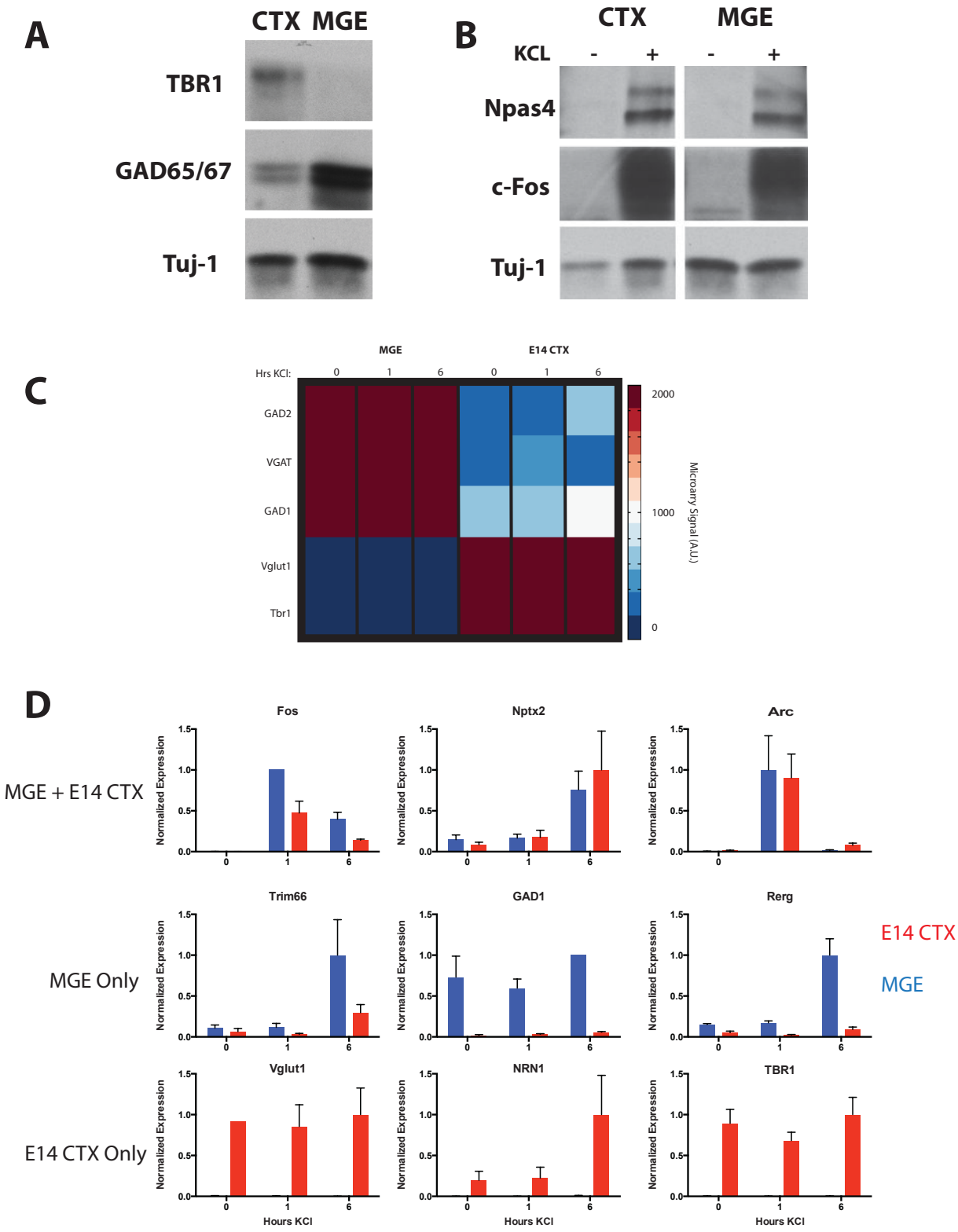

Figure 2.2 (Continued): Neuronal culture systems to assay cell-type specific inducible transcriptional programs

A) Western blot analysis of protein lysates isolated from aged matched MGE (DIV9) and E16.5 Ctx (DIV7) cultures. No TBR1 signal can be detected in MGE-cultures, while GAD65/67 is highly enriched in MGE cultures relative to E16.5 cortical cultures.
B) Western blot analysis of protein lysates isolated from aged matched MGE (DIV9) and E16.5 cortical cultures (DIV7) silenced overnight with TTX and AP-5 and depolarized with 55 mM KCl for 0 (KCl-) or 2 hours (KCl+). Both cultures robustly express Npas4 and c-Fos protein in response to KCl stimulation.
C) DIV9 MGE or E14 Cortical Cultures silenced overnight with TTX and AP-5 and depolarized with 55 mM KCl for 0, 1 or 6 hours. RNA was harvested and sent for genome-wide microarray analysis. Heatmap shows probeset intensity of known cell-type specific genes demonstrating that MGE-derived cultures have greatly increased signal from probesets directed against GAD1, GAD2, and VGAT, while E14 cortical cultures have greatly increased signal from probesets direct against TBR1 and VGLUT1.
D) Quantitative RT-PCR analysis was performed on DIV9 MGE and E14 cortical cultures that has been silenced overnight with TTX and AP-5, and depolarized with 55 mM KCl for 0, 1, or 6 hours. RNA was purified and qPCR analysis was conducted for genes that were induced by activity in both cultures (Fos, Nptx2, and Arc, top row), genes that were specifically expressed in MGE cultures (Trim66, GAD1, Rerg, middle row), or genes that were expressed specifically in E14 cortical cultures (Vglut1, NRN1, TBR1, bottom row). Expression values are normalized to the largest value in the experiment, and error bars represent SEM across three biological replicates.

Figure 2.3: The transcriptional program induced by activity in inhibitory neurons

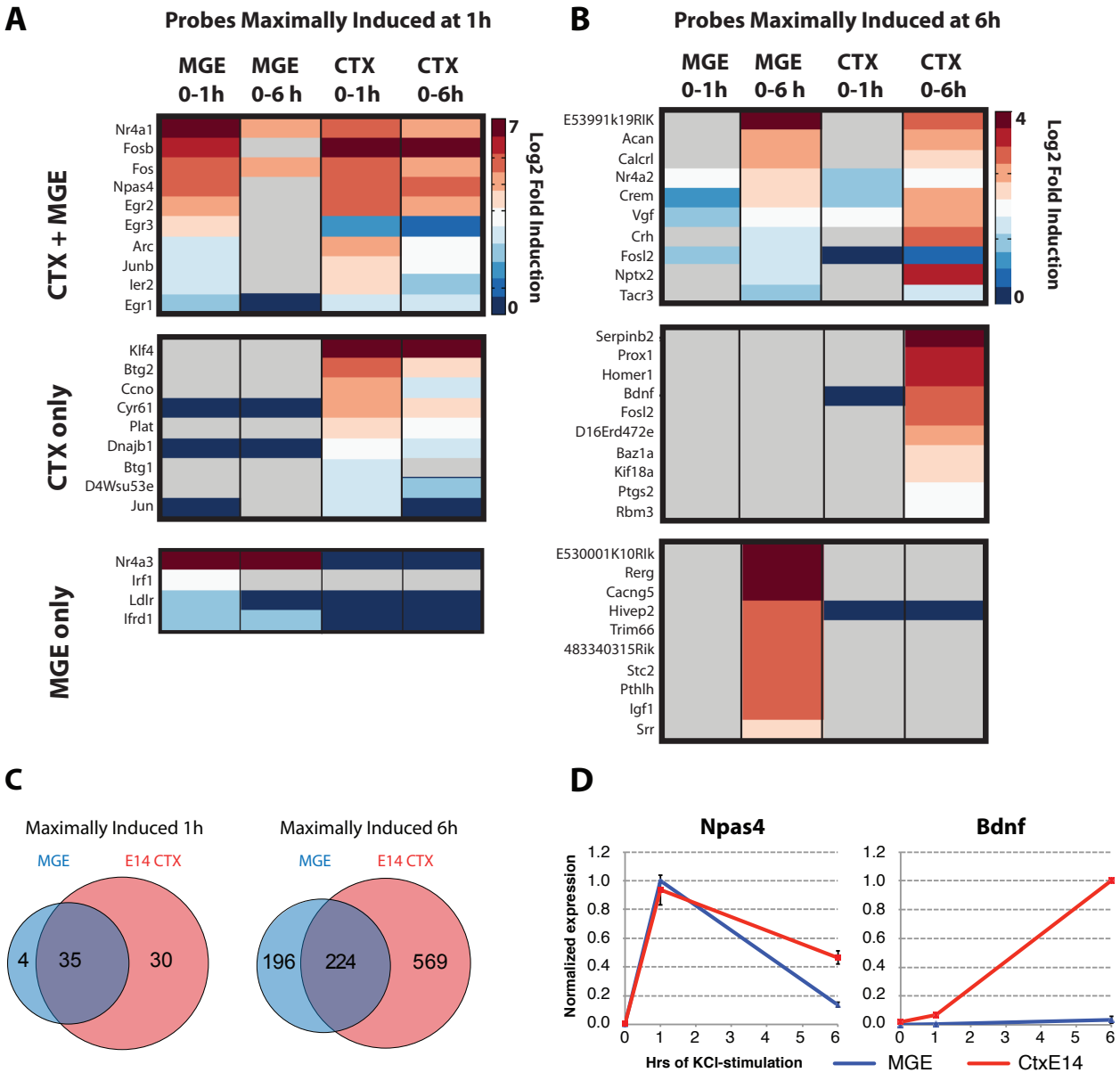

Figure 2.3 (Continued): The transcriptional program induced by activity in inhibitory neurons.

Genome wide microarray analysis was performed on DIV9 MGE and E14 cortical cultures that had been silenced overnight with TTX and AP-5 and depolarized for 0, 1, or 6 hours with 55 mM KCl. The 0-1h fold inductions and 0-6h fold induction were calculated, and induced probesets were sorted into seven categories, those maximally induced at 1 hour or 6 hours in both MGE and E14 Ctx cultures, Ctx only, or MGE only, respectively. An additional group (not shown) was created for probesets that were induced in both MGE and E14 cortical cultures, but had peak induction at distinct timepoints.

A) Heatmaps showing probesets most induced at 1 hour in both MGE and E14 Ctx cultures (top), E14 Ctx only (middle), or MGE only (bottom). Heatmaps show the Log2 fold induction of the probeset in each culture at each time point. Gray boxes indicate that the probe intensity was below expression threshold at the indicated time point.

B) Heatmaps showing example probesets induced at 6 hour in both MGE and E14 Ctx cultures (top), E14 Ctx only (middle), or MGE only (bottom). Heatmaps show the Log2 fold induction of the probeset in each culture at each time point. Gray boxes indicate that the probe intensity was below expression threshold at the indicated time point.

C) Venn diagrams showing the number of probesets maximally induced at 1 hour (left) or 6 hours after membrane depolarization (right) in MGE (blue), E14 ctx (red), or both (purple). Almost all probesets induced in MGE cultures at 1 hour are also induced in E14 cortical cultures, whereas a large fraction of MGE late-response genes are not induced in excitatory neuron cultures.

D) Quantitative RT-PCR from DIV9 MGE and E14 Ctx cultures silenced overnight and stimulated by membrane depolarization for 0, 1, or 6 hours. Npas4 is expressed and induced in both culture types, while Bdnf, a major Npas4 target gene in excitatory neurons, is not detected in MGE cultures either at baseline or in response to membrane depolarization.

transcriptional response to membrane depolarization is very similar in MGE and E14 cortical cultures. As in excitatory neurons, the set of early-response genes induced by membrane depolarization of inhibitory neurons is strongly enriched for regulators of transcription (12 out of 39, GO term 'Transcription Factor Activity', $P = 2 \times 10^{-5}$). Strikingly, 11 of the 12 transcriptional regulators acutely induced by neuronal activity in MGE-derived cultures are also induced in excitatory neurons. These shared transcriptional regulators were highly induced by neuronal activity, and included immediate early genes such as Fos, FosB, Egr1-3, Nr4a1 and Npas4 that are known to robustly and rapidly respond to activity and to mediate important neuronal functions (Figure 2.3A),(Greer and Greenberg, 2008),Lin, 2008 #957},(Jones et al., 2001). Thus, neuronal activity causes the induction of a common early-induced program of gene expression that is shared between excitatory and inhibitory neurons and is heavily enriched for transcriptional activators.

In contrast to the early-induced transcriptional program, late-response genes are enriched for regulators of synapse development and plasticity that function directly at synapses (Flavell and Greenberg, 2008). We asked whether the early-response transcription factors induced in both MGE and E14 cortical cultures regulate the same set of late-response genes in both cultures, or if they regulate cell-type specific sets of late-response genes. To this end, we identified probesets maximally induced six hours after membrane depolarization in either MGE or E14 cortical cultures, and found a high number of late-induced probesets in both cultures (MGE: 420 probesets; E14 CTX: 793 probesets); however, only ~22% of these probesets (224 out of 989) were induced in both MGE and E14 cortical cultures, indicating that excitatory and inhibitory neurons induce substantially different late-response programs of gene expression in response to neuronal activity (Figure 2.3C). To validate these microarray studies, we performed quantitative RT-PCR experiments that showed that the microarrays faithfully report cell-type specific induction in response to membrane depolarization (Figure 2.2D). Thus, inhibitory and excitatory neurons share a common set of rapidly induced transcription factors that appear to regulate distinct sets of late-response genes.

One of the primary functions of the activity-induced transcriptional program in excitatory neurons is to decrease the activity of excitatory neurons by negatively regulating excitatory synaptic input and promoting increased inhibitory input onto excitatory neurons (Sala et al., 2005), (Lin et al., 2008) (Chowdhury et al., 2006; Flavell et al., 2006). Strikingly, some of the key activity-induced regulators of synaptic function are induced by activity in E14 cortical cultures but not in MGE cultures. These genes include Grasp and Homer1, scaffolds for group 1 metabotropic glutamate receptors, as well as Bdnf, a molecule intimately associated with both excitatory and inhibitory synaptic plasticity and development (Figure 2.3B) (Hong et al., 2008), (Brakeman et al., 1997), (Ye et al., 2000). The fact that these synaptic regulator genes are induced by activity only in E14 cortical cultures suggests that activity-induced transcriptional programs might mediate cell-type specific biological functions. We therefore further investigated the activity-dependent genes program in inhibitory neurons.

We asked if the identity of late-response genes selectively induced in MGE cultures could provide insight into the function of the activity-dependent transcriptional program in inhibitory neurons. One of the genes that is most highly induced upon membrane depolarization of MGE-cultures that is not induced in E14 cortical cultures is Cacng5, an atypical TARP (Transmembrane AMPA Receptor Regulating Protein) that selectively regulates calcium-permeable AMPA receptors (Figure 2.3B), (Kato et al., 2008),(Soto et al., 2009). This suggests that activity may modulate the function of excitatory synapses on inhibitory neurons through an AMPA receptor-dependent mechanism. Though the specific role of Cacng5 in inhibitory neurons has not been established, other TARPs promote increased AMPA receptor activation in excitatory neurons, suggesting that a role of neuronal activity in inhibitory neurons may be to positively regulate excitatory synapses on inhibitory neurons (Tomita et al., 2004),(Chen et al., 2000).

Intriguingly, another gene that is highly induced selectively in MGE cultures gives rise to an unannotated RNA that is a likely precursor for the microRNA mir-670; consistent with this finding, cell-type specific profiling of microRNAs previously found that mir-670 is highly enriched in GABAergic neurons (Figure

2.3B), (He et al., 2012). MicroRNAs mediate wide-ranging functions, including regulating dendritic spine development, and activity-dependent induction of mir-670 may be a mechanism by which neuronal activity controls gene expression or synapse development in inhibitory neurons (Schratt et al., 2006). Additional activity-regulated genes specifically induced in inhibitory neurons include Trim66, a putative transcriptional repressor, and two potent secreted factors, Igf-1 and Pthlh, Analogous to the effects of Bdnf activation on synapses that form on excitatory neurons, these secreted factors may affect the formation or function of excitatory or inhibitory synapses on inhibitory neurons (Figure 2.3B).

To begin to assess the importance of the activity-dependent gene program in inhibitory neurons, we reasoned that in might be useful to investigate the function of one of the rapidly induced transcriptional regulators rather than the function of specific late response genes. We hypothesized that early-response transcription factors function as master regulators of the neuronal response to activity, inducing distinct late response genes in different neuronal cell types, thereby eliciting biological responses that are key to the function of the neuronal cell type within a neuronal circuit. Thus, knocking out the function an activity-regulated transcription factor might allow us to identify the importance of the activity-regulated gene program in inhibitory neurons, and to understand how, by acting in these neurons, this gene program contributes to neural circuit function.

Towards this end we focused our attention on the early-response transcription factor Npas4. In excitatory neurons Npas4 activates transcription of Bdnf, thereby promoting an increase in the number of inhibitory synapses that are present on excitatory neurons (Lin et al., 2008). However, despite the robust induction of Npas4 in MGE cultures, Bdnf is not expressed at detectable levels in inhibitory neurons even upon exposure of these cultures to a strong depolarizing stimulus (Figure 2.3D). Thus, the transcriptional targets of Npas4 in inhibitory and excitatory neurons are at least in part distinct, and the analysis of Npas4 function in inhibitory neurons should reveal the importance of the activity-regulated gene program in these neurons.

Npas4 is induced by neuronal activity across inhibitory neuron subtypes

To investigate the function of Npas4 in inhibitory neurons, we first asked whether Npas4 expression is induced in inhibitory neurons *in vivo* upon sensory stimulation and if so which inhibitory neuron subtypes express Npas4. Induction of Npas4 expression in the mouse brain has been observed in a variety of contexts, including in the amygdala after fear conditioning, in the hippocampus after exposure to an enriched environment, in the striatum after drug administration, and in the visual cortex after exposure of dark reared animals to light (Lin et al., 2008),(Ramamoorthi et al., 2011),(Guo et al., 2012),(Flavell et al., 2008). Despite these reports, it remained unknown if physiological stimuli induce Npas4 expression in inhibitory neurons *in vivo*. To this end, we generated mice in which genetically defined subtypes of inhibitory neurons were fluorescently labeled and maintained these mice in standard laboratory housing until postnatal day 20 (P20) (Taniguchi et al., 2011),(Madisen et al., 2010),(Stenman et al., 2003). At P20, the mice were dark-housed for 4 days and perfused either without having been exposed to light (dark housed), or after 2.5 hours of light exposure (light exposed).

We immunolabeled brain sections with antibodies against Npas4 and quantified the percentage of each inhibitory neuron subtype that stained positive for Npas4. No Npas4 positive inhibitory neurons were observed in the visual cortex of dark housed mice; however, upon light exposure we found induction of Npas4 expression in all inhibitory neuron types (Figure 2.4C-D). Notably, Npas4 was expressed in a greater percentage of SST and VIP positive neurons than in PV positive neurons (Figure 2.4D). This pattern of Npas4 induction across different inhibitory neurons subtypes was also observed when inhibitory neuron subtypes were labeled using antibodies against inhibitory neuron subtype markers instead of genetically encoded fluorescent reporters (Figure 2.5A).

To determine if this variation in Npas4 induction between inhibitory neuron subtypes reflects differences in their innate transcriptional properties, we grew mixed cortical cultures (E16.5 Ctx), which contain ~20% inhibitory neurons. These cultures were silenced, depolarized with KCl, and stained with antibodies directed

Figure 2.4: Npas4 is induced in inhibitory neurons by neuronal activity

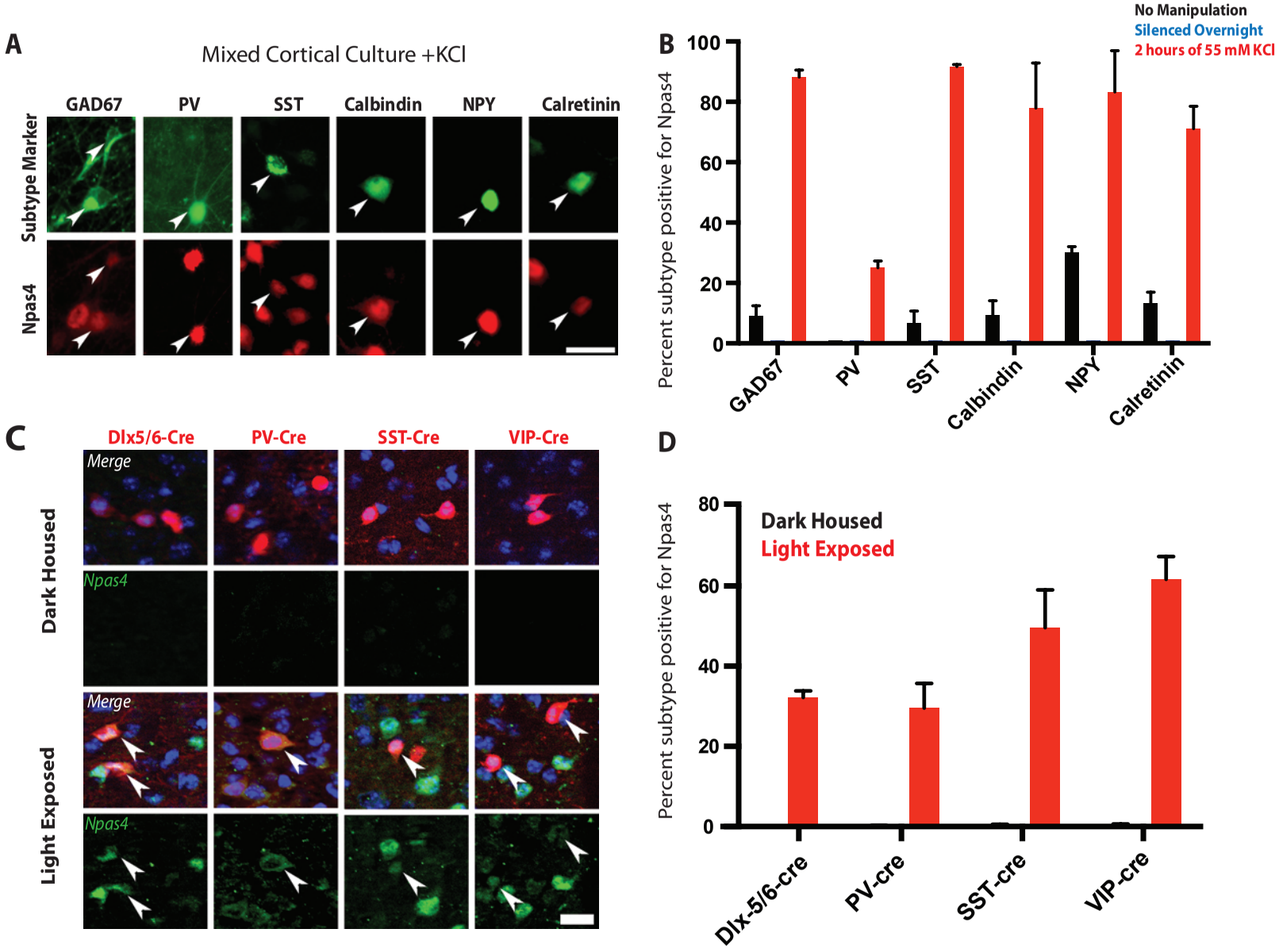

Figure 2.4 (Continued): Npas4 is induced in inhibitory neurons by neuronal activity

A) Representative images of immunolabeling for Npas4 (red) and antibodies directed against markers of different inhibitory neuron subtypes (green, arrowheads) in DIV14 mixed cortical cultures after 2 hours of depolarization with elevated KCl (Scale bar = 10 μm).
B) Percentage of different inhibitory neuron subtypes positive for Npas4 immunostaining in unperturbed DIV14 cortical cultures (black), after silencing overnight with TTX and AP-5 (blue), or after silencing overnight and subsequent exposure to 55 mM KCl for 2 hours (red) (Error bars represent SEM from three biological replicates).
C) Representative images of immunolabeling for Npas4 (green) in the visual cortex of P24 mice in which different types of inhibitory neurons are genetically labeled by a tdTomato cre reporter (red). After dark housing there is almost no Npas4 expression in the visual cortex, but after dark housing and 2.5 hours of light-exposure, Npas4 expression is induced in both inhibitory neurons (arrowheads) and surrounding excitatory neurons (Scale bar = 5 μm).
D) The percentage of inhibitory neuron subtypes positive for Npas4 immunostaining in visual cortex from P24 mice dark housed for four days (black) or dark housed and subsequently light exposed for 2.5 hours (red, error bars represent SEM from three biological replicates).

Figure 2.5: Npas4 is expressed in multiple inhibitory neuron subtypes

A

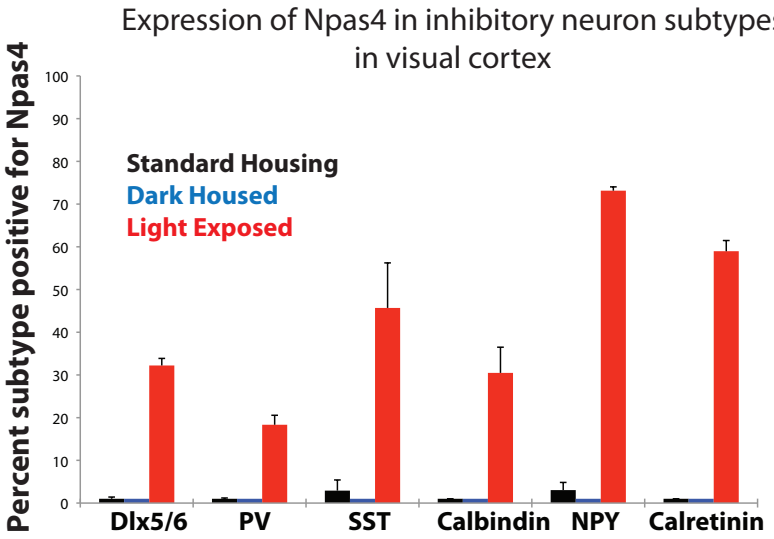

B

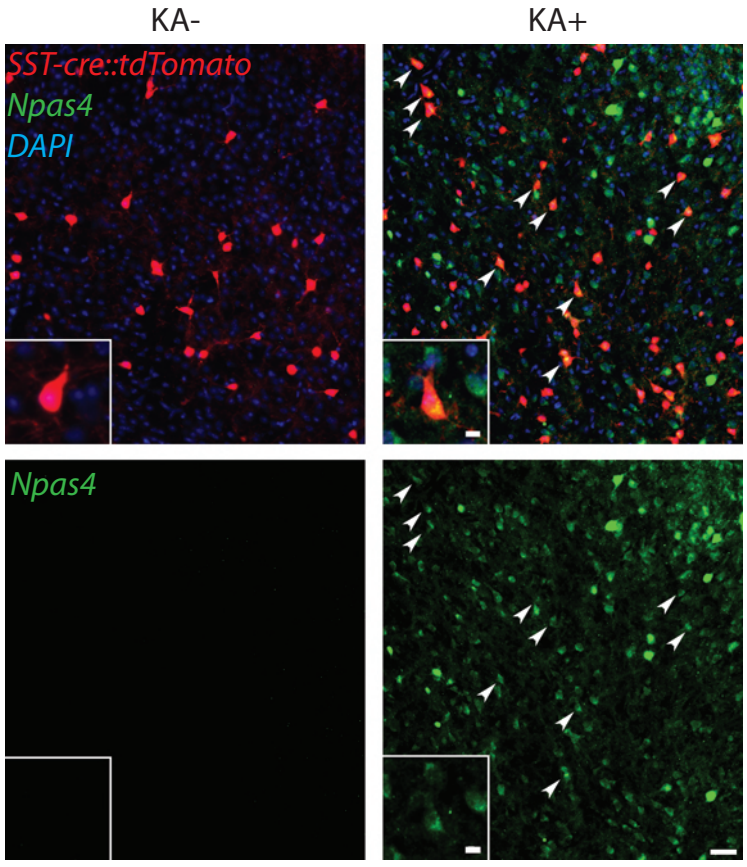

Figure 2.5 (Continued): Npas4 is expressed in multiple inhibitory neuron subtypes

A) Bar graph showing the percentage of inhibitory neuron subtypes that stained positive for Npas4 in the visual cortex of P24 wild-type mice raised in standard housing (black), dark housed for four days (blue), or dark housed and subsequently light exposed for 2.5 hours (red). Inhibitory neuron subtypes were labeled using antibodies directed against protein markers of inhibitory neurons. Error bars represent SEM from three biological replicates.
B) Neuronal activity induces Npas4 expression in SST neurons in young animals. Immunolabeling for Npas4 (green) in P11 mouse visual cortex shows before (KA-, left) or two hours after administration of 3 mg/ml kainic acid (KA+, right). SST neurons that stained positive for Npas4 are labeled with white arrowheads (Scale bar = 10 μm, 5 μm on inset).

against Npas4 and markers of different inhibitory neuron subtypes. Using immunofluorescence microscopy, we quantified the percentage of each inhibitory subtype that stained positive for Npas4. We found that no inhibitory neurons expressed Npas4 after the cultures were silenced, but that most inhibitory neurons expressed Npas4 after membrane depolarization (Figure 2.4A-B). The sole exceptions were PV-expressing neurons: only one quarter (25 ± 2.27% of PV-positive neurons) expressed Npas4 after depolarization. This observation suggests that the Npas4-expressing PV-positive neurons may represent a distinct set of PV neurons uniquely capable of inducing Npas4 expression. Similar profiles of both Npas4 and c-Fos induction are seen across inhibitory subtypes in response to other activity stimuli, including bath application of NMDA and kainate, which directly activate glutamate receptors, or picrotoxin, which inhibits GABA receptors (data not shown). These data indicate that while Npas4 is broadly induced across inhibitory neuron subtypes in response to neuronal activity, its expression may be restricted to a subclass of PV positive inhibitory neurons.

Npas4 regulates the development of excitatory, but not inhibitory, synapses formed on somatostatin positive inhibitory neurons

Having shown that Npas4 is induced in inhibitory neurons *in vivo* by sensory stimulation, we sought to determine the function of Npas4 in inhibitory neurons. We pursued the investigation into Npas4's function in somatostatin-expressing neurons because they robustly express Npas4 both in culture and *in vivo*, are genetically accessible, and have a well defined biological role mediating feedback inhibition to pyramidal cell dendrites (Silberberg and Markram, 2007),(Taniguchi et al., 2011). To determine Npas4's function in SST neurons, we used a genetic strategy to selectively remove Npas4 from SST neurons. To this end, we prepared dissociated E16.5 cortical cultures from embryos heterozygous for an allele expressing Cre recombinase under the control of the somatostatin locus, and an allele harboring a Cre-dependent tdTomato fluorescent reporter. These embryos

were homozygous for either a WT-allele of Npas4 (WT) or an Npas4-allele flanked by LoxP-sites allowing for Cre-conditional knockout of Npas4 (cKO) (Lin et al., 2008). SST-cre effectively labeled SST expressing neurons in these cultures, as over 98% of tdTomato positive neurons were also positive for somatostatin by immunofluorescence (Figure 2.6A). Furthermore, SST-Cre efficiently excised the floxed Npas4 allele, as KCl-induced Npas4 expression in labeled SST neurons was abolished in the cKO cultures (Figure 2.6B).

We first asked whether, as in excitatory neurons, Npas4 regulates the development of inhibitory synapses formed onto SST positive neurons. To this end, we quantified the density of inhibitory synapses formed onto SST neurons by immunolabeling WT and cKO cultures with two independent sets of markers for inhibitory synapses: GABAR β2/3 / GAD65 and GABAR γ2 / VGAT. We determined the density of inhibitory synapses by counting the number of pre- and post-synaptic marker co-clusters that overlapped with fluorescently labeled SST neuron dendrites, and dividing by the total dendritic area. This analysis revealed that deletion of Npas4 had no effect on the density of inhibitory synapses formed onto SST expressing neurons, consistent with the finding that Bdnf is not expressed by inhibitory neurons (Figure 2.7C-D).

To determine whether Npas4 regulates the development of excitatory input to SST neurons, we performed similar experiments to quantify the density of excitatory synapses formed onto SST neurons. We found that selective deletion of Npas4 in SST neurons resulted in significantly lower excitatory synapse density as measured by overlap of both PSD-95/Synapsin-1 and Vglut1/GluA1 (Figure 2.7A-B). Deletion of Npas4 had no effect on cell survival (data not shown), and did not appear to result in a generalized deterioration of cell health, since neither total cell size nor the complexity of proximal dendrites was significantly affected by loss of Npas4 (Figure 2.7C-D). These results indicate that Npas4 specifically controls the development of excitatory, but not inhibitory, synaptic inputs onto SST neurons. Strikingly, this phenotype is the opposite of Npas4's previously described function in excitatory neurons, suggesting that its biological role is cell-type specific (Lin et

Figure 2.6: Selective removal of Npas4 from SST neurons in dissociated E16.5 cortical cultures

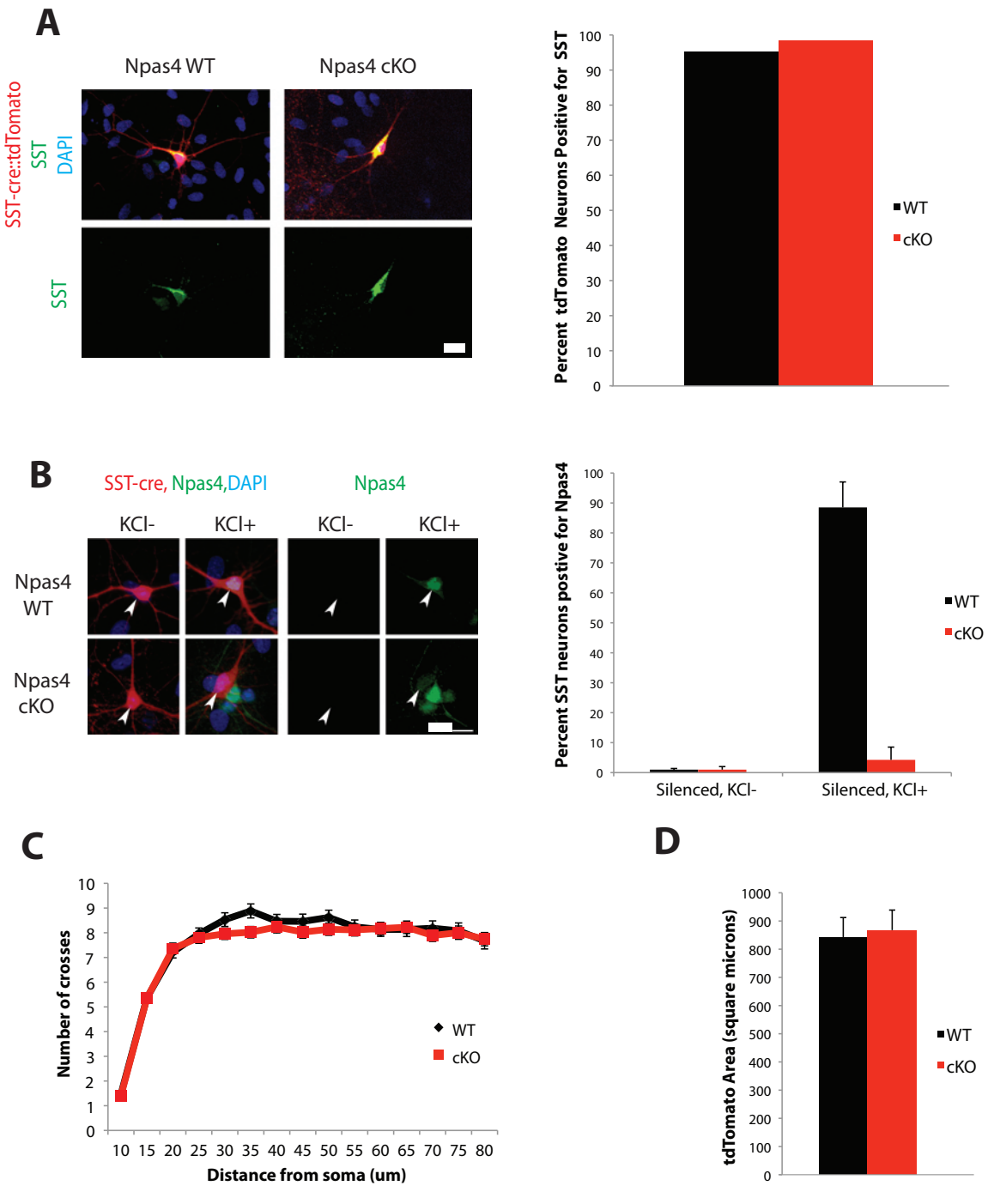

Figure 2.6 (Continued): Selective removal of Npas4 from SST neurons in dissociated E16.5 cortical cultures

A) SST-Cre faithfully labels SST neurons in dissociated cortical cultures. Left, representative images of immunolabeling for somatostatin in Npas4 WT or cKO DIV14 cortical cultures in which expression of SST-cre is reported by a tdTomato cre reporter allele (Scale bar = 10 μm). Right, quantification of the percentage of SST-cre::tdTomato labeled cells that stain positive for SST protein.
B) SST-Cre efficiently recombines the floxed Npas4-cKO allele in SST neurons in culture. Left, example images from Npas4 WT (top) or Npas4 cKO (bottom) DIV14 E16.5 cortical cultures silenced overnight (KCl-) or silenced overnight and subsequently depolarized for 2 hours with 55 mM KCl (KCl+). Labeled SST neurons (red, arrowheads) are stained for Npas4 (green, scale bar = 10 μm). Right, graph showing the percentage of labeled SST neurons that stain positive for Npas4 before or after depolarized (error bars represent SEM from 2 biological replicates).
C) Selective deletion of Npas4 does not significantly alter the complexity of proximal dendrites in SST neurons in E16.5 cortical cultures. Sholl analysis of tdTomato-labeled SST neurons in cortical cultures at DIV 14 either WT or cKO for Npas4 indicates that genetic ablation of Npas4 in SST interneurons does not affect proximal dendrite complexity.
D) Lack of Npas4 does not significantly alter dendritic area in SST neurons in E16.5 cortical cultures. Quantification of total dendritic area of tdTomato-labeled SST interneurons in cortical cultures at DIV 14 either WT or cKO for Npas4 (error bars represent SEM from three independent biological replicates).

Figure 2.7: Deletion of Npas4 in SST neurons in vitro results in decreased density of excitatory, but not inhibitory, synapses

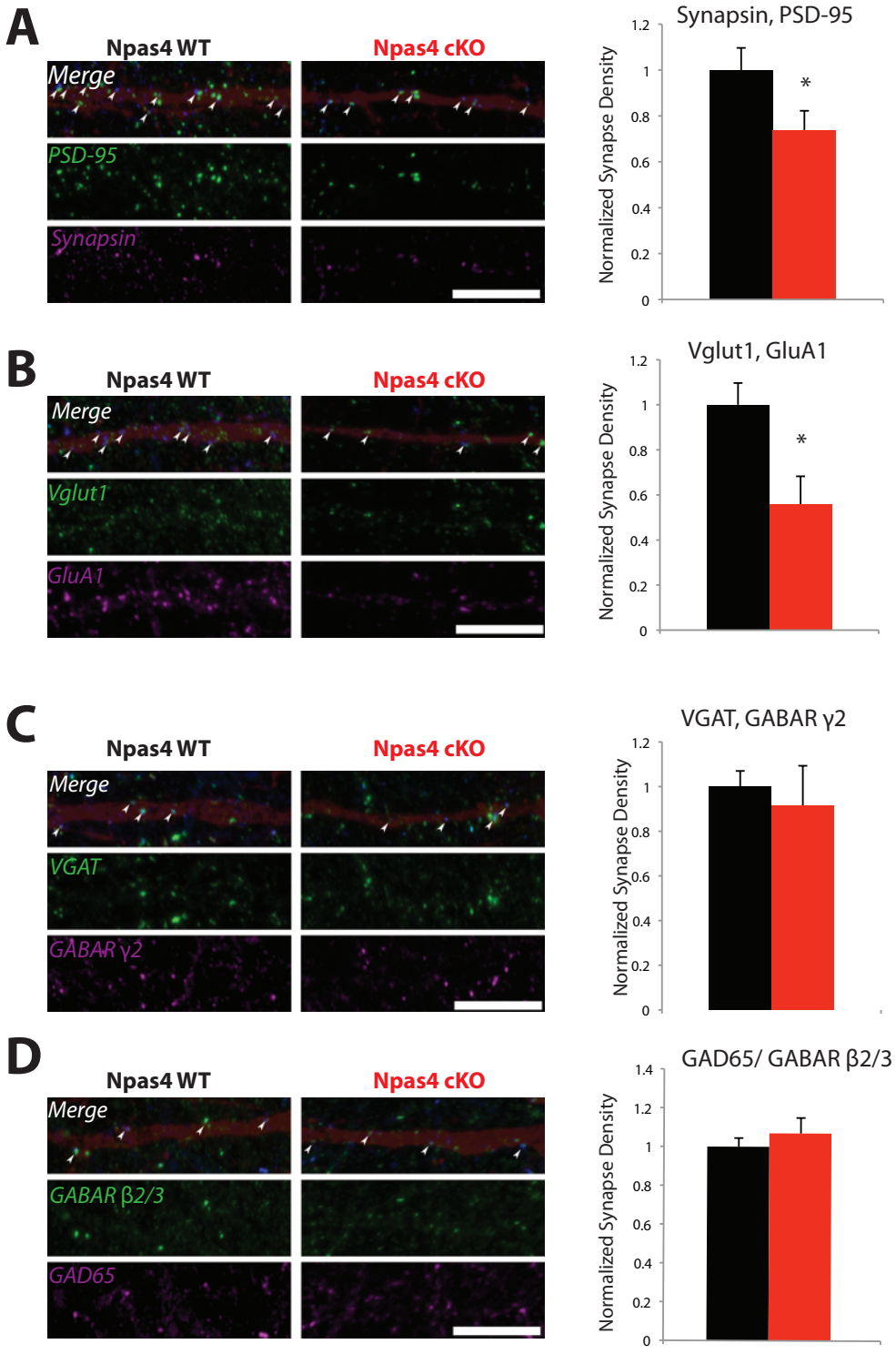

Figure 2.7 (Continued): Deletion of Npas4 in SST neurons *in vitro* results in decreased density of excitatory, but not inhibitory, synapses.

Dissociated cortical cultures were prepared from E16.5 Npas4 WT or cKO embryos with SST neurons labeled by tdTomato reporting SST-cre expression. At DIV14, cultures were immunolabeled for pairs of pre- and postsynaptic markers (Left, scale bars = 10 μm). Synapse density is expressed as the normalized density of co-clustered pre and post-synaptic markers along tdTomato positive dendrites (red, translucent); graphs on the right represent the mean and SEM of 3 independent biological replicates.

A) Example images of excitatory synapse markers PSD-95 (green) and Synapsin-1 (magenta). The density of PSD-95/Synapsin-1 co-clusters (arrows) was significantly decreased in SST neurons lacking Npas4 ($P < 0.03$, WT n = 97, cKO n=62 neurons).

B) Example images of excitatory synapse markers Vglut1 (green) and GluA1 (magenta). The density of GluA1/Vglut1 co-clusters (arrows) was significantly decreased in SST neurons lacking Npas4 ($P < 0.03$, WT n= 74, cKO n=100 neurons).

C) Example images of inhibitory synapse markers VGAT (green) and GABA-R γ2 (magenta). No change in the density of VGAT / GABA-R γ2 co-clusters (arrows) was detected in SST neurons lacking Npas4 ($P < 0.534$, WT n = 73, cKO n=84 neurons).

D) Example images of inhibitory synapse markers GABA-R β2/3 (green) and Gad65 (magenta). No change in the density of GAD65 / GABA-R β2/3 co-clusters was detected in SST neurons lacking Npas4 ($P < 0.43$, WT n = 68, cKO n=71 neurons).

al., 2008). This data supports the hypothesis that common activity-induced transcription factors regulate cell-type specific functions.

We next asked whether, in addition to controlling synapse number in neuronal cultures, Npas4 also controls the development of functional excitatory synapses onto SST neurons *ex vivo*. To this end, we used the previously described genetic strategy to conditionally delete Npas4 from tdTomato labeled SST neurons. We focused these experiments on the visual cortex at P10-12 for several reasons: first, this age matched the developmental stage of experiments performed in culture, and therefore provided the best conditions to translate the phenotype in cultured SST neurons into the intact organism. Furthermore, large calcium waves sweep through the cortex before eye opening, providing a strong source of neuronal activity, increasing the likelihood of uncovering an activity-dependent phenotype (Garaschuk et al., 2000),(Rochefort et al., 2009). Finally, focusing on an earlier point in development increases the likelihood of capturing primary phenotypes caused by removal of Npas4. *In vivo*, SST-cre efficiently excised the Npas4 floxed allele, and SST-cre labeled somatostatin expressing neurons, but not VIP or PV positive neurons (Figure 2.8B-C). Notably, Npas4 is observable in SST neurons at P11, and is robustly expressed in SST neurons after kainate seizure at this age (Figure 2.5B).

To test whether Npas4 controls the development of functional excitatory synapses formed onto SST neurons, we prepared acute brain slices containing primary visual cortex from brains of P10-P12 WT or cKO mice, obtained whole-cell patch-clamp recordings from SST neurons, and measured miniature excitatory postsynaptic currents (mEPSCs, Figure 2.9A). Pharmacologically isolated mEPSCs were blocked by NBQX and CPP, demonstrating that they are mediated by glutamate receptors (Figure 2.10C, n = 3). Conditional deletion of Npas4 resulted in a significant decrease in the frequency of mEPSCs (WT: 0.91±0.168 Hz, n = 15 versus cKO 0.39±0.054 Hz, n = 19; P = 0.003, Figure 2.9C). We did not observe any change in mEPSC amplitude or kinetics, suggesting that deletion of Npas4 from SST neurons selectively alters mEPSC frequency (WT: 23.19 ± 1.54 pA, n = 15 versus cKO 23.64 ± 1.68 pA, n = 19; P = 0.847, Figure 2.9B, 2.10D). Reduced mEPSC event frequency can

Figure 2.8: Selective deletion of Npas4 from SST neurons in vivo

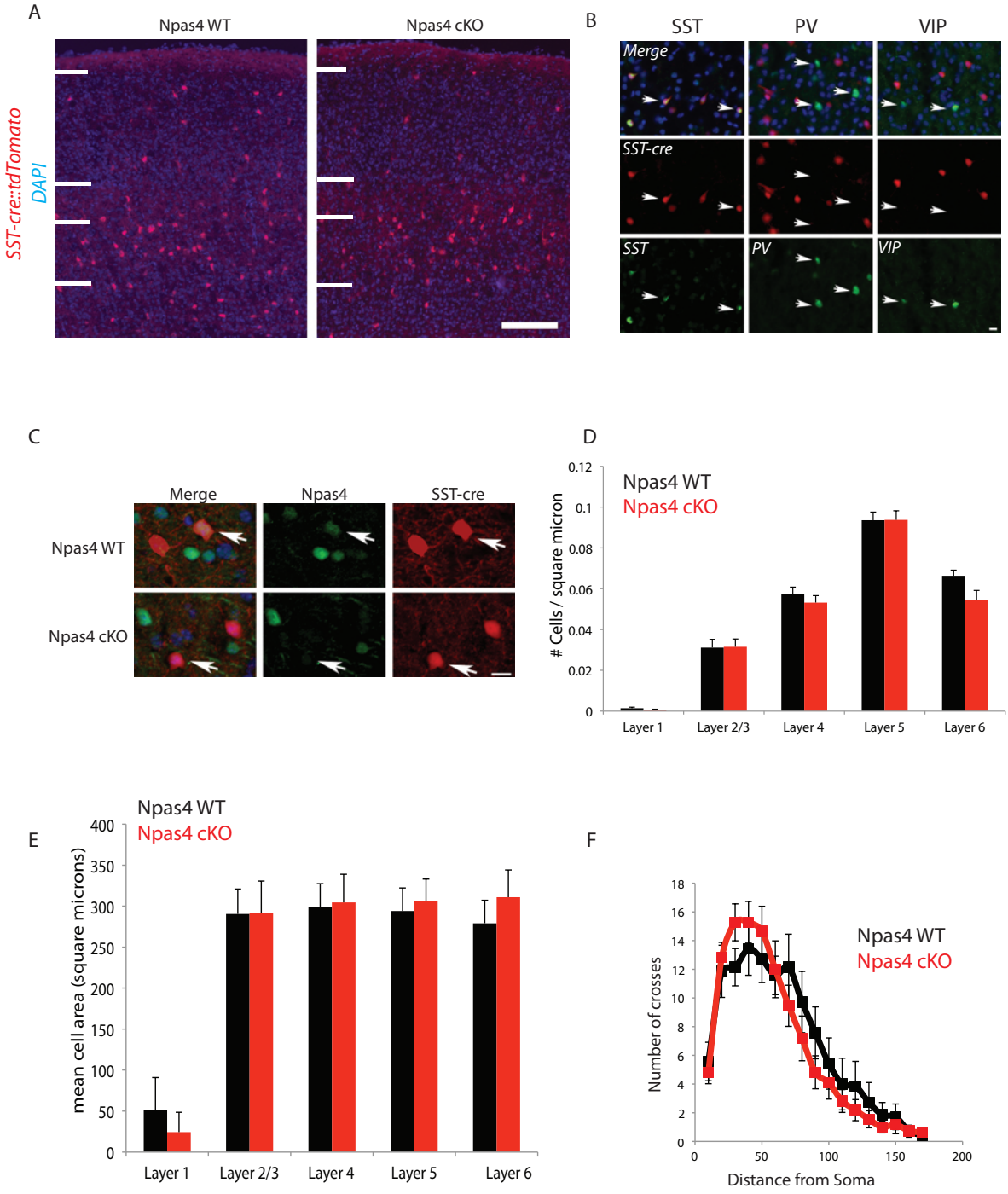

Figure 2.8 (Continued): Selective deletion of Npas4 from SST neurons *in vivo*

A) Example images of coronal sections through the visual cortex of P10-12 Npas4 WT ($Npas4^{wt/wt}$, left) or cKO ($Npas4^{fl/fl}$, right) SST-$Cre^{wt/Cre}$ x $tdTomato^{wt/ki}$ mice. DAPI (blue) marks nuclei and tdTomato (red) reports SST-Cre expression to label SST positive inhibitory neurons (Scalebar = 250 μm).
B) Validation of SST-Cre specificity in the visual cortex. tdTomato reporting SST-Cre expression (red) labels neurons that stain positive for somatostatin, but not parvalbumin or vasointestinal peptide (green, arrows). (Scalebar = 10 μm).
C) SST-Cre excises the floxed Npas4 allele. P24 Npas4 WT (top) or cKO (bottom) were dark housed starting at P20 and exposed to light for 2 hours at P24. Npas4 (green) is expressed in roughly half of SST neurons (red) in visual cortex in WT, but is absent from SST neurons in the visual cortex of Npas4 cKO neurons (arrow).
D) Lack of Npas4 does not affect layer distribution or total number of SST neurons in the visual cortex. Quantification of tdTomato-labeled SST neuron density by cortical layer indicates that conditional deletion of Npas4 does not impact SST neuron survival or migration (Error bars represent SEM from three biological replicates).
E) Lack of Npas4 does not affect soma size of SST neurons in the visual cortex. Quantification of average cell body area by cortical layer suggests that conditional deletion of Npas4 from SST neurons does not impact soma size (Error bars represent SEM from three independent biological replicates).
F) Sholl analysis of Npas4 WT or cKO SST neurons in the P11 visual cortex visualized by a DAB reaction against neurobiotin injected using a patch pipette. Lack of Npas4 in SST neurons does not significantly affect dendritic complexity of these neurons ($P = 0.244$, repeated measures ANOVA, WT n =9, cKO n = 11).

Figure 2.9: Npas4 regulates the development of functional excitatory synapses onto SST positive inhibitory neurons

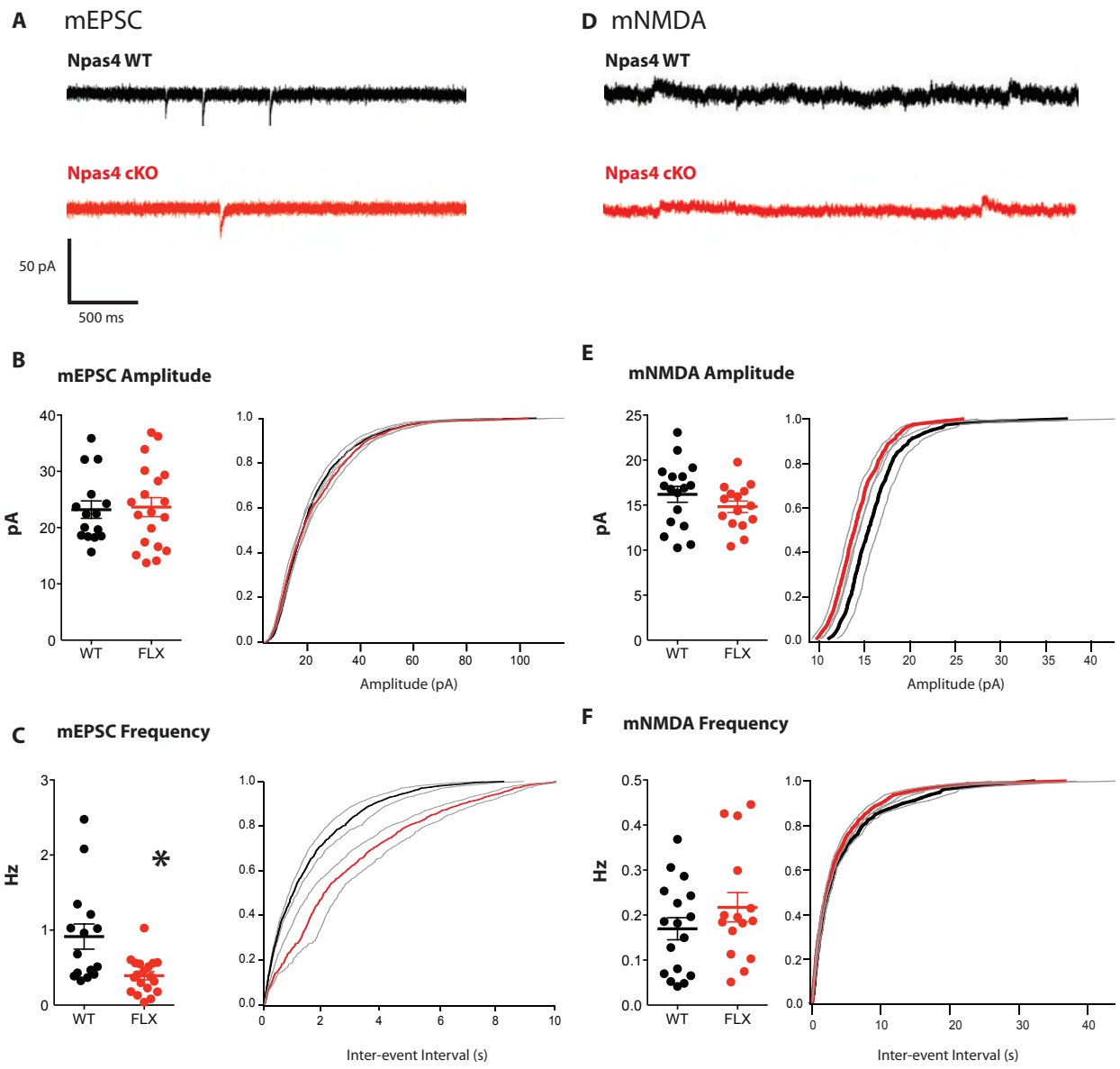

Figure 2.9 (Continued): Npas4 regulates the development of functional excitatory synapses onto SST inhibitory neurons

A) Example traces of mEPSCs recorded from wild type (black) or Npas4 cKO (red) SST positive inhibitory neurons in acute slices of visual cortex from P10-12 animals (WT n= 15, cKO n=19, scalebar = 50 pA, 500 ms).
B) Selective deletion of Npas4 in SST neurons does not significantly affect mEPSC amplitude (P = 0.847, Mann-Whitney U-Test). Left, circles represent the average event amplitude for individual neurons from WT (black) or Npas4 cKO (red) animals, while the bars represent population averages and SEM. Right, cumulative distribution plot shows the mean and SEM (gray lines) of the mEPSC amplitude distribution from all neurons sampled.
C) Selective deletion of Npas4 in SST neurons significantly decreases mEPSC frequency (P <0.003, Mann-Whitney U-Test). Left, circles represent mEPSC frequency of individual neurons from WT (black) or Npas4 cKO (red) animals, while bars are population averages and SEM. Right, cumulative distribution plot shows the mean and SEM (gray lines) of the inter-event interval distributions from all neurons sampled in each genotype.
D) Example traces of NMDA mediated miniature events (mNMDA) recorded from wild type (black) or Npas4 cKO (red) SST positive neurons in acute slices of visual cortex from P10-12 animals (WT n= 17, cKO n=15, scalebar = 50 pA, 500 ms).
E) Selective deletion of Npas4 in SST interneurons does not significantly alter mNMDA amplitude (P = 0.224, Mann-Whitney U-Test). Left, circles represent the average event amplitude for individual neurons from WT (black) or Npas4 cKO (red) brains, while bars are population averages and SEM. Right, cumulative distribution shows the mean and SEM (gray lines) of the amplitude distribution from all neurons sampled.
F) Selective deletion of Npas4 in SST interneurons does not significantly affect mNMDA event frequency (P = 0.244, Mann-Whitney U-Test). Left, circles represent average event frequency for individual neurons from WT (black) or Npas4 cKO (red) animals, while bars show population averages and SEM. Right, cumulative

Figure 2.9 (Continued):

distribution shows the mean and SEM (gray lines) of the inter-event interval for all neurons sampled.

Figure 2.10: Selective deletion of Npas4 from SST neurons does not affect mIPSCs or event kinetics

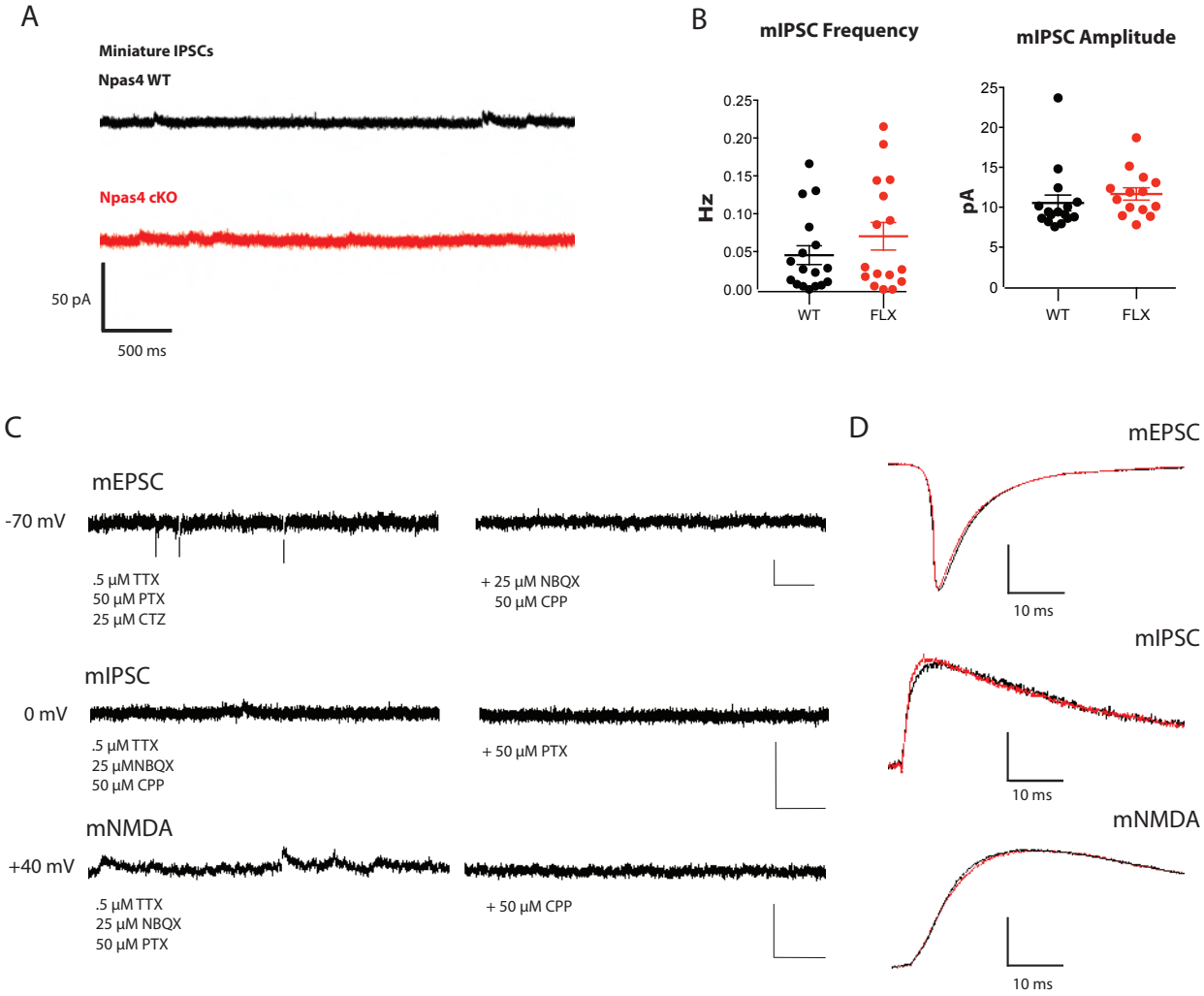

Figure 2.10 (Continued): Selective deletion of Npas4 from SST neurons does not affect mIPSCs or event kinetics

A) Example traces of mIPSC from Npas4 WT (black, top) or cKO (red, bottom) SST neurons in acute slices from P11 visual cortex (Scale bar = 50 pA, 500 ms).
B) Deletion of Npas4 in SST inhibitory neurons does not significantly alter mIPSC frequency or amplitude (WT n= 17, cKO n=16; P = 0.261 and 0.386, respectively, by Mann-Whitney U-Test). Circles are individual cells from Npas4 WT (black) or Npas4 cKO (red) brains, bars represent population mean and SEM.
C) Pharmacological blockade of miniature currents. Top, example trace of mEPSCs held at -70 mV; events were blocked by application of NBQX and CPP. Middle, example trace of mIPSCs held at 0 mV; events were blocked by application of picrotoxin. Bottom, example traces of NMDA mediated miniature currents held at +40 mV. Events were blocked by application of CPP. Blockade of mNMDA currents did not result in a decrease in average trace noise. Scalebars for all traces are 50 pA and 500 ms for all traces, n = 2 cells for each pharmacological blockade.
D) Normalized average traces from wild type (black) or Npas4 cKO (red) SST neurons for mEPSCs (top), mIPSCs (middle), and mNMDA currents (bottom). Scalebars = 10 ms.

arise from decreased presynaptic probability of release or from fewer functional excitatory synapses. The reduction in the density of excitatory synapses formed onto SST neurons in culture, combined with the fact that excitatory inputs to SST neurons are not genetically perturbed in either WT or cKO mice, suggests that the decrease in mEPSC frequency may reflect a change in the number of functional synapses.

However, a decrease in the number of functional synapses could reflect either a decrease in the total number of structural synapses or a decrease in the number of synapses that contain AMPA receptors. To distinguish between these two possibilities, we measured the miniature excitatory postsynaptic currents mediated by NMDA receptors (mNMDAs, Figure 2.9D). A change in either presynaptic probability of release or in the number of physical synaptic contacts should result in decreased mNMDA frequency similar to the observed change in mEPSC frequency; however, normal mNMDA currents in SST neurons lacking Npas4 would be consistent with reduced AMPA receptor numbers at a subset of excitatory synapses.

NMDA mediated miniature events were isolated by holding neurons at +40 mV and blocking AMPA and inhibitory currents with NBQX and picrotoxin, respectively. mNDMA currents were blocked by the application of the NMDA receptor antagonist CPP (Figure 2.10C, n = 2). No significant difference in mNMDA event frequency was detected upon deletion of Npas4 (WT: 0.169±0.024 Hz, n = 17; cKO: 0.217±0.0325 Hz, n = 15, p = 0.244, Figure 2.9F). Furthermore, neither the amplitude of mNMDA currents nor the average event kinetics was significantly affected by Npas4 deletion (WT: 16.19±0.87 pA, n = 17; cKO: 14.817±0.64 pA, n = 15, p = 0.224, Figure 2.9E, 2.10D). The NMDA receptor mediated component of a single mEPSC is often a small fraction of the magnitude of the total current, so it was not surprising that the absolute frequency of mNMDA events was lower than the frequency of mEPSCs in wild-type SST neurons (Watt et al., 2000),(Burgard and Hablitz, 1993). These results are consistent with a model in which selective deletion

of Npas4 from SST inhibitory neurons results in a decrease in the number of excitatory synapses that contain AMPA receptors.

Finally, to determine whether Npas4 also regulates inhibition onto SST neurons, we recorded miniature inhibitory postsynaptic currents (mIPSCs) from SST neurons in acute slices made from P10-P12 visual cortex (Figure 2.10A). At this early stage of inhibitory development, mIPSC events onto SST neurons were infrequent; blockade of mIPSCs by application of picrotoxin demonstrated that the events were mediated by GABA-A receptors (Figure 2.10C, n = 2). Deletion of Npas4 from SST neurons did not result in a significant change in mIPSC frequency (WT: 0.045±0.012 Hz, n = 17; cKO: 0.07±0.018 Hz, n = 16, P = 0.261 Figure 2.10B). Miniature IPSC amplitude and average waveform kinetics were also unaffected by deletion of Npas4 (WT: 10.53 ± 0.98 pA, n=17; cKO: 11.65 ± 0.772, n = 16; p = 0.386 Figure 2.10B,D). These data are consistent with the quantification of inhibitory synapse number on SST neurons in dissociated cortical cultures, and further demonstrate that Npas4's role in SST neurons is to specifically regulate the development of excitatory synapses.

Conditional Deletion of Npas4 from Somatostatin Neurons *in vivo* does not result in morphological abnormalities

To assess whether the synaptic phenotype observed upon removing Npas4 from SST neurons could be secondary to a morphological defect, we characterized SST neurons in the visual cortex of P10-12 WT and cKO mice. The cortices of cKO mice appeared grossly normal as compared to their wild-type littermates, and we found no change in the number or laminar distribution of SST neurons across the different cortical layers, indicating that Npas4 is not required for SST neuron migration, differentiation, or survival (Figure 2.8D). Conditional deletion of Npas4 in SST neurons did not affect soma size (Figure 2.8E), and SST neurons lacking Npas4 appeared to normally extend and elaborate axons to target distal dendrites, as evidenced by the presence of bright bands of tdTomato in layer 1 of the cortex in

both genotypes (Figure 2.8A). To determine whether Npas4 is required for normal growth of SST neuron dendrites, we quantified the dendritic complexity of WT and cKO SST neurons by Sholl analysis. This analysis demonstrated that Npas4 does not regulate the dendritic complexity of SST neurons (Figure 2.8F, $P < 0.244$ repeated measures ANOVA; WT: n = 9, cKO, n = 11). In summary, morphological analysis demonstrates that selective removal of Npas4 from SST neurons affects neither overall cortical structure nor the number or morphology of the SST neurons in the cortex.

Together, these data strongly support a specific role for Npas4 in promoting development of excitatory synapses on somatostatin positive inhibitory neurons. This function for Npas4 is the opposite of its role in excitatory neurons, and strongly supports the hypothesis that activity-induced early response transcription factors are common integrators of activity that can execute cell-type specific functions. Given that inhibitory neurons do not transcribe Bdnf, Npas4's major target gene in excitatory neurons, it is likely that Npas4 regulates a distinct set of genes in inhibitory neurons. To investigate possible mechanisms by which Npas4 controls the development of excitatory synapses formed onto inhibitory neurons, we performed a genome-wide investigation to identify Npas4's transcriptional targets in inhibitory interneurons.

Npas4 Controls an Activity-Induced Transcriptional Program in Inhibitory Neurons

To identify Npas4 target genes in inhibitory neurons, we prepared MGE-derived cultures from Npas4 knockout embryos and their wild type littermates. These cultures were silenced overnight, depolarized with elevated extracellular KCl for 0, 1, or 6 hours, and total RNA was isolated. By quantitative RT-PCR analysis, we found that Npas4 was strongly induced after 1 hour of depolarization in wild type cultures, and that no Npas4 signal was detected in Npas4 knockout cultures. However, the early-response gene Fos was strongly induced by membrane depolarization in MGE cultures from both genotypes, indicating that they both

responded to membrane depolarization (Figure 2.11A). To identify transcriptional targets of Npas4 in inhibitory neurons, RNA isolated from WT and Npas4 KO MGE-derived cultures was subjected to genome wide microarray analysis.

Npas4 has been reported to regulate the expression of a broad set of early-response genes induced by membrane depolarization in excitatory hippocampal neurons (Lin et al., 2008), (Ramamoorthi et al., 2011). To determine whether Npas4 regulates similar genes in inhibitory neurons, we calculated the 0-1 hour fold induction (1 hour signal / 0 h signal) for every probeset, and identified probesets induced 2-fold or more in wild type MGE cultures (n = 83). The induction of these probesets was not significantly altered by the removal of Npas4 (Figure 2.11B, P = 0.1052, Wilcox signed-rank test). Since Npas4 does not regulate the induction of early-response genes in inhibitory neurons, we next asked whether Npas4 controls the induction of late-response genes. To this end, we calculated the 0-6 hour fold induction (6 hour signal / 0 hour signal) for every probeset, and identified probesets induced 2-fold or more in wild type MGE cultures after 6 hours of membrane depolarization (n = 432). We found that loss of Npas4 significantly decreased the 0-6 hour fold induction of these late-response genes, demonstrating that Npas4 regulates a transcriptional response to neuronal activity in inhibitory neurons (Figure 2.11C, $P < 1 \times 10^{-20}$, Wilcox signed-rank test). The decreased induction of late-response genes likely reflects Npas4's role as a transcriptional activator, since there is no corresponding population of probesets that is more highly induced when Npas4 is removed (Figure 2.11C). Importantly, only a sub-population of late-response genes is misregulated upon loss of Npas4, suggesting that Npas4 regulates a specific program of late-induced genes. To validate the microarrays, we performed qPCR analysis of activity regulated Npas4 target genes in an independent biological replicate, and found that this validation faithfully reproduced both the induction of the late response genes by membrane depolarization and their misregulation upon removal of Npas4 (Figure 2.11D).

To gain insight into the mechanism by which Npas4 regulates synapse development, we next sought to identify the specific late-response genes that are regulated by Npas4. To this end, we divided the 6-hour microarray signal of every

late-induced probeset in Npas4 KO MGE cultures by the 6-hour signal in wild type MGE cultures, allowing us to directly compare the magnitude of the effect of removing Npas4 across all probesets (Figure 2.11E). Using this approach, we identified the Npas4 target genes that were most greatly affected by loss of Npas4 in MGE cultures (Figure 2.11F).

To determine how the transcriptional program regulated by Npas4 in inhibitory neurons differs from excitatory neurons, we asked whether these MGE Npas4 target genes were expressed in E14 cortical cultures, and – if so – whether they were regulated by activity. We found that Npas4 target genes in MGE cultures fell into three categories: expression of some target genes such as Rerg and Chst15 were strongly enriched in inhibitory neurons compared to excitatory neurons. Others, such as Pdzrn3 and Ppm1h, were expressed at similar levels in excitatory and inhibitory neurons, but were only induced by activity in inhibitory neurons. Finally, a third class of genes including Kcna1, Nptx2, and Gpr3 were activity regulated in both cell-types (Figure 2.12A-B). This analysis reveals that in inhibitory neurons, Npas4 regulates a set of activity-dependent late-response genes that is distinct, but not disjoint, from the set of activity-induced late-response genes it regulates in excitatory neurons.

Regulation of Npas4 target genes in SST neurons *in vivo* by neuronal activity

We next asked how Npas4 target genes might mediate Npas4's control of excitatory input to somatostatin neurons. Given the diversity of Npas4 target genes, we hypothesized that multiple target genes acting through distinct mechanisms mediate this function. Npas4 targets genes in inhibitory neurons are predicted to be active in a variety of biological contexts, including regulation of phosphorylation (Ppm1h, Mylk, Stac), membrane excitability (Kcna1), signal transduction (Gpr3, Npr3, Rerg), transcriptional regulation (Zbtb1, Bach2, Lmo2), ubiquitylation (Pdzrn3), scaffolding (Frmpd3), and AMPA receptor trafficking (Nptx2). Few of these targets have been previously described in inhibitory neurons, but some have known functions related to synapses in other systems. For instance, Gpr3 is an

Figure 2.11: Npas4 regulates a cell-type specific activity induced transcriptional program in inhibitory neurons

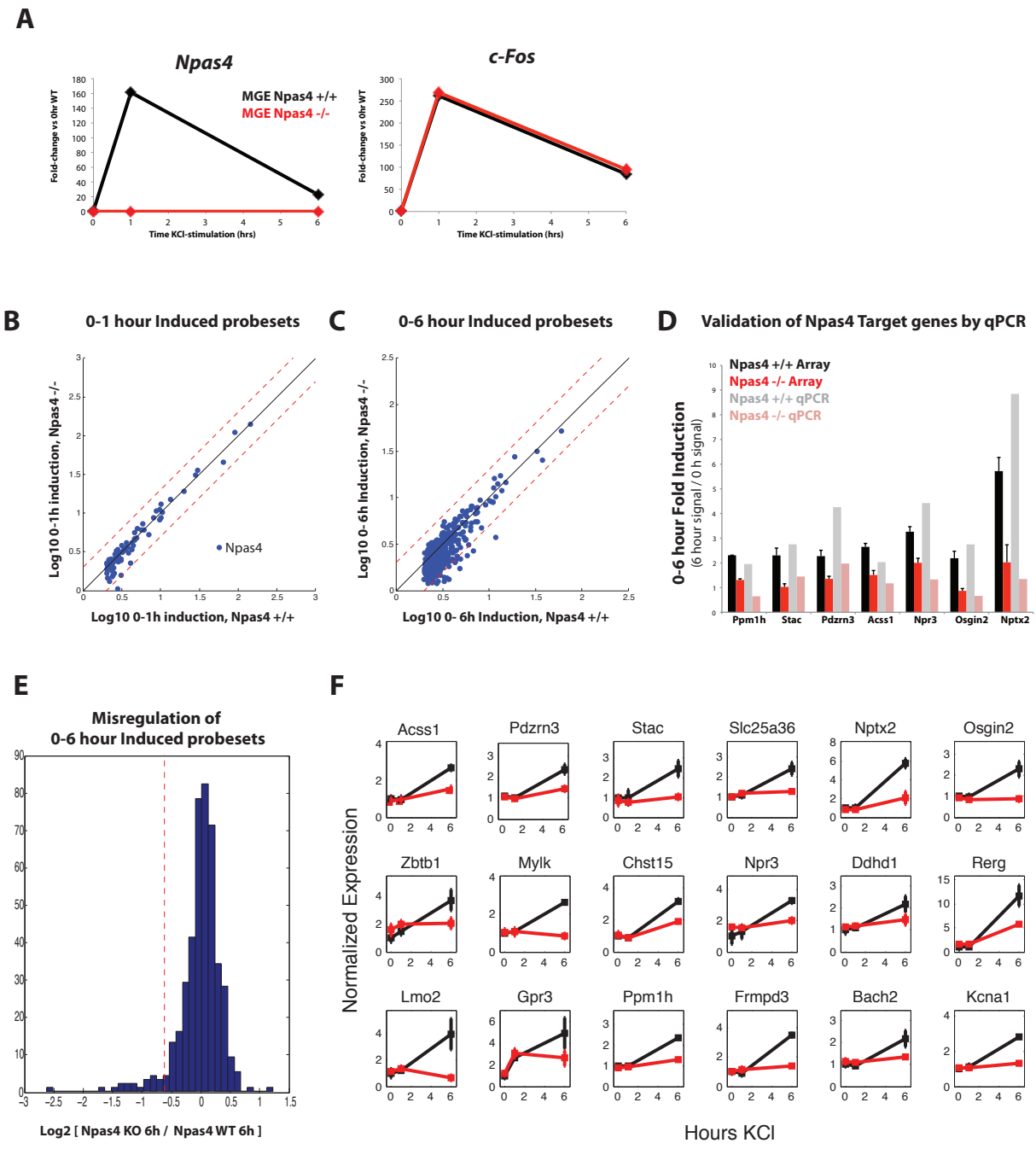

Figure 2.11 (Continued): Npas4 regulates a cell-type specific activity-induced transcriptional program in inhibitory neurons.

A) Quantitative RT-PCR for Npas4 and c-Fos from MGE-derived cultures prepared from E14 wild-type (black) or Npas4 knockout (red) littermate embryos. Cultures were grown to DIV8, silenced overnight with TTX and AP-5, and depolarized for 0, 1, or 6 hours with 55 mM KCl.
B) Genome-wide microarray analysis of depolarized Npas4 +/+ or -/- MGE cultures. Npas4 does not significantly affect the fold-induction of probesets induced 2-fold or more in wild-type MGE cultures. For every probeset induced 2-fold or more in WT MGE cultures at 1 hour (blue dots), the Log10 0-1h fold induction in WT MGE cultures (x-axis) is plotted against the Log10 0-1h fold induction in Npas4 -/- MGE cultures (y-axis). The black line is unity, while the red dotted lines demarcate a 2-fold change in either direction. The solitary outlier is a probeset against Npas4 itself.
C) Npas4 regulates the induction of a set of late-response genes. Scatterplot of every probeset induced 2-fold or more after 6 hours of KCl depolarization in WT MGE cultures (blue dots). The Log10 0-6 hour fold induction in WT MGE cultures is plotted against the Log10 0-6 hour fold induction in Npas4 -/- MGE cultures. The black line is unity, while the red dotted lines demarcate a 2-fold change in either direction.
D) Quantitative RT-PCR validation of the microarray. An independent biological replicate of MGE cultures from E14 Npas4 +/+ or -/- littermate embryos was prepared, silenced overnight with TTX and AP-5 at DIV8, and depolarized for 0 or 6 hours. Quantitative RT-PCR analysis was performed on seven Npas4 target genes, and 0-6 hour fold induction from Npas4 +/+ (gray) or Npas4 -/- (pink) was compared to the 0-6 hour fold induction of the array signal from Npas4 +/+ (black) or -/- (red) MGE cultures.
E) Identification of highly misregulated Npas4 target genes in MGE-derived cultures. Histogram shows the Log2 of the Npas4 -/- 6 hour array signal divided by the Npas4 +/+ 6 hour array signal for every probeset induced 2-fold or more in WT MGE

Figure 2.11 (Continued):

cultures. The dotted red line marks the threshold used to identify highly misregulated probesets. Probesets to the left of the red line are reduced by more than 35% 6 hours after depolarization upon loss of Npas4. Filtering using the six-hour timepoint instead of 0-6 hour fold-induction eliminates the possibility of picking up targets that appear misregulated due to changes at the 0 hour time point. F) Set of high confidence Npas4 target genes in MGE cultures. Plots show the time of depolarization (hours), versus normalized probeset intensity. All time points from Npas4 +/+ MGE cultures (black) and Npas4 -/- MGE cultures (red) are normalized to Npas4 +/+ 0 hour sample. Error bars represent SEM of two independent microarray experiments.

Figure 2.12: Cell-type specificity of Npas4 MGE target genes

A

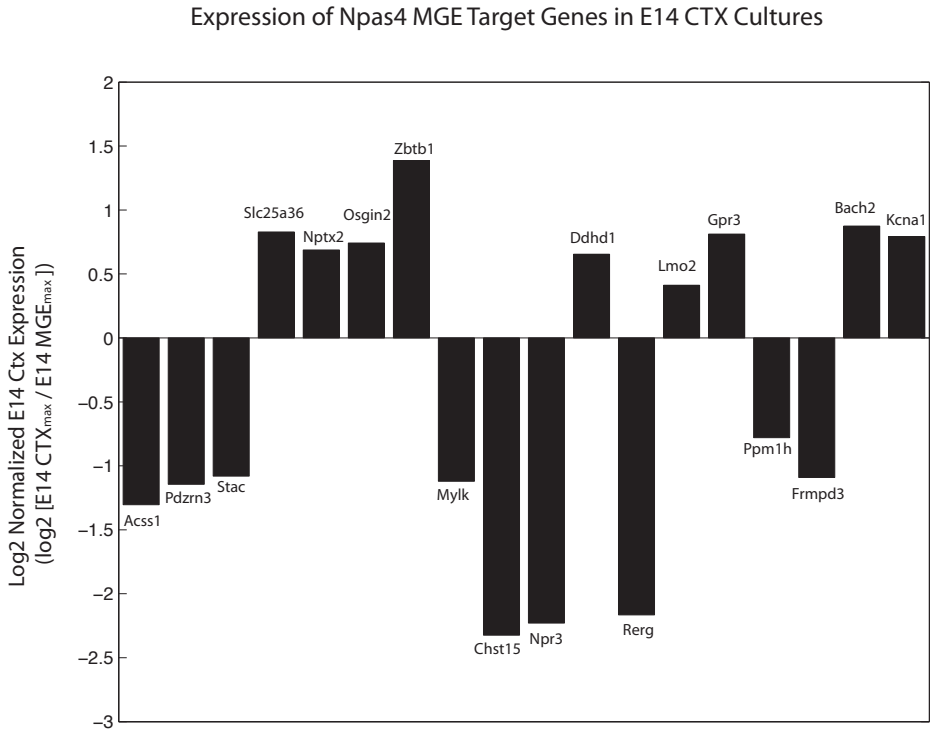

B

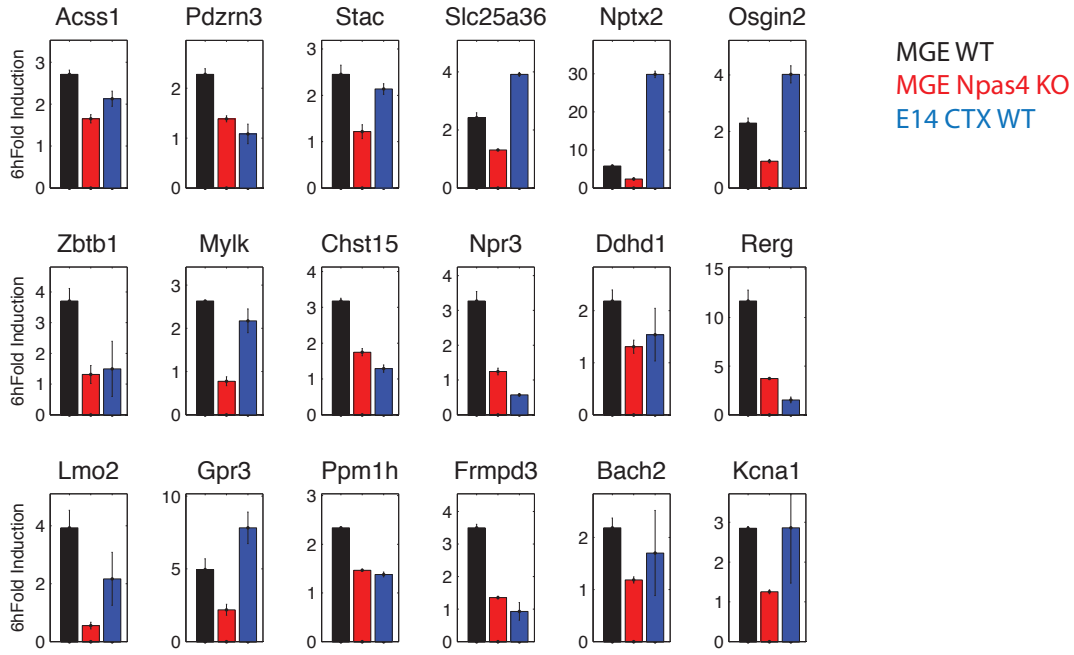

Figure 2.12 (Continued): Cell-type specificity of Npas4 MGE target genes

A) Bar graph for high confidence MGE Npas4 target genes showing their expression level in E14 cortical cultures relative to MGE cultures. The highest probeset intensity across all experimental conditions in WT E14 Cortex was divided by the highest probeset intensity across all experimental conditions in WT MGE-derived cultures, and the Log2 of this value was plotted. A value of 0 indicates that the probeset is equally expressed in both cultures; probesets with negative values are enriched in the MGE cultures, while probesets with positive values are enriched in the E14 cortex cultures.

B) Bar graphs showing the 0-6 hour fold induction of MGE Npas4 target genes in WT MGE cultures (black), Npas4 -/- MGE cultures (red), and wild type E14 cortical cultures (blue). Some genes, including Ppm1h and Pdzrn3 are expressed in E14 cortical cultures, but are not induced in response to membrane depolarization.

adenylate cyclase activator that has been reported to modulate Aβ peptide generation in neurons, while Pdzrn3 is an E3 ubiquitin ligase that regulates neuromuscular junction development and acetylcholine receptor clustering through degradation of MusK (Lu et al., 2007),(Valverde et al., 2009). Additionally, Nptx2 encodes Narp, which mediates excitatory synapse unsilencing in cell-types with smooth dendrites by recruiting AMPA receptors directly to the synapse (Koch and Ullian, 2010),(O'Brien et al., 2002; O'Brien et al., 1999; Xu et al., 2003).

To further investigate which target genes may be involved in mediating Npas4's control over excitatory synapse development in SST neurons, we asked which target genes are induced in SST neurons in response neuronal activity *in vivo*. To this end, we utilized the Ribotag mouse (Sanz et al., 2009), which harbors a cre-conditional HA-tagged ribosomal subunit that allows immunoprecipitation of ribosomally associated RNA from a population of cells defined by expression of Cre recombinase. We placed mice heterozygous for both the ribotag allele and SST-cre in the dark for two weeks and then exposed them to light for 0, 1, 3, or 7.5 hours, whereupon we dissected the visual cortex. Ribosomally associated RNA was immunoprecipitated (IPed) from SST-cre expressing neurons, and RNA was purified and amplified from both the IP (RNA from SST neurons) and input (RNA from entire visual cortex). We assessed the purity of the IP fraction by measuring the fold enrichment of IP over input across all experimental conditions by quantitative RT-PCR. This analysis revealed that, as expected, both somatostatin and GAD1 mRNA was highly enriched in the fraction of RNA that was IPed from SST neurons. In contrast, Vglut1, VIP, and Bdnf mRNA was significantly depleted from the IP fraction, reflecting the lack of expression of these genes in SST neurons, while Npas4 and c-Fos mRNA was present at similar levels in the IP and input fractions, reflecting their strong induction in both SST neurons and many other cortical neurons (Figure 2.13A). We next used this approach to assess whether candidate Npas4 target genes were expressed in SST neurons; we found that with the exception of Acss1, all of the genes that we tested were present in the SST neuron IP fraction (Figure 2.13B). Some genes such as Nptx2 and Pdzrn3 were present at similar concentrations in the IP and input fractions, indicating they are broadly expressed in the cortex; others

Figure 2.13: Npas4 targets genes are induced by physiological stimulation in SST neurons *in vivo*

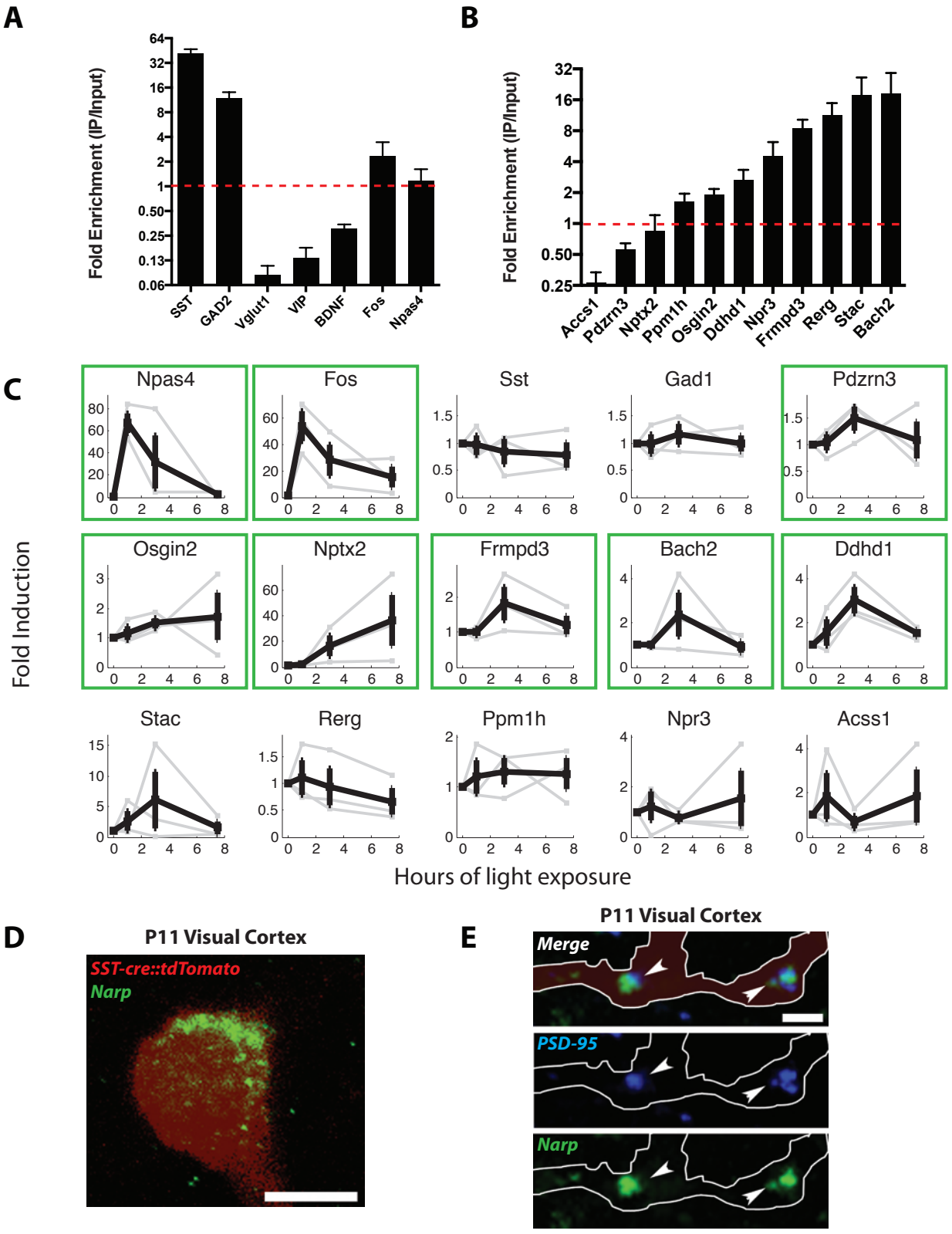

Figure 2.13 (Continued): Npas4 target genes are induced by physiological stimulation in SST neurons *in vivo*

A) Quantitative RT-PCR for a set of control genes was performed on RNA immunoprecipitated from SST neurons in the visual cortex of mice heterozygous for SST-cre and the Ribotag allele; qPCR was also performed on RNA isolated from the visual cortex input fraction from the same animals. The graph plots the average fold enrichment (IP / input) across all experimental conditions (n = 3 biological replicates, error bars represent SEM). Somatostatin and GAD2 are highly enriched in RNA immunoprecipitated from SST neurons relative to the input fraction. Vglut1, VIP, and Bdnf are substantially de-enriched in the immunoprecipitated RNA, reflecting their lack of expression in SST neurons. Fos and Npas4 have enrichment scores near 1, reflecting their similar expression in SST and excitatory neurons.
B) Plot shows the average fold enrichment (IP / Input) across all experimental conditions for selected Npas4 inhibitory target genes. Genes such as Nptx2 and Ppm1h have average fold enrichment near 1, meaning they are present at similar concentrations in the IP and input fractions. Others, such as Bach2, Frmpd3, and Stac are highly enriched in RNA IPed from SST neurons relative to the input fraction. Of the candidate target genes tested, only Acss1 is significantly de-enriched in the IP relative to the input.
C) Six week old animals heterozygous for the Ribotag allele and SST-cre were dark housed for two weeks and subsequently exposed to light for 0, 1, 3, or 7.5 hours, whereupon the visual cortex was dissected, and RNA was immunoprecipitated from SST-neurons. Subplots show the fold-induction of each candidate gene (y-axis) at each time point after light exposure (x-axis). Fold inductions were determined by dividing the normalized RNA signal at each time point by the zero hour time point for each biological replicate (gray lines, n = 3). The mean and standard error (black lines) were calculated from the fold inductions of three biological replicates. Green boxes mark genes likely induced by light stimulation in SST neurons (induced in 2 out of 3 replicates at the same time point). The early-response genes Npas4 and Fos were robustly upregulated in SST neurons one hour after light stimulation, while

Figure 2.13 (Continued):

somatostatin and GAD1 RNA did not change upon stimulation. Nearly half of the tested candidate genes were induced in SST neurons by physiological stimulation *in vivo*.

D) Coronal sections from P11 mice heterozygous for SST-cre and the tdTomato cre reporter allele were stained with an antibody directed against narp (green). This representative image is from a single confocal optical section, and shows perisomatic localization of narp in cortical SST neurons consistent with narp synthesis in those cells. Scale bar is 10 μm.

E) Brain sections from P11 mice with tdTomato labeled SST neurons were stained with antibodies against PSD-95 (blue) and narp (green). This high magnification maximal intensity projection shows that narp puncta can colocalize with PSD-95 puncta (arrowheads) on SST-neuron dendrites (white outline). Scalebar is 1 μm.

such as Bach2, Frmpd3, and Stac were highly enriched in the IP fraction, suggesting that they may be selectively expressed in SST neurons.

To determine which target genes were induced in SST neurons by light stimulation, we performed quantitative RT-PCR analysis on the RNA IPed from SST neurons at each time point after light exposure, and then calculated the fold-induction at each time point. This analysis showed that ribosomally associated Npas4 and c-Fos mRNA were highly induced one hour after light exposure, whereas ribosomal association of somatostatin and Gad1 mRNA was not changed by light exposure. We applied this analysis to eleven Npas4 MGE target genes and found that half (6 of 11) were induced by light stimulation (Figure 2.13C). Strikingly, among these induced genes are three Npas4 target genes with putative synaptic functions. These genes are Nptx2/narp, which is well known to cluster AMPA receptors, Pdzrn3, which regulates neuromuscular junction development by promoting the degradation of MuSK, and Fmrpd3. Although Fmrpd3 has no described function, it is highly enriched in SST neurons and is related to Fmrpd4 (Preso), which directly associates with PSD-95 and regulates dendritic spine morphogenesis in excitatory neurons (Lu et al., 2007),(O'Brien et al., 2002),(Lee et al., 2008).

In particular, Npas4-mediated induction of Nptx2 in SST neurons provides an appealing hypothesis to explain the mechanism by which Npas4 regulates the development of excitation: activity induces Npas4 expression, which in turn promotes accumulation of Narp, recruiting AMPA receptors to developing excitatory synapses on SST neurons. To determine if activity-induced transcription of Nptx2 results in increased Narp protein in SST neurons, we dark housed and subsequently light exposed mice with fluorescently labeled SST neurons, and immunostained brain sections with a specific antibody against Narp (Figure 2.14A). We found that light stimulation more than doubles the number of SST neurons positive for somatic Narp staining (Figure 2.14B).

Npas4's effect on the development of excitatory synapses on SST neurons is apparent in the visual cortex of P11 mice without a stimulation paradigm; we hypothesized that if Npas4-mediated transcription of Nptx2 in SST neurons is part

Figure 2.14: Narp is induced in SST neurons in response to activity

A

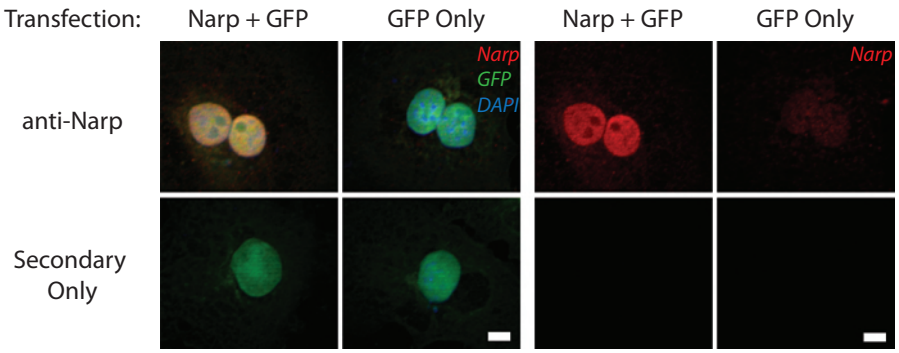

B

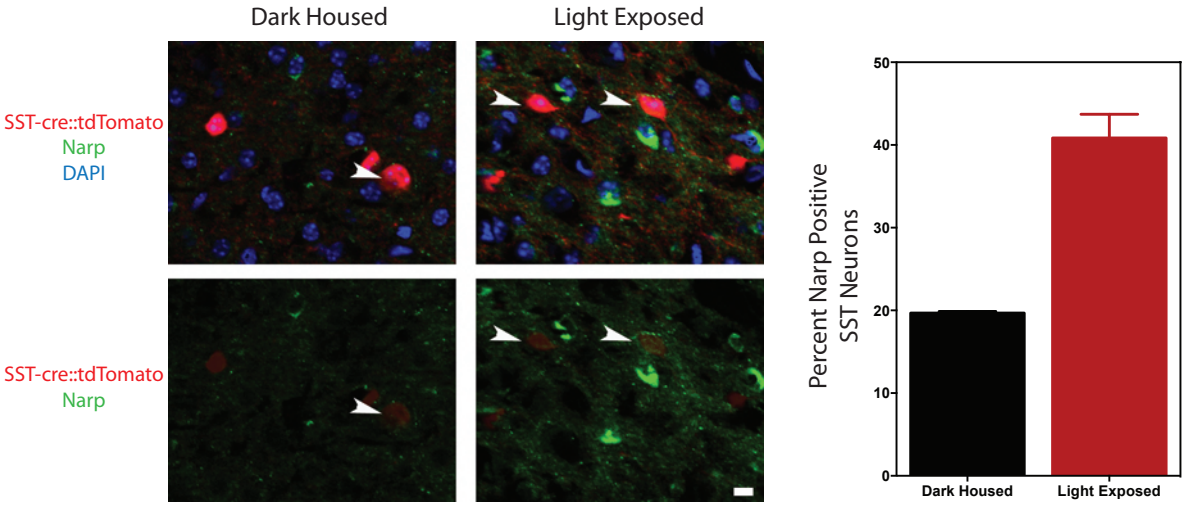

Figure 2.14 (Continued): Narp is induced in SST neurons in response to activity

A) Cos cells were transfected with either Nptx2 cDNA (Open Biosystems) and GFP (Left) or only GFP (right) and stained with an antibody against Narp (top) or only secondary antibodies (bottom). Narp antibody specifically recognizes the gene product encoded by Nptx2 cDNA by immunostaining. Right, narp signal only.
B) Staining of sections from P24 wild-type mouse brains either dark housed for four days, or dark housed and subsequently light exposed for 2.5 hours stained with antibodies directed against narp (green) and DAPI (blue). SST neurons are labeled by tdTomato. The fraction of SST neurons that contain somatic narp puncta (arrowheads) is increased upon light exposure (graph, right).

of the mechanism by which Npas4 regulates development of excitatory synapses on P11, then Narp should be present in SST neurons at synaptic sites in P11 cortex. To test this hypothesis, we perfused P11 mice in which SST neurons were labeled with tdTomato reporting expression of SST-cre, and stained brain sections with antibodies direction against Narp and PSD-95. We observed perisomatic narp immunofluorescence in cortical SST neurons in single optical sections consistent with an intracellular localization, suggesting that narp is synthesized in these SST neurons (Figure 2.14D, 27 of 42 SST neurons positive for perisomatic narp staining). Finally, we asked whether narp was also present at excitatory synapses on SST neurons. Though the density of labeled SST neurons made reconstructing full dendritic arbors impossible, we were able to resolve short segments of tdTomato labeled SST neuron dendrites. We observed Narp colocalization with PSD-95 in these dendrites, strongly supporting the hypothesis that Narp mediates part of Npas4's effect on the development of excitatory synapses to SST neurons (Figure 2.14E). In conclusion, our analysis of inducible Npas4 target genes in SST neurons revealed that multiple genes with likely functions in synaptic development or plasticity are induced by neuronal activity in SST neurons *in vivo*, and therefore represent potential molecular mechanisms by which neuronal activity regulates the development and maturation of synaptic input to SST inhibitory neurons.

Discussion

Synapses on inhibitory neurons are acutely modified by activity, but the molecular mechanisms that control the development and maturation of synaptic input to inhibitory neurons remain largely unknown. In excitatory neurons, a complex activity-induced program of gene expression controls multiple aspects of synaptic development. Recent work demonstrating the requirement of CREB for normal synaptic plasticity in hippocampal interneurons, as well as the lack of expression of the CREB coactivator CRTC1 in GABAergic neurons, suggested that inhibitory neurons may induce a unique program of activity dependent transcription to regulate synapses; however, the specific genes transcribed in inhibitory neurons in response to activity, as well as their particular function in synaptic development, remained unknown (Ch'ng et al., 2012),(Ran et al., 2012).

Here, we show that inhibitory neurons induce a large and unique program of activity-dependent gene expression that allows these neurons to adapt to activity in a cell-type specific manner. We find that most early-induced transcriptional regulators are expressed in both inhibitory and excitatory neurons, but that many of their late-induced transcriptional targets, which include regulators of synaptic development that act locally at the synapse, are induced in a cell-type specific manner. To investigate the function of the activity-dependent transcription program in inhibitory neurons, we focused on Npas4, an early-induced transcription factor that promotes increased inhibitory synapses on excitatory neurons in part by promoting transcription of Bdnf. We report that Bdnf is not expressed in inhibitory neurons; instead of acting through Bdnf, Npas4 regulates an activity-induced transcriptional program specific to inhibitory neurons that controls the development of excitatory synapses on SST positive cortical inhibitory neurons.

In neuronal cultures, SST neurons that lack Npas4 receive significantly fewer excitatory synapses, but the number of inhibitory synapses they receive is normal. *In vivo*, deletion of Npas4 results in a dramatic reduction in the frequency of miniature excitatory currents mediated by AMPA receptors, but not by NMDA receptors, suggesting that Npas4 is required to promote normal AMPA receptor

number at excitatory synapses. Together, this data suggests that activity-dependent expression of Npas4 in SST neurons positively regulates the development and maturation of excitatory synapses on SST neurons. Interestingly, mEPSCs on Npas4 deficient SST neurons have normal amplitude, implying that the accumulation of synaptic AMPA receptors regulated by Npas4 may be an all-or-none process: a given synapse either has a normal complement of AMPA receptors or too few receptors to be detected. Although the identities of specific synaptic inputs to SST neurons have yet to be fully characterized, it is possible that the all-or-none nature of this phenotype reflects the activity-dependent regulation of a specific set of excitatory inputs.

Npas4's role in the development of excitatory synapses on SST neurons is the reciprocal of the effect of Npas4 in excitatory neurons, where it positively regulates the number of inhibitory synapses on excitatory neurons. The directionality of Npas4's cell-type specific functions can be examined in the context of neuronal homeostasis: in response to activity, Npas4 is induced in excitatory neurons, where it promotes increased numbers of inhibitory synapses, thereby reducing the activity level of the pyramidal neuron (Lin et al., 2008). In SST neurons, elevated activity also induces Npas4, which then acts to promote increased excitation onto the SST neuron. In isolation, this paradoxical form of homeostasis would result in continuously increasing levels of excitation; however, from a circuit perspective, increased excitatory drive to inhibitory neurons promotes increased GABA release, and should thereby result in decreased net excitation in the local circuit. SST neurons largely receive excitatory input from local cortical afferents, so levels of Npas4 in SST neurons may specifically reflect local activity levels, and could potentially serve to fine-tune the amount of feedback inhibition broadcasted throughout the local microcircuit (Xu and Callaway, 2009). In a broader sense, the reciprocal nature of Npas4's function in excitatory and inhibitory neurons demonstrates that activity dependent transcriptional pathways are adapted to reflect the distinct function of a cell in a neural circuit.

Previous reports have also suggested that excitatory synapses on inhibitory neurons are strengthened in response to elevated levels of activity through

mechanisms that include activity-dependent synthesis and release of both Bdnf and Narp – both Npas4 target genes - from excitatory neurons. These factors strengthen excitatory synapses formed onto inhibitory neurons, providing a mechanism by which inhibitory neurons can adjust the strength of their excitatory inputs in response to the activity levels of surrounding pyramidal cells (Rutherford et al., 1998),(Chang et al., 2010),(Turrigiano, 2011).

SST neurons can, in addition to promoting increased excitatory input through Npas4's transcriptional program, cell-autonomously modulate other aspects of their excitability. In response to activity blockade, SST neurons downregulate a potassium conductance, thereby increasing membrane excitability (Gibson et al., 2006). Intriguingly, Npas4 regulates the activity-dependent induction of Kcna1, a shaker-like potassium channel, in inhibitory neuron cultures, suggesting that neuronal activity may promote maintenance of this potassium conductance through this Npas4-dependent mechanism.

Npas4 mediates its function in SST neurons by regulating a unique program of activity-dependent gene expression that is distinct from the program it regulates in excitatory neurons. Our observation that Npas4's major target gene in excitatory neurons, Bdnf, is not transcribed in cultured inhibitory neurons after membrane depolarization is consistent with previous reports that failed to detect Bdnf mRNA in inhibitory neurons in non-stimulated mouse cortex (Gorba and Wahle, 1999). In addition to regulating Bdnf, Npas4 has been reported to regulate the expression of immediate early genes such as c-Fos, Arc, and Zif268 in excitatory neurons (Ramamoorthi et al., 2011),(Lin et al., 2008). However, although these genes are well induced by membrane depolarization in inhibitory neuron cultures, we find no evidence that Npas4 regulates their expression in inhibitory neurons. Instead Npas4 regulates late-response genes that include both inhibitory neuron specific genes, as well as genes that are also activity-regulated Npas4 targets in excitatory neurons. In addition, Npas4 induces expression of late-response genes that are present in excitatory neurons, but not activated by activity. Npas4 binds to activity-regulated enhancer elements to promote transcription of activity-regulated genes (Kim et al., 2010). Cell type specific differences in activity-induction could be caused

by chromatin modifications that determine cell-type specific gene expression, differential expression of transcriptional coactivators that recruit Npas4 to distinct sets of enhancers, cell-type specific factors that recruit active enhancer elements to distinct promoters, or some combination thereof.

Recent studies have begun to identify the molecular signaling pathways that promote the formation and development of synaptic input to inhibitory neurons, yet our understanding of the molecular mechanisms by which these synapses develop is limited (Fazzari et al., 2010),(Sylwestrak and Ghosh, 2012). The identification of activity dependent transcription – and Npas4 in particular – as important regulators of synapse development opens additional avenues of investigation into these mechanisms. The discovery that nearly two hundred late response genes including Cacng5 or Pthlh are induced by neuronal activity specifically in inhibitory neurons provides a new class of candidate molecules that may mediate aspects of activity-dependent plasticity in inhibitory neurons. The characterization of the specific activity-induced transcriptional program regulated by Npas4 in inhibitory neurons provides additional candidates that may be involved in activity-dependent synapse development or plasticity in inhibitory neurons. The function of many of these Npas4 target genes, including Stac, Slc25a36, Ppm1h, and Rerg has not yet been well characterized, but these proteins possess domains or homology that suggest they could mediate potent and interesting biological functions. The further identification of Npas4 target genes induced in somatostatin expressing inhibitory neurons *in vivo* in response to physiological stimulation strongly implicates these genes as potential regulators of excitatory synapse development. In particular, Pdzrn3, an E3 ubiquitin ligase, regulates MuSK degradation at the neuromuscular junction, and thereby affects acetylcholine receptor clustering (Lu et al., 2007). Pdzrn3 may similarly affect AMPA receptors in SST neurons, analogously to Ube3a, another activity dependent E3 ubiquitin ligase that promotes degradation of multiple negative regulators of excitatory synapses in excitatory neurons (Greer et al., 2010),(Margolis et al., 2010). Frmpd3 is another MGE Npas4 target that is upregulated in SST neurons *in vivo*, but unlike Pdzrn3, it is strongly enriched in both MGE cultures and SST neurons. Though its function is unknown, Frmpd3 contains a

FERM and PDZ domain, suggesting that Frmpd3 may be localized to the plasma membrane. In addition, Frmpd3 is homologous to Frmpd4 (Preso), which directly interacts with PSD-95 and regulates dendritic spine morphogenesis in excitatory neurons, suggesting that Frmpd3 may mediate an important function at excitatory synapses on SST neurons (Lee et al., 2008).

The Npas4 target gene most obviously implicated in mediating the effect of Npas4 on excitatory synapse development is Nptx2, which encodes the protein Narp. Narp is an extracellular protein that, when it associates with neural pentraxin 1, directly recruits AMPA receptors to non-spiny excitatory synapses (Xu et al., 2003), (O'Brien et al., 2002),(Sia et al., 2007). Furthermore, Narp is required to recruit AMPA receptors to excitatory synapses early in development,(Koch and Ullian, 2010). Nptx2 mRNA and Narp are upregulated by activity in SST neurons *in vivo*. Furthermore, Narp is synthesized in SST neurons and is present at excitatory synaptic sites on SST neurons at the developmental time point when we observe reduced excitatory synapse function in the absence of Npas4. Although Npas4 likely controls excitatory synapse development through the coordinated action of multiple target genes, the induction of Narp in SST neurons seems likely to be a part of this mechanism.

Intriguingly, Npas4 also regulates activity-dependent induction of Nptx2 in excitatory neurons. Although Narp's role in cortical pyramidal neurons has not been defined, Narp can cluster AMPA receptors at synaptic sites from either pre- or post-synaptic locations, suggesting that a possible function of Npas4 mediated induction of Narp in excitatory neurons may be to promote increased excitatory input to inhibitory neurons through a presynaptic mechanism (O'Brien et al., 2002),(Lin et al., 2008). Alternately, secreted Narp from excitatory neurons may specifically modulate excitatory inputs to PV inhibitory neurons, which – in contrast to SST neurons - do not express Nptx2 (Chang et al., 2010). Interestingly, Npas4 is also poorly expressed in PV inhibitory neurons relative to other inhibitory neuron subtypes. The observation that in response to a robust depolarizing stimulus PV neurons poorly express both Npas4 and Nptx2 suggests that specific subtypes of inhibitory neurons may induce unique programs of activity dependent gene

expression, and that these programs may be extensively adapted, modified, and specialized in different types of inhibitory neurons to mediate cell-type specific functional adaptations to neuronal activity.

Materials and Methods

Electrophysiology

Coronal sections (300 μm) were cut from P10-12 mouse visual cortex using a Leica VT1000S vibratome in ice-cold choline dissection media (25 mM NaHCO3, 1.25 mM NaH2PO4, 2.5 mM KCl, 7 mM MgCl2, 25 mM glucose, 0.5 mM CaCl2, 110 mM choline chloride, 11.6 mM ascorbic acid, 3.1 mM pyruvic acid). Slices were incubated in artificial cerebral spinal fluid (ACSF, contains 127 mM NaCl, 25 mM NaHCO3, 1.25 mM NaH2PO4, 2.5 mM KCl, 2 mM CaCl2, 1 mM MgCl2, 25 mM glucose) at 32°C for 30 minutes immediately after cutting, and subsequently at room temperature. All solutions were saturated with 95% O2/5% CO2, and slices were used within 6 hours of preparation. Whole-cell voltage-clamp recordings were performed in ACSF at room temperature from neurons expressing tdTomato labeled SST neurons identified under fluorescent and DIC optics. Recording pipettes were pulled from borosilicate glass capillary tubing with filaments using a P-1000 micropipette puller (Sutter Instruments) and yielded tips of 2-5 MΩ resistance. All experiments were recorded with pipettes filled with 120 mM cesium methyl sulfonate, 10 mM HEPES, 4 mM MgCl2, 4 mM Na2ATP, 0.4 mM Na2GTP, 10 mM sodium phosphocreatine and 1 mM EGTA. Osmolarity and pH were adjusted to 310 mOsm and 7.3 with Millipore water and CsOH, respectively. Occasionally 0.5% Neurobiotin (Vector Labs) or Alexa Hydrazide 488 (Invitrogen) was included in the internal solution to visualize neurons. Recordings were sampled at 20 kHz and filtered at 5 kHz. mEPSCs were isolated by holding neurons at -70 mV and exposing them to 0.5 μM tetrodotoxin, 50 μM picrotoxin and 25 μM cyclothiazide, and were blocked by application of 25 μM NBQX and 50 μM CPP. mIPSCs were isolated by holding neurons at 0 mV and exposing them to 0.5 μM tetrodotoxin, 25 μM NBQX, and 50 μM CPP and were blocked by 50 μM picrotoxin. Miniature currents mediated by NMDA receptors (mNMDAs) were isolated by holding neurons at +40 mV and exposing them to 0.5 μM tetrodotoxin, 25 μM NBQX, and 50 μM picrotoxin. mNMDA currents were blocked by application of 50 μM CPP.

Data were analyzed using Axograph X. Events were identified using a variable amplitude template-based strategy as described (Clements and Bekkers, 1997). Templates for each event type were defined as follows. mEPSC: .25 ms rise time, 3 ms decay τ, 3xSD local noise threshold. mIPSC: 1 ms rise time, 50 ms decay τ, amplitude cutoff of 2.5xSD local noise threshold. mNMDA: 6 ms rise time, 50 ms decay τ, amplitude cutoff of 3x SD local noise threshold. Local noise was determined by a taking the standard deviation of the current for a 5 ms window before rise onset. Templates were fit to traces 25 ms after rise onset in the case of mEPSCs and 50 ms after rise onset in the case of mIPSCs and mNMDAs. Events were discarded if they were larger than 100 pA or had a rise time outside the range of 0-3 ms for mEPSCs, 0-10 ms for mIPSCs, or 0-20 ms for mNDMAs. Statistical significance was evaluated using a Mann-Whitney U-test on the mean amplitude and event frequency of all individual neurons in a given experiment. Cumulative distributions of inter-event interval and amplitude were made for each cell measured and population distributions are presented as mean ± SEM of the cumulative distributions taken from each cell in a given experiment. Cumulative distribution plots are not shown for mIPSCs because the mIPSCs onto SST neurons were so infrequent at the age we recorded that despite recording for 40 minutes, we often did not sample enough events reasonably estimate the distribution. Cells were discarded if they had series resistance larger than 20 MΩ during the recordings, if average noise RMS was over 3.5 pA, or if baseline drifted more than 30% over the course of recording.

RNA isolation, Reverse Transcription, qPCR-analysis

Total RNA was extracted with Trizol reagent following the RNEasy Micro Kit's procedure (Qiagen, Valencia, CA) and RNA quality was assessed on a 2100 Bionalayzer (Agilent, Palo Alto, CA). RNA was reverse transcribed with the High Capacity cDNA Reverse Transcription kit (Life Technologies). Real time quantitative PCR reactions were performed on the LightCycler 480 system (Roche) with LightCycler® 480 SYBR Green I Master. Reactions were run in duplicates or

triplicates and Actin levels were used as an endogenous control for normalization. Real-time PCR primers were designed using the Universal ProbeLibrary (Roche). Primer sequences are available upon request.

Microarray Analysis

Total RNA was collected from E14 MGE or 14 Cortex cultures using Trizol reagent following the RNEasy Micro Kit's procedure (Qiagen, Valencia, CA) and RNA quality was assessed on a 2100 Bionalayzer (Agilent, Palo Alto, CA). For oligonucleotide microarray hybridization, 100 ng of total RNA were amplified with the Ovation RNA Amplification System V2 (NuGEN, San Carlos, CA) and the resulting cDNA was labeled, fragmented and hybridized to Affymetrix Mouse Genome 430 2.0 arrays. Preparation of cDNA and hybridization of cDNA to microarrays was conducted in the Microarray core facility at Dana-Farber Cancer Institute, and all microarrays passed standard Affymetrix quality control tests. For expression profiling of activity dependent gene expression in MGE and E14 cortical cultures, two independent biological replicates of each experiment were performed. Arrays from all experimental conditions, and all replicates, of a given condition were normalized to one another using the robust multichip averaging method (RMA normalization) using the Matlab bioinformatics toolbox (Bolstad et al., 2003). An expression threshold was set at four times the highest signal from the Npas4 probeset in the Npas4 knockout condition. Probesets were considered for further analysis if the maximum intensity in their most highly expressed experimental condition was above this threshold in both biological replicates. ~35% of probesets passed this filter. Mean values were used for subsequent analysis. Fold changes were calculated by dividing the mean intensity from either the 1 or 6 hour condition by the intensity of the 0 hour condition. Probesets were considered to be induced if their induction was 2-fold (1.5 standard deviations greater than the average fold change) or greater over 0h condition in both biological replicates. Quantitative RT-PCR experiments confirmed that changes 2-fold or greater were accurately reported by the arrays. We found 1243 inducible probesets; these

probesets were categorized into seven distinct groups: maximally induced at 1 hour in MGE only, cortex only, or both, or maximally induced at 6 hours in MGE only, cortex only, or both. A separate category was created for genes with distinct kinetics, which were maximally induced at 1 hour in one culture type, but 6 hours in the other. The fold-induction for probesets whose maximal signal was below expression threshold at a given time point was reported as NaN to indicate the culture-type nature of its expression. Complete tables of all microarray data are available in the supplemental tables.

Ribotag Analysis

Immunoprecipitation and purification of ribosomally associated RNA was performed as described (Sanz et al., 2009). Briefly, 6-week old mice were housed in the dark for two weeks before being exposed to light for 0, 1, 3, or 7.5 hours, whereupon the visual cortex was dissected and flash frozen in liquid nitrogen. Visual cortices from three individual animals were pooled for each biological replicate, and three biological replicates were performed. Equal amounts of RNA from the IP and input fractions were amplified with the Ovation RNA Amplification System V2 (NuGEN, San Carlos, CA) and quantitative RT-PCR was performed as described. RNA concentrations were determined in every experiment by normalizing Cts to actin from the 0 hour input. For fold enrichment calculations, the fold enrichment (IP / input) was calculated based on actin-normalized RNA concentrations for every time point of every biological replicate, and these values were averages to get a single IP/Input for each gene. To calculate fold induction, for each biological replicate, each time point was divided by the 0 hour signal from that replicate, such that the 0 hour signal was set to 1 in each biological replicate. The mean and standard error of fold-inductions were calculated from these values for each gene tested.

Western blots analysis

Cortical or MGE cultures were placed on ice, washed 1x with cold PBS, and immediately exposed to boiling sample buffer (75 mM Tric HCl pH 6.8, 15% glycerol, 3% SDS, 7.5% β-Mercaptoethanol). Samples were boiled for five minutes, and centrifuged at maximum speed for 5 minutes. The supernatant was resolved by SDS-PAGE, transferred to nitrocellulose, and immunoblotted. Protein levels were visualized by chemiluminescnce. Antibodies used were Rb α-c-Fos (Santa Cruz SC-52 1:200), Rb α-Npas4 (in house, 1:2,000), Ms α-Tuj-1 (Millipore MAB1637 1:10,000), Rb α-GAD65/67 (Millipore AB1511 1:10,000), Rb α-TBR1 (Abcam ab31940 1:500).

Animal Husbandry and Colony Management

Npas4 knockout and conditional knockout mice were generated in the Greenberg lab by Yingxi Lin (Lin et al., 2008). Ai9 Rosa26::tdTomato reporter mice (Madisen et al., 2010), Dlx5/6-cre (Stenman et al., 2003), PV-cre (Hippenmeyer et al., 2005), SST-cre, VIP-cre (Taniguchi et al., 2011), and Ribotag mice (Sanz et al., 2009) were obtained from Jackson labs.

For routine experimentation, animals were genotyped using a PCR-based strategy. PCR primer sequences are available upon request. For most experiments, mice heterozygous for the Npas4 conditional allele (Npas4 flx/wt) and homozygous for SST-cre (SST +/+) were crossed to mice heterozygous for the Npas4 conditional allele and homozygous for the tdTomato reporter allele (tdTomato +/+). Resulting littermates all had one copy of the SST-cre transgene and the tdTomato cre-reporter and yielded Npas4 wt/wt and Npas4 flx/flx littermates for experimentation. The use of animals was approved by the Animal Care and Use Committee of Harvard Medical School.

Visual Stimulation and Seizure Induction

P18-20 mice reared in a standard light cycle were transferred into constant darkness for four days. Animals in the Light Exposed condition were subsequently exposed to light for 2 or 6 hours before being sacrificed. Animals in the Dark Housed condition were anaesthetized in the dark and their eyes were covered with tape before being sacrificed.

Seizures were induced in P24 mice by intraperitoneal injection of kainic acid (4 mg/ml) at a dose of 20 mg kainic acid per kg body mass. Control animals were injected with equivalent volumes of PBS. Mice were anaesthetized and perfused 2.5 hours after injection. Seizure induction in P10-12 animals was accomplished by administering 3 mg of kainic acid per kg body weight by intraperitoneal injection. At the indicated time post-injection, the visual cortex was dissected out and flash frozen in liquid nitrogen for subsequent RNA purification.

Neuronal Cell Culture

For isolation of RNA, immunocytochemistry and synaptic puncta quantification experiments, mixed cortical cultures were prepared from E16.5 mouse embryos as described (Xia et al., 1996). Briefly, $1.25x10^5$ cells per well were plated on a glial support layer on glass coverslip coated with poly-D-lysine (20 μg/mL) and laminin (3.4 μg/ml). Cultures were maintained in neurobasal medium supplemented with B27 (Invitrogen), 1 mM L-glutamine, and 100 U/ml penicillin/streptomycin, and one third of the media in each well was replaced every other day.

MGE-derived dissociated cultures were established by dissecting the MGEs from E14 embryos as previously described (Bortone & Polleux, 2009), dissociating them into a single cell suspension (Polleux & Ghosh, 2002) and plating the resulting single cell suspension at a density of $1x10^5$ per dish onto 35 mm glass bottom petri dishes (MatTek) coated with poly-D-lysine (20 μg/mL) and laminin (3.4 μg/ml). The cultures were maintained in neurobasal medium supplemented with B27

(Invitrogen), 1 mM L-glutamine, and 100 U/ml penicillin/streptomycin. After one week in culture, one third of the medium was replaced every other day.

For western blotting or RNA purification of mixed cortical cultures or E14 cortical cultures, cells were dissociated and plated at a density of $1x10^6$ per well on 6 well plates coated with poly-D-lysine (20 μg/mL) and laminin (3.4 μg/ml) and cultured in neurobasal medium supplemented with B27 (Invitrogen), 1 mM L-glutamine, and 100 U/ml penicillin/streptomycin, and one third of the media in each well was replaced every other day.. .

For KCl-mediated depolarization of neurons, neuronal cultures were treated overnight with 1 μM TTX and 100 μM APV to silence spontaneous activity prior to stimulation. Neurons were depolarized with 55 mM extracellular KCl as described (Tao et al., 1998) and lysed at the indicated time point.

Synaptic Puncta Staining and quantification of synapse density

Cultured neurons were washed with PBS and fixed with 4% paraformaldehyde and 1% sucrose in PBS for 8 minutes at room temperature. Following PBS washes, neurons were blocked in 1x GDB (0.1% gelatin, 0.3% Triton X-100, 4.2% 0.4 M phosphate buffer, 9% 5 M NaCl), incubated with the primary antibody in 1x GDB overnight at 4° C, washed 4 x 10 minutes in PBS, and then incubated with the secondary antibody in 1x GDB for 1 hour at room temperature. Neurons were then washed 4 x 10 minutes in PBS and once in distilled water before being mounted in Fluoromount-G (SouthernBiotech). The following primary antibodies were all used at a concentration of 1:250: Ms α-PSD-95 (Millipore MAB1596), Rb α-Synapsin-1 (Millipore, AB1543), Ms α-GABAR β2/3 (MAB341), Ms α-Vglut-1 (Millipore MAB5905), Rb α-GluR1 (Millipore AB1504), Rb α-GABAR γ2 (Millipore AB5559), Rb α-GAD65 (Millipore AB5082), Ms α-VGAT (Synaptic Systems 131 011). Alexa Fluor secondary antibodies (Invitrogen) were used at a concentration of 1:250.

Images were acquired on a Zeiss Axio Imager microscope with a 63x objective with the use of an apotome. Within each set of synaptic markers in a given experiment, all images were acquired with identical exposure times and apotome settings. Settings were selected such that no pixels were beyond the range of the detector. For each neuron, a Z stack of 6-8 sections with a step size of 0.5 μm was collected, and a maximal intensity projection was created and used for analysis. Neurons were analyzed blind to genotype or experimental condition. Custom ImageJ macros were used to remove the somatic region from the image and to create a mask of the GFP or tdTomato labeled cytoplasm. A custom matlab program was used to determine synapse density. Briefly, for each channel in each experiment the mean pixel intensity was determined, and a threshold was set at three standard deviations above the mean. Similar results were obtained using either 2 or 4 standard deviations above the mean. Each channel of each image was masked and binarized, and the mask of overlap of all three channels was made. Connected components greater than three pixels in size were identified and counted. Synapse density was determined by dividing the number of triple overlap co-clusters by the area of the neuron. For each biological replicate, means were determined from at least 15 neurons imaged from multiple coverslips. Because absolute values of synapse density vary significantly between biological replicates, within each set of markers in each biological replicate, the control-group mean was set to 1 and synapse density in other groups normalized to this value. Normalized mean data was used to analyze significance by ANOVA using matlab.

Morphometric reconstruction and Sholl Analysis

For Sholl analysis performed on cultured neurons, the GFP or tdTomato mask used for synapse assays was fed into a custom matlab program. Briefly, the user identified the soma center, and the program generates a series of concentric circles at set intervals, and counts the number of crosses of the mask with each

circle. Mean and SEM are the means absolute values for every neuron imaged across every biological replicate.

For morphological reconstruction of somatostatin neurons *in vivo*, neurons were identified by tdTomato expression reporting SST-cre activation. Since all SST neurons were labeled, distal processes were impossible to resolve. SST neurons were intracellularly filled using a patch pipette of 2-3.5 MΩ resistance with an internal solution containing 0.5% neurobiotin (Vector Labs) and allowed to dialyze for 40 minutes. After slow and careful removal of the pipette from the cell, the slice was immediately fixed in 4% PFA in 0.1 M phosphate buffer (PB) with 0.2% picric acid overnight at 4°C. The next day the slices were washed 3x20 minutes in 0.1M PB, then cryoprotected in 30% sucrose in 0.25 M PB, then frozen in tissue freezing medium (Triangle Biomedical Sciences) on dry ice and stored at -80° C. Slices were defrosted in 0.1 M PB and washed 3x20 minutes in 0.1 M PB to remove excess freezing medium. Slices were treated with 1% hydrogen peroxide in 0.1M PB for 30 minutes, washed 3x20 minutes in PBS, then treated with 0.4% Triton X-100 for 1 hour. Following triton, slices were incubated with AB reagent (Vector Labs) prepared according to manufacturers instructions for 2 hours. Slices were rinsed 3x20 minutes in PBS, then exposed to Immpact DAB (Vector Labs) prepared according to manufacturer's instructions until slices turned light brown. Slices were immediately transferred to PBS and washed 3x20 minutes in PBS. Finally, slices were dehydrated in a series of brief washes of increasing ethanol concentrations, and then washed twice in xylenes before being mounted in permount (Fisher Scientific). Cells were visualized using a Nikon 80i upright microscope with a 100x Nikon Plan Fluor oil, 1.3 Na objective and were traced live using neurolucida. Sholl analysis was performed on neurolucida reconstructions using neurolucida explorer.

Immunocytochemistry

Neurons were fixed in 4% PFA and 1% sucrose in PBS for 8 minutes at room temperature, then washed in PBS 3x20 minutes. Coverslips were blocked for 1 hour

(5% Normal Goast Serum, 0.1% Triton X-100 in PBS) then incubated in primary antibody in block overnight at 4°C. Coverslips were washed 4x10 minutes in PBS, and incubated in secondary antibody in block for one hour at RT away from light. Coverslips were washed 4x10 mins in PBS and 1x in distilled water before being mounted in fluoromount-G (SouthernBiotech) and stored at 4°C before imaging. Primary antibodies used were: Rb α-c-Fos (Santa Cruz sc-52, 1:500), Rb α-Npas4 (in house, 1:500), Rb α-somatostatin (Millipore AB5494 1:500), Rat α-somatostatin (Millipore AB354 1:100), Sheep α-NPY (Millipore AB1583 1:200), Ms α-calretinin (Swant 6B3 1:500), Ms α-calbindin (Swant 300 1:500), Goat α-parvalbumin (Swant PVG 214 1:200), Rb α-parvalbumin (Swant PV25 1:500), Ms α-GAD67 (Millipore MAB5406 1:500), Rb α-narp (Novus Biologicals 32250002 1:1000). Secondary antibodies were Alexa Fluors (Invitrogen) used at a concentration of 1:500.

Perfusions and Immunohistochemistry

Animals were anesthetized with 300 μL 10% ketamine and 1% xylazine in PBS by intraperitoneal injection. When animals were fully anaesthetized, as judged by lack of response to tail pinch, animals were transcardially perfused with ice cold PBS for one minute followed by six minutes of cold 4% PFA, 1% sucrose in PBS. Brains were dissected out and postfixed for one hour at 4°C, followed by 3x30 minute washes in cold PBS, and cryoprotection overnight in 20% sucrose in PBS at 4°C. For narp staining experiments, brains were postfixed in 1% PFA at 4°C for two days. The following day, brains were placed in tissue freezing medium (Triangle Biomedical Sciences) and frozen on dry ice and stored at -80°C. Brains were subsequently cryosectioned using a Leica CM1950 cryo(Kim et al., 2010)stat at a thickness of 20 μm. Brains from different experimental conditions were placed on the same slide to minimize variation. After cryosectioning, slides were either stained immediately or stored at -20°C for up to six months. Brains sections were initially blocked for one hour (0.3% Triton X-100, 0.2% Tween-20, 3% Normal Goat Serum and 3% BSA), followed by incubation of primary antibody overnight at 4°C in

block. The next day, brains were washed 3x15 minutes in PBS-T (PBS with 0.25% Triton X-100), incubated with secondary antibody and DAPI in block for 1 hour at RT, then washed 3x15 minutes in PBS-T, once in distilled water, and mounted in fluoromount-G (SouthernBiotech). Primary and secondary antibodies were the same as described for use in Immunocytochemistry, and all were used at concentrations of 1:1000.

Cell Counting Experiments

Cultured neurons or brains were imaged using a Zeiss Axio Imager microscope with either a 10x or 20x objective with an apotome. In all cases exposures were set as to ensure less that 0.4% of the pixels were saturated, and exposures were kept constant throughout a given experiment for each channel. Custom ImageJ and matlab macros were employed to quantify the fraction of a given neuron marker type positive for a transcription factor. Briefly, thresholds were determined based on multiple user defined negative regions for each channel. Channels were thresholded and binarized and a mask of each channel was created. Connected components greater than 6 pixels in size in the DAPI channel mask determined the total number of nuclei in a region. The number of connected components greater than 4 pixels positive for both DAPI and a cell-type marker were counted to produce the number of cells of a given type in an image or region of interest. Finally, the number of objects greater than 4 pixels in size positive for DAPI, a cell-type specific marker, and a transcription factor were counted to determine the number of a given cell-type positive for that transcription factor. These values, along with the area of the image or region of interest were used to calculate all relevant densities or percentages. At least three separate images per biological replicate were used to determine mean values for each biological replicate, and at least three biological replicates (animals or individual cultures) were used to determine mean and SEM of reported values. In some cases the total area and Feret diameter of binarized connected components were measured and recorded to estimate cell size.

Acknowledgements

We would like to acknowledge Caleigh Mandel-Brehm and Chinfei Chen for advice and technical support with electrophysiology experiments, David Harmin for bioinformatics advice, and Brenda Bloodgood for preliminary recordings from MGE cultures. We would further like to acknowledge Pingping Zhang for providing valuable mouse colony management assistance. Microarray experiments were conducted at the Dana-Farber Cancer Institute Microarray core facility, and neurolucida reconstructions were performed at the Childrens Hospital Boston cellular imaging core facility.

Chapter 3:

General discussion

Npas4-regulated gene expression programs

Our investigation into the cell-type specific nature of activity-induced transcriptional programs has increased our understanding of how activity controls the development of distinct neurons in a neuronal circuit. We showed that Npas4 regulates different sets of genes in inhibitory and excitatory neurons, yet the comprehensive comparison of the transcriptional programs regulated by Npas4 in these two cell-types had not yet been made. Previous genome-wide analysis of Npas4 target genes was performed using mixed E16.5 cortical cultures, which contain ~20% inhibitory neurons, making it impossible to determine the specific cellular origin of the microarray signal (Lin et al., 2008). To identify the genes specifically regulated by Npas4 in excitatory neurons, we made E14 cortical cultures from littermate wild type or Npas4 knockout embryos. We silenced cultures overnight, depolarized with elevated KCl for 0, 1, or 6 hours, and performed genome-wide microarray analysis. We found that Npas4 regulates the induction of many activity-regulated genes in excitatory cortical neurons: these genes included known excitatory neuron targets such as Bdnf, but not other reported Npas4 targets, including c-Fos, Zif268, and Arc (Lin et al., 2008),(Ramamoorthi et al., 2011). The reason for this discrepancy of our data with published reports is not known, but one possible explanation is the experimental preparation that was used. We used E14 cortical cultures made from Npas4 knockout mice to identify Npas4 targets in excitatory neurons, whereas c-Fos, Zif268, and Arc were identified as Npas4 targets using mixed hippocampal cultures made from an Npas4 conditional knockout mouse that were infected with a Cre-expressing lentivirus. It is possible that knockout of Npas4 from birth yields different results than acute knockout using a Cre-expressing lentivirus, and it is also possible that Npas4 regulates distinct programs of gene expression in hippocampal and cortical excitatory neurons.

We asked how Npas4 inhibitory neuron target genes were regulated in excitatory neuron cultures, and we found that Npas4 target genes in inhibitory neurons fall into three categories: 1) genes that are expressed at very low levels in excitatory neurons, 2) genes that are expressed in excitatory neurons, but only

activity-regulated in inhibitory neurons, and 3) genes that are regulated by membrane depolarization and Npas4 in both excitatory and inhibitory neurons. Strikingly, we do not find any genes that are activity-regulated in both cultures, but regulated by Npas4 in only one cell type (Figure 3.1).

Genes such as Nptx2, which are activity regulated Npas4 targets in both cell-types, need little further discussion: the transcriptional mechanisms involved in their activation are likely similar in different types of neurons. In inhibitory neurons, the inability of Npas4 to elicit expression of genes like Bdnf, which are never expressed in inhibitory neurons, is likely due to mechanisms operating on the level of chromatin, not differential function of Npas4 between cell-types. Supporting this hypothesis, ChIP-Seq experiments performed in the Greenberg lab in E16.5 mixed cortical cultures have shown that the gene bodies of cell-type specific genes such as Bdnf or Igf-1 harbor overlapping active (H3K4me3) and repressive (H3K27me3) histone marks. This bivalent modification state featuring both repressive and active chromatin is highly unusual, and has been previously reported in embryonic stem cells that are poised to differentiate. However, primary neurons dissociated from E16.5 mouse embryos are already terminally differentiated. Bdnf and Igf-1 are selectively expressed upon activity in excitatory and inhibitory neurons, respectively. Because these ChIP-Seq experiments were performed on material from mixed cortical cultures, one interpretation of this data is that active (H3K4me3) marks on the Bdnf gene body represent ChIP signal from excitatory neurons, while the repressive (H3K27me3) ChIP signal is from inhibitory neurons, and visa versa for the ChIP signal in the Igf-1 gene body. ChIP experiments for active and repressive chromatin modifications performed on nuclei isolated from MGE and E14 CTX cultures could directly test this hypothesis.

Other evidence supporting a chromatin-based mechanism for cell-type specific gene expression is our preliminary observation that in inhibitory neurons, Npas4 binds to the Bdnf promoter and an enhancer in an intron in the Bdnf locus. If true, this finding would suggest that Npas4 simply binds to any available site on the genome, even if the chromatin state ensures that the target gene cannot be transcribed. The logic behind such a system is unclear; it may simply reflect the fact

Figure 3.1: Npas4 induces a unique transcriptional program in MGE-derived cultures

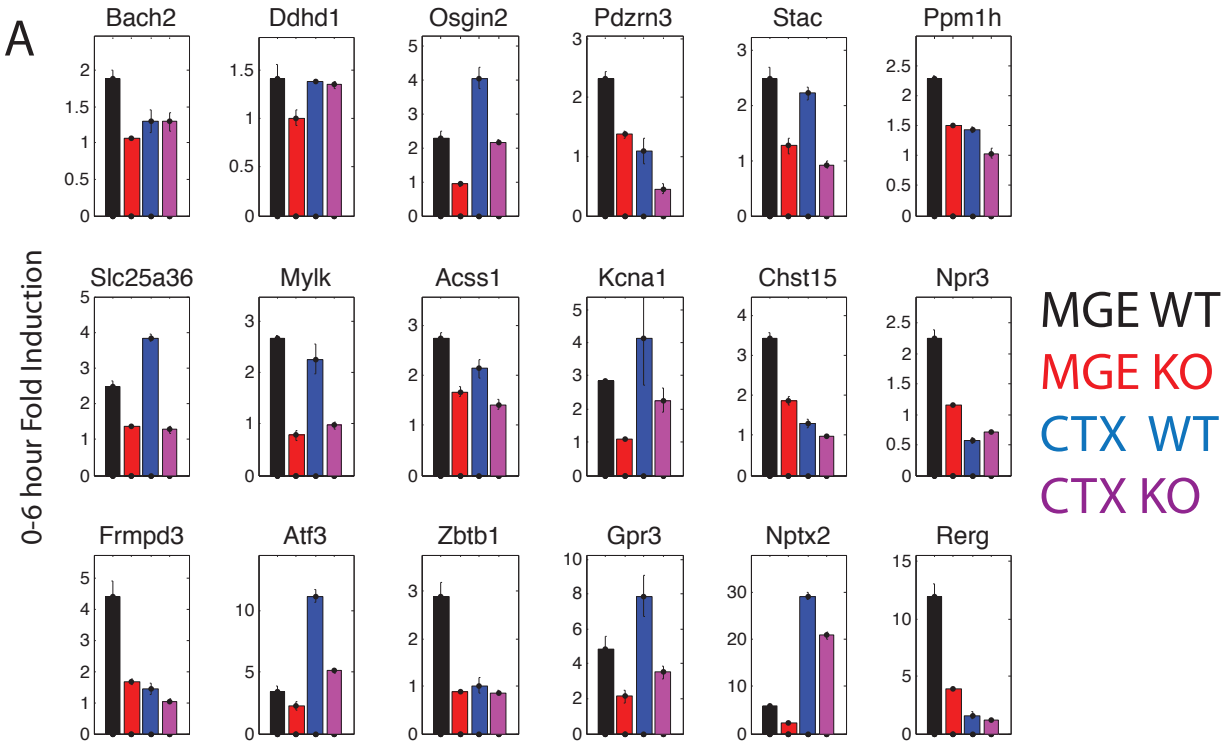

Figure 3.1 (Continued): Regulation of MGE Npas4 target genes in excitatory neurons

A) To compare the effects of membrane depolarization and removal of Npas4 in different cell types, we analyzed microarrays from depolarized Npas4 +/+ or Npas4 -/- MGE and E14 cortex cultures. For each Npas4 MGE target gene, the 0-6 hour fold induction (6 hour signal / 0 hour signal) is plotted from MGE WT (black), MGE Npas4 KO (red), E14 Ctx WT (Blue), and E14 Ctx Npas4 KO (purple). Three classes of genes are found: 1) Genes such as Rerg and Frmpd3 are selectively expressed in MGE cultures. 2) Genes such as Bach2 and Ppm1h are expressed at similar levels in both cultures, but only responsive to activity and regulated by Npas4 in MGE cultures. 3) Genes such as Nptx2, Stac, and Mylk are activity-regulated Npas4 targets in both culture types.

in response to activity, Npas4 is synthesized far in excess of the amount needed to saturate available binding sites in the genome. Npas4 and other immediate early transcription factors may therefore serve as a general signal indicating that activity has occurred, with any specificity in the transcriptional response arising through other mechanisms. It remains to be determined whether Npas4 is preferentially recruited to specific genomic loci in low-activity regimes where Npas4 is present at non-saturating concentrations, or whether it binds stochastically to available binding sites in this regime.

Finally, genes such as Zbtb1 and Ppm1h are activity-regulated Npas4 targets in inhibitory neurons, are not regulated by activity or Npas4 in excitatory neurons, and are expressed at similar levels in both cell types (Figure 3.1). Since genes that fall into this category are expressed in both inhibitory and excitatory neurons, their cell-type specific inducibility is unlikely to be mediated by chromatin modification throughout their gene bodies. However, it is possible that activity-induced enhancer elements may have distinct chromatin marks in different cell-types. If true, the availability of activity-dependent enhancers could be controlled by the developmental history of the cell. Performing ChIP-Seq experiments for the relevant chromatin modifications in MGE and E14 cortical cultures could readily test this hypothesis.

Finally, cell-type specific induction of commonly expressed genes may occur through non-chromatin based mechanisms. For instance, cell-type specific binding partners could recruit Npas4 to distinct sets of activity-regulated enhancers in different cell types, thereby causing different sets of genes to be induced in response to activity. An alternate hypothesis is that Npas4 binds to the same cohort of enhancers in both excitatory and inhibitory neurons, but these active enhancers are then recruited to distinct sets of promoters in different cell types through an independent mechanism. Genome-wide identification of Npas4 binding sites in a pure population of inhibitory neurons could begin to test these hypotheses, and they could be further tested by use of 5C (Carbon-Copy Chromosome Conformation Capture) to identify enhancer-promoter interactions in MGE and E14 cortical cultures. The function of such cell-type specific interactions could potentially be

interrogated using TALERs (transcription activator-like effector recombinases) to activate inactive enhancers or inactivate active enhancers in a cell-type specific manner (Mercer et al., 2012).

Cell-type Specific Activity-Dependent Transcription

Gene expression studies in the nervous system have shown that distinct cell-types have different gene expression profiles (Sugino et al., 2006). However, whether each separate cell-type expresses a unique set of the activity-dependent gene expression program, or whether the principle differences in this response exist only between excitatory and inhibitory neurons, remains unknown. Our finding that a relatively small fraction of PV positive inhibitory neurons can express Npas4 hints that there may be differences in the activity-dependent gene expression programs induced in distinct interneuron subtypes. Supporting this hypothesis, we find that SST neurons express Nptx2, while previous reports suggest that Nptx2 is not transcribed PV neurons (Chang et al., 2010).

An ongoing project in the Greenberg lab aims to specifically determine whether experience induces distinct transcriptional programs in discreet subtypes of inhibitory neurons. To identify cell-type specific experience-induced genes, ribosomally associated mRNAs were immunoprecipitated from populations of neurons defined by expression of Cre under control of the Emx1, GAD2, PV, SST, or VIP promoters (Taniguchi et al., 2011),(Sanz et al., 2009). To identify transcripts induced by experience, two month-old mice were kept in standard housing, housed in the dark for two weeks, or dark housed and subsequently exposed to light for varying lengths of time. The visual cortex was dissected and RNAs were IPed, purified, amplified, and analyzed by deep sequencing. This approach allows us to compare and contrast the experience-induced transcriptional programs induced by sensory experience *in vivo* in discreet classes of neurons.

Although our analysis of this experiment remains ongoing, preliminary data strongly suggests that every class of neuron we evaluated induces one or more unique genes in response to activity. Interestingly, the activity-dependent gene

expression programs across interneuron cell-types may be nearly as dissimilar to each other as they are to excitatory neurons. However, embedded in this diversity, we identified a core set of activity-induced genes that are induced in every type of neuron we analyzed. Supporting our earlier work using neuronal cultures, this group of conserved activity-induced genes consists mostly of immediate early transcriptional regulators induced in all cell-types.

This global analysis, though still ongoing, appears to extend and support our hypothesis that common activity-induced transcriptional regulators control cell-type specific cohorts of genes to mediate cell-type specific functional responses to activity. The case of Igf-1 in is another example of a cell-type specific activity-induced gene apparently mediating a unique functional response to activity. We identified Igf-1 as an activity-induced gene specifically induced in MGE cultures; however, Igf-1 induction is not affected by loss of Npas4. Separate experiments in the Greenberg lab demonstrated that Igf-1 is selectively induced in VIP positive interneurons. Igf-1 is a well-characterized growth factor, so we hypothesized that activity-induced Igf-1 in VIP neurons would promote increased excitation onto those neurons. However, when Igf-1 is selectively deleted from VIP positive neurons using VIP-cre and a conditional Igf-1 allele, the frequency of mEPSCs on VIP neurons is substantially increased (Figure 3.2). This data suggests that Igf-1 negatively regulates excitation onto VIP neurons. The functional role of VIP neurons in a neuronal circuit has yet to be published as of this date, but there is an emerging understanding that VIP positive inhibitory neurons provide strong inhibitory input onto SST interneurons. From a homeostatic perspective, SST and PV neurons, which directly inhibit pyramidal neurons, are subject to mechanisms that promote increased excitation in response to activity. In contrast, because of their putative disinhibitory role, VIP neurons may be subject to homeostatic logic similar to pyramidal neurons, and recruit mechanisms to decrease their excitation in response to activity. Thus, Igf-1 may function analogously to Bdnf in the nervous system; the use of Igf-1 instead of Bdnf by VIP neurons may allow neighboring cells in a circuit to discriminate between the source of activation and response appropriately.

Figure 3.2: Selective deletion of Igf-1 in VIP postiive inhibitory neurons increases mEPSC frequency

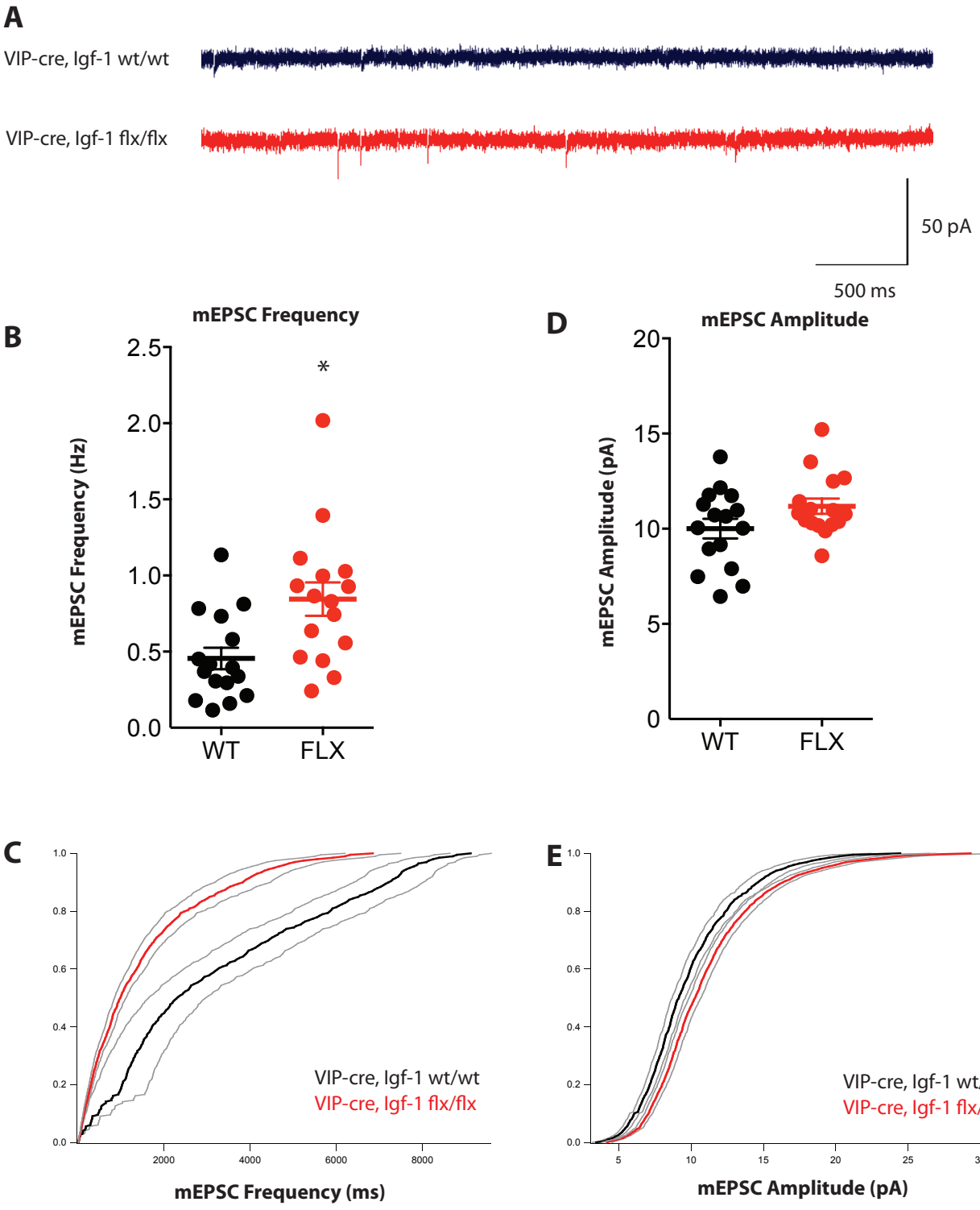

Figure 3.2 (Continued): IGF-1 negatively regulates excitatory inputs to VIP positive interneurons

A) Example traces of mEPSCs recorded in acute slices of visual cortex from P19-20 animals heterozygous for VIP-cre and a tdTomato cre reporter. These animals were either wild type (black) or were homozygous for a floxed IGF-1 allele (red). mEPSCs were recorded in the presence of TTX, picrotoxin, and cylcothiazide and filtered at 5 kHz. Scale bar is 500 ms and 50 pA.
B) Plot showing the frequency (Hz) of mEPSC onto VIP positive inhibitory neurons. Circles are the mean event frequency from single cells, and the bars represent the group mean and SEM. VIP neurons with IGF-1 conditionally deleted have significantly higher mEPSC frequency ($P < 0.01$, Mann Whitney U-Test. WT: $n = 17$, FLX: $n = 16$).
C) Cumulative distribution of mEPSC inter-event interval (ms) for WT (black) and IGF-1 Flx (red). Colored lines are the mean cumulative distribution from every neuron, and SEM is plotted in gray.
D) Plot showing amplitude (pA) of mEPSC onto VIP positive inhibitory neurons. Circles are the mean event frequency from single cells, and the bars represent the group mean and SEM. Conditional deletion of IGF-1 from VIP positive neurons does not significantly affect mEPSC amplitude.
E) Cumulative distribution of mEPSC amplitude (pA) for WT (black) and IGF-1 Flx (red). Colored lines are the mean cumulative distribution from every neuron, and SEM is plotted in gray.

In the past, the study of activity-induced genes has substantially increased our understanding of the specific mechanisms by which the nervous system responds and adapts to experience. The appreciation that different types of neurons utilize the same core early transcriptional response to activity as a scaffold to initiate a unique transcriptional and functional response deepens our understanding of how activity shapes the nervous system. In the future, continuing to refine our understanding of the cell-type specificity of this activity-dependent transcriptional response, combined with the study of specific genes *in vivo* in physiologically relevant contexts, will complement an emerging understanding of the organization of neuronal microcircuits and lend insight into the molecular mechanisms by which specific neuronal circuits develop and are modified by experience.

Chapter 4:

In vivo analysis of synaptic puncta using Array Tomography

Introduction

Synaptic connectivity is a defining feature of the nervous system. Synaptic activity controls neuronal firing, and plasticity of synaptic connections is thought to be the mechanistic basis of learning and memory (Carol, 1976),(Carew et al., 1984). Synapses are complex subcellular compartments, and their formation, stability, maturation, strength, size, and complements of signaling components are all subject to regulatory processes (Sheng and Kim, 2011),(Sudhof, 2012). This large complexity means that individual synapses can be very different from each other, resulting in an astounding molecular heterogeneity across central synapses. Understanding the function of a synapse at a mechanistic level is a major goal of neurobiology, and this goal ultimately requires the identification and characterization of the complete catalog of protein components localized to synaptic compartments. Accordingly, an immense effort by hundreds of investigators over many decades has been devoted to studying the molecular components, morphology, and function of synapses. Electron microscopy has been the gold standard for assessing synapse morphology, while electrophysiology is indispensible for the study of synapse function. Synaptic proteins have been isolated and studied using a variety of biochemical approaches, including purification of proteins enriched in synaptosomes (Filiou et al., 2010), (Bai and Witzmann, 2007),(Schrimpf et al., 2005). Finally, fluorescent microscopy has been a fruitful approach for studying many facets of synapses (Rahamimoff and Melamed, 1993).

Despite the incredible amount of information accumulated using these approaches, they each have drawbacks. Although electron microscopy remains the gold standard for synapse morphology, reconstruction of large EM volumes remains a very challenging task; moreover, methods for analysis of synapses at the EM level has not progressed far beyond visual identification and scoring (Mishchenko et al., 2010). Significant efforts have been aimed at establishing methods for high-throughput serial electron microscopy, but while this approach has proved

successful, the large effort and infrastructure required to analyze large datasets means that for the immediate future, large-volume serial EM will not be widely available as a standard assay (Bock et al., 2011). Furthermore, serial EM cannot be used to identify molecular components of synapses. Electrophysiology analysis of synapses, though incredibly powerful, is limited by available pharmacology, and cannot directly interrogate important aspects of synaptic biology in native brain tissue (for example, it cannot routinely assay weak synapses distal to the soma, or identify scaffolding proteins vital to synapse function). Existing proteomic approaches lack the resolution to interrogate individual synapses. Finally, light microscopy analysis of synapses in brain tissue is limited by two important factors. Standard fluorescent microscopy is limited to four spectrally distinct channels. Second, the size of synaptic structures are well below the theoretical resolution of a light microscope, which is around ~220 nm in the lateral (X-Y) plane and ~600 nm in the axial (Z) plane (Wang and Smith, 2012). Thus, fluorescent microscopy of synaptic proteins in brain tissue is limited to simultaneously localizing four proteins with an inherent uncertainty in localization anywhere from 4-12 times the size of the structure of interest. This inherent localization error has been widely used as a signal for identifying synapses. Because of inadequate resolution, signal from non-overlapping presynaptic and postsynaptic marker proteins appear to overlap, and quantification of this colocalization is used to count synapses, or determine if a protein localizes to a synapse (Paradis et al., 2007),(Gogolla et al., 2009a). This approach is highly likely to produce localization errors when used in brain tissue, where synapses are extremely dense.

To circumvent these two major pitfalls of conventional light microscopy, Stephen Smith's group invented and disseminated a new approach to fluorescent microscopy called array tomography (Micheva and Smith, 2007). Tissue is processed for array tomography by embedding it in an acrylic resin that allows ultrathin slices to be prepared on a microtome. Thus, the axial resolution problem of light microscopy is solved by physically sectioning the sample at a thickness of 50-100 nm. Tens or hundreds of serial ultrathin sections are splayed out on a contiguous ribbon that is adhered to a coverslip (Micheva et al., 2010e),(Micheva et

al., 2010f). Sections are stained with primary and secondary antibodies, and serial sections are imaged at preselected X-Y locations at identical spots on each section of the ribbon (Micheva et al., 2010d). Thus, instead of optically sectioning tissue, the tissue is physically sectioned, whereupon each section is imaged and then reassembled in a virtual stack (Micheva et al., 2010g). The resulting data is a Z-stack with axial resolution determined by section thickness (50-100 nm), and lateral resolution approaching the theoretical limits of fluorescent microscopy (Micheva et al., 2010b). Thus, using array tomography, synaptic markers can be localized in three dimensions in brain tissue with higher confidence than standard fluorescent microscopy approaches. The four-channel limit of standard light microscopy remains the single largest obstacle to developing a molecular taxonomy of synapses *in situ*. Array Tomography attempts to solve this problem as well: antibodies on AT ribbons can be eluted, and the ribbons can subsequently be re-stained with new sets of antibodies, and re-imaged (Micheva et al., 2010d),(Micheva et al., 2010b). The new image stack can be aligned with the previous image stack, resulting in a virtual 8-channel volume. Theoretically, this process can be repeated *ad infinitum*, to build up an N-channel matrix of fluorescent localizations of synaptic puncta, allowing a true survey of the molecular composition of synaptic sites *in vivo*.

Although array tomography has the potential to allow large-scale proteomic interrogation of every synapse across a wide area of brain tissue, the scale of the effort required, combined with the extreme fragility of the ultrathin ribbons and technical difficulties in performing the assay, only few attempts have been made to utilize the full potential of array tomography (Li et al., 2010; Micheva et al., 2010a). A more common application for array tomography is the reconstruction of ultrafine anatomy from fluorescently labeled processes (Saatchi et al., 2012),(Soiza-Reilly and Commons, 2011). Other applications include attempts to assay the localization of a protein of interest with respect to synapses using a single ultra-thin section (Eroglu et al., 2009; Kopeikina et al., 2012; Stevens et al., 2007). Additional attempts have been made to quantify synapse density on a single ultrathin section by manually counting co-clustered pre- and post-synaptic markers (Allen et al., 2012; Koffie et al., 2009). However, these approaches do not utilize the power of array tomography

Figure 4.1: Alignment and validation of synaptic marker staining on serial array tomography sections

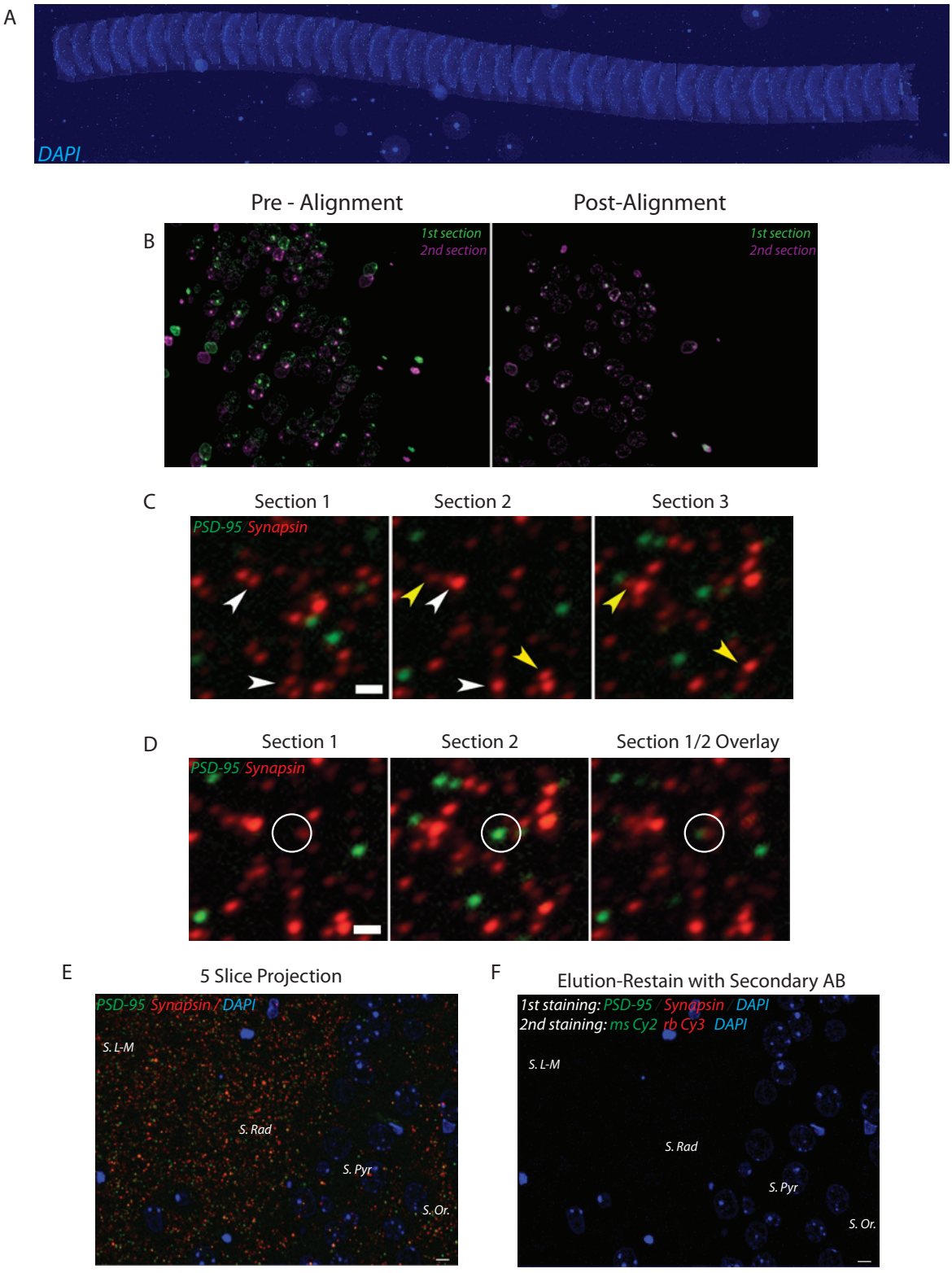

Figure 4.1 (Continued): Alignment and validation of synaptic marker staining on serial array tomography sections

A) Example image of a long ribbon of serial sections cut from hippocampus embedded in LR white at a thickness of 100 nm. DAPI staining allows visualization of the cytoarchitecture necessary for image alignment.
B) Superimposed DAPI signal from the first image section in a series (green) and the second section (magenta) before (left) and after (right) image registration protocols have been applied.
C) High magnification images of aligned serial array tomography sections stained for PSD-95 (green) and Synapsin-1 (red). Synaptic puncta are occasionally split between neighboring serial sections in the Z plane. White arrowheads point examples of split puncta from section 1 to section 2, and yellow arrowheads point to example puncta split between section 2 and section 3. Puncta are very rarely continuous across three sections. Scalebar is 1 μm.
D) High magnification image of two aligned serial array tomography sections stained for PSD-95 (green) and Synapsin-1 (red). Puncta that appear to have no synaptic partner in the X or Y axis may be associated with a synaptic partner puncta in the Z plane (right, overlay). Scalebar is 1 μm.
E) Maximal intensity projection of five serial 100 nm LR white embedded sections stained for PSD-95 (green) and Synapsin-1 (red), and DAPI (blue). Neuronal morphology can be a guide to assessing antibody specificity; observe the notable drop in synaptic puncta staining in the pyramidal layer of CA1. Scalebar is 10 μm.
F) Single plane image from the same ribbon shown in Figure 2.1E. Original antibody staining has been eluted, and the sections were restained with only secondary antibodies, demonstrating both the efficacy of the elution procedure and the lack of secondary antibody background staining. Scalebar is 10 μm.

to allow automatic and unbiased pun cta analysis in large volumes of brain tissue. When I began working with array tomography data, I found that such analysis methods did not yet exist. To use Array Tomography to count and characterize synapses *in vivo*, I set about establishing methods to analyze volumes of array tomography data.

Results

Establishing Array Tomography and Quality Control

When I began work on array tomography, methods to automatically count the number of synaptic contacts made in brain tissue had not been developed. Although co-clusters of apposed pre- and post-synaptic markers can be observed in a single ultrathin array tomography section, simply counting the number of co-clusters in a single section does not yield an accurate estimate of synapse density, since unopposed puncta may have a synaptic partner puncta that has been excluded from a single ultrathin section. To use array tomography to determine the density of pre- and post-synaptic co-clusters in a given tissue, serial sections must be created, imaged, aligned, and analyzed. The procedure for embedding tissue, serial sectioning, staining and imaging array tomography sections has been published in exquisite detail by Stephen Smith's laboratory (Micheva et al., 2010c, d, f, g). Despite the availability of detailed protocols, this approach had yet to be established independently at a new institution when I began work (additionally, these detailed protocols had not yet been published). In order to reconstruct large volumes of array tomography data, serial sections of ultrathin LR white embedded tissue must be cut into long ribbons and mounted on a coverslip (Figure 4.1A). These ribbons are imaged as a large mosaic using a 10x objective, and the constellation of DAPI stained nuclei are used to compute the X-Y center coordinate of a region of interest on every slice of the ribbon. The slices can then be imaged at high magnification. However, this online image registration is not perfect, and significant registration error exists between high-resolution images of neighboring sections in the ribbon

(Figure 4.1B, left). The image stacks must be registered and corrected for distortions using algorithms available as ImageJ plugins; proper correction is absolutely critical for obtaining aligned stacks useful data from array tomography experiments (Figure 4.1B, right).

Assessing Antibody Specificity

Array tomography sections are embedded in LR white, an acrylic resin, which provides a different environment for antigen presentation than standard frozen or paraffin embedded sections; thus antibodies validated using other immunofluorescence assays may not specifically bind their antigen on LR white sections. Stephen Smith's group and others have performed rigorous experiments to validate a cadre of antibodies against synaptic protein markers in LR white embedded sections. These validation experiments include overlay of fluorescent data from array tomography with subsequent electron micrographs on the same tissue (Micheva and Smith, 2007), but they are technically difficult and cannot easily be reproduced; independent investigators using Array Tomography must assess antibody specificity in their own hands by other means.

One method is to find puncta that are conserved across physical sections. The mean size of a pre-synaptic terminal, as assessed by electron microscopy, is around 100 nm, which is the same thickness of LR white sections cut in our experiments (Siksou et al., 2007). If antibody staining is specific and the alignment procedure has worked correctly, we should expect to observe occasional puncta that are split between serial sections. Indeed, we can observe synaptic puncta present in the exact same X-Y location in serial sections with some frequency (Figure 4.1C). Another concern is the high number of 'unapposed' puncta, which do not have a nearby synaptic partner. If antibody staining is specific, we should observe apparently unapposed puncta in the X-Y plane to actually have a synaptic partner in the Z plane on a subsequent serial section (Figure 4.1D). Quantification of these two parameters has not been formalized; instead the investigator must qualitatively

assess every stained volume to ensure that both of these features are readily observable.

It is important to note that a large number of synaptic marker puncta remain unassociated, with no apposing synaptic partner, and that this does not reflect nonspecific staining. There is no such thing as a true synaptic marker protein; there are only proteins that are enriched at synaptic compartments. Synapsin-1 labels synaptic vesicles, which are trafficked up and down long axons, and may be in reserve pools distal from the synaptic cleft. PSD-95 is enriched at synaptic sites, but it is synthesized, modified, and trafficked through the golgi and endosomes like all other proteins. Additionally, some unapposed puncta may represent nascent synapses at an early stage of development. Thus, a number of pre- and post-synaptic puncta will not be associated with a synaptic partner (Lee et al., 2010) (Goldstein et al., 2008).

Brain morphology can also be used to assess antibody specificity. The hippocampus has long been a preferred model system because of its stereotyped laminar structure (Shepherd, 2004). Excitatory neurons that reside in the pyramidal cell layer of the CA1 region of the hippocampus receive the great majority of their excitatory synaptic input on spiny dendrites that extend in either direction away from the pyramidal cell layer, and excitatory input to the soma is minimal (Megias et al., 2001). Staining for synaptic markers on array tomography sections in the hippocampus faithfully reproduces this expected pattern, with a sharp drop-off of the density of synaptic puncta in the pyramidal cell layer (Figure 4.1E).

Finally, one of the most promising aspects of array tomography is the ability to elute antibody staining after a ribbon has been imaged, and then to subsequently re-stain the same section with additional antibodies to develop a matrix that amounts to a N-channel fluorescent image. Because the harsh elution protocol has the potential to disrupt or destroy antigens (A. Mardinly, personal observations), antibody specificity must be assessed independently for each round of elution. Secondary antibody application in the absence of primary antibodies does not yield a signal on LR white sections (data not shown). Elution of primary-secondary antibody complexes and subsequent re-staining with only secondary antibodies also

does not yield a signal (Figure 4.1F). These results suggest that the elution procedure effectively removes primary-secondary antibody complexes from the ribbon, and that the elution procedure does not expose non-specific binding sites for secondary antibodies. Importantly, staining, eluting, and re-staining with the same antibody does not serve as a valid control for the specificity of that antibody. In the case of some antibodies including PSD-95, staining before elution appears to be specific by all previously discussed criteria; however, after elution and re-staining, PSD-95 puncta are randomly distributed across the pyramidal cell layer, and puncta cannot be traced through serial sections (data not shown). This result is not evidence that the initial PSD-95 staining is nonspecific, but it may imply that the elution protocol destroys the antigen causing the second round of staining to become nonspecific. Conversely, anti-synapsin antibodies label almost exactly the same puncta before and after elution (example image in Figure 4.3F). This result does not imply that the antibody is specific for the desired antigen, only that it is binding to some antigen that is not disrupted by elution and re-staining.

Analysis of Three Dimensional Data

Having established the technical protocols and necessary controls to create, stain, image, and align array tomography ribbons, we acquired virtual stacks of three-dimensional data with 100 nm axial resolution. However, analysis of this data remained challenging. Previous analysis of published array tomography data were limited to manual scoring of a single section, negating one of the most powerful aspects of the technology, the ability to analyze through a volume. Conventional methods of analyzing three dimensional fluorescent microscopy data involve converting the image stack into a maximal intensity projection, and measuring the colocalization of synaptic puncta. This approach destroys the three dimensional nature of the data, and almost guarantees the introduction of artifacts when used in brain tissue. Analysis of colocalization of pre- and post-synaptic puncta in three dimensions was similarly problematic; the increased axial and radial resolution achieved using array tomography minimizes this colocalization signal, so any viable

analysis must detect apposed puncta that barely touch instead of colocalized puncta that significantly overlap.

To approach this problem, I first created a model of the three dimensional immunofluorescence data and subsequently analyzed the model. Using bitplane imaris software, I created an idealized model that treated synaptic puncta as spheres whose center was defined by local intensity maxima: this approach was threshold-independent, meaning both bright and very puncta were included (Figures 4.2A-B). Data from Imaris was exported and fed into a custom Matlab script of my own design (termed "AT Analyzer." See material and methods for complete description of the data handling. AT Analyzer code and comments are reproduced in Appendix 3). Briefly, the core function of AT Analyzer is to calculate the distance between the centers of every possible pair of pre and post-synaptic puncta spheres. If the distance between the center points is equal to or less than the sum of the radii of the two spheres, plus an empirically determined scaling constant, then they are considered to be touching, and will be counted as a synaptic contact. To assess the efficacy of this approach, I programed AT Analyzer to export an image stack with a five-pixel cross at the location of every synapse that it identified; this stack can then be imported back into Bitplane Imaris and overlaid with the original data (Figure 4.2C), or with the spherical modeled data (Figure 4.2D). This functionality is useful for empirically determining an appropriate scaling threshold, and this threshold may vary as parameters such as slice thickness, brain region, and antibodies are changed. The ability to visually identify synapses identified by a computer script is a vital control for every experiment, and ensures that the program is neither missing real synapses nor identifying spurious synapses.

AT Analyzer Output

Although the core functionality of AT Analyzer is to calculate the number of synapses per cubic micron, the richness of the dataset allows substantially more information to be obtained. For instance, synapse density can be read out as a moving average of synapses per square micron across every axis of the volume

Figure 4.2: Volume rendering of 3D Array Tomography data for quantification of synaptic puncta

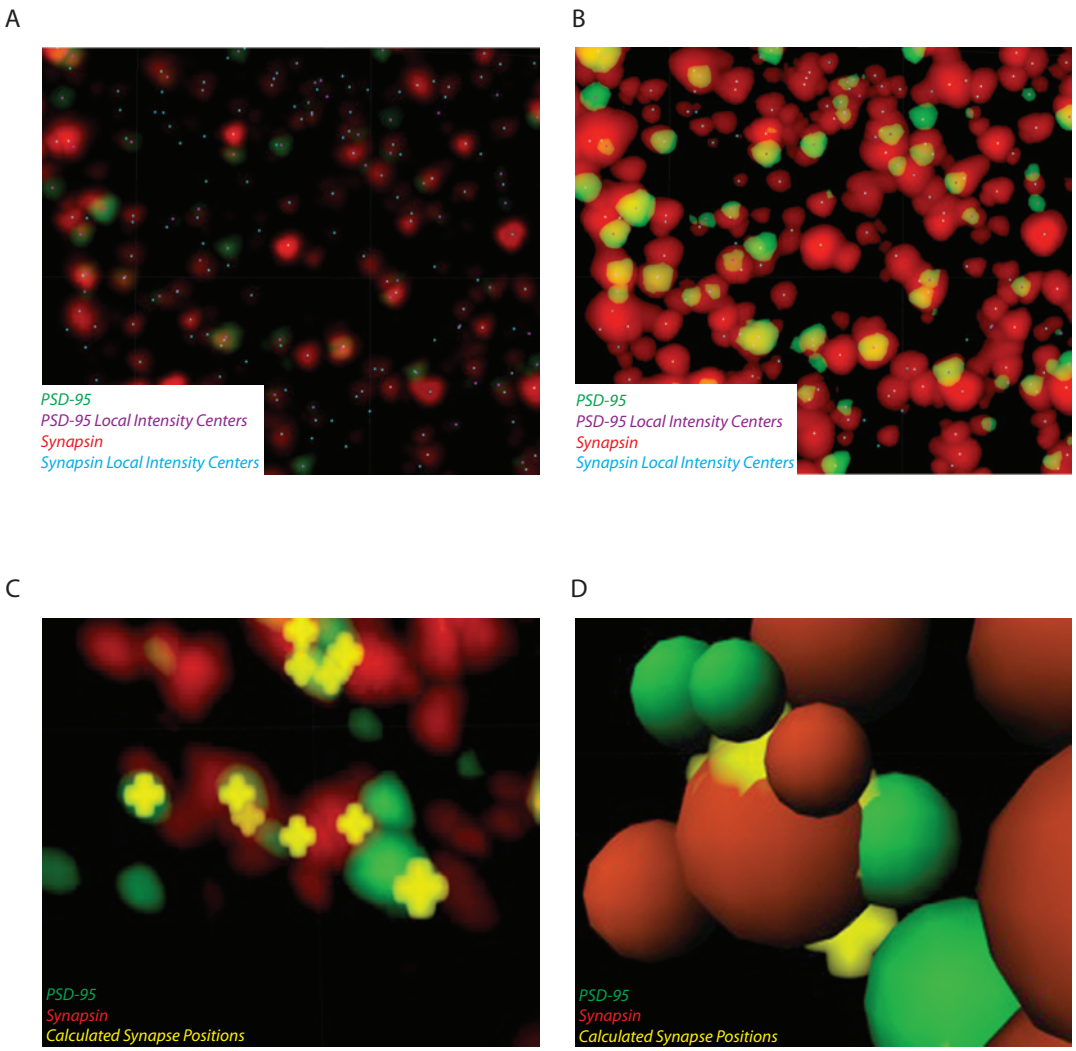

Figure 4.2 (Continued): Volume rendering of 3D Array Tomography data for quantification of synaptic puncta

A) Maximal intensity projection of 20 aligned array tomography sections taken from adult CA1 stratum radiatum. PSD-95 (green) and Synapsin-1 (red) puncta are displayed with the local intensity center for each synaptic puncta. Maximal intensity centers for local PSD-95 (purple dots) or Synapsin (blue dots) intensity mark the centers of spheres to be created to model synaptic puncta. Images in this figure are screen captures from a volumetric rendering in Imaris, and therefore have no true scale.
B) Identical image from figure 2.2A, with brightness increased to maximal levels. Local intensity centers that appeared to be centered in black space in figure 2.2A actually mark the center of a dim region of staining.
C) Maximal intensity projection of a 20 array tomography sections taken from adult CA1 stratum radiatum, and stained for PSD-95 (green) and synapsin (red). Yellow plus signs represent the locations of synaptic contacts identified by AT Analyzer.
D) Overlay of spherical volume rendering of synaptic marker staining (PSD-95, green; Synapsin-1, red) and synaptic locations calculated by AT Analyzer (yellow).

(Figure 4.3B-C). This data can be a useful tool when the volume is oriented such that a particular axis corresponds to morphology of interest (ie, determining synapse density across laminar brain structures, or a morphological feature of a labeled neuron). Another useful feature of AT Analyzer is that it outputs the density of synapses, unassociated puncta, and synapses formed by randomly localized synaptic puncta as a function of distance threshold (Figure 4.3D). This feature is useful for assessing the effect of the user-selected distance threshold. Finally, a histogram of the distances between sphere centers of synapses allows user supervision of the average synapse length, or distance between sphere centers (Figure 4.3E).

To characterize how these parameters of AT Analyzer's output dealt with highly overlapping puncta, ribbons were stained with antibodies against synapsin, imaged, and then the antibody was eluted. The ribbons were subsequently restained with synapsin again, imaged, and aligned with the previously imaged synapsin volume (Figure 4.3F). The average distance between sphere centers was ~0.05 μm, over an order of magnitude shorter than the distance between PSD-95 and synapsin centers (Figure 4.3G). Lastly, the "synapses" calculated between two pairs of synapsin puncta are insensitive to increasing the distance threshold between 0.1 μm and 0.3 μm, suggesting that this plateau represents specific interactions between puncta (Figure 4.3H). To summarize, we have established a novel approach to analyze the interaction of touching, but not overlapping, synaptic puncta in three dimensional image volumes with superior axial resolution.

Detection of Developmental Changes in Synapse Density

Next we asked whether this approach had the sensitivity to detect biologically meaningful changes in synapse density. As a positive control, we compared young mice (1 week old, P7) with adult mice (6-8 weeks of age). A period of synapse formation and growth occurs in hippocampus after P15, and quantification of synapse density in young and old mice should readily detect this

Figure 4.3: *AT Analyzer* produces unbiased, automated analysis of volume-rendered 3D array tomography data

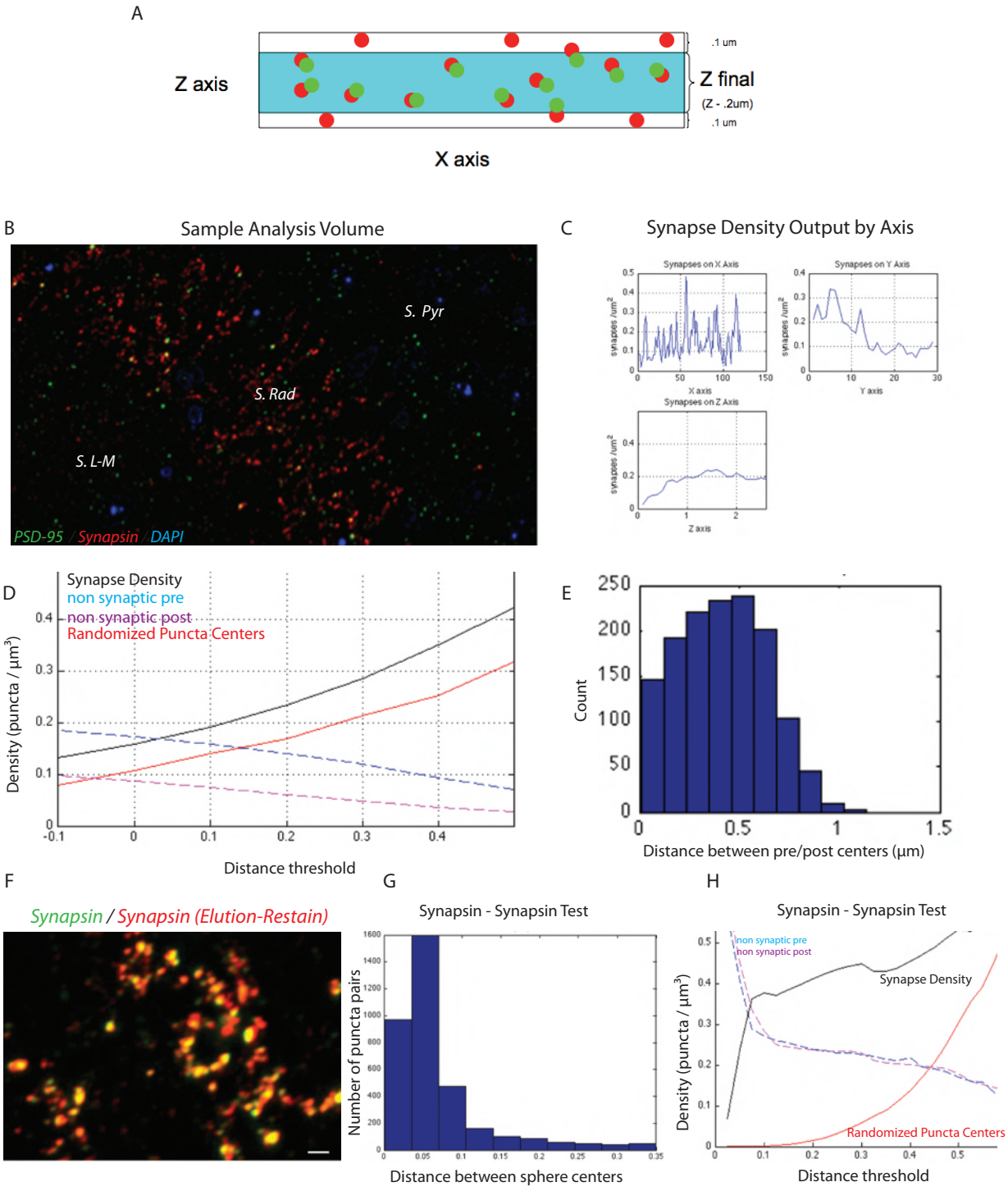

Figure 4.3 (Continued): *AT Analyzer* output and validation

A) Schematic illustrating the implementation of a fix to the Z-axis edge artifact problem. Since the X and Y axis are much longer than the Z axis, more unpaired synaptic puncta will exist along the Z axis, biasing the true density of synaptic contacts in the volume. To address this problem, post-synaptic, but not pre-synaptic, puncta with centers in the first or last section of the volume are removed, and the synapse density is determined from a new volume calculated using the reduced Z-axis.

B) Single AT section from the volume used to demonstrate *AT Analyzer* output. Section is made from adult CA1, stained for PSD-95 (green), Synapsin (red), and DAPI (blue).

C) Moving average of the synapse density across each axis of the input volume (synapse / μm^2).

D) Plots of puncta density (puncta / um^3) as a function of distance threshold, or the distance allowed between the edges of pre- and post-synaptic puncta edges in order to call a synapse. Calculated synapse density (black line) is consistently higher than synapse density where the identical set of puncta sizes have been assigned random coordinates (red line). The density of synapsin puncta unassociated with a PSD-95 puncta (blue) and PSD-95 puncta unassociated with a synapsin puncta (magenta) are also plotted.

E) Histogram showing the distribution of distances between pre- and post-synaptic local intensity centers for all synapses identified in the example volume.

F) Single plane of an array tomography volume stained for synapsin (green), eluted, and restained for synapsin again (red). Elution does not destroy the synapsin-1 antigen.

G) Distribution of the length between pre- and post-synaptic puncta when synapsin-synapsin data are run through AT Analyzer. The distance between local intensity centers is an order of magnitude shorter than when Synapsin / PSD-95 puncta are used.

Figure 4.3 (Continued):

H) Volume densities (synapses / um^3) as a function of distance threshold for synapsin- synapsin data. Black line is synapse density, synapses counted based on randomized puncta centers are shown in red, and unassociated puncta density are shown in blue and magenta, respectively.

increase in synapse density (Harris et al., 1992). To assess developmental changes in excitatory synapse density, hippocampi from pairs of adult and P7 mice were fixed and embedded, and ribbons of serial sections were sectioned at a thickness of 100 nanometers. These ribbons were stained with antibodies directed against PSD-95 and synapsin; the ribbons were imaged, reconstructed, and cropped to include only stratum radiatum (Figure 4.4A). Synapse density was calculated using AT Analyzer with a distance threshold of 0.1 μm. To reduce variability between technical replicates, ribbons from adult and P7 hippocampi were adhered to the same coverslip and handled throughout the experiment in parallel. The synapse density for each biological replicate was determined by averaging the raw values of at least five technical replicates (five independent image volumes from an individual animal acquired from at least two separate ribbons). The technical values for averaged and normalized between each biological replicate a pair-wise fashion. Group means and standard errors were calculated based on the normalized mean values of four independent biological replicates. Using this approach, each experiment includes data from at least forty separate array tomography volumes.

As expected, we detected a large increase in Synapsin-PSD-95 co-cluster density between juvenile and adult animals. This increase was accompanied by a large increase in the number of both synapsin and PSD-95 puncta (Figure 4.4B). To investigate the dynamics of this developmental increase, we determined the fraction of puncta that participated in a synaptic contact. We found that the fraction of synapsin puncta participating in a synapse did not change over development, whereas the fraction of PSD-95 puncta associated with a synapsin puncta increased by nearly 2.5 fold (Figure 4.4C). Thus, although the numbers of both PSD-95 and synapsin puncta increase over development, synapse formation appears to be driven by directing a higher proportion of total PSD-95 puncta to synaptic sites. This result may suggest the existence of mechanisms limiting the recruitment of PSD-95 to synaptic site early in development, or it may reflect a delay in the association of presynaptic terminals to available post-synaptic sites.

Figure 4.4: *AT Analyzer* method detects large developmental changes in synapse density

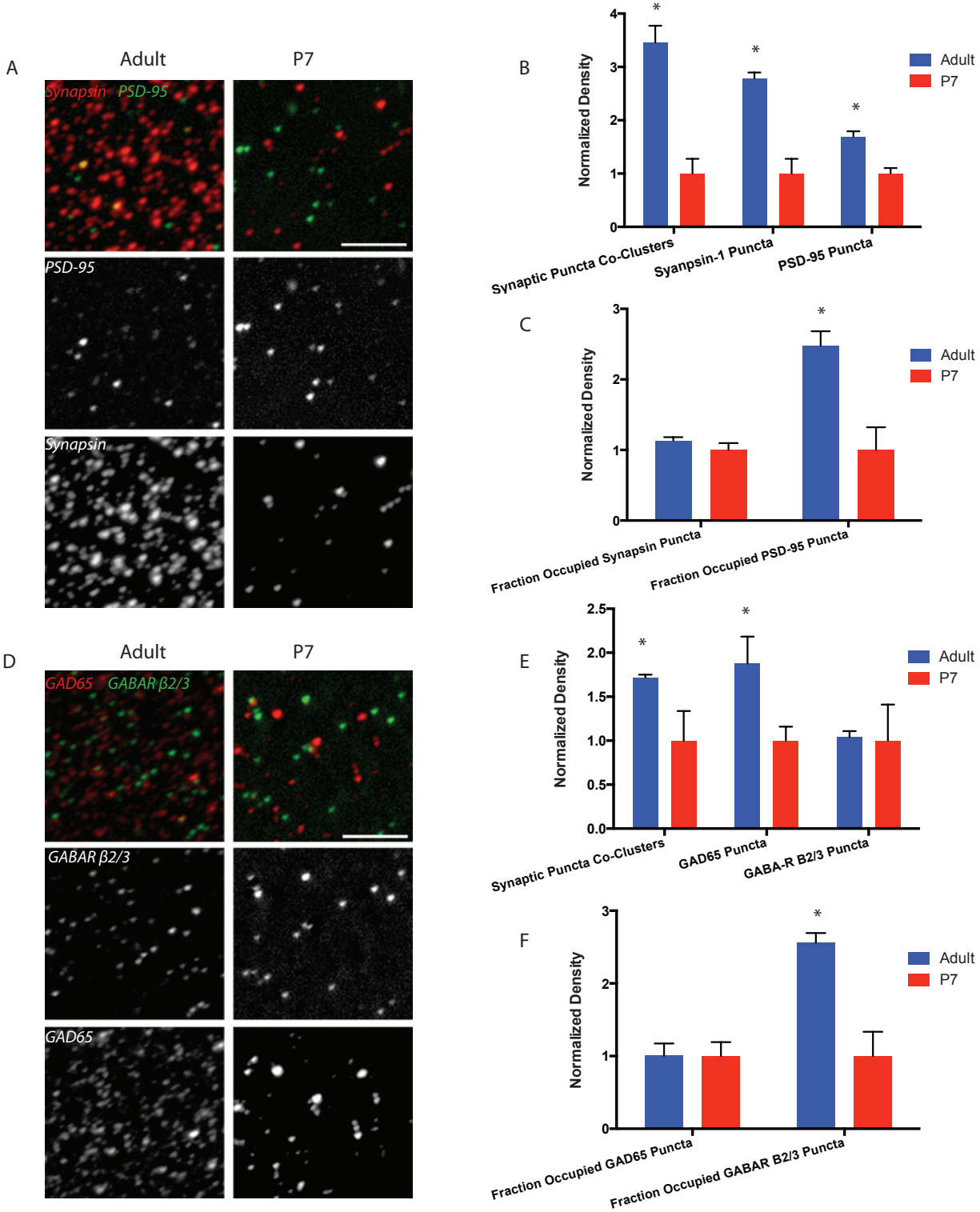

Figure 4.4 (Continued): AT Analyzer method detects large developmental changes in synapse density

A) Single array tomography section stained for PSD-95 (green) and Synapsin (red) from CA1 stratum radiatum of adult (6-8 weeks old, left) or young (1 week old, right) mice. Scalebar is 10 μm.

B) Normalized quantification of the density of synaptic contacts and synaptic puncta in young (red) and adult (blue) wild type animals in CA1 stratum radiatum. Adult animals have increased density of synapsin puncta, PSD-95 puncta, and synaptic contacts ($P < 0.05$, Mann-Whitney U-test).

C) Normalized quantification of puncta occupancy, or the fraction of puncta that are associated with an apposing synaptic partner. Left, there is no change in the fraction of synapsin puncta associated with a PSD-95 puncta over the course of development. Right, a significantly higher fraction of PSD-95 puncta is associated with synapsin puncta in adult animals ($P < 0.05$, Mann-Whitney U-test).

D) Single array tomography section stained for GABA-R β2/3 subunit (green) and GAD65 (red) from Adult (left) or young (right) CA1 stratum radiatum. Scalebar is 10 μm.

E) Normalized quantification of the density of synaptic contacts and synaptic puncta in young (red) and adult (blue) wild type animals in CA1 stratum radiatum. Adult animals have increased density of GAD65 puncta and inhibitory synaptic co-clusters, but not GABA-R β2/3 puncta ($P < 0.05$, Mann-Whitney U-test).

F) Normalized quantification of puncta occupancy, or the fraction of puncta that are associated with an apposing synaptic partner. Left, there is no change in the fraction of GAD65 puncta associated with a GABA-R β2/3 puncta over development. Right, a significantly higher fraction of GABA-R β2/3 puncta is associated with a GAD65 puncta in adult animals ($P < 0.05$, Mann-Whitney U-test).

To investigate developmental changes in inhibitory synapse density, pairs of P7 and adult hippocampi were stained with antibodies directed against GAD65 and the β2/3 subunit of the GABA-A receptor, which is an obligate subunit of synaptic GABA receptors (Figure 4.4D) (Somogyi et al., 1989). Data were acquired and normalized as described above. Large increases in both inhibitory synaptic clusters and GAD65 puncta were observed; however, no change in β2/3 subunit density was detected over development (Figure 4.4E). The number of inhibitory synapses, but not the number of β2/3 subunits increased; to account for this, as expected, the fraction of β2/3 subunits with a GAD65 partner increased dramatically over development, but the fraction of synaptic GAD65 remained unchanged (Figure 4.4F).

Thus, our application and analysis of array tomography is capable of detecting and quantifying large changes in synapse density in volumes of brain tissue. Using this approach, we detect large developmental increases in both excitatory and inhibitory synaptic density. We find that for both synapse types, large increases in the number of presynaptic puncta are not accompanied by any change in the fraction of those presynaptic puncta that participate in a synaptic contact. This trend may reflect a developmentally invariant ratio of synaptic vesicles at synaptic contacts versus vesicles being actively trafficked or stored at non-synaptic sites. For both excitatory and inhibitory synapses, a hallmark of synaptic development appears to be an increased proportion of post-synaptic proteins being sorted to synaptic sites. Whether this process is regulated by the post-synaptic cell, or is a simple reflection of increased availability of presynaptic terminals is not known.

AT Analysis of Ube3a Knockout Animals

Having demonstrated the ability of our analysis method to detect differences in synapse density in brain tissue, we sought to apply this method to questions that demanded *in vivo* analysis of synapses. One such project involved the analysis of a mouse model for Angelman Syndrome, a neurodevelopmental cognitive disorder (Williams et al., 2006). This mouse lacks the maternal copy of the Ube3a gene,

which encodes an E3 ubiquitin ligase (Jiang et al., 1998),(Miura et al., 2002). The paternal allele of Ube3a is imprinted, so a deletion of the maternal copy of Ube3a is sufficient to cause a complete null (for simplicity, Ube3a maternal -/paternal + will be referred to as Ube3a knockout) (Clayton-Smith and Laan, 2003). Ube3a is an activity-regulated gene that promotes the ubiquitylation and subsequent degradation of Arc, a classic activity regulated gene that internalizes AMPA receptors at subsets of excitatory synapses after stimulation (Greer et al., 2010). We hypothesized that in the absence of Ube3a, elevated Arc levels would result in abnormally high levels of AMPA receptor internalization. This hypothesis was supported by experiments in neuronal culture systems that demonstrated reduced surface GluR1 staining and mEPSC frequency upon deletion of Ube3a (Greer et al., 2010). Despite this data, it was not known whether these phenotypes occurred in the brain of Ube3a knockout animals.

To address this question, the hippocampi of littermate P21 wild type and Ube3a knockout mice were embedded for array tomography. Pairs of ribbons were sectioned and adhered to the same coverslips, and wild type and knockout pairs were treated identically throughout the experiment. Ribbons were stained for either GluA1 or GluN1 and SV2 to label presynaptic terminals (Figure 4.5 A,C). Three biological replicates were stained, imaged, and normalized as previously described. Synapse density was determined in stratum radiatum of CA3, and Ube3a knockout animals had a significantly lower density of synaptic GluA1-SV2 co-clusters than wild type animals (Figure 4.5B). In contrast, Ube3a knockout animals had an apparently normal density of GluN1-SV2 co-clusters (Figure 4.5D). Concomitant electrophysiological examination of Ube3a knockout mice demonstrated that they have reduced AMPA/NMDA ratios (Greer et al., 2010). To examine the morphological basis for this effect, the ratio of GluA1 to GluN1 puncta paired with an SV2 puncta was determined for each individual animal, and this ratio was then re-normalized in a pairwise manner to compare the ratio of synaptic GluA1 to GluN1 between genotypes. This analysis revealed that Ube3a KO mice had a reduced ratio of synaptic GluA1 puncta to synaptic GluN1 puncta (Figure 4.5E). Supporting these observations, the total density of GluA1 puncta was lower in Ube3a animals, but the

Figure 4.5: Array Tomography analysis of Ube3a knockout mice

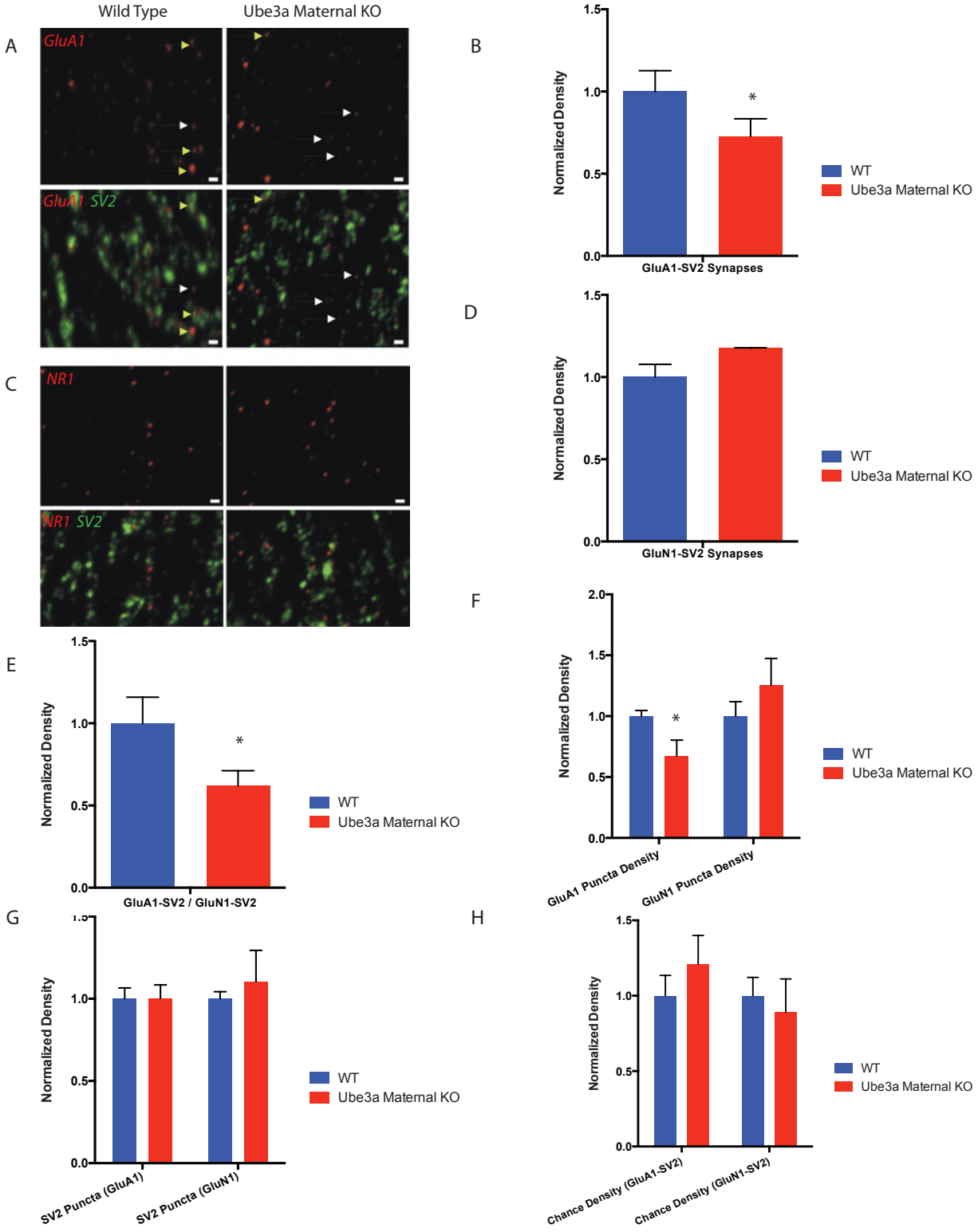

Figure 4.5 (Continued): Array tomography analysis of Ube3a knockout mice

A) Single array tomography section from the CA3 region of the hippocampus of P24 wild type (left) or Ube3a maternal knockout (right) mice, stained for GluA1 (red), and SV2 (green). White arrowheads indicate GluA1 puncta without an associated SV2 puncta, yellow arrowheads indicate GluA1 puncta with a closely associated SV2 puncta. Scalebar is 1 μm.

B) Normalized density of GluA1-SV2 synaptic co-clusters in array tomography volumes taken from wild type (blue) or Ube3a maternal KO CA3 (red). Ube3a KO mice have reduced density of synaptic GluA1-SV2 co-clusters ($P < 0.05$, Mann-Whitney U-test).

C) Single array tomography section from the CA3 region of the hippocampus of P24 wild type (left) or Ube3a maternal knockout (right) mice, stained for GluN1 (red), and SV2 (green). Scalebar is 1 μm.

D) Normalized density of GluN1-SV2 synaptic co-clusters in array tomography volumes taken from wild type (blue) or Ube3a maternal KO CA3 (red). No difference in GluR1-SV2 puncta co-cluster density was detected.

E) Normalized ratio of GluA1-SV2 puncta to GluN1-SV2 puncta in wild type (blue) or Ube3a maternal KO (red) CA3 ($P < 0.05$, Mann-Whitney U-test).

F) Normalized GluA1 and GluN1 puncta density in wild type (blue) and Ube3a maternal KO (red) in CA3. Ube3a maternal KO mice have reduced numbers of GluA1 puncta ($P < 0.05$, Mann-Whitney U-test), but not GluN1 puncta.

G) Normalized SV2 puncta density in wild type (blue) and Ube3a maternal KO (red) in CA3 in separate experiments stained for either GluN1 or GluA1.

H) Quantification of a control experiment in which data from either GluA1-SV2 or GluN1-SV2 was used, every puncta was assigned a random location *in silico*, and synapse density was calculated from the randomly localized puncta. No change is detected between wild type and Ube3a maternal KO for either experiment.

density of GluN1 and SV2 puncta were normal (Figure 4.5F-G). Furthermore, analysis of synapse density with randomized puncta locations for both GluN1 and GluA1 experiments revealed no significant change, suggesting that no unsupervised parameter in the model was driving the observed differences in the data (Figure 4.5H).

Together, these data are consistent with the hypothesis that loss of Ube3a results in abnormally elevated levels of Arc, which culminates in increased internalization of AMPA receptors. However, some confusing results from cell culture experiments from Ube3a knockout data cast confusion on the exact nature of the synaptic deficits resulting from Ube3a loss. Although disruption of Ube3a resulted in an apparent decrease in GluA1 puncta and no change in GluN1 puncta, in older neuronal cultures, a substantial increase in PSD-95 puncta density was also observed (Greer PL, unpublished observations). In order to investigate whether this data represented a cell culture artifact or a real aspect of the synaptic biology *in vivo*, we stained array tomography ribbons from wild type and Ube3a knockout animals with PSD-95 and synapsin antibodies, and imaged volumes from the CA3 region of the hippocampus (Figure 4.6A). Strikingly, we observed a substantial increase in PSD-95 - Synapsin co-clusters in Ube3a knockout animals similar to that observed in culture (Figure 4.6B). The absolute density of total synapsin and PSD-95 were not found to be significantly different between genotypes, though both PSD-95 and synapsin puncta are trending towards an increase in Ube3a knockout animals (Figure 4.6C). Finally, a much higher fraction of PSD-95 puncta was paired with a synapsin puncta in the Ube3a KO mouse (Figure 4.6D). These data indicated that the increase in PSD-95 puncta observed in neuronal cultures from Ube3a KO animals is preserved *in vivo*, and suggest that while Ube3a animals clearly have abnormal synaptic connectivity, the specific nature of these defects are not straightforward and cannot be explained by elevated Arc levels alone.

To summarize the array tomography analysis of Ube3a knockout mice, we observed fewer GluA1-SV2 co-clusters, normal levels of GluN1-SV2 co-clusters, and elevated levels of PSD-95 – Synapsin co-clusters. These changes were driven by a decrease in the number of GluA1 puncta and by an increase in the fraction of PSD-95

Figure 4.6: Array Tomography analysis of Ube3a knockout CA3 reveals elevated PSD-95/Synapsin co-clusters

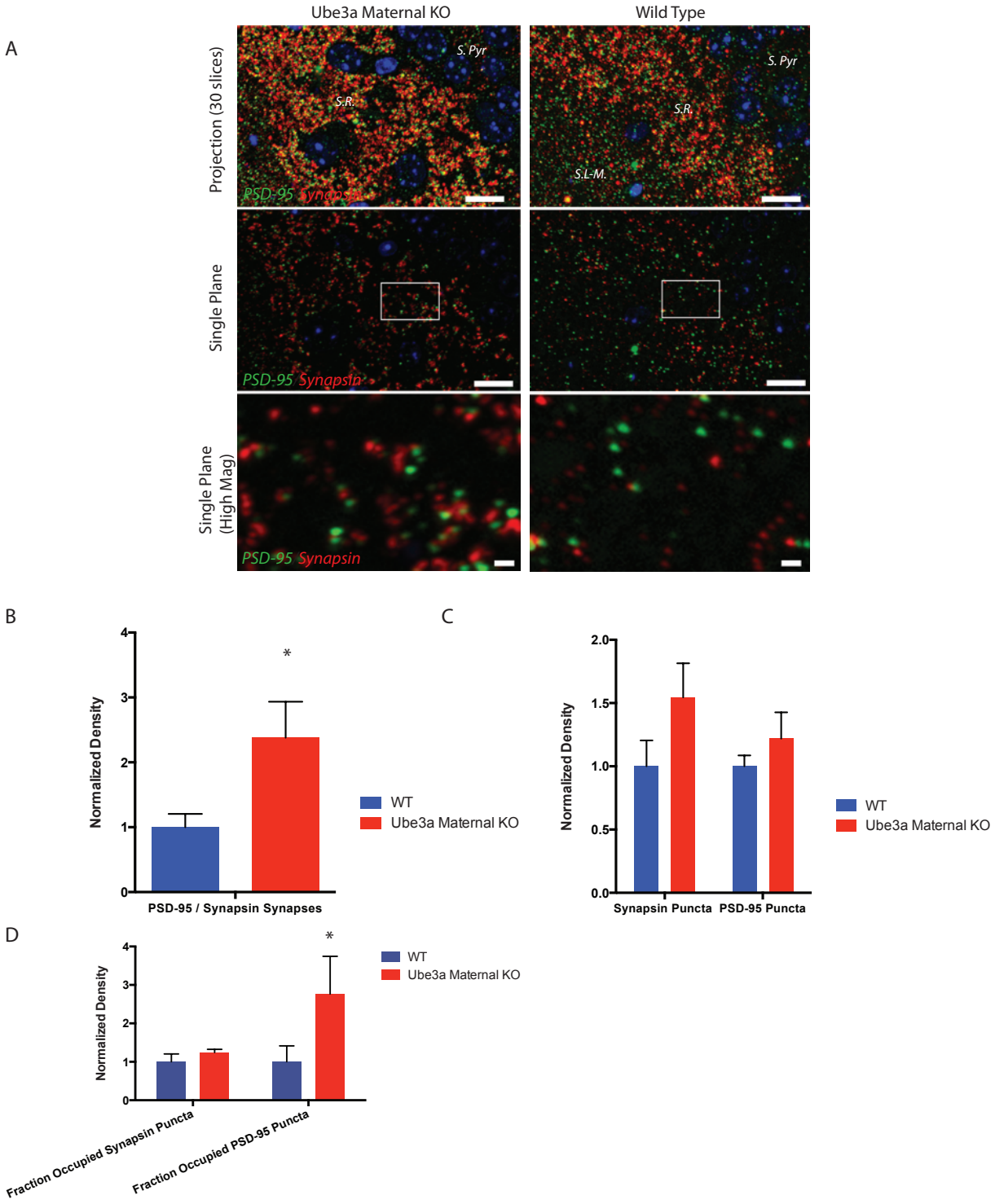

Figure 4.6 (Continued): Array tomography analysis of Ube3a knockout CA3 reveals elevated PSD-95 / Synapsin co-clusters

A) Example images of PSD-95 (green) and synapsin (red) staining from Ube3a maternal knockout or wild type CA3. Top, maximal intensity projection of 20 array tomography sections (100 nm thick) in Ube3a KO (left) or WT (right) CA3, scalebars are 10 μm. Middle, image of a single array tomography section from the projection above. Bottom, enlarged images of synaptic puncta staining, scalebar 1 μm.
B) Normalized quantification of the density of PSD-95 – Synapsin co-clusters in wild type (blue) and Ube3a maternal knockout (red) CA3 stratum radiatum ($P < 0.05$, Mann-Whitney U-test).
C) Normalized quantification of the density of PSD-95 and Synapsin puncta in wild type (blue) and Ube3a maternal knockout (red) CA3 stratum radiatum. Synapsin trend higher in Ube3a maternal knockout mice, but this change is not statistically significant.
D) Normalized quantification of the fraction of puncta in wild type (blue) or Ube3a maternal knockout (red) CA3 that are associated with a synaptic partner. A higher fraction of PSD-95 puncta is associated with a synapsin puncta in the Ube3a maternal knockout ($P < 0.05$, Mann-Whitney U-test).

puncta paired with a synaptic puncta. At least two interpretations of this data are possible: first, failure of Ube3a mediated degradation of Arc could result in increased AMPA receptor internalization, resulting in fewer GluA1-SV2 contacts, but unaltered GluN1-SV2 contacts. An ensuing decrease in excitatory drive onto these neurons could recruit homeostatic mechanisms driving synapse formation, resulting in more PSD-95 puncta paired with synapsin. However, since Arc acts preferentially on weak and inactive synapses, and is present in abnormally high levels in the Ube3a KO mice, these nascent synapses may suffer from abnormally high rates of AMPA receptor internalization (Okuno et al., 2012). However, recent reports indicating that Ube3a mediates aspects of GABAergic transmission complicate arguments based on neuronal homeostasis (Wallace et al., 2012). An alternative explanation is that the increased density of PSD-95 – Synapsin co-clusters in the Ube3a knockout represents either exuberant synapse formation or a failure to prune appropriate synapses, and these effects may be mediated by Ube3a targets other than Arc.

Analysis of Ephexin 5 Knockout Mice by Array Tomography

Another Ube3a target protein intimately involved in synapse development is Ephexin 5, a Rho-GTPase and negative regulator of synapse development. *In vitro*, disruption of Ephexin 5 results in a dramatic increase in synapse number, but it was unclear if Ephexin 5 also functioned to restrict synapse development *in vivo* (Margolis et al., 2010). To determine whether Ephexin 5 knockout mice exhibited evidence of exuberant synaptic growth, the hippocampi of wild type and Ephexin 5 knockout littermate pairs were embedded for array tomography, and ribbons were prepared as previously described. Ribbons were stained with PSD-95 and synapsin antibodies, and volumes from stratum radiatum in CA1 were imaged, aligned, and analyzed (Figure 4.7A). Quantification of the density of PSD-95 – Synapsin co-clusters revealed a large increase in the density of synaptic co-clusters in the Ephexin 5 knockout animals, supporting our understanding of Ephexin 5 function as a negative regulator of synapse growth in reduced systems (Figure 4.7B).

Figure 4.7: Array Tomography analysis of Ephexin 5 knockout CA1 reveals elevated synapse density

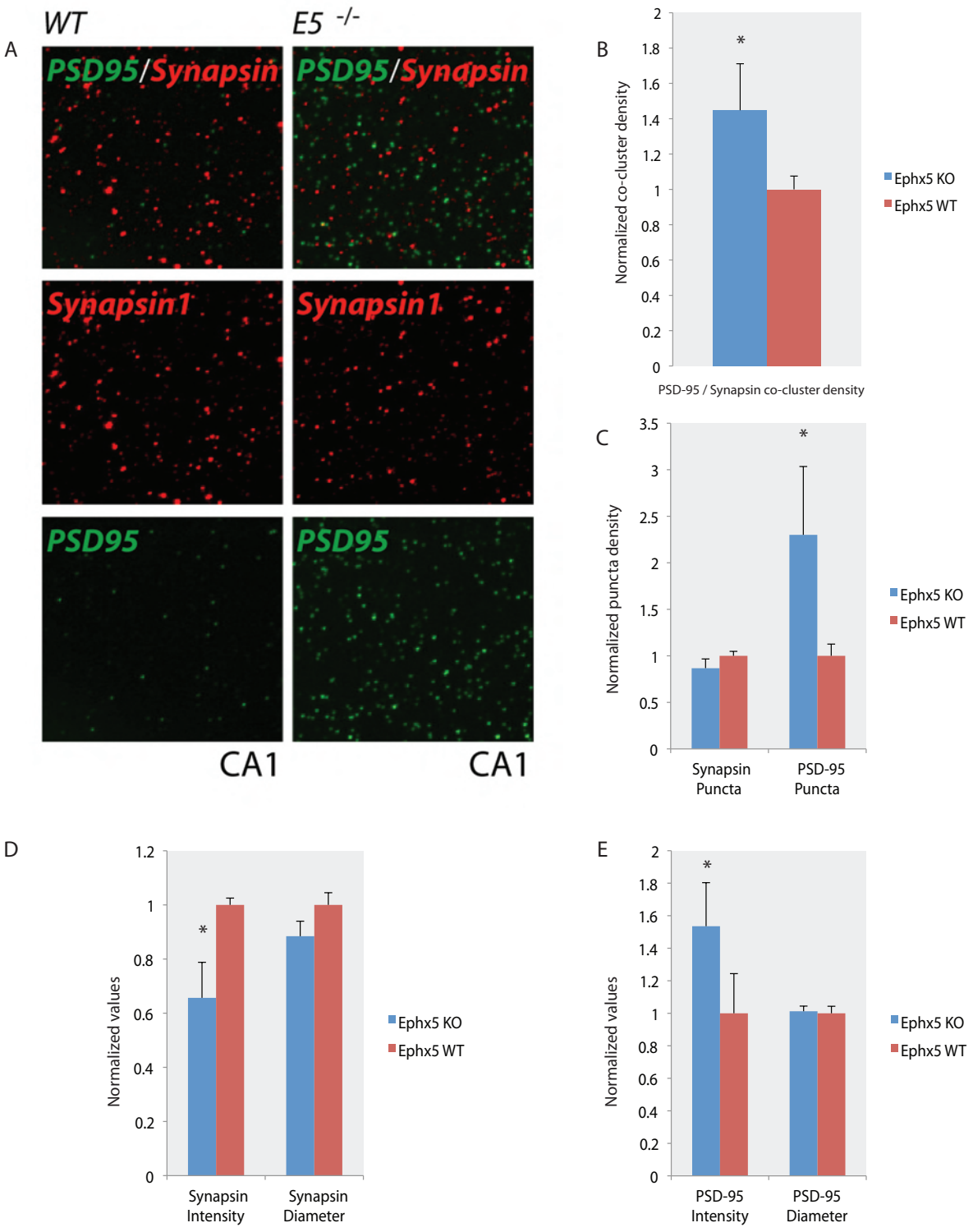

Figure 4.7 (Continued): Array Tomography analysis of Ephexin 5 knockout CA1 reveals elevated synapse density

A) Example images of PSD-95 (green) and synapsin (red) staining from stratum radiatum of wild type (left) or Ephexin 5 knockout (right) CA1.
B) Normalized quantification of PSD-95 / Synapsin co-cluster density shows elevated density of synaptic co-clusters in Ephexin 5 knockout CA1 ($P < 0.05$, Mann-Whitney U-test).
C) Normalized quantification of PSD-95 and Synapsin puncta density shows increased density of PSD-95 puncta in Ephexin 5 knockout CA1 (right, $P < 0.05$, Mann-Whitney U-test), but unchanged synapsin density.
D) Normalized quantification of synapsin puncta intensity (left) and diameter (right) in wild type (blue) and Ephexin 5 knockout mice (red). In Ephexin 5 knockout animals, synapsin puncta are less intense ($P < 0.05$, Mann-Whitney U-test), but have unchanged diameter.
E) Normalized quantification of PSD-95 puncta intensity (left) and diameter (right) in wild type (blue) and ephexin 5 knockout mice (red). In Ephexin 5 knockout animals, PSD-95 puncta are brighter ($P < 0.05$, Mann-Whitney U-test), but have unchanged diameter.

Quantification of puncta density revealed that this increase was driven by a large increase in the number of PSD-95 puncta, supporting previous data indicating that Ephexin 5 restricts synapse development through a post-synaptic mechanism (Figure 4.7C). Further analysis revealed that synapsin puncta had reduced intensity in Ephexin 5 knockout animals (Figure 4.7D). This decrease in intensity may reflect a potential strain on the number of available presynaptic vesicles given the increased number of release sites; if a fixed number of vesicles are divided between increased release sites, fewer vesicles per release site could cause reduced synapsin puncta intensity. In contrast, PSD-95 puncta are more intense in Ephexin 5 knockout animals than in wild type animals (Figure 4.7E). This observation may reflect that in addition to having more synaptic sites, Ephexin 5 animals have stronger excitatory synapses as well; this is supported by acute slice electrophysiology experiments demonstrating that both mEPSC frequency and amplitude are increased in Ephexin 5 knockout animals (Margolis et al., 2010). In summary, analysis of array tomography data demonstrated that Ephexin 5 is a negative regulator of synapse formation *in vivo,* and supported the hypothesis that it acts through a post-synaptic mechanism.

Analysis of CR3 and C3 Knockout Mice by Array Tomography

To continue application of our approach to analyzing synaptic puncta *in vivo*, we entered collaboration with Beth Steven's laboratory, which was investigating the normal function of microglia during neural development. They found that during periods of synapse pruning in the lateral geniculate nucleus (LGN), microglia engulf and destroy inappropriate synapses (Schafer et al., 2012). Evidence suggested that inappropriate synapses were tagged for destruction by complement C3, and that interaction of C3 with the complement receptor CR3, expressed in microglia, is necessary for this engulfment process. We therefore hypothesized that genetic deletion of C3 or CR3 would result in defects in the pruning process, which should manifest as a persistent increase in synapse density late in development, well after the normal pruning period was over (Schafer et al., 2012).

To test this hypothesis, array tomography ribbons were made from the LGN of pairs of P32-35 littermate wild type and CR3 KO mice, as well as wild type and C3 KO mice. Ribbons were stained for GluA1 and Vglut2, which labels presynaptic terminals of retinal ganglion cells; ribbons were subsequently imaged, aligned and analyzed. Data was handled and normalized as previously described. When the density of GluA1-Vglut2 co-clusters was quantified, it was apparent that CR3 knockout mice had increased synaptic co-cluster density (Figure 4.8A). CR3 knockout mice had normal number of GluA1 puncta (Figure 4.8B), but elevated levels of Vglut2 puncta (Figure 4.8C), consistent with a failure to prune presynaptic terminals. Similar experiments performed using C3 knockout mice demonstrated that these mice have an increase in GluA1-Vglut2 co-cluster density of similar magnitude to CR3 knockout mice (Figure 4.8D); however, neither Vglut2 nor GluR1 puncta density was altered in C3 knockout mice (data not shown). These data support the hypothesis that CR3-C3 interaction is necessary for microglia-mediated engulfment of presynaptic terminals to prune inappropriate synapses early in development. When either component is deleted, the LGN retains elevated numbers of synaptic contacts well after pruning is normally complete, indicating that both C3 and CR3 are obligate components of the signaling pathways regulating pruning (Schafer et al., 2012).

Discussion

This chapter describes the establishment, validation, and application of a method to analyze array tomography volumes of synaptic puncta in brain tissue. This method has notable advantages over previously used analyses of synaptic puncta. This approach preserves the three-dimensional nature of the data, and does not collapse superior axial resolution into a maximal intensity projection for analysis. Furthermore, by analyzing apposed (touching) pre- and post-synaptic puncta, this technique avoids reliance on the error colocalization between pre- and post-synaptic puncta. By analyzing touching pre- and post-synaptic marker puncta, this approach improves upon methods of analysis that simply count the number of

Figure 4.8: Array Tomography reveals that CR3 and C3 knockout mice have elevated synapse density in the Lateral Geniculate Nucleus

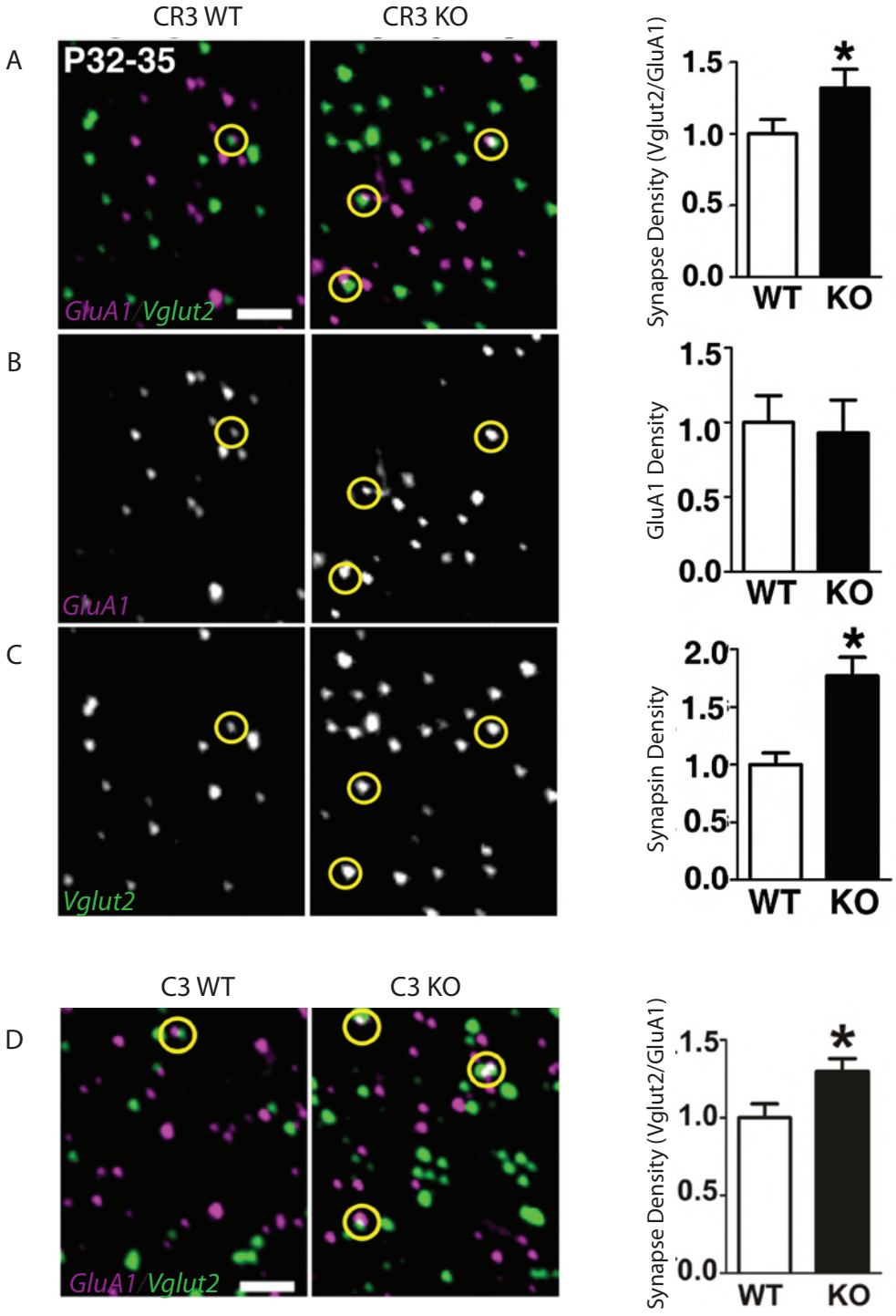

Figure 4.8 (Continued): Array Tomography reveals that CR3 and C3 knockout mice have elevated synapse density in the Lateral Geniculate Nucleus

A) Left, example from a single array tomography section of dLGN stained for GluA1 (magenta) and Vglut2 (green), from P32-35 wild type or CR3 knockout animals (scalebar 1 μm). Right, normalized quantification of GluA1-Vglut1 co-cluster density reveals elevated synapse density in CR3 knockout animals ($P < 0.05$, Mann-Whitney U-test).

B) Left, example image of GluA1 staining. Right, normalized quantification of GluA1 puncta density suggests that GluA1 puncta numbers are unchanged in CR3 knockout animals.

C) Left, example image of Vglut2 staining. Right, normalized quantification of Vglut2 puncta density suggests that Vglut2 puncta density is elevated in CR3 knockout animals ($P < 0.05$, Mann-Whitney U-test).

D) Left, example from a single array tomography section of dLGN stained for GluA1 (magenta) and Vglut2 (green), from P32-35 wild type or C3 knockout animals. scalebar 1 μm. Right, normalized quantification of GluA1-Vglut1 co-cluster density reveals elevated synapse density in C3 knockout animals ($P < 0.05$, Mann-Whitney U-test).

either synapsin or PSD-95 puncta and use them as a proxy for synapse number (Soiza-Reilly and Commons, 2011),(Micheva and Smith, 2007). Furthermore, in this approach, calculations made to determine synapse density are automated, simultaneously increasing throughput and decreasing potential for experimenter bias. Automation allows for the simultaneous analysis of many thousands of synaptic puncta: although Array Tomography cannot approach the spatial resolution of electron microscopy, we can easily analyze a hundred-fold more synapses, increasing statistical power (Mishchenko et al., 2010).

This approach to analyzing array tomography data also has significant drawbacks. First, and most prominently, our analysis requires the idealization and representation of synaptic immunofluorescence data as spheres. While many synaptic puncta are indeed sphere-like, most are not perfect spheres, so an inherent error is built into the analysis from the very start beginning. The use of an empirically determined distance threshold and visual feedback that allows the experimenter to monitor what the program calls as a synapse help mitigate this error; nevertheless, the efficacy of any model-based approach is always constrained by the fit of the model. Second, although the identification of synapses is automated and unbiased, the construction of a spherical model for each channel of synaptic puncta is neither automated nor unbiased. Thus, this approach is probably not optimal for *absolute* quantification of synapses or synaptic puncta in a volume. Instead, the power of this approach relies on its ability to detected changes between two identically handled and blinded conditions. Finally, perhaps the most powerful aspect of array tomography is the promise of multiplexing multiple rounds of antibodies on the same tissue. Regrettably, this procedure has not yet worked reliably in my hands, and accordingly my analysis system is not equipped to handle multiplexed data, though it could be modified to do so.

After our approach was developed, other groups performed array tomography experiments, confronted the same challenges, and attempted to solve them using distinct approaches. The most sophisticated approach to analyzing array tomography synaptic puncta has come from Stephen Smith's laboratory, and this approach relies on cross-correlation analysis of fluorescence intensity. Array

tomography ribbons are multiplexed with a number of synaptic markers, regions of interest are define around individual puncta of markers from a single channel (eg, synapsin), and a cross-correlation analysis of fluorescent intensity between the synapsin channel and every other channel is performed. The correlation coefficient is plotted as a function of lateral displacement of one channel: when the image is translated by 500 nm in a single dimension, the correlation rapidly falls off towards zero, suggesting that the correlation in puncta intensity is site-specific (Datwani et al., 2009). This approach is particularly suitable for multiplexed arrays, as a table of correlation coefficients between every possible pair of markers can be generated for every punctum, essentially generating a statistical profile describing the molecular content of a synapse (Micheva et al., 2010a).

This approach also has drawbacks. As discussed in the introduction, the superior resolution of array tomography means that pre- and post-synaptic markers are likely to display much less colocalization than in conventional confocal microscopy. For determining interaction between pre- and post-synaptic puncta, the cross-correlation approach still relies on the residual colocalization error signal: for example, the maximal correlation coefficient between presynaptic Bassoon and postsynaptic PSD-95 is only 0.1, and Vglut-1 and PSD-95 is 0.13 (compared to 0.7 for synapsin and Vglut1) (Micheva et al., 2010a). It is difficult to have a high degree of confidence in an approach based on shifting correlation coefficients when the maximal correlation observed in optimal conditions is very low. This cross-correlation approach for array tomography analysis appears much more useful defining the molecular components of individual pre- or post-synaptic terminals, and categorizing them accordingly.

Finally, any current discussion of array tomography would be incomplete without making reference to super-resolution microscopy, which became available shortly after the introduction of array tomography. SIM (Structured Illumination Microscopy) improved lateral resolution by a factor of 2 (~100 nm) and axial resolution by a factor of 3 (~200 nm) (Gustafsson, 2000). These resolutions compare very favorably with array tomography's capabilities; additionally, SIM has the immeasurable advantage of using conventional brain tissue preparations and

optical Z-sectioning, meaning that the labor intensive process of embedding tissue in acrylic resins and cutting ribbons of ultrathin sections can be dispensed with (Sigrist and Sabatini, 2012). PALM/STORM can achieve lateral resolution of ~30-50 nm, far greater than that of both SIM and array tomography. Indeed, STORM has been used effectively and elegantly to assess the sub-synaptic localization of synaptic proteins (Dani et al., 2010),(Sigrist and Sabatini, 2012). STORM is the superior technology for questions relating to sub-synaptic organization or localization of a given protein. However, array tomography retains some advantages over STORM: array tomography microscopy can image a much wider field of view much faster than STORM, and acquisition of Z-stacks using STORM has yet to become a common feature. Finally, when used in combination with advanced deconvolution techniques, array tomography can produce localizations on the same order of magnitude as STORM (Wang and Smith, 2012). In conclusion, the most powerful and unique aspect of array tomography is the ability to multiplex multiple sets of antibodies into the same volume. Although this procedure does not yet work reliably at multiple research institutions, it seems likely that this problem will eventually be overcome.

Material and Methods

Sample Preparation and Image Acquisition

Array tomography was performed as described (Micheva and Smith, 2007). In summary, acute hippocampal slices (300 μm thick) were fixed in 4% paraformaldehyde for 1 hour at room temperature and embedded in LR White resin using the bench top embedding protocol. Ribbons of between 30-50 serial 100 nm thick sections from each genotype were mounted side by side on gelatin subbed glass coverslips. Coverslips were immunostained with the following primary antibodies at a concentration of 1:100: α-Synapsin 1 (rb, fisher AB1543P, 1:100)

and α-PSD-95 (ms, fisher MA1-045), α-NR1 (rb, millipore AB9864), α-SV2 (ms, DSHB, Iowa), α-GAD65 (rb, Fisher AB5082MI), α-GABA-R β2/3 (Fisher MAB341MI), GluR1 (rb, millipore AB1504), Vglut2 (ms, NeuroMabs 75-067). Serial sections were imaged using a Zeiss Imager.Z1 microscope with a Photometrics CoolSNAP HQ2 camera on a PLAN APO 63x/1.4 objective. Tissue volumes were aligned using ImageJ (NIH) with the multistackreg plugin (Brad Busse). Detailed notes supplemental to the published array tomography protocols are available in Appendix 4.

Volume Analysis

Reconstructed tissue volumes were cropped and imported into Bitplane Imaris software to model synaptic puncta as spheres. Briefly, the spots function was used to generate spherical representations based on local intensity centers based on local background intensity. Modeling parameters were then adjusted so that the spots best represented the synaptic staining by eye. All sphere models were built blind to experimental condition or genotype, and identical parameters were applied to all experimental samples. Statistics for both channels were exported to a Microsoft Excel file, and rearranged for import to Matlab using a custom macro. The parameters exported were: Sphere diameter, the X, Y, and Z coordinate of the sphere center point, the sphere ID, the voxel count for each sphere, and the mean intensity of the sphere in each channel.

This information was fed into an in-house matlab script called AT Analyzer. Full code and comments are reproduced in Appendix 3. Briefly,s the size of the volume is calculated, and then corrected for the number of DAPI positive voxels in the volume, so that volumes containing different number of nuclei can be compared – before this correction was implemented, if synapse density is identical in the neuropil, identical volumes containing different number of nuclei might have had apparent differences in synapse density. Next, the program corrects for the axial edge artifact (cartooned in Figure 4.3A). Since the axial (Z plane) surface of the

sphere represent a much higher proportion of the surface area of the cube formed by the volume, a disproportionate number of puncta on the first and last slice of the volume will lack synaptic partners, since many synaptic partners will in the next section that didn't make it into the volume. To account for this, the program detects and deletes post-synaptic puncta on the extreme edges of the axial plan in the volume, but retains presynaptic puncta in those locations. The size of the volume is then reduced by the thickness of two sections in the axial axis. Thus, postsynaptic marker puncta are free to interact with presynaptic marker puncta that are an extra slice outside of the virtual stack, solving the axial edge artifact.

Next, the program identifies interacting pre and postsynaptic marker puncta. The distance from the center point of each presynaptic marker sphere to the center point of each postsynaptic marker sphere within range is calculated. If the distance between the center points is equal to or less than the sum of the radii of the two spheres, plus an empirically determined constant, the two puncta are considered to be interacting, and are counted as a synapse. The program determines the total number of synapses in the volume, as well as the total number of presynaptic marker and postsynaptic marker puncta that do not participate in a synapse, and calculates the density of each parameter. For every synapse found, the midpoint on the line between the two sphere centers is determined, and the X/Y/Z coordinates are logged as the synapse location; the length of the distance between sphere centers is also stored. This data can be loaded into a separate script called 'image_generator,' which produces a series of otherwise blank images with a five pixel cross at the location of every called synapse. This stack can be imported into bitplane imaris and overlaid with the original data to ensure that appropriate synapses are being identified, and obvious synapses are not being missed.

Several important control calculations are integrated into AT Analyzer. First, a control is performed where every puncta is assigned a completely random X/Y/Z center coordinate, and the synapse detection assay is repeated. This control ensures that the distribution of synapses detected is above what would be expected if the puncta were randomly scattered across the volume. Second, a control can be

performed where the position of every section of the Z stack is randomly shuffled; this control ensures that cross-section synapses are contributing in large measure to the detected synapse density calculation, as they are expected to. Finally, AT Analyzer will repeat all calculations at a number of distance thresholds and export all parameters (synapse, lone puncta, chance density) as a function of distance threshold to assess threshold dependency. Detailed instructions for use of AT Analyzer is available in Appendix 2, and the code of AT Analyzer and Image Generator are available in Appendix 3. Appendix 4 contains general notes to supplement published protocols for performing array tomography.

Chapter 5: References

Adesnik, H., Bruns, W., Taniguchi, H., Huang, Z.J., and Scanziani, M. (2012). A neural circuit for spatial summation in visual cortex. Nature *490*, 226-231.

Aizawa, H., Hu, S.C., Bobb, K., Balakrishnan, K., Ince, G., Gurevich, I., Cowan, M., and Ghosh, A. (2004). Dendrite development regulated by CREST, a calcium-regulated transcriptional activator. Science *303*, 197-202.

Akhtar, M.W., Kim, M.S., Adachi, M., Morris, M.J., Qi, X., Richardson, J.A., Bassel-Duby, R., Olson, E.N., Kavalali, E.T., and Monteggia, L.M. (2012). In vivo analysis of MEF2 transcription factors in synapse regulation and neuronal survival. PloS one *7*, e34863.

Allen, N.J., Bennett, M.L., Foo, L.C., Wang, G.X., Chakraborty, C., Smith, S.J., and Barres, B.A. (2012). Astrocyte glypicans 4 and 6 promote formation of excitatory synapses via GluA1 AMPA receptors. Nature *486*, 410-414.

An, J.J., Gharami, K., Liao, G.Y., Woo, N.H., Lau, A.G., Vanevski, F., Torre, E.R., Jones, K.R., Feng, Y., Lu, B.*, et al.* (2008). Distinct role of long 3' UTR BDNF mRNA in spine morphology and synaptic plasticity in hippocampal neurons. Cell *134*, 175-187.

Anggono, V., and Huganir, R.L. (2012). Regulation of AMPA receptor trafficking and synaptic plasticity. Current opinion in neurobiology *22*, 461-469.

Ascoli, G.A., Alonso-Nanclares, L., Anderson, S.A., Barrionuevo, G., Benavides-Piccione, R., Burkhalter, A., Buzsaki, G., Cauli, B., Defelipe, J., Fairen, A.*, et al.* (2008). Petilla terminology: nomenclature of features of GABAergic interneurons of the cerebral cortex. Nature reviews Neuroscience *9*, 557-568.

Atallah, B.V., Bruns, W., Carandini, M., and Scanziani, M. (2012). Parvalbumin-expressing interneurons linearly transform cortical responses to visual stimuli. Neuron *73*, 159-170.

Atallah, B.V., and Scanziani, M. (2009). Instantaneous modulation of gamma oscillation frequency by balancing excitation with inhibition. Neuron *62*, 566-577.

Bading, H., Ginty, D.D., and Greenberg, M.E. (1993). Regulation of gene expression in hippocampal neurons by distinct calcium signaling pathways. Science *260*, 181-186.

Bagnall, M.W., Hull, C., Bushong, E.A., Ellisman, M.H., and Scanziani, M. (2011). Multiple clusters of release sites formed by individual thalamic afferents onto cortical interneurons ensure reliable transmission. Neuron *71*, 180-194.

Baho, E., and Di Cristo, G. (2012). Neural activity and neurotransmission regulate the maturation of the innervation field of cortical GABAergic interneurons in an age-dependent manner. The Journal of neuroscience : the official journal of the Society for Neuroscience *32*, 911-918.

Bai, F., and Witzmann, F.A. (2007). Synaptosome proteomics. Sub-cellular biochemistry *43*, 77-98.

Bannister, A.J., and Kouzarides, T. (1996). The CBP co-activator is a histone acetyltransferase. Nature *384*, 641-643.

Barco, A., Alarcon, J.M., and Kandel, E.R. (2002). Expression of constitutively active CREB protein facilitates the late phase of long-term potentiation by enhancing synaptic capture. Cell *108*, 689-703.

Barco, A., Patterson, S.L., Alarcon, J.M., Gromova, P., Mata-Roig, M., Morozov, A., and Kandel, E.R. (2005). Gene expression profiling of facilitated L-LTP in VP16-CREB mice reveals that BDNF is critical for the maintenance of LTP and its synaptic capture. Neuron *48*, 123-137.

Barrett, C.F., and Tsien, R.W. (2008). The Timothy syndrome mutation differentially affects voltage- and calcium-dependent inactivation of CaV1.2 L-type calcium channels. Proceedings of the National Academy of Sciences of the United States of America *105*, 2157-2162.

Bartley, A.F., Huang, Z.J., Huber, K.M., and Gibson, J.R. (2008). Differential activity-dependent, homeostatic plasticity of two neocortical inhibitory circuits. Journal of neurophysiology *100*, 1983-1994.

Bartos, M., Vida, I., and Jonas, P. (2007). Synaptic mechanisms of synchronized gamma oscillations in inhibitory interneuron networks. Nature reviews Neuroscience *8*, 45-56.

Bath, K.G., and Lee, F.S. (2006). Variant BDNF (Val66Met) impact on brain structure and function. Cognitive, affective & behavioral neuroscience *6*, 79-85.

Batista-Brito, R., Machold, R., Klein, C., and Fishell, G. (2008). Gene expression in cortical interneuron precursors is prescient of their mature function. Cereb Cortex *18*, 2306-2317.

Bear, M.F., Huber, K.M., and Warren, S.T. (2004). The mGluR theory of fragile X mental retardation. Trends in neurosciences *27*, 370-377.

Beierlein, M., Gibson, J.R., and Connors, B.W. (2000). A network of electrically coupled interneurons drives synchronized inhibition in neocortex. Nature neuroscience *3*, 904-910.

Belforte, J.E., Zsiros, V., Sklar, E.R., Jiang, Z., Yu, G., Li, Y., Quinlan, E.M., and Nakazawa, K. (2010). Postnatal NMDA receptor ablation in corticolimbic interneurons confers schizophrenia-like phenotypes. Nature neuroscience *13*, 76-83.

Benedito, A.B., Lehtinen, M., Massol, R., Lopes, U.G., Kirchhausen, T., Rao, A., and Bonni, A. (2005). The transcription factor NFAT3 mediates neuronal survival. The Journal of biological chemistry *280*, 2818-2825.

Beurdeley, M., Spatazza, J., Lee, H.H., Sugiyama, S., Bernard, C., Di Nardo, A.A., Hensch, T.K., and Prochiantz, A. (2012). Otx2 binding to perineuronal nets persistently regulates plasticity in the mature visual cortex. The Journal of neuroscience : the official journal of the Society for Neuroscience *32*, 9429-9437.

Bjartmar, L., Huberman, A.D., Ullian, E.M., Renteria, R.C., Liu, X., Xu, W., Prezioso, J., Susman, M.W., Stellwagen, D., Stokes, C.C.*, et al.* (2006). Neuronal pentraxins mediate synaptic refinement in the developing visual system. The Journal of neuroscience : the official journal of the Society for Neuroscience *26*, 6269-6281.
Bliss, T.V., and Lomo, T. (1973). Long-lasting potentiation of synaptic transmission in the dentate area of the anaesthetized rabbit following stimulation of the perforant path. The Journal of physiology *232*, 331-356.

Bock, D.D., Lee, W.C., Kerlin, A.M., Andermann, M.L., Hood, G., Wetzel, A.W., Yurgenson, S., Soucy, E.R., Kim, H.S., and Reid, R.C. (2011). Network anatomy and in vivo physiology of visual cortical neurons. Nature *471*, 177-182.

Bolstad, B.M., Irizarry, R.A., Astrand, M., and Speed, T.P. (2003). A comparison of normalization methods for high density oligonucleotide array data based on variance and bias. Bioinformatics *19*, 185-193.

Bolton, M.M., Pittman, A.J., and Lo, D.C. (2000). Brain-derived neurotrophic factor differentially regulates excitatory and inhibitory synaptic transmission in hippocampal cultures. The Journal of neuroscience : the official journal of the Society for Neuroscience *20*, 3221-3232.

Bonni, A., Ginty, D.D., Dudek, H., and Greenberg, M.E. (1995). Serine 133-phosphorylated CREB induces transcription via a cooperative mechanism that may confer specificity to neurotrophin signals. Molecular and cellular neurosciences *6*, 168-183.

Bozon, B., Davis, S., and Laroche, S. (2003). A requirement for the immediate early gene zif268 in reconsolidation of recognition memory after retrieval. Neuron *40*, 695-701.

Bradley, J., Carter, S.R., Rao, V.R., Wang, J., and Finkbeiner, S. (2006). Splice variants of the NR1 subunit differentially induce NMDA receptor-dependent gene expression. The Journal of neuroscience : the official journal of the Society for Neuroscience *26*, 1065-1076.

Brakeman, P.R., Lanahan, A.A., O'Brien, R., Roche, K., Barnes, C.A., Huganir, R.L., and Worley, P.F. (1997). Homer: a protein that selectively binds metabotropic glutamate receptors. Nature *386*, 284-288.

Burgard, E.C., and Hablitz, J.J. (1993). NMDA receptor-mediated components of miniature excitatory synaptic currents in developing rat neocortex. Journal of neurophysiology *70*, 1841-1852.

Cardin, J.A., Carlen, M., Meletis, K., Knoblich, U., Zhang, F., Deisseroth, K., Tsai, L.H., and Moore, C.I. (2009). Driving fast-spiking cells induces gamma rhythm and controls sensory responses. Nature *459*, 663-667.

Cardin, J.A., Palmer, L.A., and Contreras, D. (2007). Stimulus feature selectivity in excitatory and inhibitory neurons in primary visual cortex. The Journal of neuroscience : the official journal of the Society for Neuroscience *27*, 10333-10344.

Carew, T.J., Hawkins, R.D., Abrams, T.W., and Kandel, E.R. (1984). A test of Hebb's postulate at identified synapses which mediate classical conditioning in Aplysia. The Journal of neuroscience : the official journal of the Society for Neuroscience *4*, 1217-1224.

Carmignoto, G., and Vicini, S. (1992). Activity-dependent decrease in NMDA receptor responses during development of the visual cortex. Science *258*, 1007-1011.
Carol, M.P. (1976). Neuronal circuits involved in learning: the use of modifiable synapses in the simulation of behavior. The International journal of neuroscience *7*, 9-18.

Castren, E., Zafra, F., Thoenen, H., and Lindholm, D. (1992). Light regulates expression of brain-derived neurotrophic factor mRNA in rat visual cortex. Proceedings of the National Academy of Sciences of the United States of America *89*, 9444-9448.

Cauli, B., Audinat, E., Lambolez, B., Angulo, M.C., Ropert, N., Tsuzuki, K., Hestrin, S., and Rossier, J. (1997). Molecular and physiological diversity of cortical nonpyramidal cells. The Journal of neuroscience : the official journal of the Society for Neuroscience *17*, 3894-3906.

Ch'ng, T.H., Uzgil, B., Lin, P., Avliyakulov, N.K., O'Dell, T.J., and Martin, K.C. (2012). Activity-Dependent Transport of the Transcriptional Coactivator CRTC1 from Synapse to Nucleus. Cell *150*, 207-221.

Chang, M.C., Park, J.M., Pelkey, K.A., Grabenstatter, H.L., Xu, D., Linden, D.J., Sutula, T.P., McBain, C.J., and Worley, P.F. (2010). Narp regulates homeostatic scaling of excitatory synapses on parvalbumin-expressing interneurons. Nature neuroscience *13*, 1090-1097.

Chao, H.T., Chen, H., Samaco, R.C., Xue, M., Chahrour, M., Yoo, J., Neul, J.L., Gong, S., Lu, H.C., Heintz, N.*, et al.* (2010). Dysfunction in GABA signalling mediates autism-like stereotypies and Rett syndrome phenotypes. Nature *468*, 263-269.

Chattopadhyaya, B., Di Cristo, G., Higashiyama, H., Knott, G.W., Kuhlman, S.J., Welker, E., and Huang, Z.J. (2004). Experience and activity-dependent maturation of perisomatic GABAergic innervation in primary visual cortex during a postnatal critical period. The Journal of neuroscience : the official journal of the Society for Neuroscience *24*, 9598-9611.

Chen, G., Zou, X., Watanabe, H., van Deursen, J.M., and Shen, J. (2010a). CREB binding protein is required for both short-term and long-term memory formation. The Journal of neuroscience : the official journal of the Society for Neuroscience *30*, 13066-13077.

Chen, H.X., Jiang, M., Akakin, D., and Roper, S.N. (2009). Long-term potentiation of excitatory synapses on neocortical somatostatin-expressing interneurons. Journal of neurophysiology *102*, 3251-3259.

Chen, J.L., Lin, W.C., Cha, J.W., So, P.T., Kubota, Y., and Nedivi, E. (2011). Structural basis for the role of inhibition in facilitating adult brain plasticity. Nature neuroscience *14*, 587-594.

Chen, L., Chetkovich, D.M., Petralia, R.S., Sweeney, N.T., Kawasaki, Y., Wenthold, R.J., Bredt, D.S., and Nicoll, R.A. (2000). Stargazin regulates synaptic targeting of AMPA receptors by two distinct mechanisms. Nature *408*, 936-943.

Chen, W.G., West, A.E., Tao, X., Corfas, G., Szentirmay, M.N., Sawadogo, M., Vinson, C., and Greenberg, M.E. (2003). Upstream stimulatory factors are mediators of Ca2+-responsive transcription in neurons. The Journal of neuroscience : the official journal of the Society for Neuroscience *23*, 2572-2581.

Chen, Y.J., Zhang, M., Yin, D.M., Wen, L., Ting, A., Wang, P., Lu, Y.S., Zhu, X.H., Li, S.J., Wu, C.Y.*, et al.* (2010b). ErbB4 in parvalbumin-positive interneurons is critical for neuregulin 1 regulation of long-term potentiation. Proceedings of the National Academy of Sciences of the United States of America *107*, 21818-21823.

Chen, Z.Y., Jing, D., Bath, K.G., Ieraci, A., Khan, T., Siao, C.J., Herrera, D.G., Toth, M., Yang, C., McEwen, B.S.*, et al.* (2006). Genetic variant BDNF (Val66Met) polymorphism alters anxiety-related behavior. Science *314*, 140-143.

Chowdhury, S., Shepherd, J.D., Okuno, H., Lyford, G., Petralia, R.S., Plath, N., Kuhl, D., Huganir, R.L., and Worley, P.F. (2006). Arc/Arg3.1 interacts with the endocytic machinery to regulate AMPA receptor trafficking. Neuron *52*, 445-459.

Clayton-Smith, J., and Laan, L. (2003). Angelman syndrome: a review of the clinical and genetic aspects. Journal of medical genetics *40*, 87-95.

Clements, J.D., and Bekkers, J.M. (1997). Detection of spontaneous synaptic events with an optimally scaled template. Biophysical journal *73*, 220-229.

Close, J., Xu, H., De Marco Garcia, N., Batista-Brito, R., Rossignol, E., Rudy, B., and Fishell, G. (2012). Satb1 is an activity-modulated transcription factor required for the terminal differentiation and connectivity of medial ganglionic eminence-derived cortical interneurons. The Journal of neuroscience : the official journal of the Society for Neuroscience *32*, 17690-17705.

Cobb, S.R., Buhl, E.H., Halasy, K., Paulsen, O., and Somogyi, P. (1995). Synchronization of neuronal activity in hippocampus by individual GABAergic interneurons. Nature *378*, 75-78.

Cohen, S., and Greenberg, M.E. (2008). Communication between the synapse and the nucleus in neuronal development, plasticity, and disease. Annual review of cell and developmental biology *24*, 183-209.

Cole, C.J., Mercaldo, V., Restivo, L., Yiu, A.P., Sekeres, M.J., Han, J.H., Vetere, G., Pekar, T., Ross, P.J., Neve, R.L.*, et al.* (2012). MEF2 negatively regulates learning-induced structural plasticity and memory formation. Nature neuroscience *15*, 1255-1264.

Coutellier, L., Beraki, S., Ardestani, P.M., Saw, N.L., and Shamloo, M. (2012). Npas4: a neuronal transcription factor with a key role in social and cognitive functions relevant to developmental disorders. PloS one *7*, e46604.

Cruikshank, S.J., Lewis, T.J., and Connors, B.W. (2007). Synaptic basis for intense thalamocortical activation of feedforward inhibitory cells in neocortex. Nature neuroscience *10*, 462-468.

Dani, A., Huang, B., Bergan, J., Dulac, C., and Zhuang, X. (2010). Superresolution imaging of chemical synapses in the brain. Neuron *68*, 843-856.

Dash, P.K., Karl, K.A., Colicos, M.A., Prywes, R., and Kandel, E.R. (1991). cAMP response element-binding protein is activated by Ca2+/calmodulin- as well as cAMP-dependent protein kinase. Proceedings of the National Academy of Sciences of the United States of America *88*, 5061-5065.

Datwani, A., McConnell, M.J., Kanold, P.O., Micheva, K.D., Busse, B., Shamloo, M., Smith, S.J., and Shatz, C.J. (2009). Classical MHCI molecules regulate retinogeniculate refinement and limit ocular dominance plasticity. Neuron *64*, 463-470.

De Marco Garcia, N.V., Karayannis, T., and Fishell, G. (2011). Neuronal activity is required for the development of specific cortical interneuron subtypes. Nature *472*, 351-355.

Demas, J., Sagdullaev, B.T., Green, E., Jaubert-Miazza, L., McCall, M.A., Gregg, R.G., Wong, R.O., and Guido, W. (2006). Failure to maintain eye-specific segregation in nob, a mutant with abnormally patterned retinal activity. Neuron *50*, 247-259.

Denaxa, M., Kalaitzidou, M., Garefalaki, A., Achimastou, A., Lasrado, R., Maes, T., and Pachnis, V. (2012). Maturation-Promoting Activity of SATB1 in MGE-Derived Cortical Interneurons. Cell reports *2*, 1351-1362.

Dingledine, R., Borges, K., Bowie, D., and Traynelis, S.F. (1999). The glutamate receptor ion channels. Pharmacological reviews *51*, 7-61.

Dolen, G., and Bear, M.F. (2008). Role for metabotropic glutamate receptor 5 (mGluR5) in the pathogenesis of fragile X syndrome. The Journal of physiology *586*, 1503-1508.

Dolen, G., Osterweil, E., Rao, B.S., Smith, G.B., Auerbach, B.D., Chattarji, S., and Bear, M.F. (2007). Correction of fragile X syndrome in mice. Neuron *56*, 955-962.

Dolmetsch, R.E., Pajvani, U., Fife, K., Spotts, J.M., and Greenberg, M.E. (2001). Signaling to the nucleus by an L-type calcium channel-calmodulin complex through the MAP kinase pathway. Science *294*, 333-339.

Egan, M.F., Kojima, M., Callicott, J.H., Goldberg, T.E., Kolachana, B.S., Bertolino, A., Zaitsev, E., Gold, B., Goldman, D., Dean, M.*, et al.* (2003). The BDNF val66met polymorphism affects activity-dependent secretion of BDNF and human memory and hippocampal function. Cell *112*, 257-269.

Ehlers, M.D. (2003). Activity level controls postsynaptic composition and signaling via the ubiquitin-proteasome system. Nature neuroscience *6*, 231-242.

Erisir, A., Lau, D., Rudy, B., and Leonard, C.S. (1999). Function of specific K(+) channels in sustained high-frequency firing of fast-spiking neocortical interneurons. Journal of neurophysiology *82*, 2476-2489.

Eroglu, C., Allen, N.J., Susman, M.W., O'Rourke, N.A., Park, C.Y., Ozkan, E., Chakraborty, C., Mulinyawe, S.B., Annis, D.S., Huberman, A.D.*, et al.* (2009). Gabapentin receptor alpha2delta-1 is a neuronal thrombospondin receptor responsible for excitatory CNS synaptogenesis. Cell *139*, 380-392.

Erxleben, C., Liao, Y., Gentile, S., Chin, D., Gomez-Alegria, C., Mori, Y., Birnbaumer, L., and Armstrong, D.L. (2006). Cyclosporin and Timothy syndrome increase mode 2 gating of CaV1.2 calcium channels through aberrant phosphorylation of S6 helices.

Proceedings of the National Academy of Sciences of the United States of America *103*, 3932-3937.

Espinosa, J.S., and Stryker, M.P. (2012). Development and plasticity of the primary visual cortex. Neuron *75*, 230-249.

Fagiolini, M., Fritschy, J.M., Low, K., Mohler, H., Rudolph, U., and Hensch, T.K. (2004). Specific GABAA circuits for visual cortical plasticity. Science *303*, 1681-1683.

Fagiolini, M., and Hensch, T.K. (2000). Inhibitory threshold for critical-period activation in primary visual cortex. Nature *404*, 183-186.

Fanselow, E.E., Richardson, K.A., and Connors, B.W. (2008). Selective, state-dependent activation of somatostatin-expressing inhibitory interneurons in mouse neocortex. Journal of neurophysiology *100*, 2640-2652.

Fazzari, P., Paternain, A.V., Valiente, M., Pla, R., Lujan, R., Lloyd, K., Lerma, J., Marin, O., and Rico, B. (2010). Control of cortical GABA circuitry development by Nrg1 and ErbB4 signalling. Nature *464*, 1376-1380.

Feldheim, D.A., and O'Leary, D.D. (2010). Visual map development: bidirectional signaling, bifunctional guidance molecules, and competition. Cold Spring Harbor perspectives in biology *2*, a001768.

Feller, M.B., and Scanziani, M. (2005). A precritical period for plasticity in visual cortex. Current opinion in neurobiology *15*, 94-100.

Filiou, M.D., Bisle, B., Reckow, S., Teplytska, L., Maccarrone, G., and Turck, C.W. (2010). Profiling of mouse synaptosome proteome and phosphoproteome by IEF. Electrophoresis *31*, 1294-1301.

Fino, E., and Yuste, R. (2011). Dense inhibitory connectivity in neocortex. Neuron *69*, 1188-1203.

Fischer, A., Sananbenesi, F., Wang, X., Dobbin, M., and Tsai, L.H. (2007). Recovery of learning and memory is associated with chromatin remodelling. Nature *447*, 178-182.

Flandin, P., Zhao, Y., Vogt, D., Jeong, J., Long, J., Potter, G., Westphal, H., and Rubenstein, J.L. (2011). Lhx6 and Lhx8 coordinately induce neuronal expression of Shh that controls the generation of interneuron progenitors. Neuron *70*, 939-950.

Flavell, S.W., Cowan, C.W., Kim, T.K., Greer, P.L., Lin, Y., Paradis, S., Griffith, E.C., Hu, L.S., Chen, C., and Greenberg, M.E. (2006). Activity-dependent regulation of MEF2 transcription factors suppresses excitatory synapse number. Science *311*, 1008-1012.

Flavell, S.W., and Greenberg, M.E. (2008). Signaling mechanisms linking neuronal activity to gene expression and plasticity of the nervous system. Annual review of neuroscience *31*, 563-590.

Flavell, S.W., Kim, T.K., Gray, J.M., Harmin, D.A., Hemberg, M., Hong, E.J., Markenscoff-Papadimitriou, E., Bear, D.M., and Greenberg, M.E. (2008). Genome-wide analysis of MEF2 transcriptional program reveals synaptic target genes and neuronal activity-dependent polyadenylation site selection. Neuron *60*, 1022-1038.

Flint, A.C., Maisch, U.S., Weishaupt, J.H., Kriegstein, A.R., and Monyer, H. (1997). NR2A subunit expression shortens NMDA receptor synaptic currents in developing neocortex. The Journal of neuroscience : the official journal of the Society for Neuroscience *17*, 2469-2476.

Frenkel, M.Y., and Bear, M.F. (2004). How monocular deprivation shifts ocular dominance in visual cortex of young mice. Neuron *44*, 917-923.

Frey, U., Krug, M., Brodemann, R., Reymann, K., and Matthies, H. (1989). Long-term potentiation induced in dendrites separated from rat's CA1 pyramidal somata does not establish a late phase. Neuroscience letters *97*, 135-139.

Fuchs, E.C., Zivkovic, A.R., Cunningham, M.O., Middleton, S., Lebeau, F.E., Bannerman, D.M., Rozov, A., Whittington, M.A., Traub, R.D., Rawlins, J.N.*, et al.* (2007). Recruitment of parvalbumin-positive interneurons determines hippocampal function and associated behavior. Neuron *53*, 591-604.

Gainey, M.A., Hurvitz-Wolff, J.R., Lambo, M.E., and Turrigiano, G.G. (2009). Synaptic scaling requires the GluR2 subunit of the AMPA receptor. The Journal of neuroscience : the official journal of the Society for Neuroscience *29*, 6479-6489.

Galarreta, M., and Hestrin, S. (1999). A network of fast-spiking cells in the neocortex connected by electrical synapses. Nature *402*, 72-75.

Galarreta, M., and Hestrin, S. (2001). Spike transmission and synchrony detection in networks of GABAergic interneurons. Science *292*, 2295-2299.

Galli, L., and Maffei, L. (1988). Spontaneous impulse activity of rat retinal ganglion cells in prenatal life. Science *242*, 90-91.

Gao, M., Sossa, K., Song, L., Errington, L., Cummings, L., Hwang, H., Kuhl, D., Worley, P., and Lee, H.K. (2010). A specific requirement of Arc/Arg3.1 for visual experience-induced homeostatic synaptic plasticity in mouse primary visual cortex. The Journal of neuroscience : the official journal of the Society for Neuroscience *30*, 7168-7178.

Garaschuk, O., Linn, J., Eilers, J., and Konnerth, A. (2000). Large-scale oscillatory calcium waves in the immature cortex. Nature neuroscience *3*, 452-459.

Gau, D., Lemberger, T., von Gall, C., Kretz, O., Le Minh, N., Gass, P., Schmid, W., Schibler, U., Korf, H.W., and Schutz, G. (2002). Phosphorylation of CREB Ser142 regulates light-induced phase shifts of the circadian clock. Neuron *34*, 245-253.

Gaudilliere, B., Konishi, Y., de la Iglesia, N., Yao, G., and Bonni, A. (2004). A CaMKII-NeuroD signaling pathway specifies dendritic morphogenesis. Neuron *41*, 229-241.

Genoud, C., Knott, G.W., Sakata, K., Lu, B., and Welker, E. (2004). Altered synapse formation in the adult somatosensory cortex of brain-derived neurotrophic factor heterozygote mice. The Journal of neuroscience : the official journal of the Society for Neuroscience *24*, 2394-2400.

Gentet, L.J., Kremer, Y., Taniguchi, H., Huang, Z.J., Staiger, J.F., and Petersen, C.C. (2012). Unique functional properties of somatostatin-expressing GABAergic neurons in mouse barrel cortex. Nature neuroscience *15*, 607-612.

Ghosh, A., Carnahan, J., and Greenberg, M.E. (1994). Requirement for BDNF in activity-dependent survival of cortical neurons. Science *263*, 1618-1623.

Gianfranceschi, L., Siciliano, R., Walls, J., Morales, B., Kirkwood, A., Huang, Z.J., Tonegawa, S., and Maffei, L. (2003). Visual cortex is rescued from the effects of dark rearing by overexpression of BDNF. Proceedings of the National Academy of Sciences of the United States of America *100*, 12486-12491.

Gibson, J.R., Bartley, A.F., and Huber, K.M. (2006). Role for the subthreshold currents ILeak and IH in the homeostatic control of excitability in neocortical somatostatin-positive inhibitory neurons. Journal of neurophysiology *96*, 420-432.

Gibson, J.R., Beierlein, M., and Connors, B.W. (1999). Two networks of electrically coupled inhibitory neurons in neocortex. Nature *402*, 75-79.

Ginty, D.D., Bonni, A., and Greenberg, M.E. (1994). Nerve growth factor activates a Ras-dependent protein kinase that stimulates c-fos transcription via phosphorylation of CREB. Cell *77*, 713-725.

Ginty, D.D., Kornhauser, J.M., Thompson, M.A., Bading, H., Mayo, K.E., Takahashi, J.S., and Greenberg, M.E. (1993). Regulation of CREB phosphorylation in the suprachiasmatic nucleus by light and a circadian clock. Science *260*, 238-241.

Glickfeld, L.L., and Scanziani, M. (2006). Distinct timing in the activity of cannabinoid-sensitive and cannabinoid-insensitive basket cells. Nature neuroscience *9*, 807-815.

Godecke, I., and Bonhoeffer, T. (1996). Development of identical orientation maps for two eyes without common visual experience. Nature *379*, 251-254.

Gogolla, N., Galimberti, I., Deguchi, Y., and Caroni, P. (2009a). Wnt signaling mediates experience-related regulation of synapse numbers and mossy fiber connectivities in the adult hippocampus. Neuron *62*, 510-525.

Gogolla, N., Leblanc, J.J., Quast, K.B., Sudhof, T.C., Fagiolini, M., and Hensch, T.K. (2009b). Common circuit defect of excitatory-inhibitory balance in mouse models of autism. Journal of neurodevelopmental disorders *1*, 172-181.

Goldin, M., Epsztein, J., Jorquera, I., Represa, A., Ben-Ari, Y., Crepel, V., and Cossart, R. (2007). Synaptic kainate receptors tune oriens-lacunosum moleculare interneurons to operate at theta frequency. The Journal of neuroscience : the official journal of the Society for Neuroscience *27*, 9560-9572.

Goldstein, A.Y., Wang, X., and Schwarz, T.L. (2008). Axonal transport and the delivery of pre-synaptic components. Current opinion in neurobiology *18*, 495-503.

Gonzalez, G.A., and Montminy, M.R. (1989). Cyclic AMP stimulates somatostatin gene transcription by phosphorylation of CREB at serine 133. Cell *59*, 675-680.

Gorba, T., and Wahle, P. (1999). Expression of TrkB and TrkC but not BDNF mRNA in neurochemically identified interneurons in rat visual cortex in vivo and in organotypic cultures. The European journal of neuroscience *11*, 1179-1190.

Gordon, J.A., and Stryker, M.P. (1996). Experience-dependent plasticity of binocular responses in the primary visual cortex of the mouse. The Journal of neuroscience : the official journal of the Society for Neuroscience *16*, 3274-3286.

Gorski, J.A., Zeiler, S.R., Tamowski, S., and Jones, K.R. (2003). Brain-derived neurotrophic factor is required for the maintenance of cortical dendrites. The Journal of neuroscience : the official journal of the Society for Neuroscience *23*, 6856-6865.

Greenberg, M.E., and Ziff, E.B. (1984). Stimulation of 3T3 cells induces transcription of the c-fos proto-oncogene. Nature *311*, 433-438.

Greenberg, M.E., Ziff, E.B., and Greene, L.A. (1986). Stimulation of neuronal acetylcholine receptors induces rapid gene transcription. Science *234*, 80-83.

Greer, P.L., and Greenberg, M.E. (2008). From synapse to nucleus: calcium-dependent gene transcription in the control of synapse development and function. Neuron *59*, 846-860.

Greer, P.L., Hanayama, R., Bloodgood, B.L., Mardinly, A.R., Lipton, D.M., Flavell, S.W., Kim, T.K., Griffith, E.C., Waldon, Z., Maehr, R.*, et al.* (2010). The Angelman Syndrome protein Ube3A regulates synapse development by ubiquitinating arc. Cell *140*, 704-716.

Groc, L., Heine, M., Cognet, L., Brickley, K., Stephenson, F.A., Lounis, B., and Choquet, D. (2004). Differential activity-dependent regulation of the lateral mobilities of AMPA and NMDA receptors. Nature neuroscience *7*, 695-696.

Guo, M.L., Xue, B., Jin, D.Z., Liu, Z.G., Fibuch, E.E., Mao, L.M., and Wang, J.Q. (2012). Upregulation of Npas4 protein expression by chronic administration of amphetamine in rat nucleus accumbens in vivo. Neuroscience letters.

Gustafsson, M.G. (2000). Surpassing the lateral resolution limit by a factor of two using structured illumination microscopy. Journal of microscopy *198*, 82-87.

Hall, B.J., Ripley, B., and Ghosh, A. (2007). NR2B signaling regulates the development of synaptic AMPA receptor current. The Journal of neuroscience : the official journal of the Society for Neuroscience *27*, 13446-13456.

Hall, D., Dhilla, A., Charalambous, A., Gogos, J.A., and Karayiorgou, M. (2003). Sequence variants of the brain-derived neurotrophic factor (BDNF) gene are strongly associated with obsessive-compulsive disorder. American journal of human genetics *73*, 370-376.

Hanover, J.L., Huang, Z.J., Tonegawa, S., and Stryker, M.P. (1999). Brain-derived neurotrophic factor overexpression induces precocious critical period in mouse visual cortex. The Journal of neuroscience : the official journal of the Society for Neuroscience *19*, RC40.

Hardingham, G.E., Arnold, F.J., and Bading, H. (2001). A calcium microdomain near NMDA receptors: on switch for ERK-dependent synapse-to-nucleus communication. Nature neuroscience *4*, 565-566.

Hardingham, G.E., Fukunaga, Y., and Bading, H. (2002). Extrasynaptic NMDARs oppose synaptic NMDARs by triggering CREB shut-off and cell death pathways. Nature neuroscience *5*, 405-414.

Harris, K.M., Jensen, F.E., and Tsao, B. (1992). Three-dimensional structure of dendritic spines and synapses in rat hippocampus (CA1) at postnatal day 15 and adult ages: implications for the maturation of synaptic physiology and long-term potentiation. The Journal of neuroscience : the official journal of the Society for Neuroscience *12*, 2685-2705.

Hartig, W., Derouiche, A., Welt, K., Brauer, K., Grosche, J., Mader, M., Reichenbach, A., and Bruckner, G. (1999). Cortical neurons immunoreactive for the potassium channel Kv3.1b subunit are predominantly surrounded by perineuronal nets presumed as a buffering system for cations. Brain research *842*, 15-29.

Hayashi, Y., Shi, S.H., Esteban, J.A., Piccini, A., Poncer, J.C., and Malinow, R. (2000). Driving AMPA receptors into synapses by LTP and CaMKII: requirement for GluR1 and PDZ domain interaction. Science *287*, 2262-2267.

Hayut, I., Fanselow, E.E., Connors, B.W., and Golomb, D. (2011). LTS and FS inhibitory interneurons, short-term synaptic plasticity, and cortical circuit dynamics. PLoS computational biology *7*, e1002248.

He, M., Liu, Y., Wang, X., Zhang, M.Q., Hannon, G.J., and Huang, Z.J. (2012). Cell-type-based analysis of microRNA profiles in the mouse brain. Neuron *73*, 35-48.
Hensch, T.K. (2005). Critical period plasticity in local cortical circuits. Nature reviews Neuroscience *6*, 877-888.

Hensch, T.K., Fagiolini, M., Mataga, N., Stryker, M.P., Baekkeskov, S., and Kash, S.F. (1998). Local GABA circuit control of experience-dependent plasticity in developing visual cortex. Science *282*, 1504-1508.

Hippenmeyer, S., Vrieseling, E., Sigrist, M., Portmann, T., Laengle, C., Ladle, D.R., and Arber, S. (2005). A developmental switch in the response of DRG neurons to ETS transcription factor signaling. PLoS biology *3*, e159.

Hofer, S.B., Ko, H., Pichler, B., Vogelstein, J., Ros, H., Zeng, H., Lein, E., Lesica, N.A., and Mrsic-Flogel, T.D. (2011). Differential connectivity and response dynamics of excitatory and inhibitory neurons in visual cortex. Nature neuroscience *14*, 1045-1052.

Hong, E.J., McCord, A.E., and Greenberg, M.E. (2008). A biological function for the neuronal activity-dependent component of Bdnf transcription in the development of cortical inhibition. Neuron *60*, 610-624.

Hooks, B.M., and Chen, C. (2006). Distinct roles for spontaneous and visual activity in remodeling of the retinogeniculate synapse. Neuron *52*, 281-291.

Hooks, B.M., Hires, S.A., Zhang, Y.X., Huber, D., Petreanu, L., Svoboda, K., and Shepherd, G.M. (2011). Laminar analysis of excitatory local circuits in vibrissal motor and sensory cortical areas. PLoS biology *9*, e1000572.

Horton, J.C., and Hocking, D.R. (1996). An adult-like pattern of ocular dominance columns in striate cortex of newborn monkeys prior to visual experience. The Journal of neuroscience : the official journal of the Society for Neuroscience *16*, 1791-1807.

Hu, H., Ma, Y., and Agmon, A. (2011). Submillisecond firing synchrony between different subtypes of cortical interneurons connected chemically but not electrically. The Journal of neuroscience : the official journal of the Society for Neuroscience *31*, 3351-3361.

Huang, Z.J., Kirkwood, A., Pizzorusso, T., Porciatti, V., Morales, B., Bear, M.F., Maffei, L., and Tonegawa, S. (1999). BDNF regulates the maturation of inhibition and the critical period of plasticity in mouse visual cortex. Cell *98*, 739-755.

Hubel, D.H., Wiesel, T.N., and LeVay, S. (1977). Plasticity of ocular dominance columns in monkey striate cortex. Philosophical transactions of the Royal Society of London Series B, Biological sciences *278*, 377-409.
Hubener, M. (2003). Mouse visual cortex. Current opinion in neurobiology *13*, 413-420.

Husi, H., Ward, M.A., Choudhary, J.S., Blackstock, W.P., and Grant, S.G. (2000). Proteomic analysis of NMDA receptor-adhesion protein signaling complexes. Nature neuroscience *3*, 661-669.

Impey, S., Fong, A.L., Wang, Y., Cardinaux, J.R., Fass, D.M., Obrietan, K., Wayman, G.A., Storm, D.R., Soderling, T.R., and Goodman, R.H. (2002). Phosphorylation of CBP mediates transcriptional activation by neural activity and CaM kinase IV. Neuron *34*, 235-244.

Impey, S., McCorkle, S.R., Cha-Molstad, H., Dwyer, J.M., Yochum, G.S., Boss, J.M., McWeeney, S., Dunn, J.J., Mandel, G., and Goodman, R.H. (2004). Defining the CREB regulon: a genome-wide analysis of transcription factor regulatory regions. Cell *119*, 1041-1054.

Isaac, J.T., Ashby, M.C., and McBain, C.J. (2007). The role of the GluR2 subunit in AMPA receptor function and synaptic plasticity. Neuron *54*, 859-871.
Isaacson, J.S., and Scanziani, M. (2011). How inhibition shapes cortical activity. Neuron *72*, 231-243.

Jackson, A.C., and Nicoll, R.A. (2011). The expanding social network of ionotropic glutamate receptors: TARPs and other transmembrane auxiliary subunits. Neuron *70*, 178-199.

Jiang, Y.H., Armstrong, D., Albrecht, U., Atkins, C.M., Noebels, J.L., Eichele, G., Sweatt, J.D., and Beaudet, A.L. (1998). Mutation of the Angelman ubiquitin ligase in mice causes increased cytoplasmic p53 and deficits of contextual learning and long-term potentiation. Neuron *21*, 799-811.

Jonas, P., Racca, C., Sakmann, B., Seeburg, P.H., and Monyer, H. (1994). Differences in Ca2+ permeability of AMPA-type glutamate receptor channels in neocortical neurons caused by differential GluR-B subunit expression. Neuron *12*, 1281-1289.

Jones, M.W., Errington, M.L., French, P.J., Fine, A., Bliss, T.V., Garel, S., Charnay, P., Bozon, B., Laroche, S., and Davis, S. (2001). A requirement for the immediate early gene Zif268 in the expression of late LTP and long-term memories. Nature neuroscience *4*, 289-296.

Kang, H., and Schuman, E.M. (1995). Long-lasting neurotrophin-induced enhancement of synaptic transmission in the adult hippocampus. Science *267*, 1658-1662.

Kato, A.S., Siuda, E.R., Nisenbaum, E.S., and Bredt, D.S. (2008). AMPA receptor subunit-specific regulation by a distinct family of type II TARPs. Neuron *59*, 986-996.

Kawaguchi, Y., and Kondo, S. (2002). Parvalbumin, somatostatin and cholecystokinin as chemical markers for specific GABAergic interneuron types in the rat frontal cortex. Journal of neurocytology *31*, 277-287.

Kawaguchi, Y., and Kubota, Y. (1997). GABAergic cell subtypes and their synaptic connections in rat frontal cortex. Cereb Cortex *7*, 476-486.

Kawaguchi, Y., and Kubota, Y. (1998). Neurochemical features and synaptic connections of large physiologically-identified GABAergic cells in the rat frontal cortex. Neuroscience *85*, 677-701.

Kawashima, T., Okuno, H., Nonaka, M., Adachi-Morishima, A., Kyo, N., Okamura, M., Takemoto-Kimura, S., Worley, P.F., and Bito, H. (2009). Synaptic activity-responsive element in the Arc/Arg3.1 promoter essential for synapse-to-nucleus signaling in activated neurons. Proceedings of the National Academy of Sciences of the United States of America *106*, 316-321.

Keck, T., Scheuss, V., Jacobsen, R.I., Wierenga, C.J., Eysel, U.T., Bonhoeffer, T., and Hubener, M. (2011). Loss of sensory input causes rapid structural changes of inhibitory neurons in adult mouse visual cortex. Neuron *71*, 869-882.

Kerlin, A.M., Andermann, M.L., Berezovskii, V.K., and Reid, R.C. (2010). Broadly tuned response properties of diverse inhibitory neuron subtypes in mouse visual cortex. Neuron *67*, 858-871.

Kim, T.K., Hemberg, M., Gray, J.M., Costa, A.M., Bear, D.M., Wu, J., Harmin, D.A., Laptewicz, M., Barbara-Haley, K., Kuersten, S.*, et al.* (2010). Widespread transcription at neuronal activity-regulated enhancers. Nature *465*, 182-187.

Klausberger, T., Roberts, J.D., and Somogyi, P. (2002). Cell type- and input-specific differences in the number and subtypes of synaptic GABA(A) receptors in the hippocampus. The Journal of neuroscience : the official journal of the Society for Neuroscience *22*, 2513-2521.

Koch, S.M., and Ullian, E.M. (2010). Neuronal pentraxins mediate silent synapse conversion in the developing visual system. The Journal of neuroscience : the official journal of the Society for Neuroscience *30*, 5404-5414.

Koffie, R.M., Meyer-Luehmann, M., Hashimoto, T., Adams, K.W., Mielke, M.L., Garcia-Alloza, M., Micheva, K.D., Smith, S.J., Kim, M.L., Lee, V.M.*, et al.* (2009). Oligomeric amyloid beta associates with postsynaptic densities and correlates with excitatory synapse loss near senile plaques. Proceedings of the National Academy of Sciences of the United States of America *106*, 4012-4017.

Kopec, C.D., Real, E., Kessels, H.W., and Malinow, R. (2007). GluR1 links structural and functional plasticity at excitatory synapses. The Journal of neuroscience : the official journal of the Society for Neuroscience *27*, 13706-13718.

Kopeikina, K.J., Polydoro, M., Tai, H.C., Yaeger, E., Carlson, G.A., Pitstick, R., Hyman, B.T., and Spires-Jones, T.L. (2012). Synaptic alterations in the rTg4510 mouse model of tauopathy. The Journal of comparative neurology.

Kornhauser, J.M., Cowan, C.W., Shaywitz, A.J., Dolmetsch, R.E., Griffith, E.C., Hu, L.S., Haddad, C., Xia, Z., and Greenberg, M.E. (2002). CREB transcriptional activity in neurons is regulated by multiple, calcium-specific phosphorylation events. Neuron *34*, 221-233.

Kornhauser, J.M., Ginty, D.D., Greenberg, M.E., Mayo, K.E., and Takahashi, J.S. (1996). Light entrainment and activation of signal transduction pathways in the SCN. Progress in brain research *111*, 133-146.

Korotkova, T., Fuchs, E.C., Ponomarenko, A., von Engelhardt, J., and Monyer, H. (2010). NMDA receptor ablation on parvalbumin-positive interneurons impairs hippocampal synchrony, spatial representations, and working memory. Neuron *68*, 557-569.

Kovalchuk, Y., Hanse, E., Kafitz, K.W., and Konnerth, A. (2002). Postsynaptic Induction of BDNF-Mediated Long-Term Potentiation. Science *295*, 1729-1734.
Kuhlman, S.J., Tring, E., and Trachtenberg, J.T. (2011). Fast-spiking interneurons have an initial orientation bias that is lost with vision. Nature neuroscience *14*, 1121-1123.

Kullmann, D.M., Moreau, A.W., Bakiri, Y., and Nicholson, E. (2012). Plasticity of inhibition. Neuron *75*, 951-962.

Kwok, R.P., Lundblad, J.R., Chrivia, J.C., Richards, J.P., Bachinger, H.P., Brennan, R.G., Roberts, S.G., Green, M.R., and Goodman, R.H. (1994). Nuclear protein CBP is a coactivator for the transcription factor CREB. Nature *370*, 223-226.

Kyriazi, H.T., Carvell, G.E., Brumberg, J.C., and Simons, D.J. (1996). Quantitative effects of GABA and bicuculline methiodide on receptive field properties of neurons in real and simulated whisker barrels. Journal of neurophysiology *75*, 547-560.

Lamsa, K.P., Heeroma, J.H., Somogyi, P., Rusakov, D.A., and Kullmann, D.M. (2007). Anti-Hebbian long-term potentiation in the hippocampal feedback inhibitory circuit. Science *315*, 1262-1266.

Lapray, D., Lasztoczi, B., Lagler, M., Viney, T.J., Katona, L., Valenti, O., Hartwich, K., Borhegyi, Z., Somogyi, P., and Klausberger, T. (2012). Behavior-dependent specialization of identified hippocampal interneurons. Nature neuroscience.

Lau, A.G., Irier, H.A., Gu, J., Tian, D., Ku, L., Liu, G., Xia, M., Fritsch, B., Zheng, J.Q., Dingledine, R.*, et al.* (2010). Distinct 3'UTRs differentially regulate activity-dependent translation of brain-derived neurotrophic factor (BDNF). Proceedings of the National Academy of Sciences of the United States of America *107*, 15945-15950.

Lazarus, M.S., and Huang, Z.J. (2011). Distinct maturation profiles of perisomatic and dendritic targeting GABAergic interneurons in the mouse primary visual cortex during the critical period of ocular dominance plasticity. Journal of neurophysiology *106*, 775-787.

Lee, H.W., Choi, J., Shin, H., Kim, K., Yang, J., Na, M., Choi, S.Y., Kang, G.B., Eom, S.H., Kim, H.*, et al.* (2008). Preso, a novel PSD-95-interacting FERM and PDZ domain protein that regulates dendritic spine morphogenesis. The Journal of neuroscience : the official journal of the Society for Neuroscience *28*, 14546-14556.

Lee, H.W., Kim, Y., Han, K., Kim, H., and Kim, E. (2010). The phosphoinositide 3-phosphatase MTMR2 interacts with PSD-95 and maintains excitatory synapses by modulating endosomal traffic. The Journal of neuroscience : the official journal of the Society for Neuroscience *30*, 5508-5518.

Lee, S.H., Kwan, A.C., Zhang, S., Phoumthipphavong, V., Flannery, J.G., Masmanidis, S.C., Taniguchi, H., Huang, Z.J., Zhang, F., Boyden, E.S.*, et al.* (2012). Activation of specific interneurons improves V1 feature selectivity and visual perception. Nature *488*, 379-383.

Levenson, J.M., O'Riordan, K.J., Brown, K.D., Trinh, M.A., Molfese, D.L., and Sweatt, J.D. (2004). Regulation of histone acetylation during memory formation in the hippocampus. The Journal of biological chemistry *279*, 40545-40559.

Li, H., Radford, J.C., Ragusa, M.J., Shea, K.L., McKercher, S.R., Zaremba, J.D., Soussou, W., Nie, Z., Kang, Y.J., Nakanishi, N.*, et al.* (2008). Transcription factor MEF2C influences neural stem/progenitor cell differentiation and maturation in vivo. Proceedings of the National Academy of Sciences of the United States of America *105*, 9397-9402.

Li, L., Tasic, B., Micheva, K.D., Ivanov, V.M., Spletter, M.L., Smith, S.J., and Luo, L. (2010). Visualizing the distribution of synapses from individual neurons in the mouse brain. PloS one *5*, e11503.

Lien, C.C., and Jonas, P. (2003). Kv3 potassium conductance is necessary and kinetically optimized for high-frequency action potential generation in hippocampal interneurons. The Journal of neuroscience : the official journal of the Society for Neuroscience *23*, 2058-2068.

Lin, Y., Bloodgood, B.L., Hauser, J.L., Lapan, A.D., Koon, A.C., Kim, T.K., Hu, L.S., Malik, A.N., and Greenberg, M.E. (2008). Activity-dependent regulation of inhibitory synapse development by Npas4. Nature *455*, 1198-1204.

Liu, B.H., Li, P., Li, Y.T., Sun, Y.J., Yanagawa, Y., Obata, K., Zhang, L.I., and Tao, H.W. (2009). Visual receptive field structure of cortical inhibitory neurons revealed by two-photon imaging guided recording. The Journal of neuroscience : the official journal of the Society for Neuroscience *29*, 10520-10532.

Liu, B.H., Li, P., Sun, Y.J., Li, Y.T., Zhang, L.I., and Tao, H.W. (2010). Intervening inhibition underlies simple-cell receptive field structure in visual cortex. Nature neuroscience *13*, 89-96.

Liu, B.H., Li, Y.T., Ma, W.P., Pan, C.J., Zhang, L.I., and Tao, H.W. (2011). Broad inhibition sharpens orientation selectivity by expanding input dynamic range in mouse simple cells. Neuron *71*, 542-554.

Lovett-Barron, M., Turi, G.F., Kaifosh, P., Lee, P.H., Bolze, F., Sun, X.H., Nicoud, J.F., Zemelman, B.V., Sternson, S.M., and Losonczy, A. (2012). Regulation of neuronal input transformations by tunable dendritic inhibition. Nature neuroscience *15*, 423-430, S421-423.

Lowel, S. (1994). Ocular dominance column development: strabismus changes the spacing of adjacent columns in cat visual cortex. The Journal of neuroscience : the official journal of the Society for Neuroscience *14*, 7451-7468.

Lu, Z., Je, H.S., Young, P., Gross, J., Lu, B., and Feng, G. (2007). Regulation of synaptic growth and maturation by a synapse-associated E3 ubiquitin ligase at the neuromuscular junction. The Journal of cell biology *177*, 1077-1089.

Lyford, G.L., Yamagata, K., Kaufmann, W.E., Barnes, C.A., Sanders, L.K., Copeland, N.G., Gilbert, D.J., Jenkins, N.A., Lanahan, A.A., and Worley, P.F. (1995). Arc, a growth factor and activity-regulated gene, encodes a novel cytoskeleton-associated protein that is enriched in neuronal dendrites. Neuron *14*, 433-445.

Lyons, G.E., Micales, B.K., Schwarz, J., Martin, J.F., and Olson, E.N. (1995). Expression of mef2 genes in the mouse central nervous system suggests a role in neuronal maturation. The Journal of neuroscience : the official journal of the Society for Neuroscience *15*, 5727-5738.

Ma, Y., Hu, H., and Agmon, A. (2012). Short-term plasticity of unitary inhibitory-to-inhibitory synapses depends on the presynaptic interneuron subtype. The Journal of neuroscience : the official journal of the Society for Neuroscience *32*, 983-988.

Ma, Y., Hu, H., Berrebi, A.S., Mathers, P.H., and Agmon, A. (2006). Distinct subtypes of somatostatin-containing neocortical interneurons revealed in transgenic mice. The Journal of neuroscience : the official journal of the Society for Neuroscience *26*, 5069-5082.

Madisen, L., Zwingman, T.A., Sunkin, S.M., Oh, S.W., Zariwala, H.A., Gu, H., Ng, L.L., Palmiter, R.D., Hawrylycz, M.J., Jones, A.R.*, et al.* (2010). A robust and high-throughput Cre reporting and characterization system for the whole mouse brain. Nature neuroscience *13*, 133-140.

Maffei, A., Nataraj, K., Nelson, S.B., and Turrigiano, G.G. (2006). Potentiation of cortical inhibition by visual deprivation. Nature *443*, 81-84.

Maffei, L., and Galli-Resta, L. (1990). Correlation in the discharges of neighboring rat retinal ganglion cells during prenatal life. Proceedings of the National Academy of Sciences of the United States of America *87*, 2861-2864.

Maghsoodi, B., Poon, M.M., Nam, C.I., Aoto, J., Ting, P., and Chen, L. (2008). Retinoic acid regulates RARalpha-mediated control of translation in dendritic RNA granules during homeostatic synaptic plasticity. Proceedings of the National Academy of Sciences of the United States of America *105*, 16015-16020.

Mao, Z., Bonni, A., Xia, F., Nadal-Vicens, M., and Greenberg, M.E. (1999). Neuronal activity-dependent cell survival mediated by transcription factor MEF2. Science *286*, 785-790.

Mao, Z., and Wiedmann, M. (1999). Calcineurin enhances MEF2 DNA binding activity in calcium-dependent survival of cerebellar granule neurons. The Journal of biological chemistry *274*, 31102-31107.

Margolis, S.S., Salogiannis, J., Lipton, D.M., Mandel-Brehm, C., Wills, Z.P., Mardinly, A.R., Hu, L., Greer, P.L., Bikoff, J.B., Ho, H.Y.*, et al.* (2010). EphB-mediated degradation of the RhoA GEF Ephexin5 relieves a developmental brake on excitatory synapse formation. Cell *143*, 442-455.

Marie, H., Morishita, W., Yu, X., Calakos, N., and Malenka, R.C. (2005). Generation of silent synapses by acute in vivo expression of CaMKIV and CREB. Neuron *45*, 741-752.

Marin, O. (2012). Interneuron dysfunction in psychiatric disorders. Nature reviews Neuroscience *13*, 107-120.

Markram, H., Toledo-Rodriguez, M., Wang, Y., Gupta, A., Silberberg, G., and Wu, C. (2004). Interneurons of the neocortical inhibitory system. Nature reviews Neuroscience *5*, 793-807.

Masland, R.H. (1977). Maturation of function in the developing rabbit retina. The Journal of comparative neurology *175*, 275-286.

Mataga, N., Mizuguchi, Y., and Hensch, T.K. (2004). Experience-dependent pruning of dendritic spines in visual cortex by tissue plasminogen activator. Neuron *44*, 1031-1041.

Mataga, N., Nagai, N., and Hensch, T.K. (2002). Permissive proteolytic activity for visual cortical plasticity. Proceedings of the National Academy of Sciences of the United States of America *99*, 7717-7721.

McAllister, A.K., Lo, D.C., and Katz, L.C. (1995). Neurotrophins regulate dendritic growth in developing visual cortex. Neuron *15*, 791-803.

McDowell, K.A., Hutchinson, A.N., Wong-Goodrich, S.J., Presby, M.M., Su, D., Rodriguiz, R.M., Law, K.C., Williams, C.L., Wetsel, W.C., and West, A.E. (2010).

Reduced cortical BDNF expression and aberrant memory in Carf knock-out mice. The Journal of neuroscience : the official journal of the Society for Neuroscience *30*, 7453-7465.

McGarry, L.M., Packer, A.M., Fino, E., Nikolenko, V., Sippy, T., and Yuste, R. (2010). Quantitative classification of somatostatin-positive neocortical interneurons identifies three interneuron subtypes. Frontiers in neural circuits *4*, 12.

Megias, M., Emri, Z., Freund, T.F., and Gulyas, A.I. (2001). Total number and distribution of inhibitory and excitatory synapses on hippocampal CA1 pyramidal cells. Neuroscience *102*, 527-540.

Meister, M., Wong, R.O., Baylor, D.A., and Shatz, C.J. (1991). Synchronous bursts of action potentials in ganglion cells of the developing mammalian retina. Science *252*, 939-943.

Mercer, A.C., Gaj, T., Fuller, R.P., and Barbas, C.F., 3rd (2012). Chimeric TALE recombinases with programmable DNA sequence specificity. Nucleic acids research *40*, 11163-11172.

Metsis, M., Timmusk, T., Arenas, E., and Persson, H. (1993). Differential usage of multiple brain-derived neurotrophic factor promoters in the rat brain following neuronal activation. Proceedings of the National Academy of Sciences of the United States of America *90*, 8802-8806.

Micheva, K.D., Busse, B., Weiler, N.C., O'Rourke, N., and Smith, S.J. (2010a). Single-synapse analysis of a diverse synapse population: proteomic imaging methods and markers. Neuron *68*, 639-653.

Micheva, K.D., O'Rourke, N., Busse, B., and Smith, S.J. (2010b). Array tomography: high-resolution three-dimensional immunofluorescence. Cold Spring Harbor protocols *2010*, pdb top89.

Micheva, K.D., O'Rourke, N., Busse, B., and Smith, S.J. (2010c). Array tomography: imaging stained arrays. Cold Spring Harbor protocols *2010*, pdb prot5526.

Micheva, K.D., O'Rourke, N., Busse, B., and Smith, S.J. (2010d). Array tomography: immunostaining and antibody elution. Cold Spring Harbor protocols *2010*, pdb prot5525.

Micheva, K.D., O'Rourke, N., Busse, B., and Smith, S.J. (2010e). Array tomography: production of arrays. Cold Spring Harbor protocols *2010*, pdb prot5524.

Micheva, K.D., O'Rourke, N., Busse, B., and Smith, S.J. (2010f). Array tomography: rodent brain fixation and embedding. Cold Spring Harbor protocols *2010*, pdb prot5523.

Micheva, K.D., O'Rourke, N., Busse, B., and Smith, S.J. (2010g). Array tomography: semiautomated image alignment. Cold Spring Harbor protocols *2010*, pdb prot5527.

Micheva, K.D., and Smith, S.J. (2007). Array tomography: a new tool for imaging the molecular architecture and ultrastructure of neural circuits. Neuron *55*, 25-36.

Mishchenko, Y., Hu, T., Spacek, J., Mendenhall, J., Harris, K.M., and Chklovskii, D.B. (2010). Ultrastructural analysis of hippocampal neuropil from the connectomics perspective. Neuron *67*, 1009-1020.

Miura, K., Kishino, T., Li, E., Webber, H., Dikkes, P., Holmes, G.L., and Wagstaff, J. (2002). Neurobehavioral and electroencephalographic abnormalities in Ube3a maternal-deficient mice. Neurobiology of disease *9*, 149-159.

Montminy, M.R., and Bilezikjian, L.M. (1987). Binding of a nuclear protein to the cyclic-AMP response element of the somatostatin gene. Nature *328*, 175-178.

Moosmang, S., Haider, N., Klugbauer, N., Adelsberger, H., Langwieser, N., Muller, J., Stiess, M., Marais, E., Schulla, V., Lacinova, L.*, et al.* (2005). Role of hippocampal Cav1.2 Ca2+ channels in NMDA receptor-independent synaptic plasticity and spatial memory. The Journal of neuroscience : the official journal of the Society for Neuroscience *25*, 9883-9892.

Morales, B., Choi, S.Y., and Kirkwood, A. (2002). Dark rearing alters the development of GABAergic transmission in visual cortex. The Journal of neuroscience : the official journal of the Society for Neuroscience *22*, 8084-8090.

Murphy, T.H., Worley, P.F., and Baraban, J.M. (1991). L-type voltage-sensitive calcium channels mediate synaptic activation of immediate early genes. Neuron *7*, 625-635.

Myers, S.J., Dingledine, R., and Borges, K. (1999). Genetic regulation of glutamate receptor ion channels. Annual review of pharmacology and toxicology *39*, 221-241.

Ninan, I., Bath, K.G., Dagar, K., Perez-Castro, R., Plummer, M.R., Lee, F.S., and Chao, M.V. (2010). The BDNF Val66Met polymorphism impairs NMDA receptor-dependent synaptic plasticity in the hippocampus. The Journal of neuroscience : the official journal of the Society for Neuroscience *30*, 8866-8870.

Nusser, Z., Sieghart, W., Benke, D., Fritschy, J.M., and Somogyi, P. (1996). Differential synaptic localization of two major gamma-aminobutyric acid type A receptor alpha subunits on hippocampal pyramidal cells. Proceedings of the National Academy of Sciences of the United States of America *93*, 11939-11944.

O'Brien, R., Xu, D., Mi, R., Tang, X., Hopf, C., and Worley, P. (2002). Synaptically targeted narp plays an essential role in the aggregation of AMPA receptors at excitatory synapses in cultured spinal neurons. The Journal of neuroscience : the official journal of the Society for Neuroscience *22*, 4487-4498.

O'Brien, R.J., Xu, D., Petralia, R.S., Steward, O., Huganir, R.L., and Worley, P. (1999). Synaptic clustering of AMPA receptors by the extracellular immediate-early gene product Narp. Neuron *23*, 309-323.

Oe, S., and Yoneda, Y. (2010). Cytoplasmic polyadenylation element-like sequences are involved in dendritic targeting of BDNF mRNA in hippocampal neurons. FEBS letters *584*, 3424-3430.

Okaty, B.W., Miller, M.N., Sugino, K., Hempel, C.M., and Nelson, S.B. (2009). Transcriptional and electrophysiological maturation of neocortical fast-spiking GABAergic interneurons. The Journal of neuroscience : the official journal of the Society for Neuroscience *29*, 7040-7052.

Okuno, H., Akashi, K., Ishii, Y., Yagishita-Kyo, N., Suzuki, K., Nonaka, M., Kawashima, T., Fujii, H., Takemoto-Kimura, S., Abe, M.*, et al.* (2012). Inverse synaptic tagging of inactive synapses via dynamic interaction of Arc/Arg3.1 with CaMKIIbeta. Cell *149*, 886-898.

Oliveria, S.F., Dell'Acqua, M.L., and Sather, W.A. (2007). AKAP79/150 anchoring of calcineurin controls neuronal L-type Ca2+ channel activity and nuclear signaling. Neuron *55*, 261-275.

Ooe, N., Saito, K., and Kaneko, H. (2009). Characterization of functional heterodimer partners in brain for a bHLH-PAS factor NXF. Biochimica et biophysica acta *1789*, 192-197.

Oray, S., Majewska, A., and Sur, M. (2004). Dendritic spine dynamics are regulated by monocular deprivation and extracellular matrix degradation. Neuron *44*, 1021-1030.

Packer, A.M., and Yuste, R. (2011). Dense, unspecific connectivity of neocortical parvalbumin-positive interneurons: a canonical microcircuit for inhibition? The Journal of neuroscience : the official journal of the Society for Neuroscience *31*, 13260-13271.

Pang, P.T., Teng, H.K., Zaitsev, E., Woo, N.T., Sakata, K., Zhen, S., Teng, K.K., Yung, W.H., Hempstead, B.L., and Lu, B. (2004). Cleavage of proBDNF by tPA/plasmin is essential for long-term hippocampal plasticity. Science *306*, 487-491.

Paradis, S., Harrar, D.B., Lin, Y., Koon, A.C., Hauser, J.L., Griffith, E.C., Zhu, L., Brass, L.F., Chen, C., and Greenberg, M.E. (2007). An RNAi-based approach identifies molecules required for glutamatergic and GABAergic synapse development. Neuron *53*, 217-232.

Park, S., Park, J.M., Kim, S., Kim, J.A., Shepherd, J.D., Smith-Hicks, C.L., Chowdhury, S., Kaufmann, W., Kuhl, D., Ryazanov, A.G.*, et al.* (2008). Elongation factor 2 and fragile X mental retardation protein control the dynamic translation of Arc/Arg3.1 essential for mGluR-LTD. Neuron *59*, 70-83.

Patterson, S.L., Abel, T., Deuel, T.A., Martin, K.C., Rose, J.C., and Kandel, E.R. (1996). Recombinant BDNF rescues deficits in basal synaptic transmission and hippocampal LTP in BDNF knockout mice. Neuron *16*, 1137-1145.

Perkinton, M.S., Sihra, T.S., and Williams, R.J. (1999). Ca(2+)-permeable AMPA receptors induce phosphorylation of cAMP response element-binding protein through a phosphatidylinositol 3-kinase-dependent stimulation of the mitogen-activated protein kinase signaling cascade in neurons. The Journal of neuroscience : the official journal of the Society for Neuroscience *19*, 5861-5874.

Peterson, B.Z., DeMaria, C.D., Adelman, J.P., and Yue, D.T. (1999). Calmodulin is the Ca2+ sensor for Ca2+ -dependent inactivation of L-type calcium channels. Neuron *22*, 549-558.

Petralia, R.S., Esteban, J.A., Wang, Y.X., Partridge, J.G., Zhao, H.M., Wenthold, R.J., and Malinow, R. (1999). Selective acquisition of AMPA receptors over postnatal development suggests a molecular basis for silent synapses. Nature neuroscience *2*, 31-36.

Petrij, F., Giles, R.H., Dauwerse, H.G., Saris, J.J., Hennekam, R.C., Masuno, M., Tommerup, N., van Ommen, G.J., Goodman, R.H., Peters, D.J.*, et al.* (1995). Rubinstein-Taybi syndrome caused by mutations in the transcriptional co-activator CBP. Nature *376*, 348-351.

Pfeiffer, B.E., Zang, T., Wilkerson, J.R., Taniguchi, M., Maksimova, M.A., Smith, L.N., Cowan, C.W., and Huber, K.M. (2010). Fragile X mental retardation protein is required for synapse elimination by the activity-dependent transcription factor MEF2. Neuron *66*, 191-197.

Pham, T.A., Impey, S., Storm, D.R., and Stryker, M.P. (1999). CRE-mediated gene transcription in neocortical neuronal plasticity during the developmental critical period. Neuron *22*, 63-72.

Philpot, B.D., Sekhar, A.K., Shouval, H.Z., and Bear, M.F. (2001). Visual experience and deprivation bidirectionally modify the composition and function of NMDA receptors in visual cortex. Neuron *29*, 157-169.

Pizzorusso, T., Medini, P., Berardi, N., Chierzi, S., Fawcett, J.W., and Maffei, L. (2002). Reactivation of ocular dominance plasticity in the adult visual cortex. Science *298*, 1248-1251.

Plant, K., Pelkey, K.A., Bortolotto, Z.A., Morita, D., Terashima, A., McBain, C.J., Collingridge, G.L., and Isaac, J.T. (2006). Transient incorporation of native GluR2-lacking AMPA receptors during hippocampal long-term potentiation. Nature neuroscience *9*, 602-604.

Plath, N., Ohana, O., Dammermann, B., Errington, M.L., Schmitz, D., Gross, C., Mao, X., Engelsberg, A., Mahlke, C., Welzl, H.*, et al.* (2006). Arc/Arg3.1 is essential for the consolidation of synaptic plasticity and memories. Neuron *52*, 437-444.

Ploski, J.E., Monsey, M.S., Nguyen, T., DiLeone, R.J., and Schafe, G.E. (2011). The neuronal PAS domain protein 4 (Npas4) is required for new and reactivated fear memories. PloS one *6*, e23760.

Pouille, F., Marin-Burgin, A., Adesnik, H., Atallah, B.V., and Scanziani, M. (2009). Input normalization by global feedforward inhibition expands cortical dynamic range. Nature neuroscience *12*, 1577-1585.

Prusky, G.T., and Douglas, R.M. (2003). Developmental plasticity of mouse visual acuity. The European journal of neuroscience *17*, 167-173.

Pulipparacharuvil, S., Renthal, W., Hale, C.F., Taniguchi, M., Xiao, G., Kumar, A., Russo, S.J., Sikder, D., Dewey, C.M., Davis, M.M., *et al.* (2008). Cocaine regulates MEF2 to control synaptic and behavioral plasticity. Neuron *59*, 621-633.

Qian, Z., Gilbert, M.E., Colicos, M.A., Kandel, E.R., and Kuhl, D. (1993). Tissue-plasminogen activator is induced as an immediate-early gene during seizure, kindling and long-term potentiation. Nature *361*, 453-457.

Quinlan, E.M., Philpot, B.D., Huganir, R.L., and Bear, M.F. (1999). Rapid, experience-dependent expression of synaptic NMDA receptors in visual cortex in vivo. Nature neuroscience *2*, 352-357.

Rahamimoff, R., and Melamed, N. (1993). Visualization of synaptic structure and function with confocal microscopy: calcium fluctuations and oscillations. Neuroscience research *16*, 173-180.

Ramamoorthi, K., Fropf, R., Belfort, G.M., Fitzmaurice, H.L., McKinney, R.M., Neve, R.L., Otto, T., and Lin, Y. (2011). Npas4 regulates a transcriptional program in CA3 required for contextual memory formation. Science *334*, 1669-1675.

Ramanan, N., Shen, Y., Sarsfield, S., Lemberger, T., Schutz, G., Linden, D.J., and Ginty, D.D. (2005). SRF mediates activity-induced gene expression and synaptic plasticity but not neuronal viability. Nature neuroscience *8*, 759-767.

Ran, I., Laplante, I., and Lacaille, J.C. (2012). CREB-dependent transcriptional control and quantal changes in persistent long-term potentiation in hippocampal interneurons. The Journal of neuroscience : the official journal of the Society for Neuroscience *32*, 6335-6350.

Ranson, A., Cheetham, C.E., Fox, K., and Sengpiel, F. (2012). Homeostatic plasticity mechanisms are required for juvenile, but not adult, ocular dominance plasticity. Proceedings of the National Academy of Sciences of the United States of America *109*, 1311-1316.

Redmond, L., Kashani, A.H., and Ghosh, A. (2002). Calcium regulation of dendritic growth via CaM kinase IV and CREB-mediated transcription. Neuron *34*, 999-1010.
Reyes, A., Lujan, R., Rozov, A., Burnashev, N., Somogyi, P., and Sakmann, B. (1998). Target-cell-specific facilitation and depression in neocortical circuits. Nature neuroscience *1*, 279-285.

Roberts, A.C., Diez-Garcia, J., Rodriguiz, R.M., Lopez, I.P., Lujan, R., Martinez-Turrillas, R., Pico, E., Henson, M.A., Bernardo, D.R., Jarrett, T.M., *et al.* (2009). Downregulation of NR3A-containing NMDARs is required for synapse maturation and memory consolidation. Neuron *63*, 342-356.

Rochefort, N.L., Garaschuk, O., Milos, R.I., Narushima, M., Marandi, N., Pichler, B., Kovalchuk, Y., and Konnerth, A. (2009). Sparsification of neuronal activity in the visual cortex at eye-opening. Proceedings of the National Academy of Sciences of the United States of America *106*, 15049-15054.

Rochefort, N.L., Narushima, M., Grienberger, C., Marandi, N., Hill, D.N., and Konnerth, A. (2011). Development of direction selectivity in mouse cortical neurons. Neuron *71*, 425-432.

Rosen, L.B., Ginty, D.D., Weber, M.J., and Greenberg, M.E. (1994). Membrane depolarization and calcium influx stimulate MEK and MAP kinase via activation of Ras. Neuron *12*, 1207-1221.

Royer, S., Zemelman, B.V., Losonczy, A., Kim, J., Chance, F., Magee, J.C., and Buzsaki, G. (2012). Control of timing, rate and bursts of hippocampal place cells by dendritic and somatic inhibition. Nature neuroscience *15*, 769-775.

Rudy, B., Fishell, G., Lee, S., and Hjerling-Leffler, J. (2011). Three groups of interneurons account for nearly 100% of neocortical GABAergic neurons. Developmental neurobiology *71*, 45-61.

Rudy, B., and McBain, C.J. (2001). Kv3 channels: voltage-gated K+ channels designed for high-frequency repetitive firing. Trends in neurosciences *24*, 517-526.
Rutherford, L.C., Nelson, S.B., and Turrigiano, G.G. (1998). BDNF has opposite effects on the quantal amplitude of pyramidal neuron and interneuron excitatory synapses. Neuron *21*, 521-530.

Saatchi, S., Azuma, J., Wanchoo, N., Smith, S.J., Yock, P.G., Taylor, C.A., and Tsao, P.S. (2012). Three-dimensional microstructural changes in murine abdominal aortic aneurysms quantified using immunofluorescent array tomography. The journal of histochemistry and cytochemistry : official journal of the Histochemistry Society *60*, 97-109.

Saghatelyan, A.K., Dityatev, A., Schmidt, S., Schuster, T., Bartsch, U., and Schachner, M. (2001). Reduced perisomatic inhibition, increased excitatory transmission, and impaired long-term potentiation in mice deficient for the extracellular matrix glycoprotein tenascin-R. Molecular and cellular neurosciences *17*, 226-240.

Sakata, K., Woo, N.H., Martinowich, K., Greene, J.S., Schloesser, R.J., Shen, L., and Lu, B. (2009). Critical role of promoter IV-driven BDNF transcription in GABAergic transmission and synaptic plasticity in the prefrontal cortex. Proceedings of the National Academy of Sciences of the United States of America *106*, 5942-5947.

Sala, C., Roussignol, G., Meldolesi, J., and Fagni, L. (2005). Key role of the postsynaptic density scaffold proteins Shank and Homer in the functional architecture of Ca2+ homeostasis at dendritic spines in hippocampal neurons. The

Journal of neuroscience : the official journal of the Society for Neuroscience *25*, 4587-4592.

Sala, C., Rudolph-Correia, S., and Sheng, M. (2000). Developmentally regulated NMDA receptor-dependent dephosphorylation of cAMP response element-binding protein (CREB) in hippocampal neurons. The Journal of neuroscience : the official journal of the Society for Neuroscience *20*, 3529-3536.

Sanz, E., Yang, L., Su, T., Morris, D.R., McKnight, G.S., and Amieux, P.S. (2009). Cell-type-specific isolation of ribosome-associated mRNA from complex tissues. Proceedings of the National Academy of Sciences of the United States of America *106*, 13939-13944.

Sato, M., and Stryker, M.P. (2010). Genomic imprinting of experience-dependent cortical plasticity by the ubiquitin ligase gene Ube3a. Proceedings of the National Academy of Sciences of the United States of America *107*, 5611-5616.

Schafer, D.P., Lehrman, E.K., Kautzman, A.G., Koyama, R., Mardinly, A.R., Yamasaki, R., Ransohoff, R.M., Greenberg, M.E., Barres, B.A., and Stevens, B. (2012). Microglia sculpt postnatal neural circuits in an activity and complement-dependent manner. Neuron *74*, 691-705.

Schratt, G.M., Tuebing, F., Nigh, E.A., Kane, C.G., Sabatini, M.E., Kiebler, M., and Greenberg, M.E. (2006). A brain-specific microRNA regulates dendritic spine development. Nature *439*, 283-289.

Schrimpf, S.P., Meskenaite, V., Brunner, E., Rutishauser, D., Walther, P., Eng, J., Aebersold, R., and Sonderegger, P. (2005). Proteomic analysis of synaptosomes using isotope-coded affinity tags and mass spectrometry. Proteomics *5*, 2531-2541.

Schuz, A., and Palm, G. (1989). Density of neurons and synapses in the cerebral cortex of the mouse. The Journal of comparative neurology *286*, 442-455.

Schwenk, J., Harmel, N., Zolles, G., Bildl, W., Kulik, A., Heimrich, B., Chisaka, O., Jonas, P., Schulte, U., Fakler, B.*, et al.* (2009). Functional proteomics identify cornichon proteins as auxiliary subunits of AMPA receptors. Science *323*, 1313-1319.

Shadlen, M.N., and Newsome, W.T. (1998). The variable discharge of cortical neurons: implications for connectivity, computation, and information coding. The Journal of neuroscience : the official journal of the Society for Neuroscience *18*, 3870-3896.

Shalizi, A., Gaudilliere, B., Yuan, Z., Stegmuller, J., Shirogane, T., Ge, Q., Tan, Y., Schulman, B., Harper, J.W., and Bonni, A. (2006). A calcium-regulated MEF2 sumoylation switch controls postsynaptic differentiation. Science *311*, 1012-1017.

Shatz, C.J., and Stryker, M.P. (1978). Ocular dominance in layer IV of the cat's visual cortex and the effects of monocular deprivation. The Journal of physiology *281*, 267-283.

Shatz, C.J., and Stryker, M.P. (1988). Prenatal tetrodotoxin infusion blocks segregation of retinogeniculate afferents. Science *242*, 87-89.

Sheng, M., and Kim, E. (2011). The postsynaptic organization of synapses. Cold Spring Harbor perspectives in biology *3*.

Sheng, M., McFadden, G., and Greenberg, M.E. (1990). Membrane depolarization and calcium induce c-fos transcription via phosphorylation of transcription factor CREB. Neuron *4*, 571-582.

Sheng, M., and Pak, D.T. (1999). Glutamate receptor anchoring proteins and the molecular organization of excitatory synapses. Annals of the New York Academy of Sciences *868*, 483-493.

Shepherd, G.M. (2004). The synaptic organization of the brain, 5th edn (Oxford ; New York: Oxford University Press).

Shepherd, J.D., Rumbaugh, G., Wu, J., Chowdhury, S., Plath, N., Kuhl, D., Huganir, R.L., and Worley, P.F. (2006). Arc/Arg3.1 mediates homeostatic synaptic scaling of AMPA receptors. Neuron *52*, 475-484.

Shi, S., Hayashi, Y., Esteban, J.A., and Malinow, R. (2001). Subunit-specific rules governing AMPA receptor trafficking to synapses in hippocampal pyramidal neurons. Cell *105*, 331-343.

Sia, G.M., Beique, J.C., Rumbaugh, G., Cho, R., Worley, P.F., and Huganir, R.L. (2007). Interaction of the N-terminal domain of the AMPA receptor GluR4 subunit with the neuronal pentraxin NP1 mediates GluR4 synaptic recruitment. Neuron *55*, 87-102.
Sigrist, S.J., and Sabatini, B.L. (2012). Optical super-resolution microscopy in neurobiology. Current opinion in neurobiology *22*, 86-93.

Siksou, L., Rostaing, P., Lechaire, J.P., Boudier, T., Ohtsuka, T., Fejtova, A., Kao, H.T., Greengard, P., Gundelfinger, E.D., Triller, A.*, et al.* (2007). Three-dimensional architecture of presynaptic terminal cytomatrix. The Journal of neuroscience : the official journal of the Society for Neuroscience *27*, 6868-6877.

Silberberg, G., and Markram, H. (2007). Disynaptic inhibition between neocortical pyramidal cells mediated by Martinotti cells. Neuron *53*, 735-746.

Sohal, V.S., Zhang, F., Yizhar, O., and Deisseroth, K. (2009). Parvalbumin neurons and gamma rhythms enhance cortical circuit performance. Nature *459*, 698-702.

Sohya, K., Kameyama, K., Yanagawa, Y., Obata, K., and Tsumoto, T. (2007). GABAergic neurons are less selective to stimulus orientation than excitatory neurons in layer II/III of visual cortex, as revealed by in vivo functional Ca2+ imaging in transgenic mice. The Journal of neuroscience : the official journal of the Society for Neuroscience *27*, 2145-2149.

Soiza-Reilly, M., and Commons, K.G. (2011). Quantitative analysis of glutamatergic innervation of the mouse dorsal raphe nucleus using array tomography. The Journal of comparative neurology *519*, 3802-3814.

Somogyi, P., and Klausberger, T. (2005). Defined types of cortical interneurone structure space and spike timing in the hippocampus. The Journal of physiology *562*, 9-26.

Somogyi, P., Takagi, H., Richards, J.G., and Mohler, H. (1989). Subcellular localization of benzodiazepine/GABAA receptors in the cerebellum of rat, cat, and monkey using monoclonal antibodies. The Journal of neuroscience : the official journal of the Society for Neuroscience *9*, 2197-2209.

Soto, D., Coombs, I.D., Renzi, M., Zonouzi, M., Farrant, M., and Cull-Candy, S.G. (2009). Selective regulation of long-form calcium-permeable AMPA receptors by an atypical TARP, gamma-5. Nature neuroscience *12*, 277-285.

Splawski, I., Timothy, K.W., Sharpe, L.M., Decher, N., Kumar, P., Bloise, R., Napolitano, C., Schwartz, P.J., Joseph, R.M., Condouris, K.*, et al.* (2004). Ca(V)1.2 calcium channel dysfunction causes a multisystem disorder including arrhythmia and autism. Cell *119*, 19-31.

Stellwagen, D., Beattie, E.C., Seo, J.Y., and Malenka, R.C. (2005). Differential regulation of AMPA receptor and GABA receptor trafficking by tumor necrosis factor-alpha. The Journal of neuroscience : the official journal of the Society for Neuroscience *25*, 3219-3228.

Stenman, J., Toresson, H., and Campbell, K. (2003). Identification of two distinct progenitor populations in the lateral ganglionic eminence: implications for striatal and olfactory bulb neurogenesis. The Journal of neuroscience : the official journal of the Society for Neuroscience *23*, 167-174.

Stevens, B., Allen, N.J., Vazquez, L.E., Howell, G.R., Christopherson, K.S., Nouri, N., Micheva, K.D., Mehalow, A.K., Huberman, A.D., Stafford, B.*, et al.* (2007). The classical complement cascade mediates CNS synapse elimination. Cell *131*, 1164-1178.

Steward, O., Wallace, C.S., Lyford, G.L., and Worley, P.F. (1998). Synaptic activation causes the mRNA for the IEG Arc to localize selectively near activated postsynaptic sites on dendrites. Neuron *21*, 741-751.

Sudhof, T.C. (2012). The presynaptic active zone. Neuron *75*, 11-25.

Sugino, K., Hempel, C.M., Miller, M.N., Hattox, A.M., Shapiro, P., Wu, C., Huang, Z.J., and Nelson, S.B. (2006). Molecular taxonomy of major neuronal classes in the adult mouse forebrain. Nature neuroscience *9*, 99-107.

Sugiyama, S., Di Nardo, A.A., Aizawa, S., Matsuo, I., Volovitch, M., Prochiantz, A., and Hensch, T.K. (2008). Experience-dependent transfer of Otx2 homeoprotein into the visual cortex activates postnatal plasticity. Cell *134*, 508-520.

Sylwestrak, E.L., and Ghosh, A. (2012). Elfn1 regulates target-specific release probability at CA1-interneuron synapses. Science *338*, 536-540.

Szabo, A., Somogyi, J., Cauli, B., Lambolez, B., Somogyi, P., and Lamsa, K.P. (2012). Calcium-permeable AMPA receptors provide a common mechanism for LTP in glutamatergic synapses of distinct hippocampal interneuron types. The Journal of neuroscience : the official journal of the Society for Neuroscience *32*, 6511-6516.

Tan, Z., Hu, H., Huang, Z.J., and Agmon, A. (2008). Robust but delayed thalamocortical activation of dendritic-targeting inhibitory interneurons. Proceedings of the National Academy of Sciences of the United States of America *105*, 2187-2192.

Taniguchi, H., He, M., Wu, P., Kim, S., Paik, R., Sugino, K., Kvitsiani, D., Fu, Y., Lu, J., Lin, Y.*, et al.* (2011). A resource of Cre driver lines for genetic targeting of GABAergic neurons in cerebral cortex. Neuron *71*, 995-1013.

Tao, X., Finkbeiner, S., Arnold, D.B., Shaywitz, A.J., and Greenberg, M.E. (1998). Ca2+ influx regulates BDNF transcription by a CREB family transcription factor-dependent mechanism. Neuron *20*, 709-726.

Tao, X., West, A.E., Chen, W.G., Corfas, G., and Greenberg, M.E. (2002). A calcium-responsive transcription factor, CaRF, that regulates neuronal activity-dependent expression of BDNF. Neuron *33*, 383-395.

Tian, X., Kai, L., Hockberger, P.E., Wokosin, D.L., and Surmeier, D.J. (2010). MEF-2 regulates activity-dependent spine loss in striatopallidal medium spiny neurons. Molecular and cellular neurosciences *44*, 94-108.

Timmusk, T., Palm, K., Metsis, M., Reintam, T., Paalme, V., Saarma, M., and Persson, H. (1993). Multiple promoters direct tissue-specific expression of the rat BDNF gene. Neuron *10*, 475-489.

Tolias, K.F., Bikoff, J.B., Kane, C.G., Tolias, C.S., Hu, L., and Greenberg, M.E. (2007). The Rac1 guanine nucleotide exchange factor Tiam1 mediates EphB receptor-dependent

dendritic spine development. Proceedings of the National Academy of Sciences of the United States of America *104*, 7265-7270.

Tomita, S., Fukata, M., Nicoll, R.A., and Bredt, D.S. (2004). Dynamic interaction of stargazin-like TARPs with cycling AMPA receptors at synapses. Science *303*, 1508-1511.

Torborg, C.L., Hansen, K.A., and Feller, M.B. (2005). High frequency, synchronized bursting drives eye-specific segregation of retinogeniculate projections. Nature neuroscience *8*, 72-78.

Traub, R.D., Whittington, M.A., Stanford, I.M., and Jefferys, J.G. (1996). A mechanism for generation of long-range synchronous fast oscillations in the cortex. Nature *383*, 621-624.

Tsui, C.C., Copeland, N.G., Gilbert, D.J., Jenkins, N.A., Barnes, C., and Worley, P.F. (1996). Narp, a novel member of the pentraxin family, promotes neurite outgrowth and is dynamically regulated by neuronal activity. The Journal of neuroscience : the official journal of the Society for Neuroscience *16*, 2463-2478.

Turrigiano, G. (2011). Too many cooks? Intrinsic and synaptic homeostatic mechanisms in cortical circuit refinement. Annual review of neuroscience *34*, 89-103.

Turrigiano, G.G., Leslie, K.R., Desai, N.S., Rutherford, L.C., and Nelson, S.B. (1998). Activity-dependent scaling of quantal amplitude in neocortical neurons. Nature *391*, 892-896.

Valverde, O., Celerier, E., Baranyi, M., Vanderhaeghen, P., Maldonado, R., Sperlagh, B., Vassart, G., and Ledent, C. (2009). GPR3 receptor, a novel actor in the emotional-like responses. PloS one *4*, e4704.

Van Keuren-Jensen, K., and Cline, H.T. (2006). Visual experience regulates metabotropic glutamate receptor-mediated plasticity of AMPA receptor synaptic transmission by homer1a induction. The Journal of neuroscience : the official journal of the Society for Neuroscience *26*, 7575-7580.

van Woerden, G.M., Harris, K.D., Hojjati, M.R., Gustin, R.M., Qiu, S., de Avila Freire, R., Jiang, Y.H., Elgersma, Y., and Weeber, E.J. (2007). Rescue of neurological deficits in a mouse model for Angelman syndrome by reduction of alphaCaMKII inhibitory phosphorylation. Nature neuroscience *10*, 280-282.

Verhage, M., Maia, A.S., Plomp, J.J., Brussaard, A.B., Heeroma, J.H., Vermeer, H., Toonen, R.F., Hammer, R.E., van den Berg, T.K., Missler, M.*, et al.* (2000). Synaptic assembly of the brain in the absence of neurotransmitter secretion. Science *287*, 864-869.

Wallace, M.L., Burette, A.C., Weinberg, R.J., and Philpot, B.D. (2012). Maternal loss of Ube3a produces an excitatory/inhibitory imbalance through neuron type-specific synaptic defects. Neuron *74*, 793-800.

Wang, B.S., Sarnaik, R., and Cang, J. (2010). Critical period plasticity matches binocular orientation preference in the visual cortex. Neuron *65*, 246-256.
Wang, G., and Smith, S.J. (2012). Sub-diffraction limit localization of proteins in volumetric space using Bayesian restoration of fluorescence images from ultrathin specimens. PLoS computational biology *8*, e1002671.

Wang, X., Tang, X., Li, M., Marshall, J., and Mao, Z. (2005). Regulation of neuroprotective activity of myocyte-enhancer factor 2 by cAMP-protein kinase A signaling pathway in neuronal survival. The Journal of biological chemistry *280*, 16705-16713.

Wang, X.J., and Buzsaki, G. (1996). Gamma oscillation by synaptic inhibition in a hippocampal interneuronal network model. The Journal of neuroscience : the official journal of the Society for Neuroscience *16*, 6402-6413.

Watt, A.J., van Rossum, M.C., MacLeod, K.M., Nelson, S.B., and Turrigiano, G.G. (2000). Activity coregulates quantal AMPA and NMDA currents at neocortical synapses. Neuron *26*, 659-670.

Wen, L., Lu, Y.S., Zhu, X.H., Li, X.M., Woo, R.S., Chen, Y.J., Yin, D.M., Lai, C., Terry, A.V., Jr., Vazdarjanova, A.*, et al.* (2010). Neuregulin 1 regulates pyramidal neuron activity via ErbB4 in parvalbumin-positive interneurons. Proceedings of the National Academy of Sciences of the United States of America *107*, 1211-1216.

Wiesel, T.N., and Hubel, D.H. (1963). Single-Cell Responses in Striate Cortex of Kittens Deprived of Vision in One Eye. Journal of neurophysiology *26*, 1003-1017.

Williams, C.A., Beaudet, A.L., Clayton-Smith, J., Knoll, J.H., Kyllerman, M., Laan, L.A., Magenis, R.E., Moncla, A., Schinzel, A.A., Summers, J.A.*, et al.* (2006). Angelman syndrome 2005: updated consensus for diagnostic criteria. American journal of medical genetics Part A *140*, 413-418.

Wilson, N.R., Runyan, C.A., Wang, F.L., and Sur, M. (2012). Division and subtraction by distinct cortical inhibitory networks in vivo. Nature *488*, 343-348.

Wittmann, M., Queisser, G., Eder, A., Wiegert, J.S., Bengtson, C.P., Hellwig, A., Wittum, G., and Bading, H. (2009). Synaptic activity induces dramatic changes in the geometry of the cell nucleus: interplay between nuclear structure, histone H3 phosphorylation, and nuclear calcium signaling. The Journal of neuroscience : the official journal of the Society for Neuroscience *29*, 14687-14700.

Wonders, C.P., and Anderson, S.A. (2006). The origin and specification of cortical interneurons. Nature reviews Neuroscience *7*, 687-696.

Wong, R.O., Meister, M., and Shatz, C.J. (1993). Transient period of correlated bursting activity during development of the mammalian retina. Neuron *11*, 923-938.

Wulff, P., Ponomarenko, A.A., Bartos, M., Korotkova, T.M., Fuchs, E.C., Bahner, F., Both, M., Tort, A.B., Kopell, N.J., Wisden, W.*, et al.* (2009). Hippocampal theta rhythm and its coupling with gamma oscillations require fast inhibition onto parvalbumin-positive interneurons. Proceedings of the National Academy of Sciences of the United States of America *106*, 3561-3566.

Xia, Z., Dudek, H., Miranti, C.K., and Greenberg, M.E. (1996). Calcium influx via the NMDA receptor induces immediate early gene transcription by a MAP kinase/ERK-dependent mechanism. The Journal of neuroscience : the official journal of the Society for Neuroscience *16*, 5425-5436.

Xu, D., Hopf, C., Reddy, R., Cho, R.W., Guo, L., Lanahan, A., Petralia, R.S., Wenthold, R.J., O'Brien, R.J., and Worley, P. (2003). Narp and NP1 form heterocomplexes that function in developmental and activity-dependent synaptic plasticity. Neuron *39*, 513-528.

Xu, X., and Callaway, E.M. (2009). Laminar specificity of functional input to distinct types of inhibitory cortical neurons. The Journal of neuroscience : the official journal of the Society for Neuroscience *29*, 70-85.

Xu, X., Roby, K.D., and Callaway, E.M. (2010). Immunochemical characterization of inhibitory mouse cortical neurons: three chemically distinct classes of inhibitory cells. The Journal of comparative neurology *518*, 389-404.

Ye, B., Liao, D., Zhang, X., Zhang, P., Dong, H., and Huganir, R.L. (2000). GRASP-1: a neuronal RasGEF associated with the AMPA receptor/GRIP complex. Neuron *26*, 603-617.

Yuste, R., Peinado, A., and Katz, L.C. (1992). Neuronal domains in developing neocortex. Science *257*, 665-669.

Zhang, J., Ackman, J.B., Xu, H.P., and Crair, M.C. (2012). Visual map development depends on the temporal pattern of binocular activity in mice. Nature neuroscience *15*, 298-307.

Zhao, Y., Flandin, P., Long, J.E., Cuesta, M.D., Westphal, H., and Rubenstein, J.L. (2008). Distinct molecular pathways for development of telencephalic interneuron subtypes revealed through analysis of Lhx6 mutants. The Journal of comparative neurology *510*, 79-99.

Appendix 1:

Loss of inhibitory interneurons in the dorsal spinal cord and elevated itch in Bhlhb5 mutant mice

Neuron
Article

Loss of Inhibitory Interneurons in the Dorsal Spinal Cord and Elevated Itch in *Bhlhb5* Mutant Mice

Sarah E. Ross,[1] Alan R. Mardinly,[1] Alejandra E. McCord,[1] Jonathan Zurawski,[1] Sonia Cohen,[1] Cynthia Jung,[2,3,6] Linda Hu,[1] Stephanie I. Mok,[1] Anar Shah,[1] Erin M. Savner,[1] Christos Tolias,[1] Roman Corfas,[1] Suzhen Chen,[4] Perrine Inquimbert,[4] Yi Xu,[5] Roderick R. McInnes,[2,3,6,7,8] Frank L. Rice,[9,10] Gabriel Corfas,[4] Qiufu Ma,[1,5] Clifford J. Woolf,[1,4] and Michael E. Greenberg[1,*]

[1]Department of Neurobiology, Harvard Medical School, 220 Longwood Avenue, Boston, MA 02115, USA
[2]Program in Developmental Biology
[3]Program in Genetics
The Research Institute, Hospital for Sick Children, 555 University Avenue, Toronto, ON, M5G 1L7, Canada
[4]F. M. Kirby Neurobiology Center, Department of Neurology, Children's Hospital Boston, 300 Longwood Avenue, Boston, MA 02115, USA
[5]Dana-Farber Cancer Institute, 1 Jimmy Fund Way, Boston, MA 02115, USA
[6]Department of Molecular Genetics
[7]Department of Pediatrics
[8]Institute of Medical Science
University of Toronto, Toronto, ON, M5S 1A1, Canada
[9]Center for Neuropharmacology Neuroscience, Albany Medical College, Albany, NY 12208, USA
[10]Integrated Tissue Dynamics LL, Renssalaer, NY 12144, USA
*Correspondence: michael_greenberg@hms.harvard.edu
DOI 10.1016/j.neuron.2010.02.025

SUMMARY

Itch is the least well understood of all the somatic senses, and the neural circuits that underlie this sensation are poorly defined. Here we show that the atonal-related transcription factor Bhlhb5 is transiently expressed in the dorsal horn of the developing spinal cord and appears to play a role in the formation and regulation of pruritic (itch) circuits. Mice lacking *Bhlhb5* develop self-inflicted skin lesions and show significantly enhanced scratching responses to pruritic agents. Through genetic fate-mapping and conditional ablation, we provide evidence that the pruritic phenotype in *Bhlhb5* mutants is due to selective loss of a subset of inhibitory interneurons in the dorsal horn. Our findings suggest that Bhlhb5 is required for the survival of a specific population of inhibitory interneurons that regulate pruritis, and provide evidence that the loss of inhibitory synaptic input results in abnormal itch.

INTRODUCTION

Both itch and pain serve crucial roles: they alert the organism to potential harm and trigger behavioral responses that prevent injury. However, our perceptual experience of these two sensations is qualitatively distinct, and our responses to them are very different. Itch is a skin-specific sensation that provokes the desire to scratch, thereby removing potentially harmful agents, such as a parasite, from the skin's surface. In contrast, pain can occur in any part of the body and, when it originates from the skin, triggers withdrawal, thereby removing us from harm's way (Yosipovitch et al., 2007). Both pain and itch can, however, become chronic pathological conditions (Ikoma et al., 2006). Unfortunately, effective treatment for chronic pain or itch is lacking, and progress in the development of new therapies is hampered by insufficient knowledge of the neural circuits that underlie these distinct sensations.

Our understanding of itch is limited, and the existence of itch-specific circuits is controversial (reviewed in McMahon and Koltzenburg, 1992; Schmelz, 2008). It has been hypothesized, for example, that itch might be distinguished from pain based simply on the pattern of firing or rate of discharge of C-fiber primary sensory neurons because many C-fibers respond both to algesic (pain-inducing) and pruritic (itch-inducing) compounds (Simone et al., 2004). However, recent work has supported an alternative theory—a so-called labeled-line for itch, in which a specific subset of C-fibers selectively conveys the sensation of itch from the skin to the spinal cord, where it is relayed in a unique projection pathway to the brain. A subpopulation of primary sensory neurons that respond selectively to the pruritic agent histamine are present in humans (Schmelz et al., 1997), as are second-order spinal projection neurons that respond to histamine in the cat (Andrew and Craig, 2001). Additional evidence that itch and pain are mediated by distinct neurons has emerged recently with reports that gastrin-releasing peptide receptor (GRPR)-expressing neurons in the spinal cord are specifically responsive to pruritic stimuli (Sun and Chen, 2007), and more compellingly, that selective ablation of these neurons eliminates itch but not pain (Sun et al., 2009).

Despite these advances, pruritic circuitry remains poorly understood. In particular, although itch information is integrated

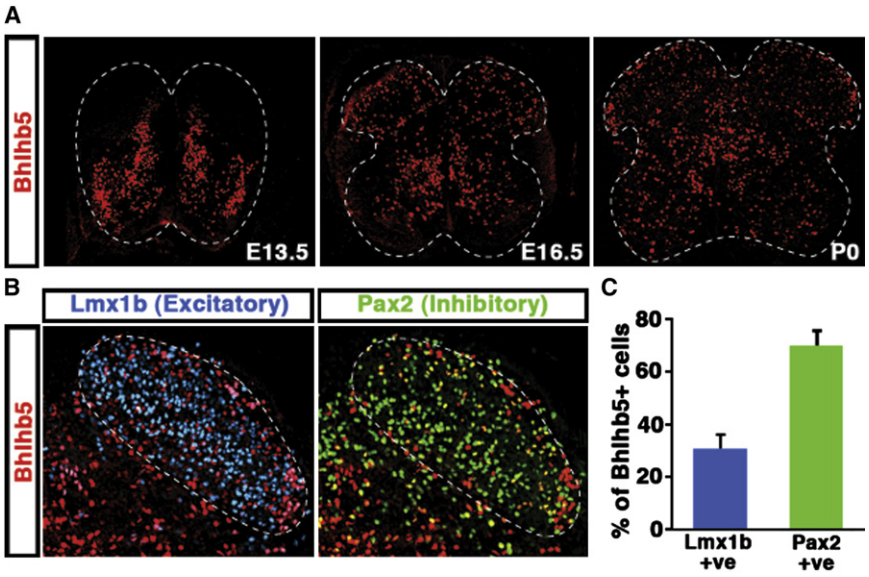

Figure 1. Bhlhb5 Is Transiently Expressed in Excitatory and Inhibitory Neurons in the Dorsal Spinal Cord

(A) Expression of Bhlhb5 protein in the mouse spinal cord embryonic day (E) 13.5, E16.5, and postnatal day 0 (P0) using anti-Bhlhb5 antibodies. The generation of Bhlhb5 antibodies used in this study is described in Figures S1A–S1C. (B) Co-staining of Bhlhb5 protein (red) with antibodies to the excitatory marker Lmx1b (blue) and the inhibitory marker Pax2 (green) in the dorsal horn of the spinal cord at P0. Dotted line denotes the dorsal horn region that was quantified in (C). (C) Quantification of the proportion of Bhlhb5-expressing neurons (Bhlhb5+) that colocalize with either Lmx1b or Pax2 indicates that Bhlhb5 is expressed in both excitatory and inhibitory neurons of the dorsal spinal cord. Data are presented as mean ± SEM. (n = 3 littermate pairs, counting 10 matched lumbar sections/pair).

and modulated within the dorsal horn of the spinal cord, the neurons involved in regulating itch await discovery. For instance, it is a common experience that inducing pain (e.g., by scratching) relieves itch (Ikoma et al., 2006). Conversely, relieving pain (e.g., with mu-opioids) induces itch (Umeuchi et al., 2003). The mutually antagonistic relationship between itch and pain suggests the involvement of inhibitory circuits within the dorsal spinal cord. However, such circuits have not been identified or characterized. A second type of modulation that occurs in the dorsal spinal cord is central sensitization, a type of sensory ''learning'' involving long-lasting changes in circuit properties that increase pain sensitivity (Woolf, 1983). This type of sensory plasticity occurs through multiple mechanisms, including an increase in the excitability of spinal cord neurons that mediate pain and a reduction in inhibitory synaptic input onto these cells (disinhibition) (reviewed in Latremoliere and Woolf, 2009). While central sensitization in response to itch (Ikoma et al., 2004), like that observed in response to pain, is thought to occur primarily in the dorsal spinal cord, the mechanisms involved are not known. Thus, there is a fundamental gap in knowledge with regard to the most basic spinal cord circuits that mediate pruritis.

Here we describe a mouse model involving mutation of the transcription factor Bhlhb5 that shows dramatically heightened responses to pruritic stimuli, enabling us to investigate the neural circuitry that underlies itch. Bhlhb5 is a neural-specific basic helix-loop-helix (bHLH) transcription factor related to the *Drosophila* proneural factor *atonal* (Ross et al., 2003). Compared to other well-studied members of this family, such as the NeuroD, Neurogenin, and Olig transcription factors, little is known about the function of Bhlhb5 in the nervous system. Previous work has identified an important role for Bhlhb5 in the retina, where it is required for the survival of some amacrine and cone bipolar cells (Feng et al., 2006). In addition, Bhlhb5 regulates the acquisition of area-specific fates in the cortex (Joshi et al., 2008). However, the function of Bhlhb5 in somatosensory systems has not been investigated.

Within the spinal cord, Bhlhb5 is transiently expressed in subsets of postmitotic neurons, suggesting a possible role in the assembly of spinal circuits. We investigated this idea by generating a series of mutant mice in which the function of the *Bhlhb5* gene is disrupted. We show that animals lacking *Bhlhb5* develop self-inflicted skin lesions and provide evidence that these lesions are due to heightened itch. To understand the molecular basis for this behavioral phenotype, we use a genetic fate mapping strategy in which Bhlhb5-expressing cells are permanently marked in vivo and uncover a crucial role for Bhlhb5 in the survival of a specific population of neurons in the superficial laminae of the dorsal horn. Furthermore, through conditional ablation, we provide evidence suggesting that loss of Bhlhb5 within inhibitory neurons in the dorsal horn results in the development of pathological skin lesions. Together, these data suggest a model in which disinhibition in the dorsal spinal cord results in abnormal itch.

RESULTS

Bhlhb5 Is Expressed within the Dorsal Horn of the Spinal Cord and Mice Lacking This Factor Develop Skin Lesions

To gain insight into the mechanisms that regulate neuronal circuit assembly in the spinal cord, we examined Bhlhb5 expression in the developing spinal cord by immunohistochemistry using several newly generated Bhlhb5-directed antibodies (Figures S1A–S1C, available online). Bhlhb5 was observed in a subpopulation of late-born neurons that migrate to the superficial layers of the dorsal horn (Figure 1A), and was transiently expressed earlier in the embryo in V1, V2, and dI6 interneurons (Figures S1D and S1E), consistent with previous reports (Liu et al., 2007). Colocalization studies using glutamatergic and GABAergic neuronal markers (Lmx1b and Pax2, respectively) (Cheng et al., 2005), revealed that approximately one-third of Bhlhb5-expressing neurons in the dorsal horn are excitatory, and two-thirds, inhibitory (Figures 1B and 1C). Expression of Bhlhb5 in the dorsal horn

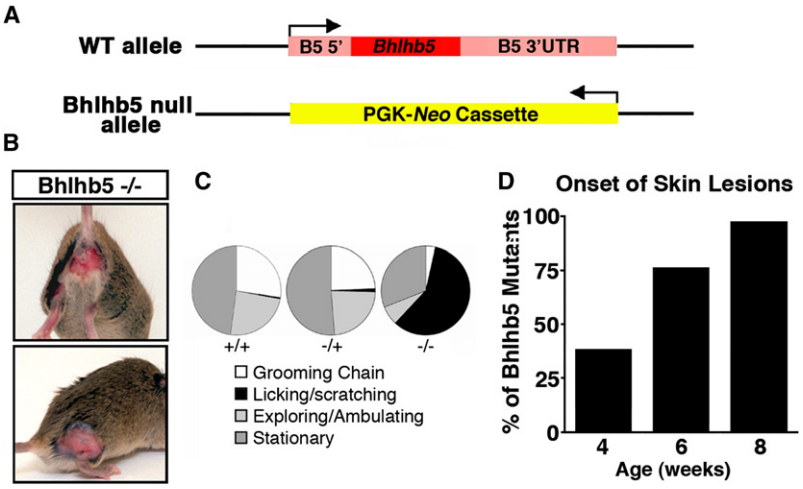

Figure 2. Loss of *Bhlhb5* Gives Rise to Mice that Develop Self-Inflicted Skin Lesions due to Excessive Licking and Scratching

(A) Schematic illustrating the *Bhlhb5* knockout allele in which the *Bhlhb5* gene is replaced by a neomycin expression cassette. Arrow indicates transcriptional start site. Also see Figure S2.

(B) Photos illustrating the skin lesions on *Bhlhb5* knockout mice.

(C) Behavioral analysis of wild-type (+/+), heterozygous (+/−), or *Bhlhb5* null (−/−) mice with pre-existing skin lesions showing proportion of time spent at each activity over a 20 min period indicates that *Bhlhb5*$^{-/-}$ mice spend the majority of their time licking and scratching at the site of lesion, whereas wild-type and heterozygous mice divide their time between normal head-to-toe grooming (grooming chain), exploring/ambulating, or resting (stationary). Note that, prior to the onset of skin lesions, *Bhlhb5*$^{-/-}$ mice do not display abnormal scratching or licking behavior. However, once a very small skin irritation develops, *Bhlhb5*$^{-/-}$ mice lick and scratch persistently such that a skin lesion develops very soon thereafter.

(D) Time course of skin lesion onset reveals that the majority of *Bhlhb5* mutants develop skin lesions between 4 and 8 weeks. Also see Figures S3A and S3D.

was prolonged, beginning shortly after the neurons exit mitosis (~E13.5) and persisting for up to 2 weeks postnatally. This extended expression of Bhlhb5 suggests a possible role for Bhlhb5 in the later aspects of neuronal differentiation, such as circuit assembly.

To investigate the function of Bhlhb5 in the developing spinal cord, we generated a *Bhlhb5* knockout mouse (Figures 2A and S2). Constitutive loss of *Bhlhb5* gave rise to mice that appeared to have severe somatosensory defects, as evidenced by self-inflicted skin lesions (Figure 2B). We observed these mice carefully and found that the skin lesions were due to excessive licking and scratching (Figure 2C). By 4 weeks of age, one-third of *Bhlhb5* mutants had developed skin lesions, and at 8 weeks of age, skin lesions were observed in almost every *Bhlhb5* knockout mouse (Figure 2D), irrespective of genetic background (129/Sv, C57Bl/6, and CD1). The skin lesions were frequently found on the perineum and the haunches (Figure S3A), but occasionally observed in many other regions, such as orafacial area. In contrast, skin lesions were never observed in wild-type or heterozygous mice.

We analyzed the epidermis of *Bhlhb5* knockout mice prior to the development of skin lesions but found that there was no evidence of abnormal innervation, as revealed by PGP9.5 staining (Figures S3B and S3C). Furthermore, electron micrographs of dorsal roots showed no evidence of neuropathy in *Bhlhb5* mutants (Figure S3D).

Bhlhb5$^{-/-}$ Mice Show Heightened Responses to Itch-Inducing Agents

Based on the skin lesions and the scratching behavior observed in *Bhlhb5*$^{-/-}$ mice, we hypothesized that these mice might be responding to an itch-like sensation. To test itch responsiveness, we examined the scratching behavior of mice that had received intradermal injections of pruritic agents into the nape of the neck. Because the presence of skin lesions was found to be a potentially confounding factor in the behavioral assays (Figures S3F–S3H), these experiments were performed using young (4-week-old) *Bhlhb5* mutant mice, prior to the onset of skin lesions. Although the signaling events that initiate itch in the skin are not well understood, they occur through at least two independent pathways (Davidson et al., 2007). One mechanism is mediated by histamine receptors, which can be activated by histamine itself or by compound 48/80, a chemical that mediates histamine release from mast cells (Kuraishi et al., 1995). The second mechanism is mediated by Protease-activated receptor2 (PAR2), which can be activated by peptide agonists such as SLIGRL-NH2 (Reddy et al., 2008). *Bhlhb5* mutants showed elevated itch responses upon activation of either histamine-dependent or PAR2-dependent mechanisms (Figure 3A). Thus, multiple pruritogens, acting through at least two distinct mechanisms, give rise to significantly elevated itch responses in *Bhlhb5* mutant mice. In addition, we tested α-methyl-5-hydroxytryptamine (αMe5HT), a serotonin analog that causes inflammation and pruritis when administered peripherally (Yamaguchi et al., 1999); chloroquine, an antimalarial drug that causes itch (as a side effect) through direct activation of sensory neurons (Sowunmi et al., 1989; Liu et al., 2009); and formalin, a pain-inducing chemical that has been found to elicit scratching when injected intradermally (Imamachi et al., 2009). Regardless of the pruritic agent used, *Bhlhb5*$^{-/-}$ mice showed significantly more scratching behavior than wild-type mice (Figure 3A).

The excessive scratching response observed in the *Bhlhb5*$^{-/-}$ mice was consistent with the possibility that the skin lesions that occur in these mice might be due to a heightened sensation of itch. In support of this hypothesis, we found that the presence of skin lesions is associated with elevated neuronal activity in the dorsal horn, a region of the nervous system in which pruritic information is thought to be integrated. Specifically, c-Fos was upregulated in the dorsal spinal cord of *Bhlhb5* mutants with

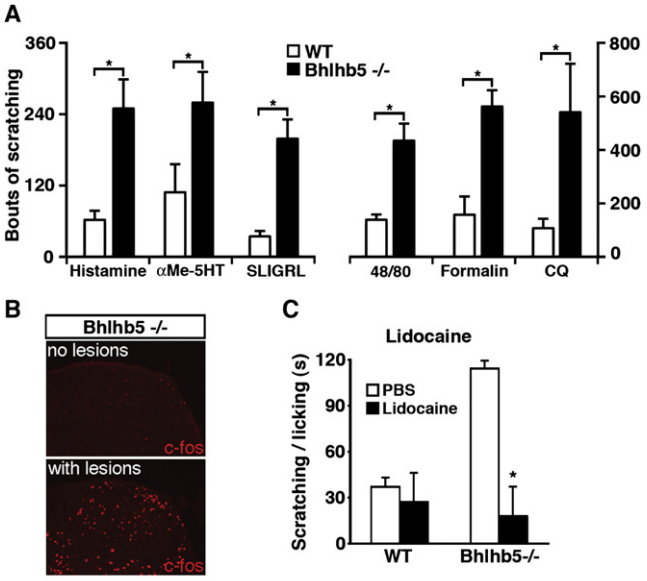

Figure 3. *Bhlhb5*$^{-/-}$ Mice Have Elevated Itch Responses

(A) *Bhlhb5*$^{-/-}$ mice show significantly enhanced scratching responses following the intradermal injection of pruritic agents into the nape of the neck. Agents tested were histamine, a serotonin analog (αMe-5HT), a PAR2 agonist (SLIGRL-NH2), compound 48/80 (48/80), formalin, and chloroquine (CQ). Experiments were performed with four or five littermate pairs that were 3 to 4 weeks old, prior to the development of skin lesions in *Bhlhb5*$^{-/-}$ mice. Data are presented as mean ± SEM, and (*) indicates significant difference relative to controls ($p < 0.05$, t test).

(B) Abnormal expression of c-Fos in the dorsal horn corresponds to the site of skin lesions in *Bhlhb5*$^{-/-}$ mice. Immunostaining with anti-c-Fos antibodies reveals elevated c-Fos expression in a segment of the dorsal horn that corresponds to the sites of a skin lesion (S1), but not in a matched segment from a *Bhlhb5*$^{-/-}$ mouse that lacks lesions.

(C) Local injection of lidocaine causes the abnormal scratching and licking behavior to attenuate in *Bhlhb5*$^{-/-}$ mice. *Bhlhb5*$^{-/-}$ mice with lesions of the perineum were used. All mice received an injection of either PBS (control) or lidocaine (to block sensory input) into the perineum. Injection of lidocaine in wild-type mice had no effect on licking and scratching behavior. Data are presented as mean ± SEM. and (*) indicates significant difference relative to treatment with vehicle ($p < 0.05$, t test).

skin lesions relative to *Bhlhb5* mutant mice that lacked lesions (Figure 3B). Moreover, c-Fos expression was observed in segments of the dorsal horn of spinal cord that correspond to the site of lesions, and not in other levels of the spinal cord (data not shown). Next, we reasoned that if *Bhlhb5*$^{-/-}$ mutant mice with skin lesions were compelled to scratch by a sensation of itch, then they would cease scratching if itch sensation were blocked. To test this idea, we used lidocaine to block sensory input from primary sensory neurons (Holstege et al., 2008). Strikingly, we found that loss of sensory input through the use of lidocaine completely attenuated the licking/scratching behavior directed toward the lesioned area (Figure 3C). Based on this finding, together with the observation that *Bhlhb5* mutants respond excessively to itch-inducing stimuli, we theorize that the skin lesions are caused by a site-specific itch that leads to the abnormal scratching and/or licking behaviors. Although we cannot know with certainty how these mice are feeling, their scratching behavior is suggestive of itch. For simplicity, we refer hereafter to the sensation that is driving the scratching behavior as itch.

Bhlhb5$^{-/-}$ Mice Have Similar Acute Nociceptive Responses but Show Evidence of Enhanced Central Sensitization

Next we investigated whether the *Bhlhb5*$^{-/-}$ mice also respond abnormally to other somatosensory modalities such as touch and pain. Upon stimulation with von Frey filaments to measure mechanical sensitivity, wild-type and *Bhlhb5*$^{-/-}$ mice showed similar paw-withdrawal thresholds (Figure 4A). When placed on a hot plate, wild-type and *Bhlhb5*$^{-/-}$ mice responded with a similar latency, indicating that thermal sensitivity is unchanged in *Bhlhb5* mutants (Figure 4B). Similarly, wild-type and *Bhlhb5* mutant animals showed no significant differences in the duration of their paw-licking behavior upon the intraplantar injection of capsaicin or mustard oil, a TRPV1 and TRPA1 agonist, respectively, indicating that loss of *Bhlhb5* does not affect nociceptive responses to chemical algesics (Figures 4C and 4D). Finally, in assays for inflammation-induced mechanical hypersensitivity, no significant differences were observed between genotypes; both wild-type and *Bhlhb5* mutant littermates showed similar levels of heightened sensitivity following the intraplantar injection of carrageenan, suggesting that mechanical allodynia is also unaffected by the loss of *Bhlhb5* (Figure 4E). Together, these results suggest that the responses to various types of noxious sensory stimuli—mechanical, thermal, and chemical—are not significantly different between wild-type and *Bhlhb5* mutants, at least in young (4-week-old) mice.

While *Bhlhb5* mutant mice showed no significant changes in their responses to most nociceptive sensory assays, the formalin test was a marked exception. In this paradigm, a biphasic behavioral response (primarily licking of the hindpaw) is seen in response to the intraplantar injection of 5% formalin. The immediate, early-phase response is due to acute activation of TRPA1-expressing primary nociceptors (McNamara et al., 2007), whereas the late-phase response is believed to be due to activity-dependent central sensitization (Tjølsen et al., 1992) and ongoing afferent input (Puig and Sorkin, 1996). Using this test we found that, although the response observed in the early phase was similar between genotypes, the response observed during the late phase was significantly different. Specifically, the licking behavior during the second phase of the formalin test was almost 4-fold greater in *Bhlhb5* mutants than in wild-type littermates (Figure 4F).

Formalin is a reactive chemical that activates TRPA1 (McNamara et al., 2007), causing widespread tissue damage and inducing pain in animals and man (Dubuisson and Dennis, 1977). Many inflammatory mediators are released in response to formalin at doses used in the standard test, including ATP and H^+ from leaking membranes, histamine from degranulated mast cells, and peptide agonists from activated proteases (Tjølsen et al., 1992). Thus, we hypothesized that, in addition to activating nociceptors, formalin treatment may also cause the release of agents that activate pruritoceptors. Consistent with this, formalin elicits primarily a scratching response rather than a wiping response when injected intradermally into the cheek

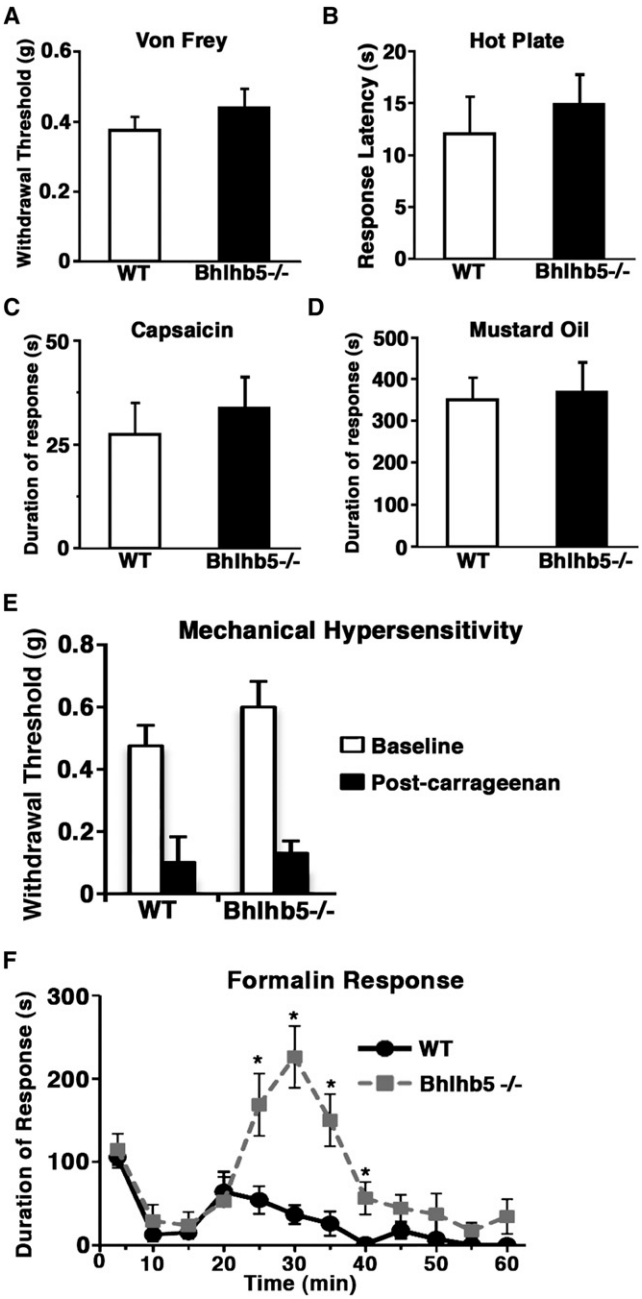

Figure 4. *Bhlhb5*$^{-/-}$ Mice Show Evidence of Enhanced Central Sensitization

(A) Mechanical sensitivity as assessed by measuring the withdrawal threshold upon application of von Frey fibers to the plantar surface of the hindpaw.

(B) Thermal sensitivity as assessed by measuring the response latency when placed on a 55°C hot plate.

(C and D) Acute nociception as assessed by measuring the duration of licking following the injection of capsaicin (C) or mustard oil (D) into the hindpaw.

(E) Mechanical hypersensitivity as assessed by measuring the withdrawal threshold prior to and 2 hr following the injection of carrageenan into the hindpaw.

(F) Upon injection of 5% formalin into the hindpaw, wild-type (WT) and *Bhlhb5*$^{-/-}$ mice show a similar response in the early phase (0–20 min); however, during the late phase (20–40 min), *Bhlhb5*$^{-/-}$ mice spend significantly more time licking their hindpaws, suggestive of enhanced central sensitization in these mice. Data are presented as mean ± SEM, and (*) indicates a significant difference relative to controls at the same time point ($p < 0.05$, Mann-Whitney U-test). These experiments were performed with six to eight littermate pairs that were 4 weeks old, prior to the development of skin lesions in *Bhlhb5*$^{-/-}$ mice. (When older mice were used in these studies, *Bhlhb5*$^{-/-}$ mice were found to have reduced responses in all behavioral assays, possibly due to the presence of skin lesions on these mice, which may have been a confounding factor; Figures S3E–S3G).

(Figure S3E). This behavioral assay is thought to distinguish between pain and itch, because the noxious irritant capsaicin elicits wiping by the forepaw whereas the pruritogen histamine evokes scratching by the hindpaw (Shimada and LaMotte, 2008). Thus, the finding that formalin induces scratching in this assay suggests that formalin may elicit itch in addition to pain. If so, the heightened response to formalin observed in *Bhlhb5*$^{-/-}$ mice might reflect, at least in part, an abnormal itch sensation. Alternatively, it is possible that the *Bhlhb5*$^{-/-}$ phenotype may include a pain component, but if so, it appears to be restricted to formalin, and not heat, capsaicin, mustard oil, or carrageenan.

Conditional Ablation Points to a Possible Role for the Dorsal Horn of the Spinal Cord in the Abnormal Itch of *Bhlhb5*$^{-/-}$ Mice

Since itch circuits are poorly characterized but are thought to involve numerous regions of the nervous system, we used conditional ablation to help identify the neurons whose dysfunction causes excessive itch in *Bhlhb5* mutants. Specifically, we generated a *Bhlhb5* allele that was flanked by loxP sites (Figures 5A and S4) and crossed it to a variety of cre-expressing mouse lines in which cre-mediated recombination occurs within discrete regions of the nervous system. The selective disruption of *Bhlhb5* in neuronal precursors by crossing the conditional *Bhlhb5* knockout to a *Nestin-cre* line (Tronche et al., 1999) gave rise to mice with skin lesions, suggesting that the scratching behavior in the *Bhlhb5*$^{-/-}$ mice is neural in origin (Figure 5B) and excluding the possibility that the self-injurious grooming behavior in the mutant mice was due to topical dermatitis. One of the regions of the nervous system in which Bhlhb5 is highly expressed is in the dorsal telencephalon (Joshi et al., 2008). However, loss of *Bhlhb5* in the dorsal telencephalon using the *Emx-cre* line (Gorski et al., 2003) was not sufficient for the development of skin lesions (Figure 5B), suggesting that higher cortical function was not involved in this phenotype. In contrast, the loss of *Bhlhb5* resulting from *Wnt1*-driven *cre* expression (Rico et al., 2002) was found to be sufficient for the development of skin lesions (Figure 5B), and the incidence of these lesions was identical in frequency, location, and severity to those observed in the *Bhlhb5* knockout mouse (data not shown). Analysis of Bhlhb5 protein expression following *Wnt1-cre*-mediated recombination confirmed that Bhlhb5 was selectively lost from the dorsal, but not the ventral, horn of the spinal cord, as expected based on the distribution of *Wnt1-cre*-mediated reporter expression (Figure 5C). In addition, *Wnt1-cre;Bhlhb5*$^{fl/fl}$ mice showed significantly elevated scratching responses in response to the pruritic agent compound 48/80 (Figure 5D). Together these data indicate

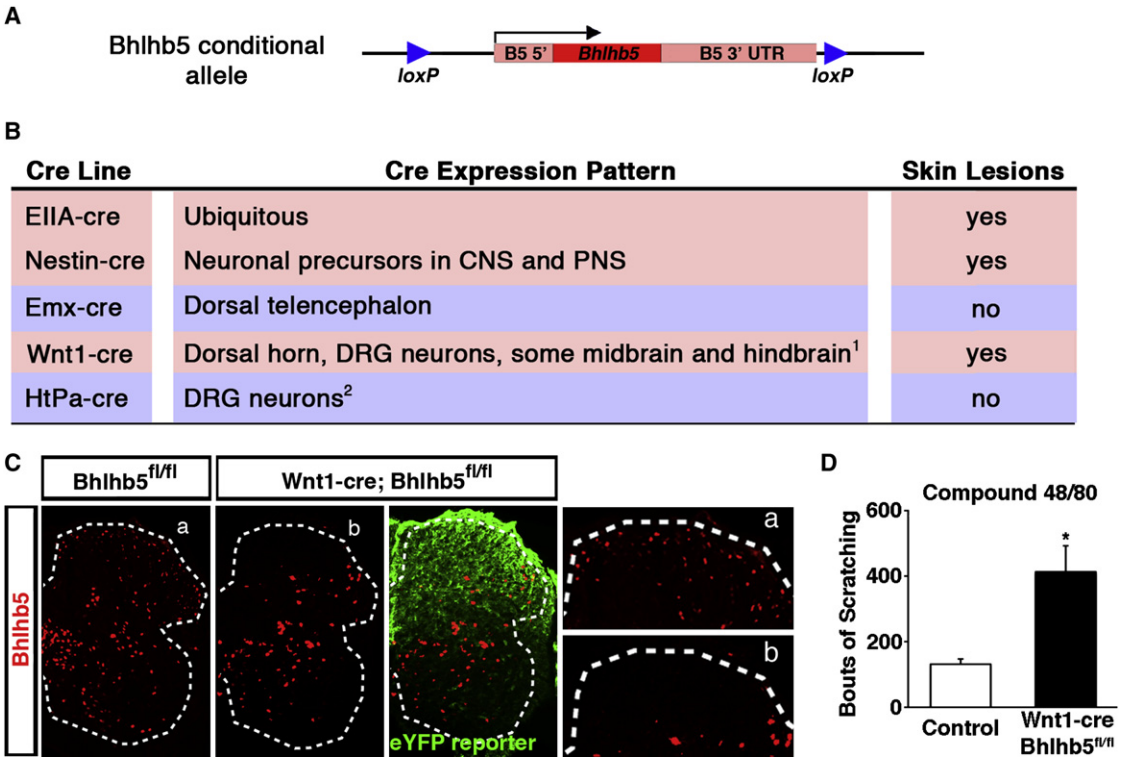

Figure 5. Conditional Ablation Points to a Possible Role of the Dorsal Horn in the Abnormal Itch in *Bhlhb5* Mutant Mice

(A) Schematic illustrating the conditional *Bhlhb5* knockout allele in which the *Bhlhb5* gene is floxed by loxP sites (▶), enabling cre-mediated recombination. Arrow indicates transcriptional start site. Also see Figure S4.

(B) Table listing the cre-expressing mouse lines used to cause selective ablation of *Bhlhb5*, together with the expression pattern of cre in each line and whether the subsequent animals develop skin lesions following cre-mediated recombination of *Bhlhb5*. [1]*Wnt1-cre* also causes recombination in the cerebellum and other neural crest-derived cells in addition to dorsal root ganglia (DRG) neurons. [2]*HtPa-cre* causes recombination in other neural crest-derived cells in addition to DRG neurons. Also see Figure S5. The expression pattern of each cre line was confirmed using cre-responsive reporter mice (data not shown).

(C) Wnt1-cre-mediated loss of *Bhlhb5*. Lumbar sections from P0 animals stained with antibodies for Bhlhb5 (red) and eYFP (green). Sections from control (left) and mutant mouse (right) are homozygous floxed at the *Bhlhb5* locus (Bhlhb5$^{fl/fl}$). In addition, the mutant mouse harbors the *Wnt1-cre* allele and the Rosa26 cre-responsive eYFP reporter (eYFP reporter). Insets are enlarged on right. eYFP staining reveals cells in which cre-mediated recombination has occurred. Note that Bhlhb5 staining is absent from the dorsal horn of mutants, but not the ventral horn.

(D) Conditional loss of *Bhlhb5* in the *Wnt1-cre* expression domain results in significantly elevated scratching responses following the injection of compound 48/80 intradermally into the nape of the neck relative to homozygous floxed control mice. Data are presented as mean ± SEM, and (*) indicates significant difference relative to controls ($p < 0.05$, t test). Though conditional loss of *Bhlhb5* pointed to a possible role of the dorsal horn in the abnormal itch, no gross defects in the dorsal spinal cord were observed in *Bhlhb5* mutant mice (Figure S6).

that loss of *Bhlhb5* within the *Wnt1-cre* expression domain is responsible for the development of abnormal itch.

Although *Wnt1*-mediated *cre* expression causes recombination in several regions in the nervous system (see Figure 5B), there were two regions in particular known to mediate pruritis: the dorsal root ganglia (DRG), which contains primary pruritoceptive neurons that initiate itch, and the dorsal horn of the spinal cord, which contains interneurons and projection neurons that integrate pruritic information and relay it to the brain (Sun et al., 2009). To help distinguish which of these two regions might be responsible for the self-injurious behavior in *Bhlhb5* mutant mice, we used the *HtPa-cre* line, which results in the loss of *Bhlhb5* in all neural-crest-derived cells (including all DRG neurons), but not in neurons of the spinal cord (Figure S5; Pietri et al., 2003). *HtPa-cre*-mediated ablation of *Bhlhb5* was not sufficient, however, for the development of skin lesions (Figure 5B). Together, these findings suggest that the loss of *Bhlhb5* within the dorsal horn is necessary for heightened itch in *Bhlhb5* mutant mice.

A Subpopulation of Bhlhb5-Expressing Neurons Is Absent from the Superficial Dorsal Horn of *Bhlhb5* Mutant Mice

While the conditional ablation studies raised the possibility that defects within the dorsal horn of the spinal cord lead to abnormal itch in *Bhlhb5* mutant mice, the cellular basis for this phenotype was unknown. Mice lacking *Bhlhb5* were found to have no obvious or major disruption of dorsal horn anatomy based on expression of a variety of spinal cord neuronal markers, including PKCγ, calbindin, calretinin, Substance P, IB4, and CGRP (Figure S6). Recent reports have suggested that DRG neurons that express gastrin-related peptide (GRP) are specific for itch

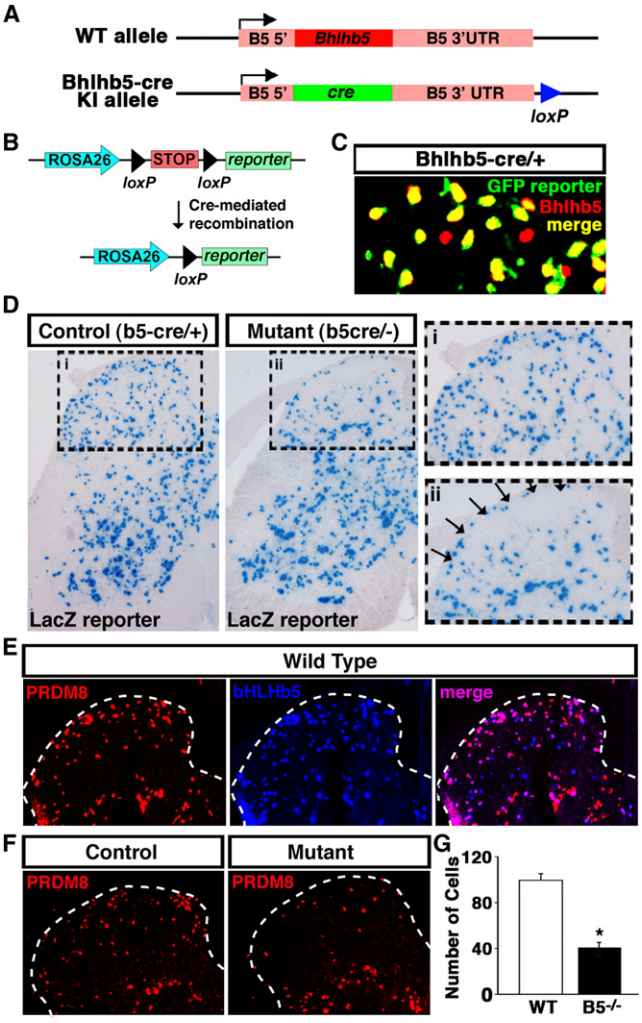

Figure 6. A Subpopulation of Bhlhb5-Expressing Neurons Is Absent from the Superficial Dorsal Horn of *Bhlhb5* Mutant Mice

(A) Schematic illustrating the *Bhlhb5-cre* knockin allele in which the coding region of the *Bhlhb5* gene was replaced with the coding region of the *cre recombinase* gene. Also see Figure S7.

(B) Diagram illustrating the mechanism whereby the *Bhlhb5-cre* allele causes irreversible recombination of the Rosa26 reporter, resulting in the removal of a stop signal and expression of the reporter (βgalactosidase or eYFP).

(C) Specificity of the *Bhlhb5-cre* allele. Representative region of dorsal spinal cord from P0 mice that are heterozygous for the *Bhlhb5-cre* allele and harbor the Rosa-eYFP reporter were stained with antibodies to Bhlhb5 (red) and eYFP (green). Note that at this time point, almost all labeled cells are double-labeled (yellow), indicating cre-mediated recombination has occurred in Bhlhb5-expressing cells.

(D) *Bhlhb5-cre* knockin reveals the fate of *Bhlhb5-cre*-marked cells in the spinal cord of control (*Bhlhb5-cre*/+) and mutant (*Bhlhb5-cre*/−) mice. Cre-responsive Rosa26-LacZ reporter is used to mark cells in which *Bhlhb5-cre* was expressed. Sections are from representative lumbar spinal cord hemisections from P28 mice. Dorsal horn is enlarged in inset for control (i) and mutant (ii) mice. Arrows indicate region of cell loss in mutant mice. Quantification reveals an ~50% loss of *lacZ*-expressing cells in the superficial dorsal horn of the spinal cord (data not shown, n = 4 pairs of mice, counting 20 matched lumber sections/pair). See also Figure S8A. Note that no sensory phenotypes are observed in control mice that are heterozygous for *Bhlhb5*, and the dorsal horn appears grossly normal based on the analysis of a number of other neural markers (Figure S6).

(E) Coimmunostaining with antibodies against Prdm8 (red) and Bhlhb5 (blue) reveal that these two factors show a very high degree of colocalization (merge; purple) in the dorsal horn of mice at P0, suggesting that Prdm8 is a marker for Bhlhb5-expressing cells.

(F) Representative lumbar sections from P0 mice stained with antibodies to Prdm8 reveal that there is a loss of Prdm8-expressing neurons in *Bhlhb5* mutants relative to controls.

(G) Quantification of Prdm8-positive (+ve) cells in the superficial dorsal horn of control (Con) and *Bhlhb5* mutant (Mut) mice. (n = 3 pairs of mice, counting 10 matched lumber sections/pair). Data are presented as mean ± SEM. *$p < 0.05$, t test.

(Sun and Chen, 2007). However, when we looked specifically at this population, we found that the number of GRP-expressing neurons in the DRG was unchanged in *Bhlhb5* mutants (data not shown), and the innervation by GRP-expressing neurons in the dorsal horn appeared unaffected by the loss of *Bhlhb5* (Figures S6G and S6H).

The absence of an easily discernable defect in the dorsal spinal cord of *Bhlhb5* mutants was not altogether unexpected given that Bhlhb5 is expressed in just a small subset of those neurons. To determine whether there is a subtle defect in itch circuitry within the dorsal spinal cord, we needed an approach to selectively define the cells that express *Bhlhb5* and observe the subsequent fate of these cells in mice lacking *Bhlhb5*. Toward this end, we generated a *Bhlhb5-cre* knockin animal (*Bhlhb5-cre*), in which the coding region of the *Bhlhb5* gene was replaced with *cre recombinase* (Figures 6A and S7). Upon crossing this *Bhlhb5-cre* line with a cre-responsive reporter line, cells in which the *Bhlhb5* gene has been activated become permanently marked with the reporter (Figure 6B), allowing the fate of *Bhlhb5*-expressing cells to be resolved at a cellular level and followed throughout the life of the animal.

For these experiments, we used three different cre-responsive indicator alleles (Rosa26-lacZ, Rosa26-eYFP, or Z/EG reporters) (Soriano, 1999) to visualize genetically marked neurons. For simplicity, we refer to these neurons as B5-cre-lacZ, B5-cre-eYPF, or B5-cre-Z/EG marked neurons, respectively. Analysis of reporter expression in newborn mice that are heterozygous for the *Bhlhb5-cre* allele revealed that B5-cre-eYFP and Bhlhb5 were almost completely colocalized, indicating that reporter expression faithfully recapitulated the endogenous expression pattern of Bhlhb5 (Figure 6C).

Upon crossing the *Bhlhb5-cre* line with the Rosa26-lacZ reporter, we found that lacZ marked a small subset of neurons throughout all laminae of the spinal cord in adult mice (Figure 6D). In mice lacking Bhlhb5, most regions of the spinal cord showed a similar pattern of B5-cre-lacZ cells. However, specifically in the superficial laminae, we found significantly fewer B5-cre-lacZ neurons in the *Bhlhb5* mutants (Figure 6D). Quantification revealed that approximately 50% of neurons that would normally have expressed Bhlhb5 were missing in the superficial dorsal horn of adult mice lacking *Bhlhb5*. Furthermore, this cell loss was observed throughout the rostro-caudal axis of the spinal cord (data not shown). To verify this finding and to rule out potential effects specific to the Rosa locus, we used the Z/EG line as a reporter and we again observed significant loss of cell bodies and neuropil in *Bhlhb5* mutants relative to control animals (Figure S8A). Coimmunostaining with CGRP

(a marker of lamina I and outer lamina II) and IB4 (a marker of inner lamina II) revealed a decrease in the number of B5-cre-Z/EG marked cells within the superficial layers in mutant mice. Given that the decrease in genetically labeled cells is observed using cre reporters that are expressed from different promoters and distinct loci, it is unlikely that these effects are due to misregulation of the reporter alleles.

While a loss of Bhlhb5 neurons seemed the most likely explanation for these findings, it remained possible that the reduction in the number of *Bhlhb5-cre*-labeled neurons in the *Bhlhb5* mutant reflected merely misregulation of the *Bhlhb5-cre* allele. To address this possibility, we searched for another marker of Bhlhb5-expressing cells with which to confirm our findings. Our studies in other regions of the nervous system (to be described elsewhere) revealed that Bhlhb5 was largely coexpressed with Prdm8, a putative zinc-finger-containing transcription factor. To assess whether Prdm8 could be used as a marker for Bhlhb5-expressing cells in the spinal cord, we performed double-immunolabeling experiments and found that Bhlhb5 and Prdm8 showed approximately 85% colocalization (Figure 6E). Next, we examined the number of Prdm8-expressing cells in the dorsal spinal cord of *Bhlhb5* mutant mice and found that they were reduced by approximately 50% (Figures 6F and 6G), corroborating that a subpopulation of Bhlhb5-expressing neurons is absent from the superficial dorsal spinal cord in *Bhlhb5* mutant mice.

Cell Loss in *Bhlhb5* Mutant Mice Reflects an Increase in Programmed Cell Death

There are several possible explanations for the decrease in *Bhlhb5-cre*-marked neurons in the superficial lamina of the dorsal horn in *Bhlhb5-cre/−* mice relative to *Bhlhb5-cre/+* mice. The neurons might never have been born, they might have migrated to the wrong lamina, or they might have died during development.

Given that Bhlhb5 is expressed exclusively in postmitotic neurons (data not shown and Liu et al., 2007), it seemed unlikely that a loss of this factor would affect mitosis. However, to rule out this possibility, we compared control mice (*Bhlhb5-cre/+; Rosa26-eYFP*) to *Bhlhb5* mutant mice (*Bhlhb5-cre/−; Rosa26-eYFP*), analyzing the numbers of neurons that were colabeled with BrdU, to label dividing neurons, and eYFP, to label neurons that were genetically marked by the *Bhlhb5-cre* allele. Neurons were labeled with BrdU at either E12.5 or E13.5, the time during which superficial dorsal horn neurons are born, and analyzed at E17.5, after they have migrated into superficial laminae (Mizuguchi et al., 2006; Wildner et al., 2006). These experiments revealed no difference in the number of genetically marked neurons that were BrdU-positive between control and *Bhlhb5* mutant mice, indicating that loss of Bhlhb5 has no effect on the number of dorsal horn neurons that are born (data not shown).

We next investigated the possibility that the decrease in the number of neurons in the superficial dorsal spinal cord of *Bhlhb5* mutant mice was due to a defect in migration. Toward this end, we quantified the number of cells that express B5-cre-eYFP in control and *Bhlhb5* mutant animals at P0. This analysis revealed that there was an ~50% decrease in the number of B5-cre-eYFP-marked neurons in the superficial dorsal horn of Bhlhb5 mutants, but that no difference existed in the number of B5-cre-eYFP-marked neurons in any other region of the spinal cord in control and mutant mice (Figures 7A–7D). The observed decrease in the number of B5-cre-eYFP-marked neurons in the superficial dorsal horn of the *Bhlhb5* mutant mice, without a corresponding increase in other regions of the spinal cord, suggests that neurons that are absent from the superficial dorsal horn have not migrated to another region of the spinal cord.

Finally, we investigated the possibility that Bhlhb5-cre-marked neurons might be lost in *Bhlhb5* mutant mice through programmed cell death. To address this, we counted the number of neurons that express activated caspase-3, a marker of apoptosis (Cryns and Yuan, 1998), and found that there was a small but significant increase in the number of apoptotic cells in the superficial dorsal horn of *Bhlhb5* mutant mice relative to controls at E18.5, with no significant difference at E17.5 or E19.5 (Figure 7E). The timing of this cell death was in agreement with the observation that *Bhlhb5* mutants display a clear loss of Bhlhb5-cre-marked cells at P0 (Figure 7C), but not at (or prior to) E17.5 (data not shown). These findings indicate that the loss of Bhlhb5-cre-labeled cells in *Bhlhb5* mutants is likely due to apoptosis during development, and suggest that Bhlhb5 is required for the survival of neurons in spinal cord pruritic circuits.

Inhibitory Neurons Underlie Abnormal Itch in *Bhlhb5*$^{-/-}$ Mice

To investigate whether excitatory or inhibitory neurons are lost upon ablation of *Bhlhb5*, we double-labeled the B5-cre-eYFP neurons with antibodies for excitatory (Lmx1b) or inhibitory (Pax2) neurons (Cheng et al., 2005) and found a partial loss of both glutamatergic and GABAergic neurons (Figure S8B). To ascertain which subset is involved in the pruritic phenotype in *Bhlhb5* mutant mice, we used two additional cre lines, *Tlx3-cre* and *Pax2-cre* (Ohyama and Groves, 2004; Xu et al., 2008). Tlx3-cre causes recombination within regions of the nervous system that include excitatory neurons within the dorsal horn (Figures 8A and 8C), whereas Pax2-cre causes recombination within regions of the nervous system that include most inhibitory neurons throughout the spinal cord (Figures 8B and 8C). To confirm that these alleles were behaving as expected, double-labeling with markers for glutamatergic (Lmx1b-expressing) and GABAergic (Pax2-expressing) neurons was performed. These experiments revealed that, upon Tlx3-cre-mediated recombination, Bhlhb5 was no longer expressed in excitatory neurons in the dorsal horn, though it remained expressed in inhibitory neurons in this region (Figure 8C). Conversely, upon Pax2-cre-mediated recombination, Bhlhb5 was no longer expressed in inhibitory neurons, though it remained expressed in excitatory neurons of the spinal cord (Figure 8C). Mice lacking *Bhlhb5* selectively in glutamatergic neurons within the dorsal horn neither developed skin lesions nor showed heightened itch responses (Figures 8D and 8E), suggesting that Bhlhb5 function within excitatory neurons is not required for the pruritic phenotype. However, use of the *Pax2-cre* line to ablate *Bhlhb5* gave rise to mice that both developed skin lesions and showed heightened responses to pruritic agents (Figures 8D and 8E). These findings suggest that the loss of Bhlhb5 in inhibitory neurons is sufficient to produce persistent abnormal itch (Figure 8F).

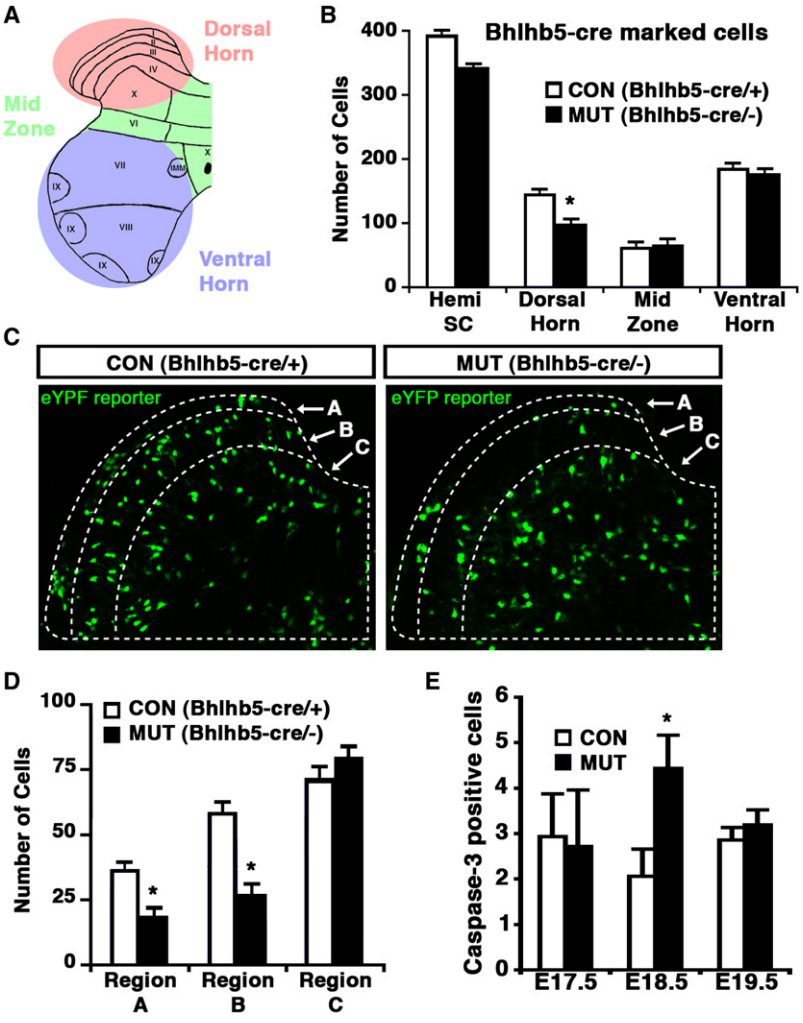

Figure 7. Cell Loss in *Bhlhb5* Mutant Mice Reflects an Increase in Programmed Cell Death

(A) Schematic illustrating regions within a hemi-spinal cord (dorsal horn, mid zone and ventral horn) that were used for quantification.

(B–D) Quantification of *Bhlhb5-cre*-marked cells in the lumbar spinal cord of control (*Bhlhb5-cre*/+) and mutant (*Bhlhb5-cre*/−) mice, visualized with the cre-responsive Rosa26-eYFP reporter at P0. (B) The number of *Bhlhb5-cre*-marked cells observed in various regions of a spinal cord hemisection was quantified. Significantly fewer *Bhlhb5-cre*-marked cells were found in the dorsal horn of *Bhlhb5* mutants relative to controls. No significant changes were observed in other regions of the spinal cord. (C) Representative images from the dorsal horn of control and mutant mice showing *Bhlhlb5-cre*-marked cells. The dorsal horn was further subdivided into regions based on anti-calretinin antibody staining (which marks region B; data not shown). Note that Rexed's laminae are not fully formed at this stage and most lamina-specific markers are not expressed. Nevertheless, region A corresponds roughly to future lamina I and region B to future lamina II. (D) Quantification of *Bhlhb5-cre*-marked neurons in regions A, B, and C, as defined above. There is a significant reduction in the number of Bhlhb5-cre marked neurons within regions A and B of the dorsal horn in mutants relative to controls. No significant change was observed within region C.

(E) Analysis of apoptotic cells in the dorsal horn of control and mutant animals at E17.5, E18.5, and E19.5, as indicated. Apoptotic neurons in the dorsal horn were identified using an antibody against cleaved caspase-3. Significantly more cleaved caspase-3-positive cells were observed in the mutant dorsal horn at E18.5 relative to littermate controls. Further analysis reveals that the absence of Bhlhb5-expressing neurons in the dorsal horn is due to the loss of both inhibitory and excitatory neurons (Figure S8B).

For (B), (D), and (E), three to five pairs of littermates were analyzed, and data represent mean ± SEM (*$p < 0.05$, Mann-Whitney U-test).

To further test the idea that abnormal circuitry within the dorsal horn causes the pruritic phenotype, we analyzed c-Fos expression (as a marker of neuronal activation) following the injection of the pruritic agent, compound 48/80, or formalin. Using this approach, we found significantly more c-Fos-expressing cells in the dorsal horn of *Bhlhb5* mutant mice, relative to controls (Figures S8C–S8F), consistent with the idea that neurons of the dorsal horn process information aberrantly in *Bhlhb5* mutant mice.

DISCUSSION

We have generated a mouse model that develops self-inflicted skin lesions and we provide evidence that this is due to abnormal itch responsiveness. Using a genetic fate mapping strategy, we provide insight into the cellular basis for this phenotype, showing that Bhlhb5 is required for the survival of a select group of neurons within the dorsal horn. Furthermore, through conditional ablation, we provide evidence that the loss of Bhlhb5 within inhibitory interneurons produces the abnormal scratching behavior that gives rise to pathological lesions.

The expression of Bhlhb5 within the dorsal horn is restricted to approximately 5% of neurons, yet its loss in the dorsal horn is very likely responsible for the abnormal itch response we detect in *Bhlhb5* mutant mice. We have identified a specific population of inhibitory neurons in the most superficial laminae of the spinal cord that require Bhlhb5 for survival and appear to be critical for regulating the normal manifestation of itch. In addition, we provide evidence that the loss of inhibitory neurons in the dorsal horn can give rise to persistent itch through a mechanism of disinhibition—decreased inhibitory synaptic input in lamina I and II of the dorsal spinal cord (Figure 8F). Thus, our data suggest that itch behavior is the result of both a peripheral activation of primary afferent pruritoceptors and central modulatory circuits. When pruritic circuits in the dorsal horn are disinhibited, as is seen in *Bhlhb5* mutant mice, the activation of pruritoceptors causes persistent itch, resulting in pathological lesions.

Bhlhb5$^{-/-}$ mice show a dramatically elevated response in the late phase of the formalin test, a finding widely thought to be due, at least in part, to enhanced central sensitization (Tjølsen et al., 1992). This type of plasticity, which occurs for both itch and pain, heightens aversive sensation through long-term changes

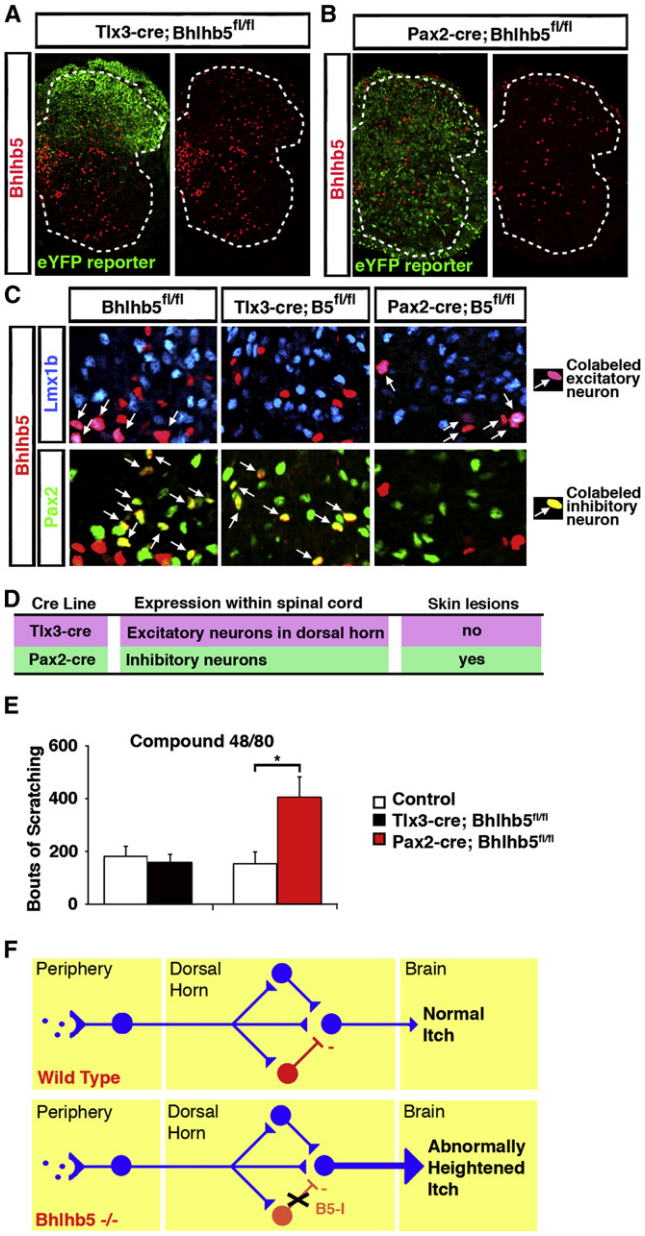

Figure 8. Abnormal Itch in *Bhlhb5* Mutant Mice May Be Due to Loss of *Bhlhb5* from Inhibitory Neurons of the Dorsal Horn

(A and B) Loss of *Bhlhb5* upon either *Tlx3-cre* (A) or *Pax2-cre* (B)-mediated excision in conditional *Bhlhb5* mutant mice ($Bhlhb5^{fl/fl}$). Lumbar hemisection from P0 mouse stained with antibodies that recognize Bhlhb5 (red) or eYFP (green) is shown.

(C) Specificity of the *Tlx3-cre* and *Pax2-cre* alleles. Representative region of dorsal spinal cord from P0 mice of the indicated genotypes that are stained with antibodies that recognize Bhlhb5 (red), Lmx1b (blue), or Pax2 (green) is shown. In control animals, Bhlhb5 colocalizes with both Lmx1b and Pax2, as indicated by the arrows. Upon Tlx3-cre-mediated excision within excitatory neurons, Bhlhb5 remains colocalized with the excitatory marker Pax2, but not the inhibitory marker Lmx1b. Conversely, upon Pax2-cre-mediated excision within inhibitory neurons, Bhlhb5 remains colocalized with the excitatory marker Lmx1b, but not the inhibitory marker Pax2.

(D) Table describing the *Tlx3-cre* and *Pax2-cre* mouse lines, together with the expression pattern of cre within the spinal cord for each line, and whether the subsequent animals develop skin lesions following cre-mediated recombination of *Bhlhb5*. (Note that cre expression in these animals is not exclusive to the spinal cord; each line also causes some recombination in other regions of the nervous system including parts of the hindbrain.)

(E) Conditional loss of *Bhlhb5* in the *Pax2-cre* domain, but not the *Tlx3-cre* domain, results in significantly elevated scratching responses following the intradermal injection of compound 48/80 into the nape of the neck relative to littermate controls lacking cre alleles. Data are presented as mean ± SEM, and (*) indicates significant difference relative to controls ($p < 0.05$, t test).

(F) Model: disinhibition gives rise to abnormally heightened itch in $Bhlhb5^{-/-}$ mice. In wild-type mice, pruritic agents at the skin's surface activate a subset of itch-mediating DRG neurons that project from the periphery to the dorsal horn of the spinal cord. This pruritic information is modulated by excitatory (blue) and inhibitory (red) neurons in the dorsal horn before being relayed to the brain and being experienced as the sensation of normal itch. In *Bhlhb5* mutant mice, there is a loss of inhibitory neurons in the dorsal horn. Thus, reduced inhibitory synaptic input in the dorsal horn (disinhibition) results in a greater itch signal that is conveyed to the brain, resulting in abnormally heightened itch that may ultimately give rise to pathological skin lesions.

in circuit properties (Ikoma et al., 2004; Latremoliere and Woolf, 2009; Woolf, 1983). We speculate that the abnormal itch observed in *Bhlhb5* mutant mice may be due to an enhanced central sensitization in response to activation of itch circuits that arises from a loss of inhibitory input in lamina I and II of the dorsal spinal cord. Thus, it is possible that normal everyday scratching might, in mutant mice with this form of aberrant central sensitization, lead to the development of a pathological itch-scratch-itch cycle. If so, this may explain why $Bhlhb5^{-/-}$ mice develop lesions in discrete areas, despite the fact that these mice have a loss of Bhlhb5-expressing neurons throughout the entire rostro-caudal axis of the dorsal horn.

The finding that local anesthetic applied to the site of lesion attenuates the scratching behavior in *Bhlhb5* mutant mice (Figure 4D) strongly suggests that activity in primary sensory neurons is involved in the itch response. However, the itch phenotype in *Bhlhb5* mutant mice is clearly not caused by this peripheral activity alone, since HtPa-cre-mediated loss of *Bhlhb5* in DRG neurons does not result in skin lesions (Figure 5B). Rather, our studies suggest that the heightened itch in *Bhlhb5* mutant mice is due to the loss of Bhlhb5 in inhibitory neurons of the dorsal spinal cord (Figure 8). Thus, we propose that peripheral neurons initiate an itch signal that is abnormally amplified in the dorsal horn of the spinal cord, resulting in scratching responses that culminate in the development of pathological skin lesions (Figure 8F). In addition, it is possible that changes in the spinal cord of *Bhlhb5* mutant mice may have an indirect effect on the activity of primary sensory neurons. This idea has precedent in models of neuropathic pain, where it has recently been observed that primary nociceptors become hyperactive as a consequence of spinal cord injury (Carlton et al., 2009).

The behavioral assays for this study were performed primarily with 4-week-old mice, an age where the circuits of the spinal cord are thought to be mature (Fitzgerald, 2005). At this age, wild-type and *Bhlhb5* mutant mice show no significant differences in their responses to a number of pain assays (Figure 3), but *Bhlhb5* mutant mice show heightened responses to pruritogens and formalin (Figure 4), consistent with the idea that there is

a selective disruption of sensory circuits in the dorsal horn of *Bhlhb5* mutant mice. In contrast, a few weeks later—subsequent to the development of skin lesions—*Bhlhb5* mutant mice show somewhat higher pain thresholds than wild-type controls (Figures S3E–S3G). One possibility is that the increased pain threshold in older mice is a secondary consequence of the skin lesions. Though the scratching behavior is likely due to itch, the ensuing tissue damage might also cause pain, and either of these sensations could be a confounding factor in behavioral assays for nociception. It remains possible, however, that *Bhlhb5* mutant mice develop reduced sensitivity to pain with a latent onset. Future studies will be required to clarify this issue.

Several recent studies have revealed that one of the central mechanisms underlying the development of pain hypersensitivity is reduced inhibitory synaptic input in the dorsal horn of the spinal cord. For instance, pharmacological blockade of either GABA or glycine receptors enhances the electrophysiological responses to the activation of primary nociceptors (Baba et al., 2003; Torsney and MacDermott, 2006). Moreover, a reduction of inhibitory synaptic transmission has been shown to play a role in pain sensitization through a variety of mechanisms, including a loss of GABAergic interneurons in the dorsal horn (Moore et al., 2002; Scholz et al., 2005) and the inhibition of glycine receptor function (Zeilhofer, 2005). However, while multiple studies have shown that pain is aggravated by reduced synaptic inhibition in the dorsal spinal cord, whether analogous mechanisms regulate pruritis was unknown. Our study clarifies this issue by uncovering a role for disinhibition in the regulation of itch.

The only itch-specific neurons in the spinal cord identified at a molecular level to date are those that express GRPR (Sun et al., 2009). Beyond these, other neurons within itch circuits of the dorsal horn remain completely unknown, underscoring a fundamental gap in current knowledge with regard to pruritic circuitry. Our study begins to bridge this gap by providing evidence that a distinct population of inhibitory interneurons within the dorsal horn functions to inhibit itch, and that loss of these neurons results in persistent itch that gives rise to pathological lesions. Thus, Bhlhb5 inhibitory neurons may represent the first inhibitory component of puritic circuits to be identified genetically. In addition, the *Bhlhb5-cre* mouse provides a genetic marker with which to identify this population of cells. Using this molecular handle, it should be possible to define the molecular, electrophysiological, and morphological characteristics of these neurons and characterize exactly how, where, and when they regulate itch. We speculate that chronic severe itch in some patients may result from a similar kind of disinihibiton to that described here, rather than from the increased activation of pruritoceptors as is commonly assumed. If so, the inhibitory neurons identified in this study may ultimately provide a cellular target for the development of therapies for chronic itch.

EXPERIMENTAL PROCEDURES

See Supplemental Experimental Procedures for details on the generation of Bhlhb5-directed antibodies, animal husbandry, colony management, immunohistochemistry, Xgal staining, and the generation of *Bhlhb5* null, *Bhlhb5* conditional knockout, and *Bhlhb5-cre* knockin mice.

Behavioral Assays

Where appropriate, mice were habituated for 20 min/day over several days. For observational studies, habituated mice were placed individually in a clear cage and videotaped for 20 min and scored for their behavior. To assess mechanical sensitivity, calibrated von Frey fibers were applied to the plantar surface of the hindpaws of mice. The smallest monofilament that evoked paw-withdrawal responses on five out of ten trials was taken as the mechanical threshold. To determine thermal pain threshold, mice were placed on a 55°C hot plate and the response latency to paw licking or jumping was recorded. For tests of acute nociception, capsaicin (2.5 μg) or mustard oil (0.75%) was injected subcutaneously into the plantar surface of the hindpaw in a 20 μl volume. For the formalin tests, the mice received 25 μl intraplantar injection of 5% formalin, and the lickings of the injected paw were recorded in 5 min intervals for 1 hr for the subsequent hour. To test for mechanical hypersensitivity, the paw withdrawal threshold was determined 2 hr after the intraplantar injection of 2% carrageenan into the hindpaw in a 20 μl volume. To test for pruritic responses, each of the pruritic compounds were injected intradermally into the nape of the neck in a 50 μl volume, and the bouts of scratching that occurred over the subsequent hour were quantified. The pruritic compounds used were histamine (1 μmol), αMe5HT (30 μg), SLIGRL-NH2 (100 nmol), compound 48/80 (100 μg) formalin (5%), and chloroquine (200 μg). To investigate the involvement of sensory feedback, *Bhlhb5*$^{-/-}$ mice that had pre-existing skin lesions in the perineum (or wild-type littermates) were injected with 200 μl of 0.3% lidocaine (or PBS, as a control) subcutaneously into the perineum. Ten minutes later, the scratching and licking behavior directed toward the perineum was assessed every 10 s for a total of 10 min.

Quantification of Neurons

For neuronal quantification experiments, three to five pairs of P0 littermates were analyzed. Ten matched lumbar sections per animal were used for quantification, spanning 2000 μm. Cell counts in various regions of the spinal cord were conducted using the cell count function of Metamorph (Molecular Devices). Metamorph cell scoring parameters were validated by manual counts and were kept constant across all conditions. To quantify apoptotic neurons, mice were analyzed in a similar fashion, and cleaved caspase-3-positive cells in the dorsal horn were counted manually. All counts were conducted blind to genotype.

SUPPLEMENTAL INFORMATION

Supplemental Information for this article includes eight figures, one table, and Supplemental Experimental Procedures and can be found with this article online at doi:10.1016/j.neuron.2010.02.025.

ACKNOWLEDGMENTS

We thank E.C. Griffith for critical readings of the manuscript; D. Harmin for help with statistical analysis; M. Gee and P. Zhang for assistance with mouse colony management; the MRDDRC Gene Manipulation Core (M. Thompson, Y. Zhou, and H. Ye); the MRDDRC Imaging Core (L. Bu); and the MRDDRC Histology Core (M. Liana). This work was supported by a Jane Coffin Childs Fellowship and a Dystonia Medical Research Foundation Fellowship to S.E.R., NIH grant R01-NS-028829 to M.E.G., and the Developmental Disabilities Mental Retardation Research Center grant NIH-P30-HD-18655 for core support.

Accepted: February 19, 2010
Published: March 24, 2010

REFERENCES

Andrew, D., and Craig, A.D. (2001). Spinothalamic lamina I neurons selectively sensitive to histamine: a central neural pathway for itch. Nat. Neurosci. *4*, 72–77.

Baba, H., Ji, R.R., Kohno, T., Moore, K.A., Ataka, T., Wakai, A., Okamoto, M., and Woolf, C.J. (2003). Removal of GABAergic inhibition facilitates polysynaptic A fiber-mediated excitatory transmission to the superficial spinal dorsal horn. Mol. Cell. Neurosci. *24*, 818–830.

Carlton, S.M., Du, J., Tan, H.Y., Nesic, O., Hargett, G.L., Bopp, A.C., Yamani, A., Lin, Q., Willis, W.D., and Hulsebosch, C.E. (2009). Peripheral and central sensitization in remote spinal cord regions contribute to central neuropathic pain after spinal cord injury. Pain *147*, 265–276.

Cheng, L., Samad, O.A., Xu, Y., Mizuguchi, R., Luo, P., Shirasawa, S., Goulding, M., and Ma, Q. (2005). Lbx1 and Tlx3 are opposing switches in determining GABAergic versus glutamatergic transmitter phenotypes. Nat. Neurosci. *8*, 1510–1515.

Cryns, V., and Yuan, J. (1998). Proteases to die for. Genes Dev. *12*, 1551–1570.

Davidson, S., Zhang, X., Yoon, C.H., Khasabov, S.G., Simone, D.A., and Giesler, G.J., Jr. (2007). The itch-producing agents histamine and cowhage activate separate populations of primate spinothalamic tract neurons. J. Neurosci. *27*, 10007–10014.

Dubuisson, D., and Dennis, S.G. (1977). The formalin test: a quantitative study of the analgesic effects of morphine, meperidine, and brain stem stimulation in rats and cats. Pain *4*, 161–174.

Feng, L., Xie, X., Joshi, P.S., Yang, Z., Shibasaki, K., Chow, R.L., and Gan, L. (2006). Requirement for Bhlhb5 in the specification of amacrine and cone bipolar subtypes in mouse retina. Development *133*, 4815–4825.

Fitzgerald, M. (2005). The development of nociceptive circuits. Nat. Rev. Neurosci. *6*, 507–520.

Gorski, J.A., Balogh, S.A., Wehner, J.M., and Jones, K.R. (2003). Learning deficits in forebrain-restricted brain-derived neurotrophic factor mutant mice. Neuroscience *121*, 341–354.

Holstege, J.C., de Graaff, W., Hossaini, M., Cano, S.C., Jaarsma, D., van den Akker, E., and Deschamps, J. (2008). Loss of Hoxb8 alters spinal dorsal laminae and sensory responses in mice. Proc. Natl. Acad. Sci. U S A *105*, 6338–6343.

Ikoma, A., Fartasch, M., Heyer, G., Miyachi, Y., Handwerker, H., and Schmelz, M. (2004). Painful stimuli evoke itch in patients with chronic pruritus: central sensitization for itch. Neurology *62*, 212–217.

Ikoma, A., Steinhoff, M., Ständer, S., Yosipovitch, G., and Schmelz, M. (2006). The neurobiology of itch. Nat. Rev. Neurosci. *7*, 535–547.

Imamachi, N., Park, G.H., Lee, H., Anderson, D.J., Simon, M.I., Basbaum, A.I., and Han, S.K. (2009). TRPV1-expressing primary afferents generate behavioral responses to pruritogens via multiple mechanisms. Proc. Natl. Acad. Sci. USA *106*, 11330–11335.

Joshi, P.S., Molyneaux, B.J., Feng, L., Xie, X., Macklis, J.D., and Gan, L. (2008). Bhlhb5 regulates the postmitotic acquisition of area identities in layers II-V of the developing neocortex. Neuron *60*, 258–272.

Kuraishi, Y., Nagasawa, T., Hayashi, K., and Satoh, M. (1995). Scratching behavior induced by pruritogenic but not algesiogenic agents in mice. Eur. J. Pharmacol. *275*, 229–233.

Latremoliere, A., and Woolf, C.J. (2009). Central sensitization: a generator of pain hypersensitivity by central neural plasticity. J. Pain *10*, 895–926.

Liu, B., Liu, Z., Chen, T., Li, H., Qiang, B., Yuan, J., Peng, X., and Qiu, M. (2007). Selective expression of Bhlhb5 in subsets of early-born interneurons and late-born association neurons in the spinal cord. Dev. Dyn. *236*, 829–835.

Liu, Q., Tang, Z., Surdenikova, L., Kim, S., Patel, K.N., Kim, A., Ru, F., Guan, Y., Weng, H.J., Geng, Y., et al. (2009). Sensory neuron-specific GPCR Mrgprs are itch receptors mediating chloroquine-induced pruritus. Cell *139*, 1353–1365.

McMahon, S.B., and Koltzenburg, M. (1992). Itching for an explanation. Trends Neurosci. *15*, 497–501.

McNamara, C.R., Mandel-Brehm, J., Bautista, D.M., Siemens, J., Deranian, K.L., Zhao, M., Hayward, N.J., Chong, J.A., Julius, D., Moran, M.M., and Fanger, C.M. (2007). TRPA1 mediates formalin-induced pain. Proc. Natl. Acad. Sci. USA *104*, 13525–13530.

Mizuguchi, R., Kriks, S., Cordes, R., Gossler, A., Ma, Q., and Goulding, M. (2006). Ascl1 and Gsh1/2 control inhibitory and excitatory cell fate in spinal sensory interneurons. Nat. Neurosci. *9*, 770–778.

Moore, K.A., Kohno, T., Karchewski, L.A., Scholz, J., Baba, H., and Woolf, C.J. (2002). Partial peripheral nerve injury promotes a selective loss of GABAergic inhibition in the superficial dorsal horn of the spinal cord. J. Neurosci. *22*, 6724–6731.

Ohyama, T., and Groves, A.K. (2004). Generation of Pax2-Cre mice by modification of a Pax2 bacterial artificial chromosome. Genesis *38*, 195–199.

Pietri, T., Eder, O., Blanche, M., Thiery, J.P., and Dufour, S. (2003). The human tissue plasminogen activator-Cre mouse: a new tool for targeting specifically neural crest cells and their derivatives in vivo. Dev. Biol. *259*, 176–187.

Puig, S., and Sorkin, L.S. (1996). Formalin-evoked activity in identified primary afferent fibers: systemic lidocaine suppresses phase-2 activity. Pain *64*, 345–355.

Reddy, V.B., Iuga, A.O., Shimada, S.G., LaMotte, R.H., and Lerner, E.A. (2008). Cowhage-evoked itch is mediated by a novel cysteine protease: a ligand of protease-activated receptors. J. Neurosci. *28*, 4331–4335.

Rico, B., Xu, B., and Reichardt, L.F. (2002). TrkB receptor signaling is required for establishment of GABAergic synapses in the cerebellum. Nat. Neurosci. *5*, 225–233.

Ross, S.E., Greenberg, M.E., and Stiles, C.D. (2003). Basic helix-loop-helix factors in cortical development. Neuron *39*, 13–25.

Schmelz, M. (2008). Itch and pain. Neurosci. Biobehav Rev. *34*, 171–176.

Schmelz, M., Schmidt, R., Bickel, A., Handwerker, H.O., and Torebjörk, H.E. (1997). Specific C-receptors for itch in human skin. J. Neurosci. *17*, 8003–8008.

Scholz, J., Broom, D.C., Youn, D.H., Mills, C.D., Kohno, T., Suter, M.R., Moore, K.A., Decosterd, I., Coggeshall, R.E., and Woolf, C.J. (2005). Blocking caspase activity prevents transsynaptic neuronal apoptosis and the loss of inhibition in lamina II of the dorsal horn after peripheral nerve injury. J. Neurosci. *25*, 7317–7323.

Shimada, S.G., and LaMotte, R.H. (2008). Behavioral differentiation between itch and pain in mouse. Pain *139*, 681–687.

Simone, D.A., Zhang, X., Li, J., Zhang, J.M., Honda, C.N., LaMotte, R.H., and Giesler, G.J., Jr. (2004). Comparison of responses of primate spinothalamic tract neurons to pruritic and algogenic stimuli. J. Neurophysiol. *91*, 213–222.

Soriano, P. (1999). Generalized lacZ expression with the ROSA26 Cre reporter strain. Nat. Genet. *21*, 70–71.

Sowunmi, A., Walker, O., and Salako, L.A. (1989). Pruritus and antimalarial drugs in Africans. Lancet *2*, 213.

Sun, Y.G., and Chen, Z.F. (2007). A gastrin-releasing peptide receptor mediates the itch sensation in the spinal cord. Nature *448*, 700–703.

Sun, Y.G., Zhao, Z.Q., Meng, X.L., Yin, J., Liu, X.Y., and Chen, Z.F. (2009). Cellular basis of itch sensation. Science *325*, 1531–1534.

Tjølsen, A., Berge, O.G., Hunskaar, S., Rosland, J.H., and Hole, K. (1992). The formalin test: an evaluation of the method. Pain *51*, 5–17.

Torsney, C., and MacDermott, A.B. (2006). Disinhibition opens the gate to pathological pain signaling in superficial neurokinin 1 receptor-expressing neurons in rat spinal cord. J. Neurosci. *26*, 1833–1843.

Tronche, F., Kellendonk, C., Kretz, O., Gass, P., Anlag, K., Orban, P.C., Bock, R., Klein, R., and Schütz, G. (1999). Disruption of the glucocorticoid receptor gene in the nervous system results in reduced anxiety. Nat. Genet. *23*, 99–103.

Umeuchi, H., Togashi, Y., Honda, T., Nakao, K., Okano, K., Tanaka, T., and Nagase, H. (2003). Involvement of central mu-opioid system in the scratching behavior in mice, and the suppression of it by the activation of kappa-opioid system. Eur. J. Pharmacol. *477*, 29–35.

Wildner, H., Müller, T., Cho, S.H., Bröhl, D., Cepko, C.L., Guillemot, F., and Birchmeier, C. (2006). dILA neurons in the dorsal spinal cord are the product

of terminal and non-terminal asymmetric progenitor cell divisions, and require Mash1 for their development. Development *133*, 2105–2113.

Woolf, C.J. (1983). Evidence for a central component of post-injury pain hypersensitivity. Nature *306*, 686–688.

Xu, Y., Lopes, C., Qian, Y., Liu, Y., Cheng, L., Goulding, M., Turner, E.E., Lima, D., and Ma, Q. (2008). Tlx1 and Tlx3 coordinate specification of dorsal horn pain-modulatory peptidergic neurons. J. Neurosci. *28*, 4037–4046.

Yamaguchi, T., Nagasawa, T., Satoh, M., and Kuraishi, Y. (1999). Itch-associated response induced by intradermal serotonin through 5-HT2 receptors in mice. Neurosci. Res. *35*, 77–83.

Yosipovitch, G., Carstens, E., and McGlone, F. (2007). Chronic itch and chronic pain: Analogous mechanisms. Pain *131*, 4–7.

Zeilhofer, H.U. (2005). The glycinergic control of spinal pain processing. Cell. Mol. Life Sci. *62*, 2027–2035.

Appendix 2: Protocol for Generating Sphere Models in Imaris and Using AT Analyzer

Array Tomography Analysis Protocol:

In Imaris:
1. Reset scaling of X, Y, and Z dimensions. For each volume, record the length of each dimension in microns.
2. Threshold the DAPI channel. Record the threshold. Using the colocalization module, record the number of voxels above threshold for DAPI (colocalize DAPI with itself).
3. For each synaptic marker channel, model the puncta as best as possible using spots generated from local intensity centers. Export spot statistics in XLS files.

Be sure that your presynaptic marker is channel 1, post is channel 2, and DAPI is channel 3.

After exporting spots or surface object data in xls format from Imaris, move back to home computer:

1. Open XLS file in excel
2. Run macro 'spots_AT' (Tools -> Macro -> Macros) or the 'ellipsoid_AT' macro, depending upon which analysis you are going to do. Doing both is fine! These macros simply copy and paste excel data into the correct columns so that matlab knows which information is in which column.
3. Save the result as a .csv file; be sure to specify if it was spots or ellipsoids. Accept all the warnings; when you close the csv file, you will be prompted to save as; don't – it is already saved.

Note: time has passed, and Microsoft excel support for macros has become increasingly terrible, and in some cases impossible. If macros are unavailable, you will have to manually copy and paste the relevant columns into a single sheet in excel. The proper data to place in each column is available at the top of the matlab file 'AT_Analyzer.M'

****VERY IMPORTANT!*****
If GFP is the fourth channel in the sample (ie, you're analyzing a GFP labeled cell)
OR
If your pre marker is not channel 1, post is not channel 2, or DAPI is not channel 3, you will have to manually cut and paste the data from the following columns to the .csv file:

DAPI MAX intensity: column 7
Pre mean intensity: column 8
Post mean intensity: column 9

GFP mean intensity: column 10

Open Matlab

1. Click File -> import data, navigate and find the first csv file; double click on it
2. A dialogue box will appear; hit 'next.' This will lead you to another box; hit 'finish'
3. On the variable list to the right, you will now have a variable called 'data.' Right click on this and rename it either 'predata' or 'postdata' depending on which file you imported.
****IMPORTANT****: if you call this file anything OTHER than 'predata' or 'postdata' the analysis will not work.
4. Repeat this process for the other file; this time there will be an additional warning after you hit finish; simply hit 'ok' and proceed.

5. Under the 'programs' folder, open the program called 'AT_Analyzer.M'
This will open up the matlab editor. Go to the very top, where you will find the data you have to input into the program.

6. Input the following data that you recorded during your imaris analysis session:

ff – this is the distance threshold; for excitatory synapses it seems to work well around .1 to .2, for inhibitory it seems to work better around 0. No matter what you put here, you well get the threshold independent data, however you can only generate more detailed reports about a specified threshold

samplename: (use some sort of systematic notation, since this is the unique identifier of this data)

this length of each dimension in microns:
xmax
ymax
zmax

dapi min (dapi threshold)
dapi vox (number of dapi + voxels)

premin (presynaptic channel threshold)
postmin (postsynaptic channel threshold) - these parameters allow you to delete puncta with an average intensity below a certain value, to compensate for high background. If you choose not to use them, set them to default 0. This will ensure all data is counted.

Leave dataoutput and cycleoutput equal to 1; only put it 0 only if you don't want data output; eg, if you're running a test.

GFP = 1/0 (yes/no).
If GFP = 1,
GFPmin = gfp channel threshold,
gfp vox, number of GFP+ voxels.

Now you are ready to run your program!

*******VERY IMPORTANT*********
Before you run your program, make sure that the directory on the left of the matlab window is the directory where you want your data stored! It is a common mistake to have matlab deposit your data into the program folder

To run your program, select 'run spacefill_syncounter.m'

When the program is completed, several things will happen.

Two figures will appear. You may save them or discard them. They pop up so you can observe quality of the data real time.

The command window on matlab will output the following variables:
syndensity
predensity
postdensity
lone predensity
lone postdensity
predistribution
postdistribution
chancedensity

These variables are exported elsewhere, so don't worry about writing them down. They're output here so you can glance at the data and make sure that nothing is totally wacky.

Now, check your directory. There should be several new files:

Samplename_data.csv = this file contains basic info about the volume at the given distance threshold
Samplename_syndata.csv = this file contains detailed data about the individual synapses in the volume at the specified distance threshold
Samplename_cycle.csv = this file contains synapse densities as a function of varying the distance threshold
Samplename_cyclechance.csv = contains chance data dependent on cycling FF

Samplename_lonepost.csv and samplename_lonepre.csv, self-explanatory by now

Make sure to clear the matlab command space before loading more data.

*****VERY IMPORTANT******
You've been running your volumes at a certain distance threshold value because I told you what seems to work best. But no matter how reproducible this is, you've got to empirically convince yourself that the given distance threshold is actually modeling your data accurately. You can do this partially by looking at its threshold dependency, but the only real way is to look at the synapses the program is outputting. To do this….

1. BEFORE you type clear into the command window, find the csv file that has been generated in your analysis folder called 'samplename_syndata.csv.' Double click on it, and the same import diaglue will appear. Hit next and then finish, and find it as a variable in the workspace. Right click, and rename it 'testsyndata'
2. Create a new folder for the output of the image stack called 'tifs'. Open the program called 'image compiler.' Copy and paste the program into the command line, and hit enter. When you ran the original program, each synapse was logged with an X, Y and Z coordinate defined as the midpoint between the pre and post puncta center point. This program generates a cross at each point
3. You should find a series of tiffs in the folder you specified, numbered 1 to zmax. Open imageJ, go to file -> import -> image sequence…, select the first image, and click ok.
4. Save the image stack as a tif, and wait until you get back on imaris
5. Open the imaris scene, and go to edit -> add channels. Load the stack. Change the color to something like yellow (red is default) and enjoy viewing the synapses that the program called in the context of the original data. Do this for a few different FFs, and you'll get a sense of where you should be analyzing the data.

Appendix 3: AT Analyzer Code and Comments

Below is the matlab code for the AT Analyzer script. It is reproduced here in the thesis so that it is clear exactly how data was handled during my array tomography experiments. I apologize in advance for the messy code; before embarking on this project I had never written a single line of code.

```
%INPUTS!!!!!
%LOAD PREDATA, POSTDATA;
%For each variable the columns need to be:   1 = puncta diameter, 2 = x
location, 3, = y location, 4 = z location 5 = sphere ID, 6 = voxel
count,
%7 = intensity max DAPI, 8 = PRE mean intesnity, 9 = POST mean
intensity, 10 = GFP or morphology intensity,

ff = .1; %distance threshold, in microns. set it to 0 for touching
spheres, negative value for overlapping spheres.

samplename = '051911_CR3_Bm2-vglut';
xmax= 50.8;
ymax= 58.8;
zmax= 2.2;

dapimin = 4.45;
dapivox = 495301;


GFP = 0;  %if GFP is in the sample, and you would only like to consider
POST GFP synapses, change to 1
GFPvox = 0;  %number of voxels positive for GFP
GFPmin = 0;  %Min GFP value to allow for GFP localized puncta

cycleoutput = 1; %if you wish to output synapse density as a function
of distance threshold
dataoutput = 1;  %if you want it to write the output, set this to 1 -
only turn to 0 for debug
shuffle = 0; %set to 1 if you want to include a control run where Z
planes are randomly shuffled.  I've found it superflous, but it's there
if you want it.


%%%%%%%%%%%%%%%%%%%%%%%%%%%%%%%%%%%%%%%%%%%%%%%%%%%%%%%%%%%%%%%%%%%%%%%
%Begin program

maxradius = .1;  %2x max radius is an upper bound on the distance of
puncta we'll even consider searching for
avgradius = .1;

%corrects volume for dapi staining and edge artifact

zmax1 = zmax - .2; %Corrects volume for Z edge artiface
volume = (xmax * ymax * zmax1); %volume in um^3
voxvolume = volume / .0010465; %volume in voxel number
dvoxvolume = voxvolume - (dapivox * 1.8971); %1.89 is empirically
```

```
determined constant to account for non-dapi stained nuclear components.
Adjusts volume for DAPI, so we're comparing neuropil to neuropil.
dumvolume = dvoxvolume / 955.566173; %(.1023*.1023*.1)^-1 = 955 vox/um3
- this constant is only apporpriate for 63x objective and 100 nm Z
sectioning of ribbons


if GFP == 1;
dumvolume = .0010465 * GFPvox;  %um^3 - if we're analyzing a GFP
labelled cell, the size of the volume is irrelevant, only the size of
the GFP staining matters
end;


%%%%%%%%%%%%%%%%%%%%%%%%%%%%%%%%%%%%%%%%%%%%%%%%%%%%
%Removes non-GFP associated postsynaptic puncta

if GFP == 1;

    thresh = GFPmin;
    numPOSTpuncta = numel(postdata(:,5));  %number of post synaptic
puncta
i = 1;
    for x = 1:numPOSTpuncta;  %for all post puncta
        if postdata(x,10) <= thresh;  %if the mean GFP intensity of the
voxelsin that puncta are below the GFP threshold
           postnonGFP(i,1) = postdata(x,5); %add the ID to the deletion
list
           i = i + 1;
        end;

    end;


   [d, inonGFP, idata] = intersect(postnonGFP,postdata(:,5)); %find the
intersection of the IDs and the IDs marked for deletion
   postdata(idata,:) = []; %deletes the interesect of puncta below
threshold;

end;



%%%%%%%%%%%%%%%%%%%%%%%%%%%%%%%%%%%%%%%%%%%%%%%%%%%%

%Removes puncta that overlap with DAPI staining


numPOSTpuncta = numel(postdata(:,5));
numPREpuncta = numel(predata(:,5));
postDAPI = [];
x = 1;
for x = 1:numPOSTpuncta;
        if postdata(x,7) > dapimin;
           postDAPI(x,1) = postdata(x,5);
```

```
        end;
    x = x + 1;
end;


if isempty(postDAPI) == 0;
 [d, ipostDAPI, idata] = intersect(postDAPI,postdata(:,5));
 postdata(idata,:) = []; %deletes the interesect of puncta below
threshold;
end;

numPOSTpuncta = numel(postdata(:,5));

preDAPI = [];
x = 1;
for x = 1:numPREpuncta;
   if predata(x,7) > dapimin;
       preDAPI(x,1) = predata(x,5);
   end;
   x = x + 1;
end;

if isempty(preDAPI) == 0;
 [d, ipreDAPI, idata] = intersect(preDAPI,postdata(:,5));
 predata(idata,:) = []; %deletes the interesect of puncta below
threshold;
end;

numPREpuncta = numel(predata(:,5));


%%%%%%%%%%%%%%%%%%%%%%%%%%%%%%%%%%%%%%%%%%%%%%%%%%%%%%%%%%%%%%%%
%Removes puncta less than V voxels - maybe some are so small that
they're
%noise?  you decide!

v = 1; %this is the largest voxel # you wish to remove

presmall = [];
 for x = 1:numPREpuncta;
        if predata(x,6) <= v;
           presmall(x,1) = predata(x,5);
        end;
       x = x + 1;
 end;

if isempty(presmall) == 0;
 [d, ipresmall, idata] = intersect(presmall,predata(:,5));
 predata(idata,:) = []; %deletes the interesect of puncta below
threshold;
end;

numPREpuncta = numel(predata(:,5));

postsmall = [];
 for x = 1:numPOSTpuncta;
```

```
        if postdata(x,6) <= v;
           postsmall(x,1) = postdata(x,5);
        end;
       x = x + 1;
 end;

if isempty(postsmall) == 0;
 [d, ipostsmall, idata] = intersect(postsmall,postdata(:,5));
 postdata(idata,:) = []; %deletes the interesect of puncta below
threshold;
end;

numPOSTpuncta = numel(postdata(:,5));



clear v;
clear x;

%%%%%%%%%%%%%%%%%%%%%%%%%%%%%%%%%%%%%%%%%%%%%%%%%%%%%%%%%%%%%%%%
%deletes postsynaptic puncta that are avgradius/2 away from Z edges

    numPOSTpuncta = numel(postdata(:,5));
    farZpost = [];
    for x = 1:numPOSTpuncta;
        if postdata(x,4) < (.1) | postdata(x,4) > (zmax - (.1));
            farZpost(x,1) = postdata(x,5);
        end;
    end;

   if isempty(farZpost) == 0;
   [d, ifarzpost, idata] = intersect(farZpost,postdata(:,5));
   postdata(idata,:) = []; %deletes puncta that have been logged in far
Z;
   end;

  numPOSTpuncta = numel(postdata(:,5));


%%%%%%%%%%%%%%%%%%%%%%%%%%%%%%%%%%%%%%%%%%%%%%%%%%%%%%%%%%%%%%%%%%%%%%%%%%%%%%%%
%%%%%%%%%%%%%%%%%%
%count synapses, records stats about them
postdatacopy = postdata;%copy the data
predatacopy = predata;%copy the data

postdata = sortrows(postdata,2);  %sorts data by X location for speed
predata = sortrows(predata,2);


b = 0;    %number of breaks
y = 1;    %presynpatic index
syncount = 0;  %Number of synapses - starts at 0
startID = 1;     %ID that the matching search begins on

for y = 1:numPREpuncta;  %for all presynaptic puncta
```

```
    dx = predata(y,2);  %reads out the X, Y, Z variable
    dy = predata(y,3);
    dz = predata(y,4);

    recentxID = startID; %what is the ID of the post puncta most
recently searched
    minID = startID - 1;

    for recentxID = startID:numPOSTpuncta; % for every POST puncta from
the last one we searched to the end....

        dx2 = postdata(recentxID,2);  %reads out Post X,Y,Z location
        dy2 = postdata(recentxID,3);
        dz2 = postdata(recentxID,4);

        recentxID = recentxID + 1;   %increases ID count

        if dx2 > (dx + maxradius + .1);   %if puncta is too far away on
the X axis to ever be a synapse...
        b = b + 1;  %count a break.  since we're sorting by distance,
if it's too far on this axis, the rest in this direct will be too far
as well.
        break;  %break

        end;

        if recentxID > numPOSTpuncta + 1;  %if we've reached the end...
        break;  %break
        end;


            umDIS =  sqrt(((dx-dx2)^2)+((dy-dy2)^2)+((dz-dz2)^2));
%calculate the distance between the puncta centers

            if ((predata(y,1)/2) + (postdata((recentxID-1),1)/2) + ff)
>= umDIS;   %If the sum of the radii + the distance threshold are equal
to or greater than distance
                syncount = syncount + 1;  %counts a synapse
                xmidx(syncount) = (dx+dx2)/2;  %records synapse X,y,z
location
                xmidy(syncount) = (dy+dy2)/2;
                xmidz(syncount) = (dz+dz2)/2;
                xpreID(syncount) = predata(y,5);  %records PRE puncta
ID
                xpostID(syncount) = postdata((recentxID-1),5); %records
POST puncta ID
                xdist(syncount) = umDIS;  %records the distance
            end;

     end;    %logs a synapse for beginning going up until its too far
away



     if minID > 0
```

```
     for minID = (startID-1):-1:1;  %starting at 1-startID, going all
the way up to 1.  all code is the same, we're just searching the other
direction up the post puncta until we hit one that is too far away

         dx2 = postdata(minID,2);
         dy2 = postdata(minID,3);
         dz2 = postdata(minID,4);


        minID = minID - 1;

        if dx2 < (dx - maxradius - .1);
         b = b + 1;
        break;
        end;

        umDIS =  sqrt(((dx-dx2)^2)+((dy-dy2)^2)+((dz-dz2)^2));

        if ((predata(y,1)/2) + (postdata((minID+1),1)/2) + ff) >=
umDIS;
                syncount = syncount + 1;  %counts a synapse if two
puncta are closer than threshold
                xmidx(syncount) = (dx+dx2)/2;
                xmidy(syncount) = (dy+dy2)/2;
                xmidz(syncount) = (dz+dz2)/2;
                xpreID(syncount) = predata(y,5);
                xpostID(syncount) = postdata((minID+1),5);
                xdist(syncount) = umDIS;
        end;


    end;
    end;
    y = y + 1;
    startID = round((recentxID + minID) / 2);
 end;

clear y;
clear umDIS;

if syncount > 0;
midz(:,1) = xmidz(1,:);  %readjustes each var from col vector to row
vector
midy(:,1) = xmidy(1,:);
midx(:,1) = xmidx(1,:);
preID(:,1) = xpreID(1,:);
postID(:,1) = xpostID(1,:);
dist(:,1) = xdist(1,:);
end;

%%%%%%%%%%%%%%%%%%%%%%%%%%%%%%%%%%%%%%%%%%%%%%%%%%%%%%%%%%%%%%%%

%finds the ID and Z position of all pre puncta located on extreme Z
plane
```

```
farZpreID = [];
fmin = avgradius/2;
fmax = zmax - avgradius/2;
n = 0;
for y = 1:numPREpuncta;
    if predata(y,4) > fmax | predata(y,4) < fmin;
        n = n + 1;
        farZpreID(n) = predata(y,5);
        farZpreZ(n) = predata(y,4);
    end;
end;


%how many pre/post syn puncta arent in a synapse?  Which puncta dont
appear in a synapse?

postalone1 = postdata(:,5);
[d, ipostID, ialone] = intersect(postID,postalone1);
postalone1(ialone) = [];  %postalone1 contains the ID of pre puncta not
in a synapse
numpostalone = numel(postalone1);

prealone1 = predata(:,5);  %prealone is vector of ID of presynaptic
puncta
[d, ipreID, ialone] = intersect(preID,prealone1);  %takes the intersect
of presynaptic puncta in a synapse and presynaptic IDs
prealone1(ialone) = [];  %sets the indeces of pre that take part in a
synapse to null.  now prealone1 contains only those Ids that dont take
part in a synapse
numprealone = numel(prealone1);

% what % of alone puncta can be accounted for by being located on far
Z?

if isempty(farZpreID) == 0;
p = intersect(prealone1, farZpreID);
fractpre = numel(p)/numel(prealone1);
else;
fractpre = 0;

end;

clear q;
clear p;

%generates fract of puncta in 50 random intervals equivilent to
avgrad/2

r = fmin + (fmax-fmin).*rand(50,1);
hi = r(:,1) + (avgradius/4);
lo = r(:,1) - (avgradius/4);  %creates 50 intervals of equivilant Z
thickness to the amount that is being called 'far z'%

for z = 1:50;
n = 0;
```

```
    for y = 1:numPREpuncta;
        if predata(y,4) < hi(z,1) & predata(y,4) > lo(z,1);
            n = n + 1;
            ID(n) = predata(y,5);  %adds one everytime a puncta occurs
within range
        end;
    end;
    p = intersect(prealone1, ID);  %list of unassociated puncat in that
interval
    fract(z) = numel(p)/numel(prealone1);  %fraction of the alone in
that given interval
end;
meanPrefract = mean(fract(:,1));  %mean fraction of Pre puncta in given
interval of avgradius


clear y;
clear n;
clear z;
clear p;
clear z;

prealone2 = numel(prealone1) - ((fractpre - meanPrefract) *
numel(farZpreID)); %number of lone pre puncta, substracting the avg
lone due to being on far Z


%%%%%%%%%%%%%%%%%%%%%%%%%%%%%%%%%%%%%%%%%%%%%%%%%%%%%%%%%%%%%%%%%%%
%finds presynaptic puncta that take part in multiple synapses

preID2 = preID;
maxpre = 0;

while isempty(preID2) == 0;
  maxpre = maxpre + 1;
  prenum(maxpre) = numel(unique(preID2));  %prenum(1) = the number of
puncta that occur at least once, etc
  [d, ipreID2, ic] = intersect(preID2,unique(predata(:,5)));
  preID2(ipreID2) = [];  %at this point preID2 is a list of things that
occur more than once
end;

%need to find a way to log D and put it thorugh cycle below to retain
IDs

x = numel(prenum);  %x = the max number of elements in prenum (that
last element should be 0)
prenumc = prenum;  %copy
for q = (x-1):-1:1;
    for z = x:-1:(q+1);
       prenumc(q) = (prenumc(q) - prenumc(z));  %prenumc(1) = the
number of puncta that occur twice, etc
    end;
end;

if sum(prenumc) ~= numel(unique(preID));
```

```
print 'shit! something funky happened with prenumc!';
end;

clear d;
clear ic;
clear ipreID2;
clear x;
clear q;
clear z;

%finds postsynaptic puncta that take part in multiple synapses
postID2 = postID;
maxpost = 0;
while isempty(postID2) == 0;
  maxpost = maxpost + 1;
  postnum(maxpost) = numel(unique(postID2));  %postnum(1) = all the ID
numbers of puncta occuring at least once
  [d, ipostID2, ic] = intersect(postID2,unique(postdata));
  postID2(ipostID2) = [];  %at this point postID2 is a list of things
that occur more than once
end;
x = numel(postnum);  %max number of elements in postnum
postnumc = postnum;
for q = (x-1):-1:1;
    for z = x:-1:(q+1);
       postnumc(q) = (postnumc(q) - postnumc(z));
    end;
end;   %postnumc(1) = number of puncta that occur twice, etc.  x-1 =
highest valence post puncta.

clear d;
clear ic;
clear ipreID2;
clear x;
clear q;
clear z;



%%%%%%%%%%%%%%%%%%%%%%%%%%%%%%%%%%%%%%%%%%%%%%%%%%%%
%Plots moving average of synapse density on X,Y,and Z axis  in 1 um
incriments
count = 0;
for x = 1:(xmax - 1);
    for x1 = 1:numel(midx);
        if midx(x1) <= (x + .5) & midx(x1) >= (x-.5);
            count = count + 1;
        end;
    localx(x) = (count / (ymax * zmax));
    end;
count = 0;
end;

count = 0;
for y = 1:(ymax-1);
    for y1 = 1:numel(midy);
    if midy(y1) <= (y + .5) & midy(y1) >= (y-.5);
```

```
            count = count + 1;
        end;
    localy(y) = (count / ((xmax * zmax)));
    end;
count = 0;
end;

cycle = 1;
count = 0;
for z = .1:.1:(zmax - .1);
    for z1 = 1:numel(midz);
        if midz(z1) <= (z + .1) & midz(z1) >= (z - .1);
            count = count + 1;
        end;
    localz(cycle,1) = (count / (.2 * xmax * ymax));
    localz(cycle,2) = z;
    end;
cycle = cycle + 1;
count = 0;
end;

%tallies the number of synapses in 1 um in either direction from point
on specified axis, to be plotted against that axis

%%%%%%%%%%%%%%%%%%%%%%%%%%%%%%%%%%%%%%%%%%%%%%%%%%%%

%calculates the synapse number and density expected if the same number
of
%pre/post puncta were randomly associated.  Essentially the same code
from
%above, with randomly assinged locations.



postdata = postdatacopy;
predata = predatacopy;

if GFP == 1;

    thresh = GFPmin; %necesasry mean GFP intensity for puncta to be
considered
    numPOSTpuncta = numel(postdata(:,5));

    for x = 1:numPOSTpuncta;
        if postdata(x,10) <= thresh;
           postnonGFP(x,1) = postdata(x,5);
        end;
    x = x + 1;
    end;


   [d, inonGFP, idata] = intersect(postnonGFP,postdata(:,5));
   postdata(idata,:) = []; %deletes the interesect of puncta below
threshold;

end;
```

```
    numPOSTpuncta = numel(postdata(:,5));

    predata(:,4) = zmax * rand(numPREpuncta,1);
    predata(:,3) = ymax * rand(numPREpuncta,1);
    predata(:,2) = xmax * rand(numPREpuncta,1);
    postdata(:,4) = zmax * rand(numPOSTpuncta,1);
    postdata(:,3) = ymax * rand(numPOSTpuncta,1);
    postdata(:,2) = xmax * rand(numPOSTpuncta,1);

    numPOSTpuncta = numel(postdata(:,5));
    farZpost = [];
    for x = 1:numPOSTpuncta;
        if postdata(x,4) < (avgradius/2) | postdata(x,4) > (zmax -
(avgradius/2));
            farZpost(x,1) = postdata(x,5);
        end;
    end;

   if isempty(farZpost) == 0;
   [d, ifarzpost, idata] = intersect(farZpost,postdata(:,5));
   postdata(idata,:) = []; %deletes puncta that have been logged in far
Z;
   end;
  numPOSTpuncta = numel(postdata(:,5));



postdata = sortrows(postdata,2);
predata = sortrows(predata,2);


b = 0;
y = 1;
chancesyncount = 0;
startID = 1;     %ID that post search begins on

for y = 1:numPREpuncta;
    dx = predata(y,2);
    dy = predata(y,3);
    dz = predata(y,4);

    recentxID = startID;
    minID = startID - 1;

    for recentxID = startID:numPOSTpuncta; % from start to last...

        dx2 = postdata(recentxID,2);
        dy2 = postdata(recentxID,3);
        dz2 = postdata(recentxID,4);

        recentxID = recentxID + 1;   %increases considered ID

        if dx2 > (dx + maxradius + .1);   %if the considered ID is too
far away, break, otherwise do normal deal
```

```
        b = b + 1;
        break;
        end;
        if recentxID > numPOSTpuncta + 1;
        break;
        end;


            umDIS =  sqrt(((dx-dx2)^2)+((dy-dy2)^2)+((dz-dz2)^2));

            if ((predata(y,1)/2) + (postdata((recentxID-1),1)/2) + ff)
>= umDIS;
                chancesyncount = chancesyncount + 1;  %counts a synapse
if two puncta are closer than threshold

            end;

     end;    %logs a synapse for beginning going up until its too far
away



     if minID > 0
     for minID = (startID-1):-1:1;  %starting at 1-startID...

         dx2 = postdata(minID,2);
         dy2 = postdata(minID,3);
         dz2 = postdata(minID,4);


        minID = minID - 1;

        if dx2 < (dx - maxradius - .1);
         b = b + 1;
        break;
        end;

        umDIS =  sqrt(((dx-dx2)^2)+((dy-dy2)^2)+((dz-dz2)^2));

        if ((predata(y,1)/2) + (postdata((minID+1),1)/2) + ff) >=
umDIS;
                chancesyncount = chancesyncount + 1;  %counts a synapse
if two puncta are closer than threshold
        end;


       end;

      end;
    y = y + 1;

    startID = round((recentxID + minID) / 2);
 end;
```

```
%%%%%%%%%%%%%%%%%%%%%%%%%%%%%%%%%%%%%%%%%%%%%%%%%%%%
%Shuffles puncta on Z axis for another control

if shuffle == 1;

n = 1;
for n = 1:20;

postdata1 = postdata;
predata1 = predata;


zslices = [0:.1:(zmax-.1)];
randzslices = randperm(numel(zslices));
randzslices1 = (randzslices - 1) / 10;
trans = zslices - randzslices1;  %zslices - trans = randzslices

%x = 1;
%for x = 1:numPOSTpuncta;
%    postdata1(x,4) = postdata1(x,4) - floor(postdata(x,4)) +
(floor(postdata1(x,4)) - trans(floor(postdata1(x,4)) + 1));
%    x = x + 1;
%end;
x = 1;
for x = 1:numPREpuncta;
    predata1(x,4) = predata1(x,4) - floor(predata(x,4)) +
(floor(predata1(x,4)) - trans(floor(predata1(x,4)) + 1));
    x = x + 1;
end;

%count synapses, records stats about them

postdata1 = sortrows(postdata1,2);
predata1 = sortrows(predata1,2);


b = 0;
y = 1;
shufflesyncount = 0;
startID = 1;     %ID that post search begins on

for y = 1:numPREpuncta;
    dx = predata1(y,2);
    dy = predata1(y,3);
    dz = predata1(y,4);

    recentxID = startID;
    minID = startID - 1;

    for recentxID = startID:numPOSTpuncta; % from start to last...

        dx2 = postdata1(recentxID,2);
        dy2 = postdata1(recentxID,3);
```

```
        dz2 = postdata1(recentxID,4);

        recentxID = recentxID + 1;   %increases considered ID

        if dx2 > (dx + maxradius + .1);   %if the considered ID is too
far away, break, otherwise do normal deal
        b = b + 1;
        break;
        end;
        if recentxID > numPOSTpuncta + 1;
        break;
        end;


            umDIS =  sqrt(((dx-dx2)^2)+((dy-dy2)^2)+((dz-dz2)^2));

            if ((predata(y,1)/2) + (postdata((recentxID-1),1)/2) + ff)
>= umDIS;
                shufflesyncount = shufflesyncount + 1;  %counts a
synapse if two puncta are closer than threshold
            end;

     end;    %logs a synapse for beginning going up until its too far
away



     if minID > 0
     for minID = (startID-1):-1:1;  %starting at 1-startID...

         dx2 = postdata1(minID,2);
         dy2 = postdata1(minID,3);
         dz2 = postdata1(minID,4);


        minID = minID - 1;

        if dx2 < (dx - maxradius - .1);
         b = b + 1;
        break;
        end;

        umDIS =  sqrt(((dx-dx2)^2)+((dy-dy2)^2)+((dz-dz2)^2));

       if ((predata(y,1)/2) + (postdata((minID+1),1)/2) + ff) >= umDIS;
             shufflesyncount = shufflesyncount + 1;  %counts a synapse
if two puncta are closer than threshold

       end;


       end;
       end;
    y = y + 1;
    startID = round((recentxID + minID) / 2);
```

```
 end;


shufflecount(n,1) = shufflesyncount;

clear zslices;
clear randzslices;
clear randzslices1;
clear trans;

n = n + 1;
end;


Mshufflecount = mean(shufflecount);
end;

%%%%%%%%%%%%%%%%%%%%%%%%%%%%%%%%%%%%%%%%%%%%%%%%%%%%%%%%%%%%%%%%%%%%%%%%%%
%%%%%%%%%%%%%%%%%%%%%%%%%%%%%%%%%%%%%%%%%%%%%%%%%%%%%%%%%%%%%%%%%%%%%%%%%%
%%%%%%%%%%%%%%%%%
postdata = postdatacopy;
predata = predatacopy;


%OUTPUT

syndensity = syncount / dumvolume;

predensity = numPREpuncta / dumvolume;
postdensity = numPOSTpuncta / dumvolume;

syndensity
predensity
postdensity
%dumvolume
%syncount
%prealone2  %corrected for far Z effects with monte carlo
lonepredensity = prealone2 / dumvolume
%numpostalone
lonepostdensity = numpostalone / dumvolume
predistribution = prenumc'
postdistribution = postnumc'
%chancesyncount
chancedensity = chancesyncount / dumvolume

if shuffle == 1;
Mshufflecount
shuffledensity = Mshufflecount / dumvolume;
shuffledensity
end;


%Create the first subplot
figure(1)
subplot(2,2,1), plot(1:xmax-1,localx); %Figure with 2 rows, 1 column,
```

```
index the first plot and plot the first graph
grid on; xlabel('X axis'); ylabel('synapses / um^2'); title('Synapses
on X Axis');
subplot(2,2,2), plot(1:ymax-1,localy); %Figure with 2 rows, 1 column,
index the second plot and plot the second graph
grid on; xlabel('Y axis'); ylabel('synapses / um^2'); title('Synapses
on Y Axis');
subplot(2,2,3), plot(localz(:,2),localz(:,1));
grid on; xlabel('Z axis'); ylabel('synapses / um^2'); title('Synapses
on Z Axis');
axis([0,2.6,0,.6]); %adjust axis

%create second subplot
figure(2)
subplot(2,2,1), hist(midz); %Figure with 2 rows, 1 column, index the
first plot and plot the first graph
grid on; xlabel('synapse Z locations'); ylabel('count'); title('synapse
Z locations');
subplot(2,2,2), hist(predata(:,4)); %Figure with 2 rows, 1 column,
index the second plot and plot the second graph
grid on; xlabel('presynapse Z locations'); ylabel('count');
title('presynapse Z locations');
subplot(2,2,3), hist(postdata(:,4));
grid on; xlabel('postsynapse Z locations'); ylabel('count');
title('postsynapse Z locations');
subplot(2,2,4), hist(dist);
grid off; xlabel('Distances between Puncta in Synapses');
ylabel('Count'); title('Distances between puncta');



%%%%%%%%%%%%%%%%%%%%%%%%%%%%%%%%%%%%%%%%%%%%%%%%%%%%%%%%%%%%%%%%%%%%%%%
%writes files of data for you!

if dataoutput == 1;
a = strcat(samplename, '_data.csv');
label = 'xmax';

dlmwrite(a, xmax,'delimiter',',')
dlmwrite(a, label,'-append','delimiter',',','coffset',1)
dlmwrite(a, ymax,'-append','delimiter',',')
dlmwrite(a, zmax,'-append','delimiter',',')

dlmwrite(a, syndensity,'-append','delimiter',',')
dlmwrite(a, predensity,'-append','delimiter',',')
dlmwrite(a, postdensity,'-append','delimiter',',')
dlmwrite(a, dumvolume,'-append','delimiter',',')
dlmwrite(a, syncount,'-append','delimiter',',')
dlmwrite(a, prealone2,'-append','delimiter',',')
dlmwrite(a, lonepredensity,'-append','delimiter',',')
dlmwrite(a, numpostalone,'-append','delimiter',',')
dlmwrite(a, lonepostdensity,'-append','delimiter',',')
dlmwrite(a, prenumc','-append','delimiter',',')
dlmwrite(a, postnumc','-append','delimiter',',')
dlmwrite(a, chancesyncount,'-append','delimiter',',')
dlmwrite(a, chancedensity,'-append','delimiter',',')
```

```
if shuffle == 1;
dlmwrite(a, Mshufflecount,'-append','delimiter',',')
dlmwrite(a, shuffledensity,'-append','delimiter',',')
end;


detailout = dataset(xmax,ymax,zmax,
syndensity,predensity,postdensity,dumvolume,syncount,prealone2,lonepred
ensity,numpostalone,lonepostdensity,prenumc,postnumc,chancesyncount,cha
ncedensity);
export(detailout,'file',a,'delimiter',',');




%outputs synapse info into spreadsheets

numsyn = numel(midx);
for x = 1:numsyn
    syndata(x,1) = midx(x,1);
    syndata(x,2) = midy(x,1);
    syndata(x,3) = midz(x,1);
    syndata(x,4) = preID(x,1);
    syndata(x,5) = postID(x,1);
    syndata(x,6) = dist(x,1);
    x = x + 1;
end;

b = strcat(samplename, '_syndata.csv');
dlmwrite(b, syndata,',');   %column 1 is x, 2 is y, 3 is z, 4 is PreID,
5 is postID, 6 is Distance b/w the 2


end;

%figure(3)
%subplot(2,2,1), hist(midx,118); %Figure with 2 rows, 1 column, index
the first plot and plot the first graph
%grid on; xlabel('synapse X coordinate'); ylabel('count');
title('Synapses on X Axis');
%subplot(2,2,2), hist(postdata(:,2),118); %Figure with 2 rows, 1
column, index the second plot and plot the second graph
%grid on; xlabel('post x coordinate'); ylabel('count');
title('postsynapses on X Axis');
%subplot(2,2,3), hist(predata(:,2),118);
%grid on; xlabel('pre x coordinate'); ylabel('count');
title('presynapses on X Axis');

%figure(4)
%subplot(2,2,1), hist(midy,82); %Figure with 2 rows, 1 column, index
the first plot and plot the first graph
%grid on; xlabel('synapse y coordinate'); ylabel('count');
title('Synapses on Y Axis');
%subplot(2,2,2), hist(postdata(:,3),82); %Figure with 2 rows, 1 column,
index the second plot and plot the second graph
%grid on; xlabel('post y coordinate'); ylabel('count');
```

```
title('postsynapses on Y Axis');
%subplot(2,2,3), hist(predata(:,3),82);
%grid on; xlabel('pre y coordinate'); ylabel('count');
title('presynapses on Y Axis');
%%%%%%%%%%%%%%%%%%%%%%%%%%%%%%%%%%%%%%%%%%%%%%%%%%%%%%%%


%Repeat the entire above program (or most of it), while varying the
%distance threshold from -.3 um to +.3 um in incriments of .05 microns.

predata = predatacopy;
postdata = postdatacopy;

ff = -.3;
num = 0;
for ff = -.3:.05:.3;

%corrects volume for dapi staining

zmax1 = zmax - avgradius; %corrects volume for syn and pre
volume = (xmax * ymax * zmax1); %in um^3
voxvolume = volume / .0010465;
dvoxvolume = voxvolume - (dapivox * 1.8971); %1.89 is empirically
determined, see xls sheet
dumvolume = dvoxvolume / 955.566173; %(.1023*.1023*.1)^-1 = 955 vox/um3

%correction for lone pre density
volume = (xmax * ymax * zmax); %in um^3
voxvolume2 = volume / .0010465;
dvoxvolume2 = voxvolume2 - (dapivox * 1.8971); %1.89 is empirically
determined, see xls sheet
dumvolume2 = dvoxvolume2 / 955.566173; %(.1023*.1023*.1)^-1 = 955
vox/um3



if GFP == 1;
dumvolume = .0010465 * GFPvox;  %um^3
end;


%%%%%%%%%%%%%%%%%%%%%%%%%%%%%%%%%%%%%%%%%%%%%%%%%%%%%%%%

%calculates the synapse number and density expected if the same number
of pre/post puncta were randomly associated
postdatacopy = postdata;
predatacopy = predata;

    numPOSTpuncta = numel(postdata(:,5));

    predata(:,4) = zmax * rand(numPREpuncta,1);
    predata(:,3) = ymax * rand(numPREpuncta,1);
    predata(:,2) = xmax * rand(numPREpuncta,1);
    postdata(:,4) = zmax * rand(numPOSTpuncta,1);
    postdata(:,3) = ymax * rand(numPOSTpuncta,1);
```

```
    postdata(:,2) = xmax * rand(numPOSTpuncta,1);

    numPOSTpuncta = numel(postdata(:,5));

    farZpost = [];
    for x = 1:numPOSTpuncta;
        if postdata(x,4) < (.1) | postdata(x,4) > (zmax - (.1));
            farZpost(x,1) = postdata(x,5);
        end;
    end;

   if isempty(farZpost) == 0;
   [d, ifarzpost, idata] = intersect(farZpost,postdata(:,5));
   postdata(idata,:) = []; %deletes puncta that have been logged in far
Z;
   end;
  numPOSTpuncta = numel(postdata(:,5));



postdata = sortrows(postdata,2);
predata = sortrows(predata,2);


b = 0;
y = 1;
chancesyncount = 0;
startID = 1;     %ID that post search begins on

for y = 1:numPREpuncta;
    dx = predata(y,2);
    dy = predata(y,3);
    dz = predata(y,4);

    recentxID = startID;
    minID = startID - 1;

    for recentxID = startID:numPOSTpuncta; % from start to last...

        dx2 = postdata(recentxID,2);
        dy2 = postdata(recentxID,3);
        dz2 = postdata(recentxID,4);

        recentxID = recentxID + 1;   %increases considered ID

        if dx2 > (dx + maxradius + .1);   %if the considered ID is too
far away, break, otherwise do normal deal
        b = b + 1;
        break;
        end;
        if recentxID > numPOSTpuncta + 1;
        break;
        end;
```

```
            umDIS =  sqrt(((dx-dx2)^2)+((dy-dy2)^2)+((dz-dz2)^2));

            if ((predata(y,1)/2) + (postdata((recentxID-1),1)/2) + ff)
>= umDIS;
                chancesyncount = chancesyncount + 1;  %counts a synapse
if two puncta are closer than threshold

            end;

     end;    %logs a synapse for beginning going up until its too far
away



     if minID > 0
     for minID = (startID-1):-1:1;  %starting at 1-startID...

         dx2 = postdata(minID,2);
         dy2 = postdata(minID,3);
         dz2 = postdata(minID,4);


        minID = minID - 1;

        if dx2 < (dx - maxradius - .1);
         b = b + 1;
        break;
        end;

        umDIS =  sqrt(((dx-dx2)^2)+((dy-dy2)^2)+((dz-dz2)^2));

        if ((predata(y,1)/2) + (postdata((minID+1),1)/2) + ff) >=
umDIS;
                chancesyncount = chancesyncount + 1;  %counts a synapse
if two puncta are closer than threshold
        end;


       end;

      end;
    y = y + 1;

    startID = round((recentxID + minID) / 2);
 end;



%%%%%%%%%%%%%%%%%%%%%%%%%%%%%%%%%%%%%%%%%%%%%%%%%%%%%%%%%%%%%%%%%%%
%deletes postsynaptic puncta that are radius/2 away from Z edges


    postdata = postdatacopy;
    predata = predatacopy;
```

```
    numPOSTpuncta = numel(postdata(:,5));
    farZpost = [];
    for x = 1:numPOSTpuncta;
        if postdata(x,4) < .1 | postdata(x,4) > (zmax - .1);
            farZpost(x,1) = postdata(x,5);
        end;
    end;

   if isempty(farZpost) == 0;
   [d, ifarzpost, idata] = intersect(farZpost,postdata(:,5));
   postdata(idata,:) = []; %deletes puncta that have been logged in far
Z;
   end;
  numPOSTpuncta = numel(postdata(:,5));



postdata = sortrows(postdata,2);
predata = sortrows(predata,2);


b = 0;
y = 1;
syncount = 0;
startID = 1;     %ID that post search begins on

for y = 1:numPREpuncta;
    dx = predata(y,2);
    dy = predata(y,3);
    dz = predata(y,4);

    recentxID = startID;
    minID = startID - 1;

    for recentxID = startID:numPOSTpuncta; % from start to last...

        dx2 = postdata(recentxID,2);
        dy2 = postdata(recentxID,3);
        dz2 = postdata(recentxID,4);

        recentxID = recentxID + 1;   %increases considered ID

        if dx2 > (dx + maxradius + .1);   %if the considered ID is too
far away, break, otherwise do normal deal
        b = b + 1;
        break;
        end;
        if recentxID > numPOSTpuncta + 1;
        break;
        end;


            umDIS =  sqrt(((dx-dx2)^2)+((dy-dy2)^2)+((dz-dz2)^2));
```

```
            if ((predata(y,1)/2) + (postdata((recentxID-1),1)/2) + ff)
>= umDIS;
                syncount = syncount + 1;  %counts a synapse if two
puncta are closer than threshold
                xpreID(syncount) = predata(y,5);
                xpostID(syncount) = postdata((recentxID-1),5);
            end;

     end;    %logs a synapse for beginning going up until its too far
away



     if minID > 0
     for minID = (startID-1):-1:1;  %starting at 1-startID...

         dx2 = postdata(minID,2);
         dy2 = postdata(minID,3);
         dz2 = postdata(minID,4);


        minID = minID - 1;

        if dx2 < (dx - maxradius - .1);
         b = b + 1;
        break;
        end;

        umDIS =  sqrt(((dx-dx2)^2)+((dy-dy2)^2)+((dz-dz2)^2));

        if ((predata(y,1)/2) + (postdata((minID+1),1)/2) + ff) >=
umDIS;
                syncount = syncount + 1;  %counts a synapse if two
puncta are closer than threshold
                xpreID(syncount) = predata(y,5);
                xpostID(syncount) = postdata((minID+1),5);
        end;


       end;

      end;
    y = y + 1;

    startID = round((recentxID + minID) / 2);
 end;
preID = [];
postID = [];



if syncount >= 1;
    preID(:,1) = xpreID(1,:);
    postID(:,1) = xpostID(1,:);
else;
```

```
    preID = 0;
    postID = 0;
end;

postalone1 = postdata(:,5);
[d, ipostID, ialone] = intersect(postID,postalone1);
postalone1(ialone) = [];  %postalone1 contains the ID of pre puncta not
in a synapse
numpostalone = numel(postalone1);

prealone1 = predata(:,5);  %prealone is vector of ID of presynaptic
puncta
[d, ipreID, ialone] = intersect(preID,prealone1);  %takes the intersect
of presynaptic puncta in a synapse and presynaptic IDs
prealone1(ialone) = [];  %sets the indeces of pre that take part in a
synapse to null.  now prealone1 contains only those Ids that dont take
part in a synapse
numprealone = numel(prealone1);


%generates fract of puncta in 50 random intervals equivilent to 1/2
radius
farZpreID = [];
fmin = avgradius/2;
fmax = zmax - avgradius/2;
n = 0;
for a = 1:numPREpuncta;
    if predata(a,4) > fmax | predata(a,4) < fmin;
        n = n + 1;
        farZpreID(n) = predata(a,5);
        farZpreZ(n) = predata(a,4);
    end;
end;

if isempty(farZpreID) == 0;

    p = intersect(prealone1, farZpreID);
    fractpre = numel(p)/numel(prealone1);

    clear q;
    clear p;
    clear a;

elseif isempty(farZpreID) == 1;
    fractpre = 0;

end;


r = fmin + (fmax-fmin).*rand(50,1);
hi = r(:,1) + (avgradius/4);
lo = r(:,1) - (avgradius/4);  %creates 50 intervals of equivilant Z
thickness to the amount that is being called 'far z'%%

for z = 1:50;
n = 0;
```

```
ID = [];
    for a = 1:numPREpuncta;
        if predata(a,4) < hi(z,1) & predata(a,4) > lo(z,1);
            n = n + 1;
            ID(n) = predata(a,5);  %adds one everytime a puncta occurs
within range
        end;
    end;
    if isempty(ID) == 0;
        p = intersect(prealone1, ID);  %list of unassociated puncat in
that interval
        fract(z) = numel(p)/numel(prealone1);  %fraction of the alone
in that given interval
    else;
        fract = 0;
    end;
end;
meanPrefract = mean(fract(:,1));


clear y;
clear n;
clear z;
clear p;
clear z;
clear a;


prealone2 = numel(prealone1) - ((fractpre - meanPrefract) *
numel(farZpreID)); %number of lone pre = num of lone pre - ((fract of
lone pre on far z - avg numb of lone pre) * num lone on far Z)

num = num + 1;
radsyn(num,1) = ff;  % the first column of radsyn is the radius
radsyn(num,2) = syncount;  %the second column of radsyn is the synapse
count
radsyn(num,3) = (syncount / dumvolume); %the third column of radsyn is
the density
radsyn(num,4) = (chancesyncount / dumvolume); %the fourth column of
radsyn is the density by chance
radsyn(num,5) = (numpostalone / dumvolume); %5th column is density of
lone puncta
radsyn(num,6) = (prealone2 / dumvolume2); %6th column is density of
alone-pre

end;


plot(radsyn(:,1),radsyn(:,3),'k',radsyn(:,1),radsyn(:,4),'r',radsyn(:,1
),radsyn(:,5),'m--',radsyn(:,1),radsyn(:,6),'b--')

if cycleoutput == 1;


synapse_density = radsyn(:,3);
chance_density = radsyn(:,4);
```

```
lonepost_density = radsyn(:,5);
lonepre_density = radsyn(:,6);
distance_threshold = radsyn(:,1);

cycout =
dataset(distance_threshold,synapse_density,chance_density,lonepost_dens
ity,lonepre_density);
yy = strcat(samplename, '_cycle_output.csv');
export(cycout,'file',yy,'delimiter',',');


end;

%%%%%%%%%%%%%%%%%%%%%%%%%%%%%%%%%%%%%%%%%%%%%%%%%%%%
Imager Generator – outputs a TIF series marking synapses output into
the 'samplename_syndata.csv' file.

%column 1 is x, 2 is y, 3 is z, 4 is PreID, 5 is postID, 6 is Distance
b/w
%the 2
%samplenamesyndata = array

pixX = xmax / .1023;
pixY = ymax / .1023;
pixZ = zmax / .1;

testsyndata(:,3) = testsyndata(:,3) * 10;  %round the Z position of
synapse to nearest img number
roundZ = round(testsyndata(:,3));
remainders = testsyndata(:,3) - roundZ(:,1);
testsyndata(:,3) = roundZ(:,1);
A = sortrows(testsyndata, 3);  %sort by Z stack

syncount = numel(testsyndata(:,3));

testsyndata(:,1) = round((testsyndata(:,1) / .1023));
testsyndata(:,2) = round((testsyndata(:,2) / .1023));

rpixY = round(pixY);
rpixX = round(pixX);

stack = (Micheva and Smith, 2007);
for Z = 1:pixZ;
    stack(Z) = {zeros(rpixY,rpixX)};
    Z = Z + 1;
end;

i = 1;
Z = 1;
for Z = 1:pixZ;
    img = stack{Z};
    for i = 1:syncount;
        if (testsyndata(i,3) == Z & (testsyndata(i,1) > 2) &
(testsyndata(i,2) > 2) & (testsyndata(i,1) < (pixX - 2)) &
(testsyndata(i,2) < (pixY -2)));
            img(testsyndata(i,2),testsyndata(i,1)) = 200;
```

```
            img((testsyndata(i,2)+1),testsyndata(i,1)) = 200;
            img((testsyndata(i,2)-1),testsyndata(i,1)) = 200;
            img(testsyndata(i,2),(testsyndata(i,1)+1)) = 200;
            img(testsyndata(i,2),(testsyndata(i,1)-1)) = 200;

        end;
    i = i + 1;
    stack{Z} = img;
    end;
Z = Z + 1;
end;

Z = 1;
for Z = 1:pixZ;
    strZ = num2str(Z);
    a = strcat(strZ,'.tif');
    imwrite(stack{Z},a,'tif','Compression','none');
end;
```

Appendix 4: Technical Notes to Supplement the Published Array Tomography Protocol

I. Sectioning:

Filter the water in the knife bath with a 0.22 μm filter attached to the syringe

Don't trim the blockface of embedded tissue with a razor before beginning sectioning. Just start sectioning until you get to tissue (at a speed of 100 μm/s)

Stain with toluidine blue to see if your block has tissue in it:
Warm the slide to adhere the tissue to the slide/coverslip
Stain with toluidine blue for 20s, then rinse with water.
Look under microscope for tissue.

- when you are fully into the tissue (confirmed with stain), raise the water level up and use tape to remove all the scum from atop the water

- now you will trim the block by hand with a razor

- use compressed air to remove pieces of LR white left around sample

- Use triangular knife to trims sides – the knife has 45 degree sides, so add an extra 15 degrees, and it trims at a 60 degree angle on each side.

- Paint some xylene:glue mix onto the top and bottom sides of the block

- have the knife zeroed at 0 degrees, and put in coverslip

- cut at 70-100 nm for puncta across sections, but at 200 nm for anatomy.

- when you have a ribbon, slowly add more water from the front corner, and use eyelash tool to smooth out the water edge on the coverslip. Attach edge of array to the coverslip, and remove water from the front slowly with a syringe to adhere the rest of the ribbon smoothly to the coverslip.

II. Staining:

In general, if an AB is 1 mg/ml, use 1:100, or 10x more concentrated than normal frozen slices.

For filling cells, Luciferase Yellow works well.

Leave primary staining overnight at 4 degrees (especially for synapsin, its 3x brighter overnight)

Spin Abs before using for 2 minutes at 13000 rpms

III. Image Acquisition:

First acquire a mosaic of the entire ribbon:
- Mark the top left and bottom right of the ribbon and it automatically makes a grid
    mark top left -> button on bottom of acq setup screen. (button is rectangle with lines extending over the shape on top left corner)
    Mark bottom right -> rectange button with arrows pointing at center of each side

- go to focus correction tab in acq setup screen, scroll along and focus at a few different spots
- hit check enable correct to confirm
- check mosaic in experiment tab in multichannel acquisition

- mosaic won't automatically save – so save it!
- then click convert tile images in mosaic tab
- go to mosaic and go to 'measure' + 'marker'
- Mark a spot on 2 section and save image w/markers
- "measure" – create table – ok
- Brads software:
    - Prep image -> mark loop
    - when done, click back on original mosaic
    - then slick 'preview stack'
    - Close, and don't save everything it opened – it saved the position list
    - change to 63x objective
    - mark/find – new – import position list _ open, open all channels/colors

when position list opens, double click so the check comes up – delete first and last slice
Find slice near middle, and turn on all colors, and measure exposures
- turn on autofocus – set the first channel to autofocus (other should be 'current'). – This should be a more punctate channel.

Check position list in multichannel acquire tab, and go!

When it is done, check through each image to see if it is in focus – if not, retake image w/same parameters + resave (overwrite same name as out of focus image).

Click 'make stack' macro on top right and reset parameters on bottom.

IV. Analysis:

In axiovision, start using .Zvi images (in a separate folder).
1. Convert ZVI files to TIFS
Export images -> make a new folder and choose 'save as'
Don't check create project folder
Check merged images if 3 channels, but more than 3 channels do not check it!
Select file type: TIF
Batch – add files you want (select all + open) then click 'run batch'
When finished close the export window
Check all images – if any are out of focus, you'll have to retake it and replace it in the stack once it is in TIF format.

Open ImageJ

- Convert tiffs to stack:
Import -> image sequence -> click on 1st image + open
Image -> color -> RGB split (splits channels)
File -> save as tif (resave each color stack so you have them separate)
-modify the images if desired:
process – enhance contrast to .1%, normalize stack,
process - subtract background (rolling ball of 20-50 pixels)

Alignment
-> Go to DAPI stack and find image roughly in the middle of stack to begin alignment (eg, if your stack has 30 sections, start on section 15).
- Plugins -> multistackreg (stackreg and turboreg must also be installed)
- 1st stack DAPI, 2nd stack DAPI. Select rigid body transformation, and click save transformation file (call it 'rigid.txt').
- click ok, let it go through every image (this might take a while)
- after it is complete, 1st stack DAPI, 2nd stack DAPI. Select Affine transformation, and click save transformation file (call it 'affine.txt').
- save newly aligned DAPI stack
Now repeat this process for all the other colors in your stack, except use 'load transformation file' file, and load the saved file that the DAPI alignment produced.
IMPORTANT! Start at the same slice number! If you started your rigid transformation with your dapi stack at slice 15 out of 30, also start the alignment of the other channels on slice 15 out of 30.

When all stacks have been aligned

- Recombination
When all colors have been aligned, go to Image – color – RGB merge, and merge them
Go to ROI manager, select what you want, add it to the list, and save ROI so that you can get the same ROI on subsequent acquisitions

Sometimes, imageJ might not align everything properly. You have two options: 1) delete every slice after the misaligned sections or 2) manually align the stack using autoaligner, then repeat the rigid and affine alignments in ImageJ.

Save your 3 color stack and load it into a 3D program of your choice (axiovision, imaris, and velocity all work).